

THESIS ON NATURAL AND EXACT SCIENCES B216

Geochemistry of Organic-Rich Metalliferous Oil Shale/Black Shale of Jordan and Estonia

MARGUS VOOLMA

TUT
PRESS

TALLINN UNIVERSITY OF TECHNOLOGY
Institute of Geology

This dissertation was accepted for the defense of the degree of Doctor of Philosophy in Earth Sciences on 02.06.2016

Supervisor:

Prof. Alvar Soesoo, Institute of Geology at Tallinn University of Technology

Opponents:

Dr. Peter Sorjonen-Ward, Ore Geology and Resource Economics Unit, Geological Survey of Finland, Finland

Dr. Leho Ainsaar, Institute of Ecology and Earth Sciences at University of Tartu, Estonia

Defence of the thesis: 05.07.2016 at Tallinn University of Technology, Ehitajate tee 5, Tallinn, 19086, Estonia

Declaration: Hereby I declare that this doctoral thesis, my original investigation and achievement, submitted for the doctoral degree at Tallinn University of Technology has not been submitted for doctoral or equivalent academic degree.

Margus Voolma

Copyright: Margus Voolma, 2016

ISSN 1406-4723

ISBN 978-9949-23-983-2 (publication)

ISBN 978-9949-23-984-9 (PDF)

LOODUS- JA TÄPPISTEADUSED B216

**Orgaanika- ja metalliderikaste
põlevkivide/mustade kiltade geokeemiast
Jordaania ja Eestis**

MARGUS VOOLMA

CONTENTS

LIST OF ORIGINAL PUBLICATIONS	6
INTRODUCTION.....	7
MATERIAL AND METHODS	9
Oil Shale.....	9
Black Shale	9
Geochemical analysis.....	9
Statistical analysis.....	10
Outline of Attarat Um Ghudran oil shale of Jordan	10
Mineralogical composition.....	12
Chemical composition	13
Outline of graptolite argillite of Estonia	15
Mineralogical composition.....	16
Chemical composition	17
DISCUSSION	18
Comparison of chemical composition and distribution patterns of metals in oil shale and black shale.....	20
Mineral matter characteristics in oil shale/black shale reflected through variation of major elements.....	21
Enriched metals in oil shale/black shale and organic matter.....	23
Trace elements variation reflecting changes in accumulation environment of black shale.....	31
CONCLUSIONS.....	38
ACKNOWLEDGEMENTS	40
REFERENCES.....	41
ABSTRACT	49
KOKKUVÕTE.....	51
ELULOOKIRJELDUS.....	53
CURRICULUM VITAE	54
PUBLICATIONS (1–5)	55

LIST OF ORIGINAL PUBLICATIONS

This thesis is based on the following papers.

1. Voolma, Margus; Soesoo, Alvar; Hade, Sigrid; Hints, Rutt; Kallaste, Toivo (2013). Geochemical heterogeneity of the Estonian graptolite argillite. *Oil Shale*, 30(3), 377 - 401.
2. Hints, Rutt; Hade, Sigrid; Soesoo, Alvar; Voolma, Margus (2014). Depositional framework of the East Baltic Tremadocian black shale revisited. *GFF*, 136, 464 - 482.
3. Hints, Rutt; Soesoo, Alvar; Voolma, Margus; Tarros, Siim; Kallaste, Toivo; Hade, Sigrid (2014). Centimetre-scale variability of redox-sensitive elements in Tremadocian black shales from the eastern Baltic Palaeobasin. *Estonian Journal of Earth Sciences*, 63(4), 233 - 239.
4. Puura, Väino; Soesoo, Alvar; Voolma, Margus; Hade, Sigrid; Aosaar, Hardi (2016). Chemical composition of the mineral matter of the Attarat Um Ghudran oil shale, Central Jordan. *Oil Shale*, 33(1), 18-30
5. Voolma, Margus; Soesoo, Alvar; Puura, Väino; Hade, Sigrid; Aosaar, Hardi (2016). Assessing geochemical variability of oil shale in the Attarat Um Ghudran deposit, Jordan. *Estonian Journal of Earth Sciences*, 65(2), 61-74.

The co-authorship of the papers reflects that they are part of collaborative research projects. The author was responsible for sample collection and preparation for analysis, geochemical data interpretation and statistical analysis.

INTRODUCTION

Oil shales/black shales (OS/BS) can be found all over the world. The dimensions of OS/BS deposits are highly variable in thickness as well as in lateral extent. OS/BS are usually organic-rich fine-grained sedimentary rocks commonly formed in low-oxygen or anoxic/euxinic conditions. Silt- and clay-size mineral matter is deposited together with organic matter (OM) mostly in marine settings. The mineral composition ranges from dominating silicate minerals (quartz, feldspars, clay minerals) to prevailing carbonate minerals (calcite, dolomite), while both types commonly contain some amount of sulfide minerals (pyrite, sphalerite), suggesting anoxic sedimentary conditions that allowed the preservation of OM in these deposits. The sulfide minerals and OM are associated with abundance of various heavy metals common in OS/BS. The assemblage of trace metals is variable, from common transition metals Mo, V, U, Pb, Zn, Ni, Cu, Co, and Cr to precious metals Ag, Au and platinum group elements (PGEs); however, the enriched heavy metals' sets vary in different OS/BS deposits. BS of Estonia, known as graptolite argillite (GA) and its continuation to the west as alum shale, is enriched with e.g. Mo, U, V, and Pb. OS of Jordan has high concentrations of e.g. Zn, Cd, Ni, Cr, Mo, and V. For the genesis of different OS/BS formations as well as for the source of metals several mechanisms have been proposed. In fact, the high content of OM is the only common factor for these fine-grained sedimentary rocks that were deposited in various depositional environments (e.g. fresh water lakes, marine basins) ranging in age from Cambrian to Paleogene.

There are numerous studies conducted on various metalliferous BS/OS deposits worldwide (Dyini, 2003, 2006) – deposits in North America (Vine & Tourtelot, 1970; Coveney et al., 1987; Quinby-Hunt et al., 1989; Wilde et al., 1989; Hatch & Leventhal, 1992; Algeo & Maynard, 2004), Australia (Lewis et al., 2010), Jordan (Abed & Amireh, 1983; Al-Harashsheh et al., 2005; Hamarneh et al., 2006; Abed et al., 2009; Dill et al., 2012; Magharbeh et al., 2012; Amer et al., 2013; Alnawafleh & Fraige, 2015; Hakimi et al., 2016), Israel (Goren, 2015), China (Steiner et al., 2001; Jiang et al., 2007; Fu et al., 2015a, 2015b; Bai et al., 2015; Zeng et al., 2015; Liu et al., 2015; Xu et al., 2013; Fu et al., 2012), Latvia (Kiipli, 1997), central Europe (Vaughan et al., 1989), and alum shale in Scandinavia (Andersson et al., 1985; Sundblad & Gee, 1984; Berry et al., 1986; Leventhal, 1990, 1991; Schovsbo, 2002), focusing on the general characteristics and different aspects of metallogenesis in those assemblages. Also, a series of investigations have been targeted on the general geochemistry and trace element distribution of Estonian GA (Petersell et al., 1981; Loog, 1982; Petersell et al., 1987; Pukkonen, 1989; Kallaste & Pukkonen, 1992; Pukkonen & Rammo, 1992; Loog & Petersell, 1994; Loog & Petersell, 1995; Lippmaa et al., 2009; Lippmaa et al., 2011; Voolma et al., 2013; Hints et al., 2014; Soesoo & Hade, 2014; Hade & Soesoo 2014).

The studied Jordanian OS and Estonian BS samples contain anomalous amounts of trace metals (e.g. V, Mo, U, Zn); however, in both cases the metal-rich OS/BS intervals cannot be distinguished from metal-poor rocks without chemical analyses (Fig. 1).

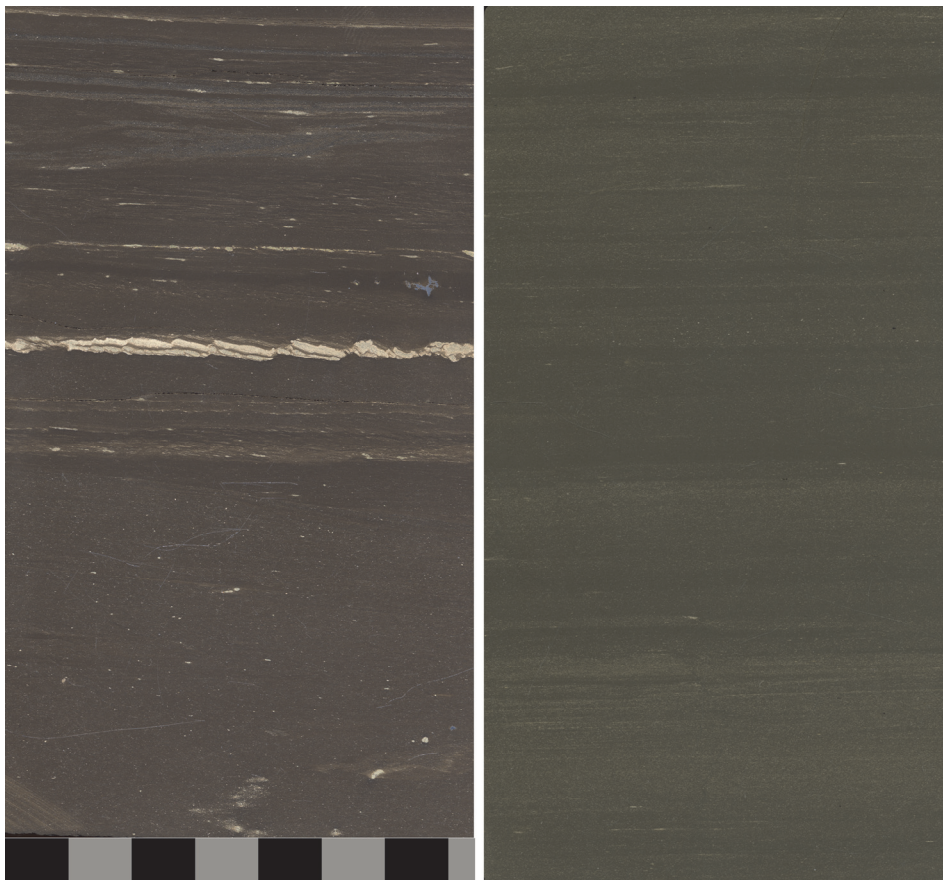


Fig. 1. Example of black shale of Estonia (left) and oil shale of Jordan (right) drill core sections.

This study is focused on the comparison of variation in geochemistry of GA in Estonia and OS of Attarat Um Ghudran (AUG) deposit in Jordan (within the Jordan Oil Shale Energy (JOSE) concession area) with emphasis on enriched trace metals – their distribution patterns, possible provenance and mode of occurrence in these organic-rich sedimentary rocks. Firstly, a comparative study of organic-rich sedimentary deposits, GA of Estonia and OS of Jordan, is presented to determine/highlight main similarities as well as variations and distribution patterns of major components along with enriched metals, using OS/BS from two very different geological settings – deep-water calcareous OS versus more proximal shallow-water settings with siliciclastic input. Some aspects (oil yield,

heat of combustion, etc.) involved in describing the organic-rich sedimentary deposit are out of scope (or the data are too limited to compare) of this study and are omitted. Secondly, statistical analysis method is used to spot and highlight the changes in BS cross-section having rather homogeneous major element composition next to heterogeneous trace metal composition. Hierarchical clustering of samples could reveal internal structure of the formation, possibly helping to interpret the processes behind high variation of trace metals during the accumulation of GA.

MATERIAL AND METHODS

Oil Shale

During 2007-2013, the JOSE Company explored a concession area of about 73 km² located in the southern border zone of AUG deposit, next to Wadi Maghar (WM). JOSE has drilled a regular grid of boreholes with a full coring of the up to 90 m thick OS seam and its lower and upper contact layers. Drill cores were halved and samples for quality assessment were taken with a 0.5 to 2.0m interval. All lithological layers thicker than 0.5 m were sampled separately, coarse-crushed and sent to Estonia for analyzing. The halved drill cores were logged and photographed in Jordan. JOSE is the owner of all rock material and geochemical data (AUG OS) used for interpretation in this study.

Black Shale

Samples of the Türisalu Formation (Fm.) were taken from Pakri Peninsula (59.37668N, 24.03648E), the 4.2-m thick BS sequence of the Uuga Cliff outcrop was sampled with 20-cm interval.

Drill cores SP2 and SP3 on Suur-Pakri Island, NW Estonia, are located less than a kilometer apart: SP2 (59°20'13.07"N, 23°53'54.74"E, WGS84) and SP3 (59°20'15.33"N, 23°54'33.8"E, WGS84); GA in these drill cores is 4.6 m and 4.4 m thick, respectively. A quarter of the BS in both drill cores was sampled and analyzed by 2-cm interval. Siliciclastic beds belonging to the Kallavere Fm. and the Varangu Fm. near the lower and upper contacts with the Türisalu Fm. were also sampled. Core loss is 1.08 m for SP3 and 1.0 m for SP2.

Geochemical analysis

The samples were analyzed at the Institute of Geology at Tallinn University of Technology. Preparation and analytical methods were similar for OS and BS samples. Loss on ignition (LOI) was determined from 1 g of pulverized sample material at 500°C and 920°C, for 18 BS samples also at 400°C. XRF analysis was conducted with S4 Pioneer Spectrometer (Bruker AXS GmbH), using X-ray tube with a rhodium anode, which operated at 3 kW. The samples were measured with

a manufacturer's standard as MultiRes modification (pre-calibrated standardless method). In-house standard ES-2 ("Dictyonema Shale") was used as reference material (Kiipli et al., 2000). Detection limits for trace elements analyzed with XRF are 10 ppm for Ni, Cu, Zn, Ga, Ge, As, Se, Br, Rb, Sr, Y, Zr, Nb, Mo, U, and Th; 20 ppm for Sc, V, Cr, Co, Ag, Cd, Sn, Sb, Te, Pb, and W; 50 ppm for I, Cs, Ba, La, Ce, and Nd, and 0.1% for F.

Statistical analysis

The BS dataset for the present statistical analyses is composed of 21 data rows as chemical analyses and 13 columns as elements (21 samples by 13 elements). Two methods of multivariate analysis were used for data assessment: (i) principal components analysis (PCA) and (ii) hierarchical clustering of PCA groups. Both analyses were carried out by using software 'R' (package 'FactoMineR') and RExcel. More detailed description, the formulas used and the mechanism of the construction for these parameters are given by Le et al. (2008) and Husson et al. (2010, 2011).

Outline of Attarat Um Ghudran oil shale of Jordan

Cretaceous to Paleogene sedimentary sequences of the Afro-Arabian shelf sea contain vast volumes of OM (Sharland et al., 2001; Powell & Moh'd, 2011). Jordan, a country devoid of oil, is extraordinarily rich in OS resources. In 1983, Abed and Amireh (1983) summarized the early (1959-1980) publications on OS occurrences in Jordan. Subsequent prospecting and exploration campaigns organized by the Government (Hamarnah et al., 2006) cleared the way for developers interested in acquiring concessions in order to initiate the resource exploration and feasibility studies by interested companies. The Estonian-Jordanian JOSE Company applied for the concession in southern part of the AUG deposit, located on the Central Jordan desert plateau at altitudes 700-800 m above sea level, about 100 km SSE of Amman and 40 km east of village Qattrana (Fig. 2).

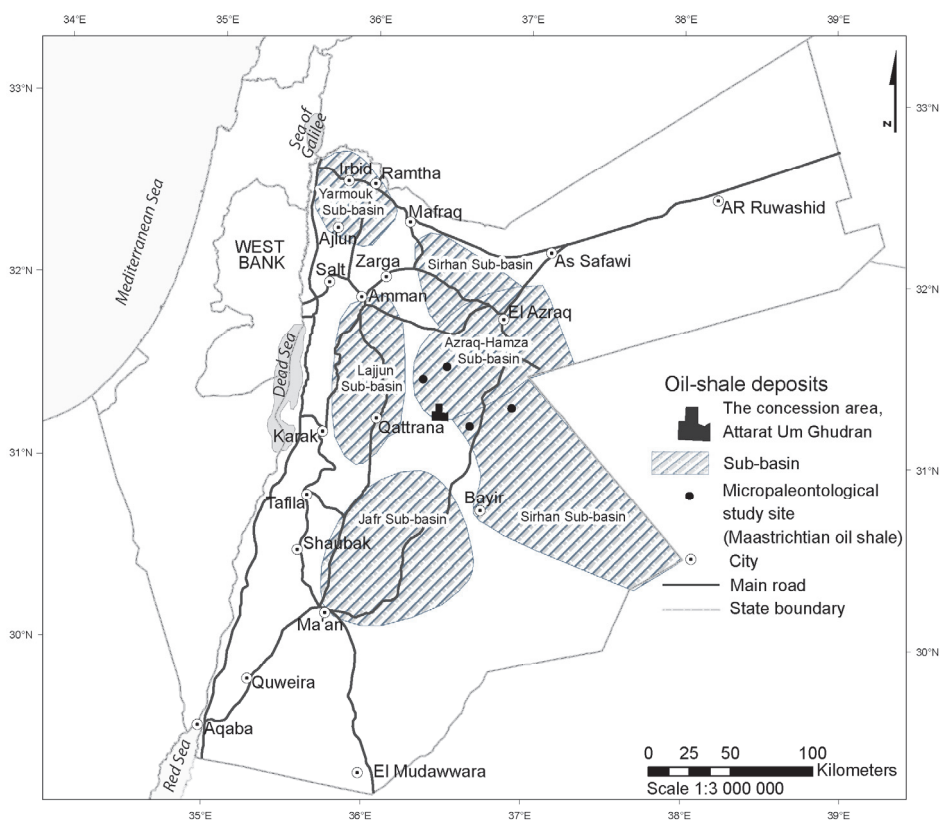


Fig. 2. Approximate location of the JOSE exploration area in the Late Mesozoic to Mid-Paleogene epicontinental sea platform of Jordan subjected to formation of internal shelf basins structured by shallow swells; solid circles – micropaleontological age studies of drill cores or cuttings (modified from Alqudah et al., 2015).

The richest oil shale-grade deposits are of the Late Cretaceous Maastrichtian age, in which OM is presented as kerogen (Abed & Amireh, 1983). It originates from fossilized phytoplankton and zooplankton that flourished and deposited on the southern continental shelf of the Tethys Ocean (Abed et al., 2009). According to a classification by Hutton (1987) the largest Jordanian OS deposits belong to the family of marinite OS (Hamarnah et al., 2006; DeWolfe et al., 2010).

Geologically, the territory of Jordan is located in the NW part of the Arabian Plate. Starting in the Palaeozoic, a thick sedimentary cover evolved during several phases (Sharland et al., 2001; Powell & Moh'd, 2011). Systematic lithofacies studies of Cretaceous to Eocene succession in central and southern Jordan (Powell & Moh'd, 2011) revealed that (i) the area is characterized by passive continental margin depositional sequences, which pass upward from alluvial/paralic to carbonate shelf and pelagic ramp settings, and (ii) sedimentation during the Santonian to Maastrichtian was characterized by a hemi-pelagic chalk-chert-

phosphorite lithofacies association, deposited in shallow to moderate water depths on a homoclinal ramp setting, although thicker coeval sequences were deposited in extensional rifts.

During Early Cretaceous through Eocene, the large temporarily submerged shallow marine clastic and carbonate platform surrounded the continental area of the Arabian Shield in the south and was surrounded by deep marine clastic and carbonate platform of Neo-Tethys in NW (the Mediterranean Neo-Tethys Domain) and NE (the Eastern Neo-Tethys Domain) - see Fig. 1A in Alqudah et al. (2015). Due to upwelling systems, the shallow marine deposits contain rich OS and phosphate accumulations there (Abed, 2013).

A comprehensive and representative study of nannofossils from OS sequences of Jordan was committed and OS sequences of Maastrichtian, Paleocene, Early Eocene and Middle Eocene age were identified (Alqudah et al., 2014a, 2014b, 2015). The data revealed that the thickest OS sequences are located in deep sub-basins that developed in connection with synsedimentary subsidence of seabed in active fault zones.

The AUG and WM OS deposits form a uniform, north-south striking elongated AUG-WM basin that is located in desert area of Central Jordan (Hamarneh et al., 2006; Alali, 2006). Based on reconstructions by Alqudah et al. (2014a, 2014b, 2015), the uniform area of AUG and WM OS deposits lies in the transition zone between the deepest zones of the El-Lajjun Sub-basin with Maastrichtian OS (in the west) and Azraq-Hamza Sub-basin with Maastrichtian-Eocene and locally with over 500 m thick Eocene OS (in the east). Some 100 km to the south, the Jafr Sub-basin with Maastrichtian-Eocene OS (locally over 250 m thick) is situated (Fig. 2).

Mineralogical composition

In addition to small-scale dolomitic limestone layers, two large types of OS can be distinguished in the cross-section: (i) mudstone OS that is dark brown to black, almost massive or very finely laminated, and (ii) wackestone OS that contains varying amount of grains (fossil shells and shell debris) and concretions (Puura et al., 2016). According to SEM-EDS observations, grains and concretions in the OS are dominantly calcitic or, in places, carbonate fluorapatite in composition.

In general, according to XRD studies the mineral composition of OS is limited to calcite, carbonate fluorapatite, quartz (with additional tridymite-cristobalite in certain intervals) and smectite with minor pyrite, sphalerite, and barite identified so far (Puura et al., 2016). The variation through cross-section is significant: the content of calcite varies from 8 to 88%, quartz up to 51% (cristobalite+tridymite up to 47%), and dolomite from below the detection limits (approximately <2%) up to 80%, apatite up to 40%, and clay minerals up to 31%. The corresponding chemical and mineralogical composition is similar to that of the Lajjun deposit located westward from the current study area as described by Hufnagel (1984) and Abed et al. (2009).

Chemical composition

Despite the dominating carbonate composition of the OS suite, the chemical composition in AUG OS seam still varies significantly in the cross-section. Major element composition studies indicate that SiO_2 and CaO range between 3 to 70 wt% and 10 to 50 wt%, respectively, and show strong inverse correlation. The usually low MgO and P_2O_5 contents rise randomly up to 16 wt%. Al_2O_3 and S concentrations are locally up to 7 wt%. OM content in the deposit varies from very low 4 wt% up to 38 wt%.

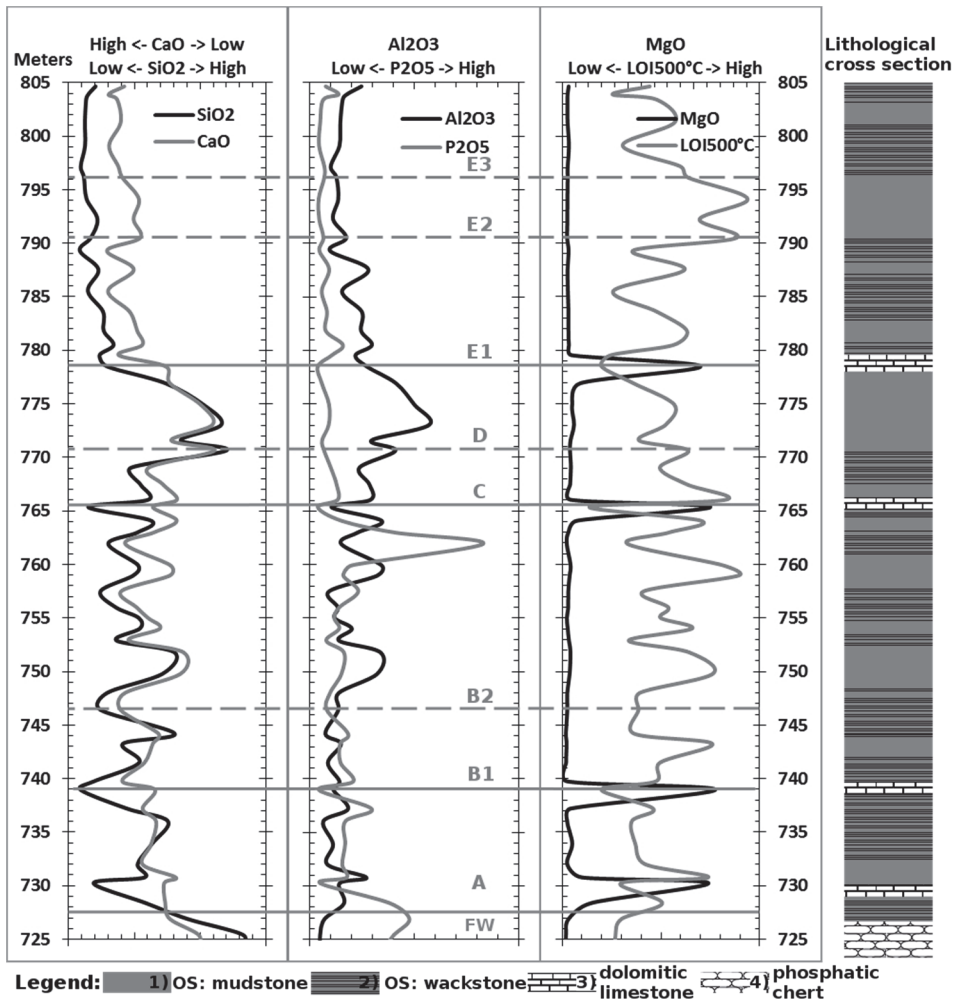


Fig. 3. OS cross-section with main characteristic elements defining the layered structure (from Puura et al., 2016).

Significant variation occurs also in trace metal contents, ranging between 100 and 2700 ppm for Zn and V; Ni, Cr and Mo show concentrations from few tens of ppm-s up to 600 ppm.

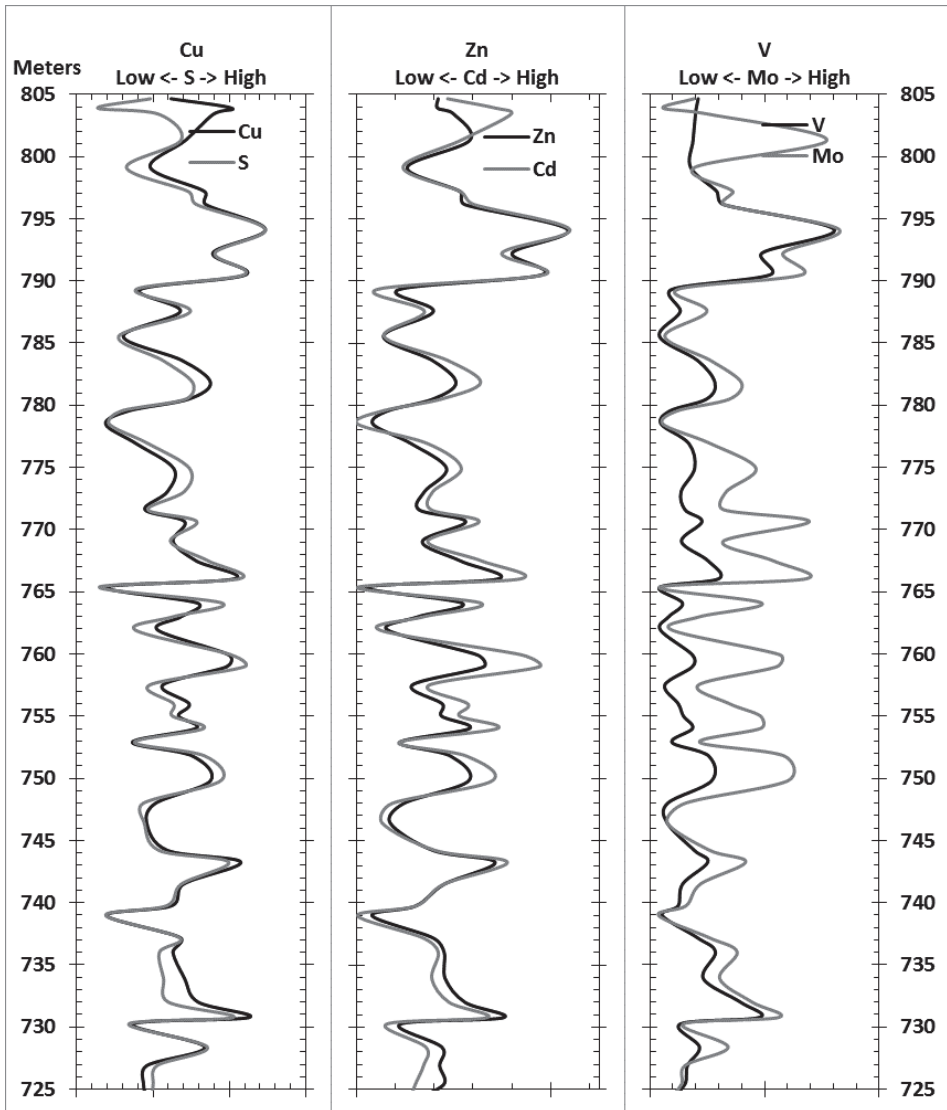


Fig 4. The content of trace metals varies in a wide range, however, trace metals show strong covariation in OS sequence.

Geochemical variation of major and trace elements significantly depends on the layered structure of the OS unit. Apart from lithological OS types, there are geochemical distinctions separating different OS layers, indexed from A to E3. Unlike the rest of layers, certain OS layers show distinct enrichment/depletion in some elements, for example kerogen- and trace metal-rich (layer E2), SiO₂-rich

(layer D), CaO-rich and SiO₂-poor (layers E3 and E1), and P₂O₅-rich (layer A). The dolomitic limestone interlayers show compositionally extreme values for certain elements, high MgO and low kerogen and trace metals (layers A/B, B/C, D/E) (Fig. 3, Fig. 4).

Results of PCA and hierarchical clustering of the OS sample collection (also used in the following comparison with BS) provide considerable information on the geochemical pattern – regularities in distribution of sample clusters within and between the different OS layers. The variation of chemical composition of the OS unit is basically expressed and visualized with six specific geochemical groups (clusters) of samples, spatial distribution of which allows summarizing the main changes in composition and shapes general chemical patterns of the deposit. The study revealed that significant general trends and fluctuations in the entire OS unit as well as differences in the chemical composition of the individual OS layers occur namely in accordance with the layered structure and have most likely been generated by considerable changes in sedimentation conditions. Minor variations as well as specific geochemical stability intervals occur in internal structure of the layers. The inconstant composition of the OS unit has resulted from different intensity of accumulation of chemical components being almost independent from each other: (i) CaO of calcite; (ii) SiO₂ of quartz (cristobalite-tridymite); (iii) Al₂O₃ and related elements of clay minerals; (iv) P₂O₅ of apatite; (v) OM carrying S and trace metals (Zn, Mo, Cr, etc.). Exceptional elevated concentrations of MgO in the barren carbonate interlayers are likely due to diagenetic processes but derived from specific limestones deposited without load of clay components, apatite and OM carrying S and trace metals (Voolma et al., 2016).

Because the mineral matter had only diluting effect on OM carrying S and trace metals the highly variable major elements composition of OS still allows the comparison of enriched trace-metal trends with BS (GA of Estonia).

Outline of graptolite argillite of Estonia

The Tremadocian BS of the Türisalu Fm. make up a laterally extensive organic-rich siliceous mudstone bed in northern Estonia, eastern part of the Baltic Palaeobasin. On a regional scale, GA belongs to the wide but patchy belt of the Middle Cambrian to Lower Ordovician BS extending from Lake Onega district in the east to the Caledonian front, Oslo region and Jutland Peninsula in the west (Andersson et al., 1985; Kaljo et al., 1986; Heinsalu & Bednarczyk, 1997; Buchardt et al., 1997).

GA in Estonia belongs to the Türisalu Fm., it is overlain by glauconitic sandstones and clays of the Varangu Stage and underlain by the phosphatic quartzose sandstone of the Kallavere Fm. (Heinsalu & Viira, 1997). According to biostratigraphic data, the unit is diachronous (Heinsalu et al., 2003) and varies in thickness from less than half a meter in northeastern Estonia to more than 6 m in northwestern Estonia (Fig. 5).

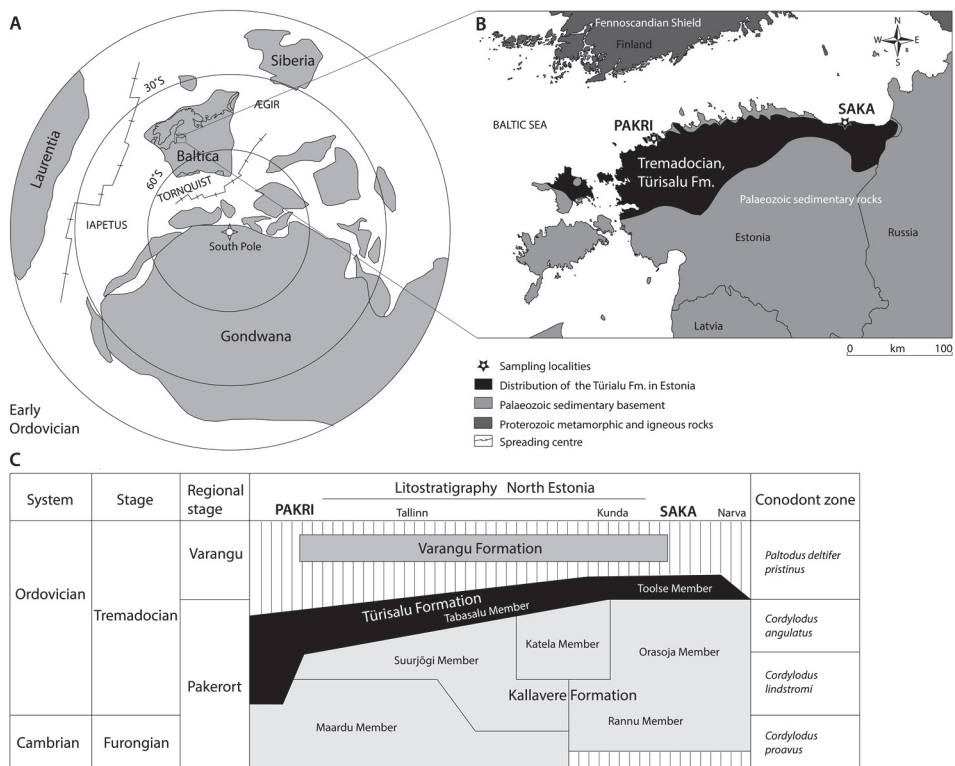


Fig. 5. A. Palaeogeography of Baltica in the Early Ordovician (after Cocks & Torsvik, 2005). B. Modern distribution of the Türisalu Fm. and sampling localities Pakri (outcrop and drillcores) and Saka. C. Lithostratigraphy of the Tremadocian deposits of Estonia after Heinsalu et al. (2003). Figure from (Hints et al., 2014)

Recent findings suggest that the Türisalu Fm. exemplifies transgressive, but rather shallow water reducing marine muds with spatially heterogeneous properties (Voolma et al., 2013; Hints et al., 2014).

Mineralogical composition

GA is a fine-grained kerogen-rich siliceous deposit characterized by high content of OM (15–20%) and pyrite (2.4–6.0%), and very low thermal maturity (Petersell, 1997). The mineral assemblage of GA is according to previous studies dominated by K-feldspars, quartz and clay minerals (Utsal et al., 1982; Loog et al., 2001). In the lateral as well as vertical dimension the contents of major rock-forming minerals show slight but pronounced variation patterns (Utsal et al., 1982; Kleesment & Kurvits, 1987; Loog et al., 2001). The average content of quartz in GA gradually rises eastward with the corresponding clay mineral decrease. In NE Estonia, the argillite complex is intercalated with numerous quartzose silt beds

(Loog & Petersell, 1995). From authigenic sulfides, the occurrence of pyrite, marcasite, sphalerite and galena has been documented. In outcrops and drill cores secondary gypsum and jarosite commonly appear. In general, a higher degree of sulfide mineralization within GA is associated with the occurrence of silt interbeds. Those interbeds might also host a higher amount of other minor authigenic compounds typical for GA – phosphates (mainly apatite as biogenic detritus and nodules), carbonates (calcite and dolomite as cement and concretions), barite and glauconite. Besides the highly resistant terrigenous accessory phases (zircon, tourmaline, garnet), considerable abundance of micas in GA beds has been documented (Utsal et al., 1982; Kleesment & Kurvits, 1987).

Chemical composition

In this study the focus is on results of a centimetre-scale study of enriched trace metal distribution in the Tremadocian BS in two closely spaced drill core sections from Suur-Pakri Island and Pakri outcrop, NW Estonia. The high-resolution bed-to-bed study performed on geochemical variation from the above sampling sites show that major elements vary relatively little across the examined GA sequences, while several trace elements show rather high variation (Fig. 6). Analyses indicate that the GA assemblage is siliceous, high-K, Mn-poor and with variable Fe and S contents. The studies of vertical sequences of GA show the existence of pronounced fine-scale trace metal variability in the GA. The examined samples were detected to be enriched in U, V, Mo and Pb, Zn with respect to average BS, the results obtained thus agreeing with previously published data on the geochemistry of GA. The content of enriched elements was, however, recorded to change greatly over the examined sequences, suggesting a notably more complex nature of trace metal distribution in GA than previously assumed. Redox-sensitive metals U and Mo, and to a lesser extent also V, showed loose covariance with OM content (LOI 500°C), apparently indicating their trapping mainly via OM tied species, and the enrichment primarily linked to OM sequestration.

In general, the dominance of common marine redox sensitive elements among enriched metals in GA favors syngenetic enrichment as the major process of trace metal sequestration. On the other hand, the remarkably high concentration of enriched elements in GA and the variable covariance patterns imply that element sequestration solely from seawater due to Eh gradients is likely an insufficient model for explaining the observed large-scale trace-metal heterogeneity in GA.

The comparison with OS, with somewhat similar trace-metal assemblage, but entirely different and extremely variable mineral matter (calcareous, siliceous, and phosphatic) composition might give hints for new interpretations.

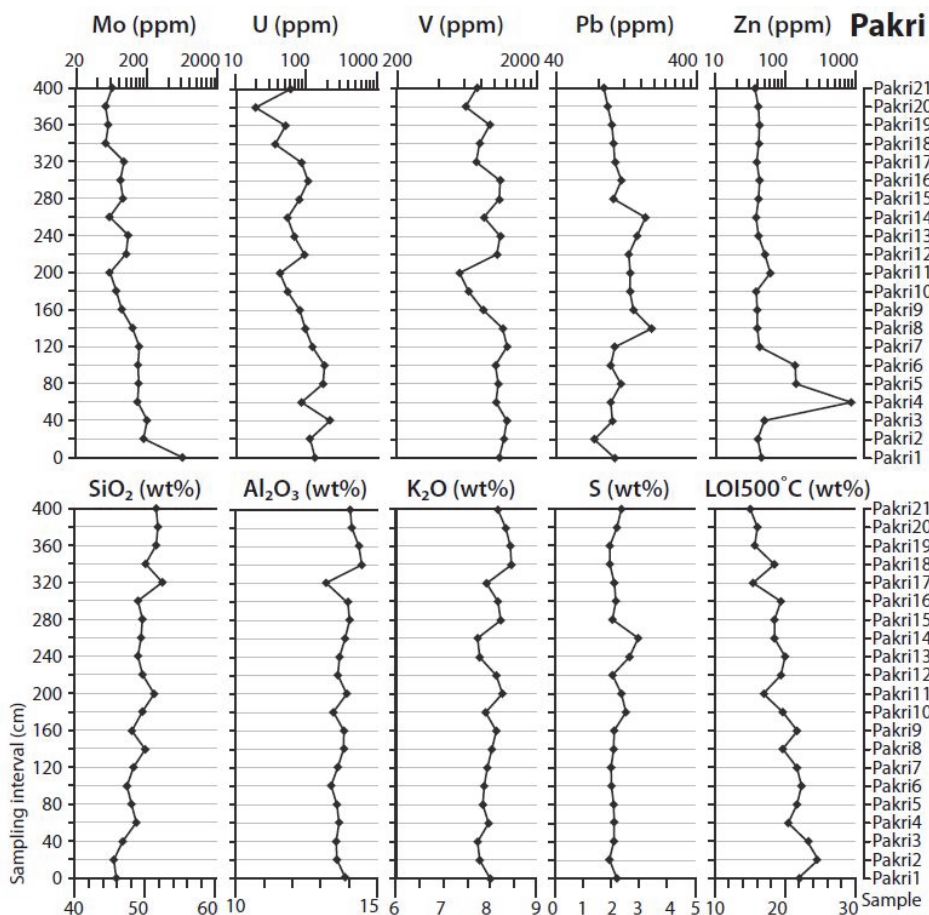


Fig. 6. Vertical distribution profiles of major compounds SiO_2 , Al_2O_3 , K_2O , S, $\text{LOI}_{500^\circ\text{C}}$ and enriched trace metals Mo, U, V, Pb, Zn from Pakri GA sections.

DISCUSSION

Organic-rich deposits ranging from shallow estuarine to ocean-floor varieties act as a significant sink for a number of redox-sensitive elements (e.g. Calvert & Pedersen, 1993; Morford & Emerson, 1999). The distribution of redox-sensitive elements in ancient organic-rich deposits have shown to be useful proxies for interpreting the redox-structure of palaeoseawater, primary productivity and palaeohydrography (e.g. Algeo & Maynard, 2004; Algeo & Lyons, 2006; Brumsack, 2006; Algeo & Tribouillard, 2009).

Trace metal enrichment in BS is mostly explained by two alternative theories: (i) syngedimentary sequestration of metals under oxygen-deficient conditions from marine water, (e.g. Holland, 1979; Algeo & Maynard, 2004; Schovsbo, 2002), or

(ii) flushing of the sediments by metal-enriched syngenetic brines or contemporaneous exhalation of such brines into marine basin (e.g. Coveney & Glascock, 1989; Jiang et al., 2007; Yu et al., 2009; Petersell et al., 1987; Loog & Petersell, 1995). However, these theories are challenged by the works that underline the influence of source rocks and particulate precursor material on the final character of metal enrichment in BS (e.g. Leventhal & Hosterman, 1982), or the crucial role of diagenetic redistribution processes induced by late diagenetic brines (e.g. Coveney et al., 1987; Peacor et al., 2000). The dominance of common marine redox-sensitive elements among enriched metals in BS/OS favors syngenetic enrichment as the major process of trace metal sequestration. The redox-sensitive elements mostly occur as soluble species under the oxidizing conditions. Under the oxygen-depleted conditions, however, the redox-sensitive elements are typically present as insoluble species (metal-organic complexes, sulfides, and metal oxyhydrates) and thus tend to sequester into sediments. The whole metal trapping process is strongly linked with OM breakdown and sulfate reduction processes, which initiate the crystallization of sulfides. In addition to the redox-sensitive trace elements, other elements like Fe and Mn found commonly enriched in BS, are essential recyclers in redox partitioning in marine systems (Chester, 2000). Consequently, based on numerous comparative studies of trace element accumulation in modern and ancient organic-rich sediments (e.g. Nijenhuis et al., 1999; Brumsack, 2006), it has been suggested that oxygen availability in sedimentary environment could have had sole control over the development of enriched trace metal associations in different BS (e.g. Algeo & Maynard, 2004).

Redox-sensitive metals tend to form mobile species under oxic conditions and immobile species in reducing environments, therefore typically accumulating in sediments near redox boundaries. However, several recent investigations suggest that the reduction and sequestration of redox-sensitive metals occurs via various speciation pathways and thus parallel assessment of the behavior of different redox-sensitive elements might potentially give a much more detailed picture of primary environments than single-element-based approaches (e.g. Algeo & Maynard 2004; Tribouvillard et al. 2006).

The differences in trace element composition of OS and BS might in some instances reflect variations in source material fluxes. First of all this relates to non-reactive elements with negligible solubility in surface environments transported to the sedimentary basin mainly in the composition of terrigenous (volcanic) matter such as residual heavy minerals, secondary weathering products or volcanic ash. According to Vine & Tourtelot (1970), the detrital fraction of most BS is characterized by the elements Al, Ti, Zr, Ga, and Sc (very low in OS) and may also commonly include Be, B, Ba, Na, K, Mg, and Fe. Additional elements generally considered insensitive to secondary processes include Nb, Y, Th, Ta, Hf, and the REEs (also very low in OS) (Taylor & McLennan, 1985).

Comparison of chemical composition and distribution patterns of metals in oil shale and black shale

Average, maximum and minimum concentrations and standard deviation (SD) for OS/BS datasets are presented in Table 1. Compared to OS, GA has more stable major element composition in the studied sequences, indicated by low SD values.

Table 1. Average, maximum, and minimum concentrations of oil shale and black shale samples. Major elements as mass% and trace elements as ppm. For reference concentrations of average shale (AS) (Wedepohl 1971, 1991) are presented. In italics are elements (Cu, Se, Cd, Ba, Zr) below detection limits in few samples, for average calculation for elements below detection limit, value inserted was 10% of detection limit; Pb and Rb average content in OS is based on only 40 samples, not representative of full sequence

	OS 410				BS 373				
	Mean	SD	Min	Max	Mean	SD	Min	Max	AS
LOI500°C	15.95	5.65	4.13	38.28	20.82	2.24	12.67	25.87	
LOI920°C	36.87	7.27	10.33	53.64	23.17	2.12	17.24	28.15	
SiO₂	18.48	12.36	2.59	71.70	50.28	1.62	46.42	55.58	58.89
TiO₂	0.08	0.05	0.02	0.29	0.75	0.03	0.59	0.86	0.77
Al₂O₃	2.06	1.18	0.38	6.97	12.95	0.36	11.60	14.20	16.70
Fe₂O₃	0.64	0.28	0.21	1.77	5.20	0.87	4.31	12.28	6.86
K₂O	0.25	0.13	0.06	0.62	7.70	0.22	6.74	8.52	3.60
MgO	1.34	2.61	0.22	15.50	1.17	0.08	0.99	2.07	2.65
CaO	34.19	7.96	10.79	49.26	0.26	0.29	0.10	4.45	2.20
P₂O₅	2.76	2.06	0.31	16.58	0.15	0.09	0.07	1.00	0.16
S	2.66	0.96	0.54	6.22	2.63	0.49	1.94	6.12	0.24
Mo	143	93	12	614	152	60	51	616	1
V	430	301	78	2040	1090	178	508	1520	130
U			<10	50	115	39	22	257	4
Zn	852	424	100	2784	356	2007	29	30699	95
Ni	175	82	28	865	162	38	65	320	68
Cu	60	22	<10	131	122	18	87	309	45
Pb	4.2*				112	45	58	484	
Cr	294	97	83	626	72	7	55	90	90
Zr	38	11	<10	85	137	9	95	180	160
Rb	9.5*				124	7	83	138	140
Sr	685	158	229	1855	70	5	47	99	300
Ba	94	231	<50	2409	391	24	297	458	580
Cd	90	50	<20	261			<20	252	0.13
Se	40	162	<10	3196			<10	13	0.6
As			<10	64	60	21	42	236	10

Mineral matter characteristics in oil shale/black shale reflected through variation of major elements

Mineral matter composition in BS is clearly SiO₂-dominated, being on average 50.28 wt% (SD 1.26), while in OS CaO is prevailing with average 34.19 wt% (SD 7.96). However, SiO₂ is also dominant in certain intervals in the AUG deposit (Fig. 7; Table 1). In marine sediments as OS and BS dominated by CaO or SiO₂, CaO mainly resides in calcite and SiO₂ in quartz/opal when the dominating source is biogenic. However, SiO₂ in large quantities may also originate from terrigenous sources as quartz, and SiO₂ together with Al₂O₃ as feldspars, clay minerals, or ferromagnesian minerals. Strong inverse correlation of CaO and SiO₂ and wide range in concentrations suggest biogenic/marine source for these elements in OS, while BS samples plot next to AS suggesting dominating detrital origin and very low content or absence of carbonates (Fig. 7). The Al₂O₃ content varies between 11.6 and 14.2 wt% and its average concentration 12.95 wt% is significantly higher in BS compared to 2.06 wt% in OS. SiO₂ and Al₂O₃ ratio and covariation usually indicates abundance of clay minerals and quartz in sediments. BS samples plot tightly together close to the AS, while OS samples diffuse towards higher SiO₂ values, suggesting excess silica content, relative to aluminum and low clay content (Fig. 7).

TiO₂ average content is ten times lower in OS (0.08 wt%) compared to BS (0.75 wt%). Titanium shows a strong correlation with aluminum in both sediments, indicating possible detrital origin (Fig. 7). In sedimentary rocks Ti/Al is commonly interpreted to reflect changes in terrigenous input and provenance areas (e.g. Taylor & McLennan, 1985; Rudnick & Gao, 2010; Boyle, 1983). On Fig. 7, OS samples plot on a single line approaching the AS, and BS samples slightly left towards lower aluminum or higher titanium content. CaO, SiO₂, Al₂O₃ and TiO₂ content and distribution patterns suggest very low input of terrigenous minerals in OS contrasting BS.

While in OS the high content of major elements in all samples is limited with SiO₂ and CaO, in BS also K₂O and Fe₂O₃ are present in high (>5 wt%) quantities. K₂O content is significantly higher in BS (7.70 wt%) compared to OS (0.25 wt%) (Fig. 7), while good correlation with aluminum is evident for both rocks. The elevated K₂O content is a typical feature of the BS of the Türisalu Fm., where silt-size particles dominate over clay fraction and which contains abundant authigenic K-feldspar (Loog et al., 2001). The high potassium content is likely connected with the abundance of authigenic K-feldspar in those beds, thus differentiating Estonian GAs from the Scandinavian alum shale, where clay minerals occur as the dominant K-rich phases (Snäll, 1988).

Fe₂O₃ average content (0.64 wt%) is significantly lower in OS compared to BS (5.20 wt%). In OS samples good correlation between Fe₂O₃ and Al₂O₃ is evident, while in BS no covariance with aluminum occurs (Fig. 7). The average content of MgO is rather similar in both rocks, however, higher concentrations occur in several layers of dolomitic limestone present in the OS sequence (Fig. 7).

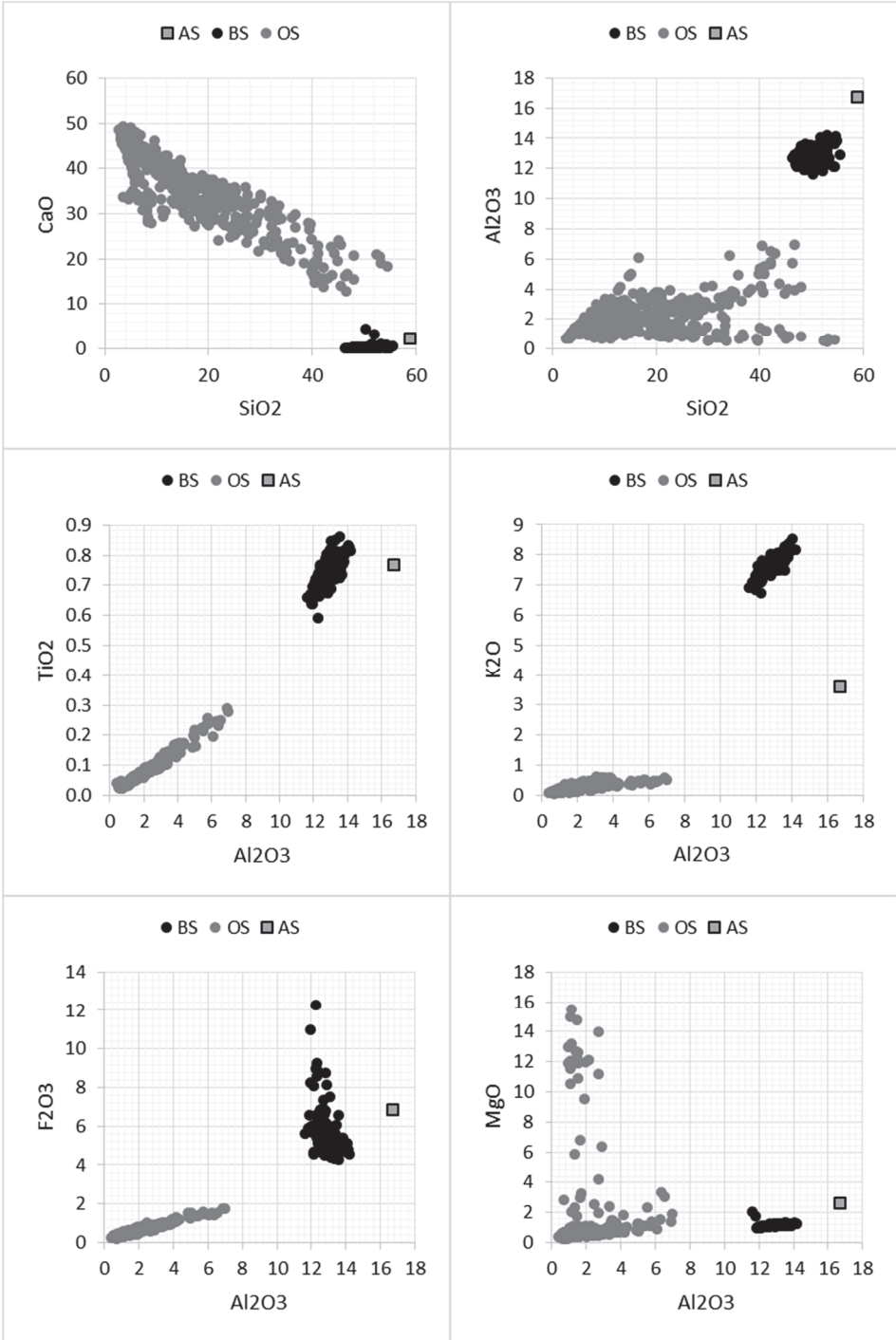


Fig. 7. Cross plots of 410 OS, 373 BS samples and average shale (AS) for reference. **CaO-SiO₂** – in OS samples inverse correlation and wide range of concentrations occur, in BS very low CaO content is contrasting rather monotonous and dominating SiO₂; AS plots

close to BS samples; $\text{Al}_2\text{O}_3\text{-SiO}_2$ – OS samples show excess SiO_2 content relative to mostly <5 wt% Al_2O_3 content; BS samples with rather uniform Al_2O_3 , SiO_2 content plot tightly together on line from origin through AS; $\text{TiO}_2\text{-Al}_2\text{O}_3$ – both OS and BS samples show strong correlation, however in OS concentrations are clearly lower relative to BS close to AS; $\text{K}_2\text{O-Al}_2\text{O}_3$ – good correlation for OS samples is evident, while the content relative to AS is lower, while BS has noticeably higher potassium content; $\text{Fe}_2\text{O}_3\text{-Al}_2\text{O}_3$ – in OS samples good correlation exists, while in BS scattering towards higher Fe_2O_3 content occurs in some samples; $\text{MgO-Al}_2\text{O}_3$ – BS and majority of OS samples plot close to a line from origin through AS, dolomitic limestone samples in OS sequence scatter from this trend;

Summarizing the major elements trends of OS and BS relative to AS shows that: (BS) excluding elevated potassium and in some samples iron, the concentrations are rather monotonous and similar to average shale values plotting on or close to line from AS extrapolated to zero, suggesting dominantly terrigenous origin for mineral matter; (OS) samples have clearly elevated calcium and lower silica content showing strong inverse correlation, relative to the aluminum content, and compared with AS, the biogenic source for mineral matter seems to be dominating. Additionally, strong correlation of titanium, potassium, iron and magnesium (with exception of dolomite samples) with aluminum, but clearly lower concentrations relative to AS suggest very low terrigenous input.

Enriched metals in oil shale/black shale and organic matter

Under oxic seawater conditions many trace elements are transported to the seafloor as oxides, hydroxides or adsorbates on other particulates. These elements may have marine hydrogenous source – scavenged from seawater, or biogenic source. The distribution of Cd, Cu, Cr, Ni, Se, V, and Zn in the water column, relative to PO_4^{3-} , NO_3^- , and Si(OH)_4 , limiting nutrients of phytoplankton, indicate that organic detritus is the major carrier of many minor elements from seawater to the sea floor. These nutrients are extracted from seawater in the photic zone during photosynthesis and returned to the ocean at depth by way of bacterial respiration. The amount of OM (and trace metals) that reaches seafloor is variable and largely dependent of the depth and primary productivity as well as redox conditions – sulfate-reducing (euxinic), denitrification (anoxic) or oxic (Piper & Isaacs, 1995). Distinguishing the detrital (terrigenous), marine hydrogenous and biogenic fractions as carriers of minor elements indicates the possible source of trace metals and fixation/enrichment mechanism in sediment.

Organic-rich OS and BS are characterized by a high content of redox-sensitive metals U, Mo, V and some chalcophile elements Ni, Cu, Zn and also Pb in BS (Table 1). Figs. 8-11 presents redox-sensitive elements, OM and sulfide forming elements content and trends in OS/BS samples.

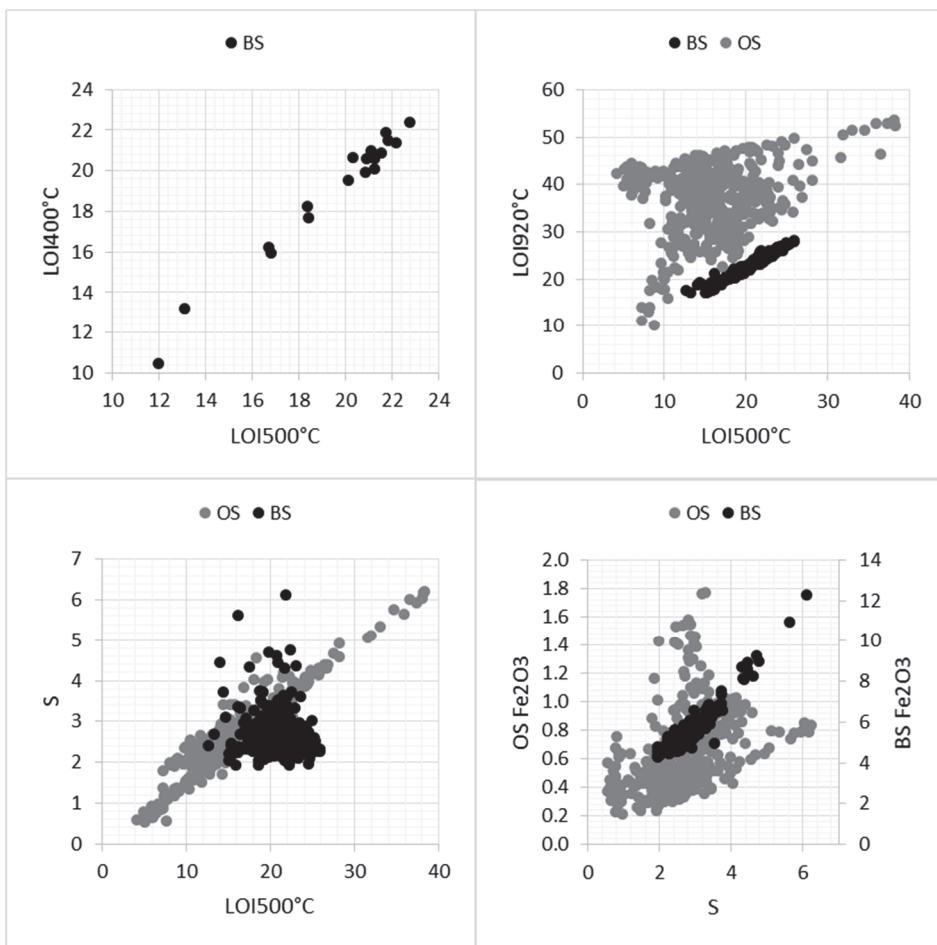


Fig. 8. Cross plots of 410 OS and 373 BS samples. **LOI400°C-LOI500°C** – in 18 black shale samples confirm that mass loss at 500C is mainly reflecting organic matter content; **LOI920°C-LOI500°C** – in OS samples calcite and organic matter content varies in great range having no correlation however, while BS samples display strong correlation between organic matter and pyrite (LOI920°C reflecting mainly mass loss of pyrite decomposition); **S-LOI500°C** – very strong correlation suggest dominantly organic nature for sulfur in OS samples, while in BS no covariation exist; **S-Fe₂O₃** – in OS samples no correlation occur, while BS samples display good correlation;

The LOI500°C variations, which could in most part be interpreted in terms of OM abundance in organic-rich deposits, are, however, dependent on other additional processes such as decomposition of sulfides and carbonates and dehydration of clays. However, the decomposition of sulfides and carbonates should occur at higher temperatures and is reflected by LOI920°C. The compositional data show rather low carbonate content and uniform clay mineral abundance in the BS. In OS the carbonate content varies in large range and lacks the correlation with OM, while in BS LOI920°C, reflecting the decomposition of pyrite, values are

approximately 10% higher and in good correlation with LOI500°C reflecting OM. To rule out the possibility that finely dispersed pyrite decomposition contributed to mass loss at 500°C, LOI400°C was determined for 18 samples. Almost equal LOI400°C values determined in 18 samples suggest that mass loss at 500°C is mainly related to OM content (Fig. 8). OM content reflected by LOI500°C varies considerably in both rock types (Fig. 8).

Sulfur average content (2.6 wt%) is similar for both deposits. In OS sulfur is dominantly organic (Al-Harashseh et al., 2005), while in BS strong correlation with Fe₂O₃ suggests large quantity of pyrite and that sulfur is residing mainly in pyrite (in Pyrite (FeS₂) Fe₂O₃/S = 2.5) (Fig. 8). The scattering trend and excess S propose lower abundance of sulfide minerals in OS, likely hosting minor fraction of trace metals. Indeed, abundant pyrite beds are present in black shale detectable by naked eye (Fig. 1), while SEM observations of OS confirmed presence of finely dispersed pyrite and (Cd-rich) sphalerite. Also Fe₂O₃ strong correlation with Al₂O₃ (Fig. 7) might indicate its detrital source in OS.

However, while BS has high Fe content clearly related to pyrite, OS and BS both have very low Mn contents, elements which in marine sediments through Mn-Fe cycling play important role regarding trace metals. As manganese is mobile in reducing sedimentary environments, its main role is the transfer of trace elements from the water column to the sediments. It is known that Mn oxides trap trace metals from diffusing to overlying waters (Tribovillard et al., 2006). Moreover, iron displays a pattern of redox cycling similar to that of Mn. However, there is a significant difference - Fe is systematically involved in iron-sulfide precipitation within reducing sediments and waters. The main trace elements which are influenced by Mn-Fe cycling are 2⁺ - cation elements as Ni, Cu, Zn, Co, Pb, and also V, Mo, and Cr. The trace metals can be adsorbed onto Fe-Mn-oxyhydroxides, by this way they are transported from the water column to the sediment. The elements can later be released upon reductive dissolution of the oxyhydroxides at or below the water-sediment interface. By this mechanism, a selection of trace metals is then available for new reactions, for instance, the capture in solid solutions by authigenic sulfides, such as pyrite in reducing environments (Tribovillard et al., 2006).

Trace metals are also delivered into marine sediment in association with OM. In oxic marine waters several trace metals behave as micronutrients, such as Ni, Cu, Zn, and Cd. These metals may be present as trace-metal soluble cations or as complexes with humic/fulvic acids. However, Cd is usually present only as Cd²⁺ in the water column or sediment, and is associated with OM. Upon OM decay, the trace metals may be released from organometallic complexes to pore waters and under reducing conditions may be incorporated as a solid solution phase into pyrite, or form independent sulfide phase (Tribovillard et al., 2006), for example Cd-rich sphalerite in OS and abundant pyrite in BS.

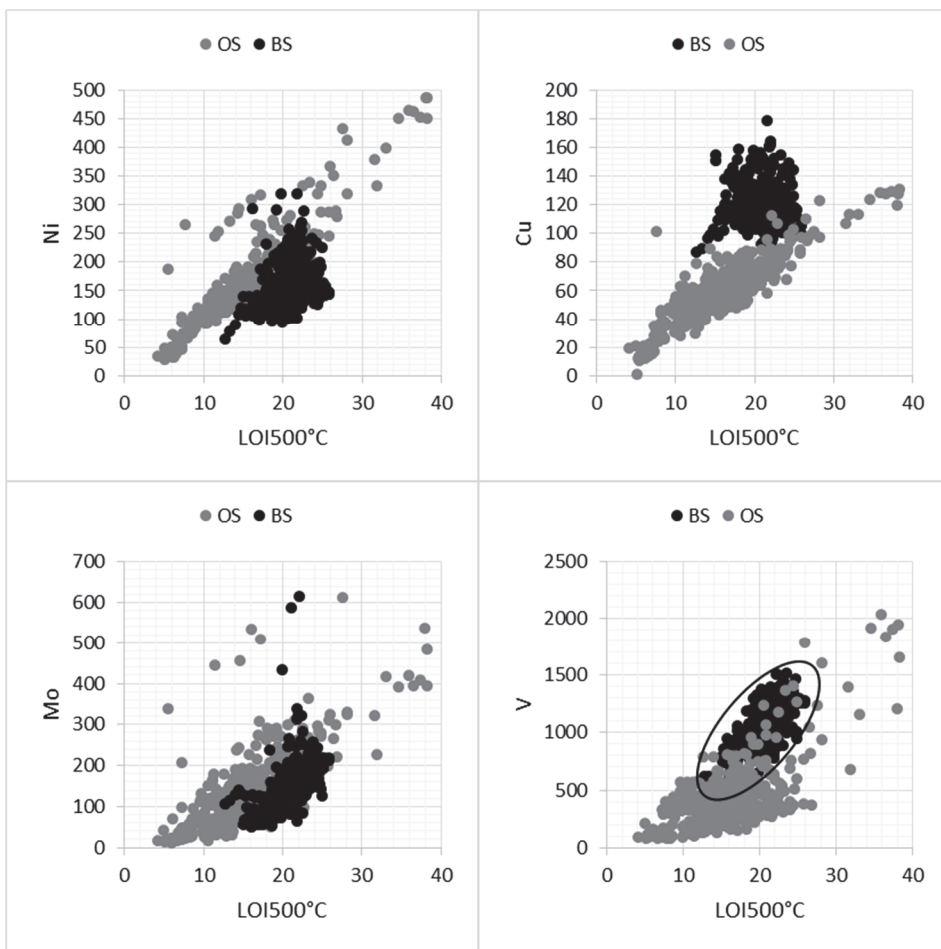


Fig. 9. Cross plots of 410 OS and 373 BS samples. **Ni-LOI500°C** – in OS the content varies in great range and good correlation is evident, while in BS no clear trend is observed; however, the samples do overlap; **Cu-LOI500°C** – in OS the concentrations vary in great range and show strong correlation, while BS samples plot tightly together with no clear trend; **Mo-LOI500°C** – OS and BS samples overlap, also in both rock samples loose covariation is evident; **V-LOI500°C** – OS and BS samples are partly overlapping showing also loose correlation with OM, in OS the concentrations are lower and more scattered.

Comparing OS and BS, Ni and Cu display similar trends and vary in wide range, in OS the average content of Cu is lower (OS=60; BS=122), while Ni content is alike (OS=175; BS=162). Mo content similarly varies in great range (12-616 ppm), while V content is approximately two times higher in BS (OS= 430; BS=1090). In OS Zn and Cd also show high concentrations and strong covariation with OM, while in BS Cd content in most samples is <20ppm (except samples with very high Zn content) and in majority of samples Zn content remains below 50 ppm. In addition to Cd, also Se is significantly enriched in OS compared with

BS. The low crustal abundance of Cd and Se and their high concentration in OS suggest marine source, controlled by bioaccumulation and low dilution by terrigenous material. The accumulation of minor elements within the marine fraction of sediment may reflect the level of primary productivity in the photic zone, assuming a stoichiometry for the biogenic fraction of minor elements preserved in the sediment. The suite of minor elements that show an enrichment in excess of that due solely to the rain rate of organic matter onto the sea floor defines the redox conditions of bottom water under which the sediment accumulates (Piper & Isaacs, 1995). According to Tribovillard et al. (2006) interpretation of the trace element–TOC covariation patterns, the Ni and Cu enrichment under anoxic conditions indicates deposition mainly in the form of organometallic complexes. Elements like U and V have a limited diffusion into the sediments and precipitation as authigenic phases at redox boundary. Under euxinic conditions insoluble metal sulfides and oxyhydroxides will precipitate in quantity directly from the water column or at the sediment–water interface resulting in strong U and V enrichments. It is known that U and V usually reside mainly in authigenic mineral phases rather than organic phases (Algeo and Maynard, 2004). This is in contrast to elements such as Ni, Cu and Mo that are concentrated in organic phases.

Internal recycling is particularly relevant for nutrient-type trace metals (Zn, Cd, Cu, Ni), which alike the macronutrients nitrate, phosphate, and silicic acid undergo multiple cycles of assimilation into biogenic particulate material within surface waters and release or remineralization at depth. In this manner an element can undergo many internal cycles within the ocean prior to ultimate burial in sediments (Bruland & Lohan, 2003); as a result, the final assemblage as well as content of these elements in sediment may vary.

On Cu-Ni graph (Fig. 11) OS samples display fairly good correlation and plot on a line overlapping the line extrapolated from origin through average concentration of seawater (SW). BS samples scatter randomly, relative to OS towards higher Cu content positioning them on AS trend line. Comparing Cu-Ni and Cu-Zn as well as Ni-Zn (not plotted) trends suggest excess Zn relative to copper and nickel, while Zn-Cd ratio corresponds to SW (Fig. 11). All these trace metals display good correlation with LOI500°C. For OS these trends refer to dominantly biogenic source and high primary productivity. Due to varying amount of OM deposition, and high bottom water oxygen consumption, anoxic to euxinic conditions developed at seafloor and lower water column. Different and also varying conditions for BS and OS formations during the accumulation is most evident from the trends of trace-metals and abundance of pyrite. In case of BS nearly all Fe is pyritized (Fig. 8 Fe₂O₃-S plot) probably indicating more effective recycling and the presence of free H₂S⁻, while in OS low input of reactive Fe is indicated by good correlation between Fe₂O₃ and Al₂O₃ (unreactive is incorporated into silicates – clay minerals, Fig. 7). In OS dominantly pyrite together with abundant cadmium-rich sphalerite is present (based on SEM observation sphalerite even

seems to be dominating). Highly scattered occurrence in OS mud groundmass is interpreted to indicate syngenetic origin for pyrite and sphalerite. The lower Cu and Ni content relative to Zn (and Cd) suggest that remineralization and fixation to the final sediment occurred under anoxic (no free H_2S) conditions and was more effective for the latter trace metals and Cu and Ni may have been partly released/escaped.

Strong covariation of nutrient-type trace metals as well as good correlation with OM and proportions corresponding to average SW (Fig. 11), suggest marine source and deposition in the form of organometallic complexes under anoxic conditions for OS, while more complex and varying settings apply for BS.

Some trace metals (U, Cr, Zn, Pb) display very different characteristics in OS and BS (Fig. 10), which may be related to dissimilar source for these metals or accumulation environment, also later diagenetic processes may have modified the content of some metals.

Besides hydrogenous, the sources of trace metals may be non-hydrogenous – e.g. detrital or hydrothermal. Trace metals dominantly controlled by the detrital flux display good correlation with Ti and Al which are commonly overwhelmingly of detrital origin and are usually immobile during diagenesis. This is often the case for Cr and rarely for U, Mo and V (Tribovillard et al., 2006). In OS Cr content (average 294 ppm) varies in great range and shows strong positive correlation with OM (Fig. 10) suggesting non-detrital origin, while in BS the average content 72 ppm is similar to AS and shows small fluctuations similar to Al_2O_3 , indicating detrital provenance. Also Cr and Zr are considered to be immobile elements and reflect detrital fraction in sedimentary rocks (e.g. Vine & Tourtelot, 1970). On Cr vs Zr plot (Fig. 11) OS and BS follow two separate trends. BS samples plot tightly together on AS trend line, suggesting traditional interpretation as indicators of terrigenous input for these elements. OS samples form parallel trend with SW slightly offset towards Zr. The small discrepancy may be due to minor detrital fraction contribution in OS, however considering the six-fold difference in Cr content and parallel trend with SW strongly suggest marine source at least for chromium.

Hydrothermal fluxes also represent potentially important source of trace metals, including Ba, Sr, Pb, Zn and Mn, commonly hosted in minerals such as barite, celestite, galena, blende and rhodocrosite (Tribovillard et al., 2006). In OS Pb content is below 20 ppm in all samples (average 4.2 ppm based on limited data – 40 samples), while in BS (average 122 ppm) up to 484 ppm concentrations are detected. While in OS highly variable Zn content is strongly correlated with OM

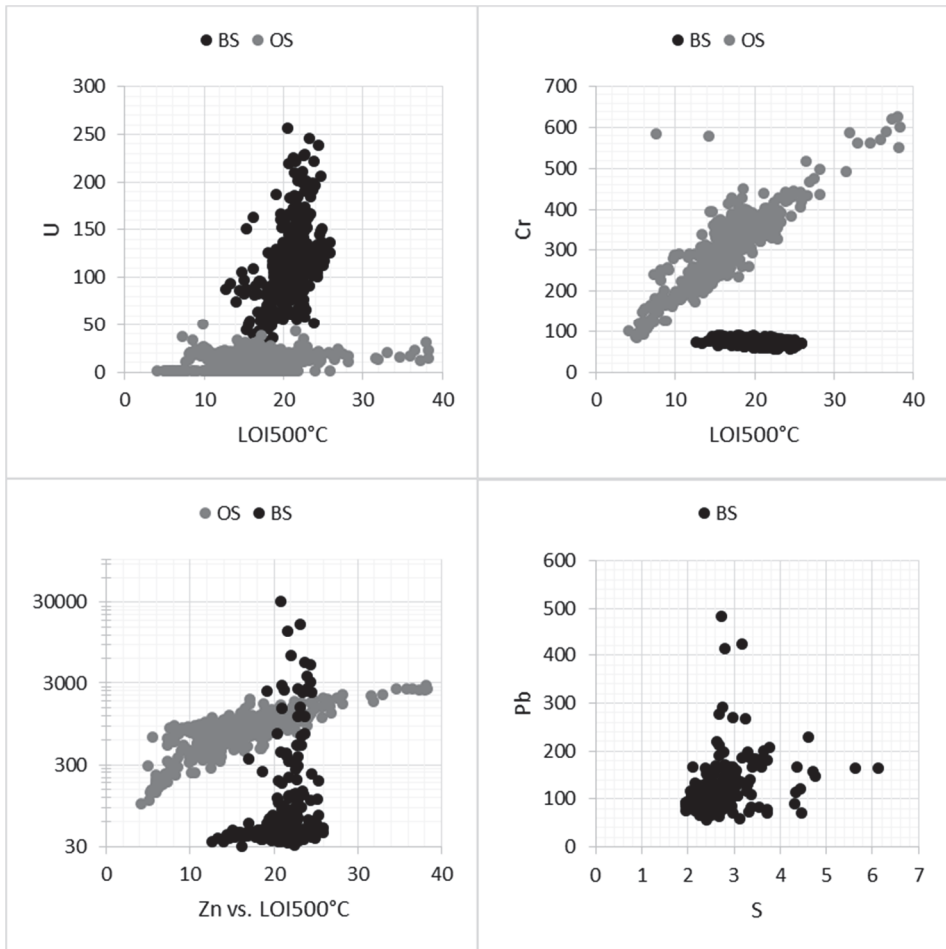


Fig. 10. Cross plots of 410 OS and 373 BS samples. **U-LOI500°C** – in OS U content shows no correlation with OM and is unevenly distributed in cross-section, the content varies from <10ppm to 50ppm, while in BS several times higher concentrations range between 22-257 ppm and show loose correlation with OM; **Cr-LOI500°C** – in OS strong covariance is evident, while in BS chromium content is evenly around 70 ppm; **Zn-LOI500°C** (log. scale!) – in OS samples good correlation between Zn and OM is evident, while in BS besides monotonous approximately 40 ppm zinc content in majority of samples extremely high up to 30000 ppm concentrations occur; **Pb-S** – in BS samples lead shows rather scattered trend and content varies in wide range (in OS lead content is <20ppm, not plotted).

in BS beside monotonous approximately 40 ppm content, extremely enriched intervals occur with concentrations up to 30699 ppm (Fig. 10). Recent studies in Caledonian Nappe complexes, (e.g Grimmer & Greiling, 2012), suggest the existence of subduction zone related volcanic arc complexes within the Iapetus Ocean near the western border of the Baltica palaeocontinent in the Late Cambrian and Tremadoc. The associated volcanic activity in these areas could supply

overlying waters with extra trace metal budgets and modify regional marine trace metal signals, enhancing the trace metal content of marine water.

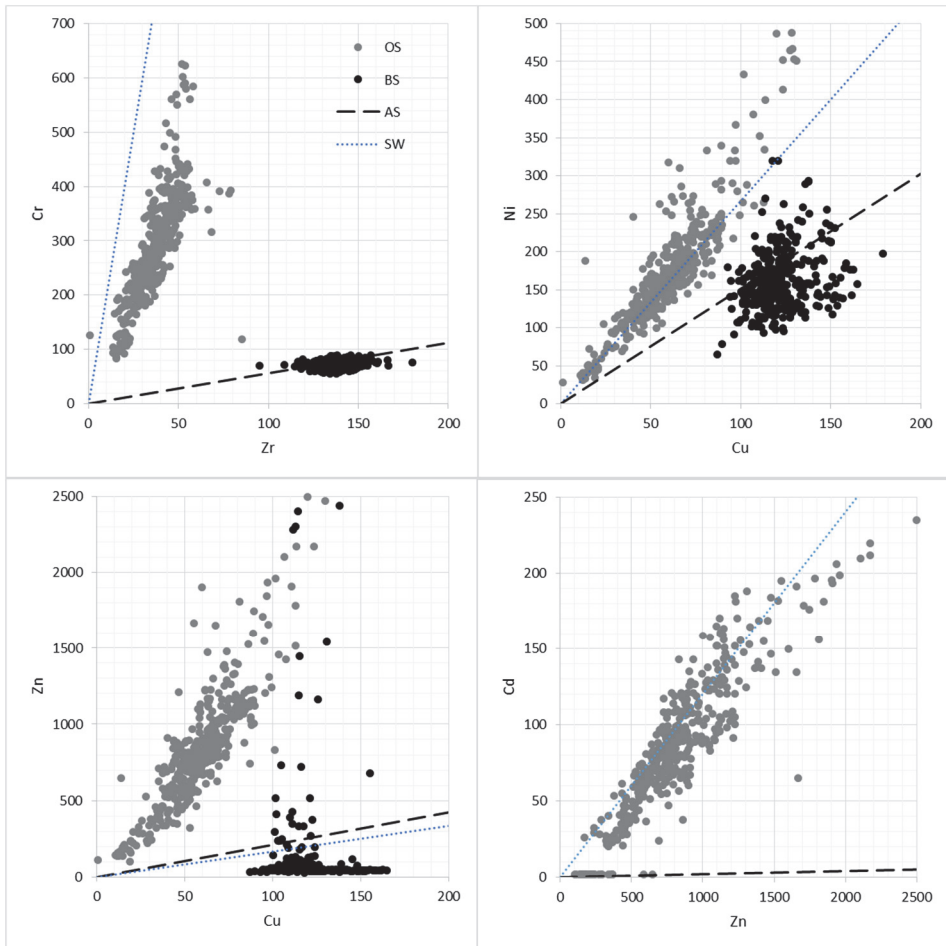


Fig. 11. Cross plots of 410 OS and 373 BS samples. **Cr-Zr** – BS samples plot on AS line suggesting detrital provenance, while in OS high Cr and low Zr contents suggest very low terrigenous input for these samples and marine source for Cr; **Ni-Cu** – while BS samples show rather scattering trend mostly plotting on AS line, OS samples display good correlation and plot on SW line; **Zn-Cu** – in BS besides extremely enriched samples, Zn content is lower than both AS and SW relative to Cu, while opposite trend applies for OS samples. However, **Cd-Zn** ratio corresponds well to average SW; AS-average shale; SW-sea water (elements concentrations from (Bruland & Lohan, 2003))

Trace element accumulations in sedimentary environments can be hosted by various phases, such as in metal sulfides, in solid solution in pyrite, insoluble oxides and oxyhydroxides, phosphate, sulfate, organometallic complexes and trace metals can also be adsorbed onto organic or mineral surfaces. Consequently, the behavior of certain trace element is highly variable during diagenesis, mainly

depending on the pH and Eh conditions of the burial environment. In the absence of post-depositional replenishment of oxidizing agents, sulfides are stable and the elements engaged with Fe - sulfides typically do not move during later diagenesis. This immobility is generally the case with Mo, V, Cd, Ni, Co, Cu, Zn and Pb. In contrast, in case of post-depositional oxygen replenishment, the influence is great when the penetration depth into the sediments is large and, in cases, may lead to uranium remobilization in regions where authigenic uranium has accumulated (Tribovillard et al., 2006). In case of oil shale where significant enrichments in V, Cr, Cd and Mo are observed, with U being enriched only at a lesser degree, it may indicate that small quantities of dissolved oxygen may have caused the solubility and loss of U from the sediments that had previously experienced reducing conditions. In OS samples the absence of U (<10ppm) is noticeable relative to other redox-sensitive elements.

Trace elements variation reflecting changes in accumulation environment of black shale

BS cross section from Pakri Peninsula represented by 21 samples, with sampling interval of 20 cm, characterized by selected 13 elements, was studied applying statistical analysis methods. Variables as chemical elements were selected to reflect different processes. Zr, Cr, Al/Ti represent detrital input and changes in sedimentary sequence. Organic matter (OM reflected by LOI500°C) together with nutrient-type elements Zn, Ni, Cu, (also Cr) mirror the changes in primary productivity and is important transporter of trace metals from water column to the sediment either via biochemical processes or scavenging (adsorption) onto sinking particulate particles. Redox-sensitive elements V, Mo, U, Cr, as well as Fe and S might reflect changes in bottom water conditions during accumulation. Pb and possibly Zn might indicate hydrothermal input.

Linking geochemical patterns of a sediment succession with a number of known and unknown geological factors requires a complex multi-step multivariate analysis. As a first step, the statistical analysis is applied in order to define the variations and highlight changes in selected major and trace element compositions that may be linked to certain fluctuations in the course of accumulation of the primary BS sediment and other contemporary and later processes. One of the well-known statistical tools is principal components analysis (PCA), which is the general name for a technique that uses sophisticated underlying mathematical principles to transform a number of possibly correlated variables into a smaller number of variables called principal components. In general terms, PCA uses a vector space transform to reduce the dimensionality of large datasets (like geochemical analyses). Using mathematical projection, the original dataset which may have involved many variables, can often be interpreted in just a few variables (the principal components). The examination of the reduced dimension dataset will allow the user to spot trends, patterns and outliers in the data, far more easily

than would have been possible without performing the PCA. Two methods of multivariate analysis were used for data assessment: (i) PCA and (ii) hierarchical clustering of PCA groups.

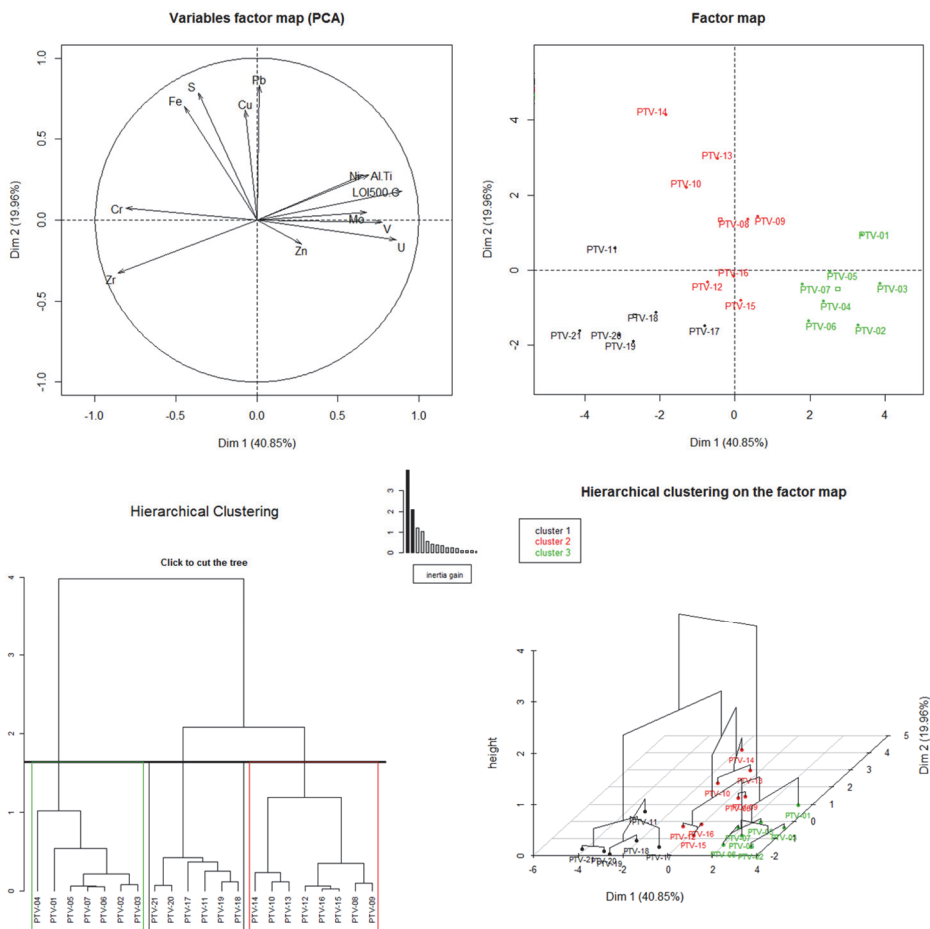


Fig. 12. Principal components and hierarchical cluster analysis graphical representation. On variables factor map on a plane induced by PC1 and PC2 variables (chemical elements) relationship is demonstrated. On factor map relationship between samples and PCs is presented. Hierarchical clustering tree demonstrates relationship between different samples and clusters. Hierarchical clustering on the factor map depicts relationship between different samples/clusters and PCs.

First two principal components (PC) account for 40.85% and 19.96% of data variability, respectively. In order to visualize interrelationships between PC and chemical elements, the planes constructed by pairs of principal components PC1 to PC2 are presented (Fig. 12 Variables factor map). The distance between the chemical component projected onto a plane and the correlation circle with radius one demonstrates the correlation of the variable and principal components. The

distance from an axis shows the quality of how well the element is projected onto a corresponding plane. The proximity of variables on the plane means also strong association between individual elements. Plot of samples on the plane PC1–PC2 demonstrates association between samples and principal components (Fig. 12 Factor map). Hierarchical clustering tree demonstrates the interrelation of individual samples and clusters as well as association with PCs on hierarchical clustering on the factor map (Fig. 12).

PC1 – The first PC describes 41% of the data variance. It is strongly correlated with many variables and describes samples of cluster 3 (C3) (Fig. 12), with the highest correlation with OM (LOI500°C), and also Al/Ti, U, V, Mo, and Ni. Strong correlation between these elements suggests that they vary together. Strong negative correlation is with Zr and Cr indicating covariation of these elements, differentiating samples of cluster 1 (C1). This component can be interpreted as a measure of trace-element carrying OM versus detrital (Zr, Cr) silicate mineral matter content.

PC2 – The second PC accounts for 20% of data variability and is strongly correlated with Pb, Cu, S and Fe, all elements incorporated into sulfides (Fig. 12). This component describes samples of cluster 2 (C2) (Fig. 12).

PC3 – The third PC accounts for 11% of data variability and is most strongly correlated with Zn opposed by Cu (not plotted).

Based on the biostratigraphic framework and a recent time scale calibration (Cooper & Sadler, 2012), the primary muds of the Türisalu Fm. should have been deposited within a maximum time frame of ~ 5 My (Hints et al., 2014). Whereas the long-term accumulation rates apparently stayed very low during sedimentation of the primary organic-rich muds of the Türisalu Fm., the sedimentary fabrics in the BS suggest dynamic deposition, frequent reworking of sea bottom and changes in deposition rates (Hints et al., 2014). The studies of modern organic-rich muds have revealed usefulness of high-resolution sampling within a limited geographic range (e.g. Algeo & Lyons, 2006), allowing more reliable distinction between possible driving factors behind the synsedimentary trace metal sequestration and more consistent environmental interpretations.

As recorded from the chemical composition of the BS sequence, during the deposition of approximately 4.2 m of BS in a considerable time period, stable and variable conditions of accumulation alternated. The borders of these variations become visible by the help of hierarchical clustering of samples using PCA. The hierarchical clustering separates three distinct groups of samples. The principal components describing different clusters and the relation of elements to clusters on planes constructed by components is visualized on Fig. 12.

Hierarchical clustering resulted with three groups of samples, whereas clusters 1 and 2 (C1 and C2) are more closely related than cluster 3 (C3) (Fig. 12). The position of individual samples from different clusters in the BS cross-section reveals three-stage internal structure of the sequence: its lower part includes 7 samples belonging to C3, the middle part by 8 samples belonging to C2 and one

sample of C1, capped with 5 samples of C1 (Fig. 13). Such distribution indicates that at least two major changes occurred during the deposition of BS affecting the final chemical composition.

On the following BS cross-sections (Figs. 13-15) the background of graph is color-coded representing the BS sequence and the positions of individual samples according to a cluster they belong to. For interpretation of processes behind clusters different elements used in PCA are plotted.

Starting from the base, samples belonging to C3 form 1.4 m thick unit with similar characteristics of the sedimentary fabric almost uniformly characterized as finely laminated, while for the middle (C2) and upper (C1) part, BS fabrics of massive to moderately laminated, normal grading as well as microbial lamination are described (Fig. 13).

The lower third of the formation is most organic-rich gradually decreasing towards the upper part: average LOI_{500°C} in C3 is 22.3, in C2 and C1 is 19.6 and 16.4 wt%, respectively (Fig. 13). The decrease in OM means that mineral matter is gradually rising towards the upper part; however, Ti/Al ratio commonly interpreted to reflect changes in terrigenous input and provenance areas (e.g. Boyle, 1983), shows invariable (except a small peak at PTV-17) pattern in cross-section suggesting common source during the course of BS accumulation. However, increased clastic material input is supported by Zr (reflects zircon) and SiO₂/Al₂O₃ (higher ratio reflects quartz) increasing trend towards the upper part (Fig. 14). Small decrease in Al/Ti in C1 may indicate higher input of heavy minerals, also Fe₂O₃ content is enriched relative to S (Fig. 15) in these samples compared to the rest of the sequence, indicating increase in Fe residing in silicates. Variations in characteristic sedimentary fabrics, changing proportions of OM and mineral matter, and mineral matter invariable source suggest that major changes at C3-C2 and C2-C1 boundary are most likely affected by primary productivity, preservation of OM and changing redox conditions. However, the increase in MM towards the upper part of the deposit may also indicate higher sedimentation rates diluting the organic component.

Redox-sensitive elements (V, U, Mo) display rather different patterns when comparing the clusters. In C3 in the lower part of formation, V displays rather unvarying pattern, whereas U and Mo content varies in great range, while starting from PTV-8 (from base at 1.4 m), in samples of C1 and C2 all these elements display good correlation (Fig. 14). Similarly to OM, the highest content of these elements occurs in C3.

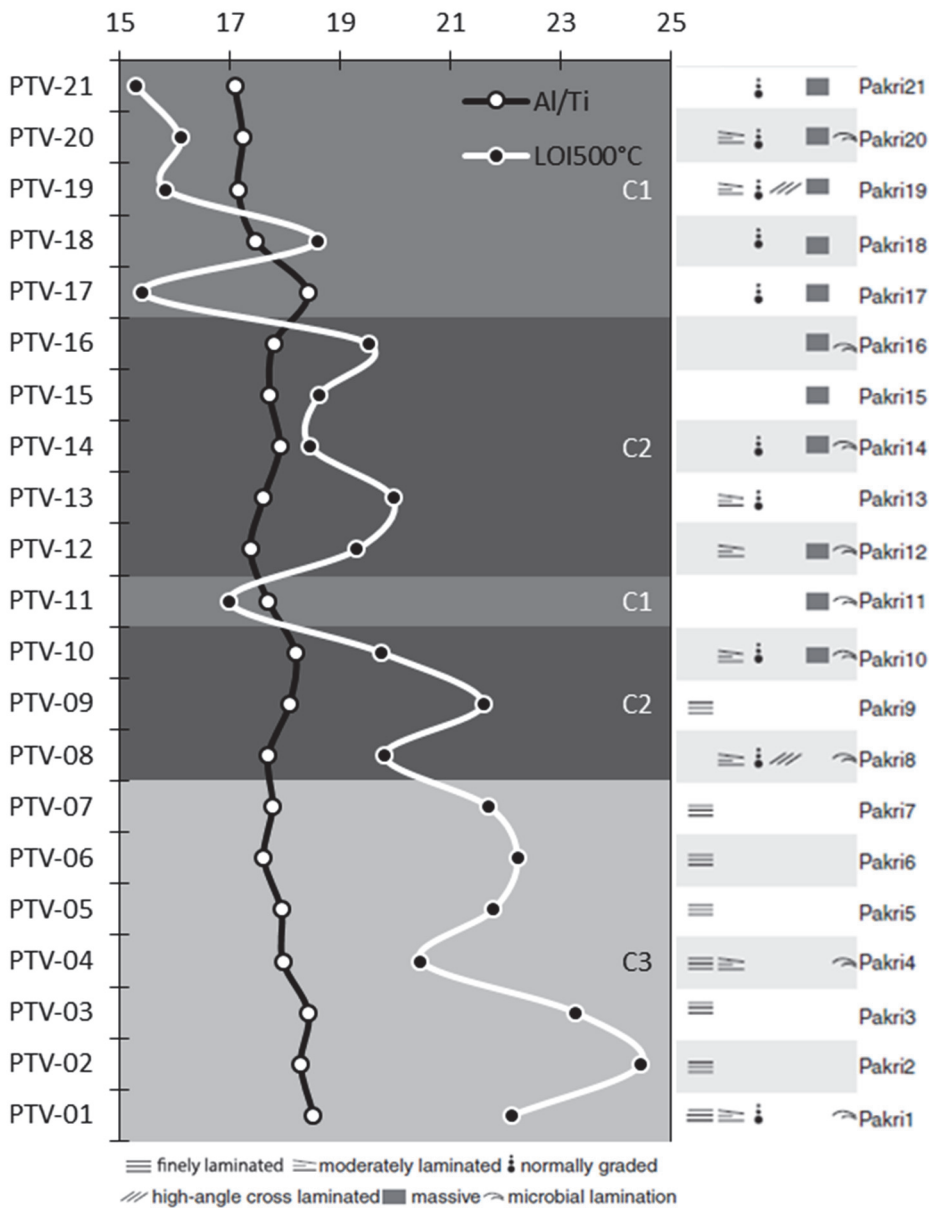


Fig. 13. Black shale sequence from Pakri Peninsula. The distribution of samples belonging to different clusters are plotted using different colors on background. On the right sedimentary fabrics observed in the Pakri cross-section are plotted (figure from Hints et al., 2014).

The high content of OM and redox-sensitive elements indicate overall bottom water and sediment oxygen depletion. High variation in concentrations of redox-sensitive elements as well as sharp peaks of pyrite (Fe, S,) and other sulfide forming elements (Pb), suggest periods with more reducing or even sulfidic

bottom waters (Fig. 15). Samples of C2 are characterized by higher content of Pb, Cu, Fe and S. Changing conditions are also suggested by deviations in redox-sensitive elements (V, U, Mo) covariation patterns. Also, for example Cr displays similar pattern with Zr in C3, while in C2 (starting from sample PTV-10) and C1 rather different behavior, excess Cr relative to Zr is evident (Fig. 14).

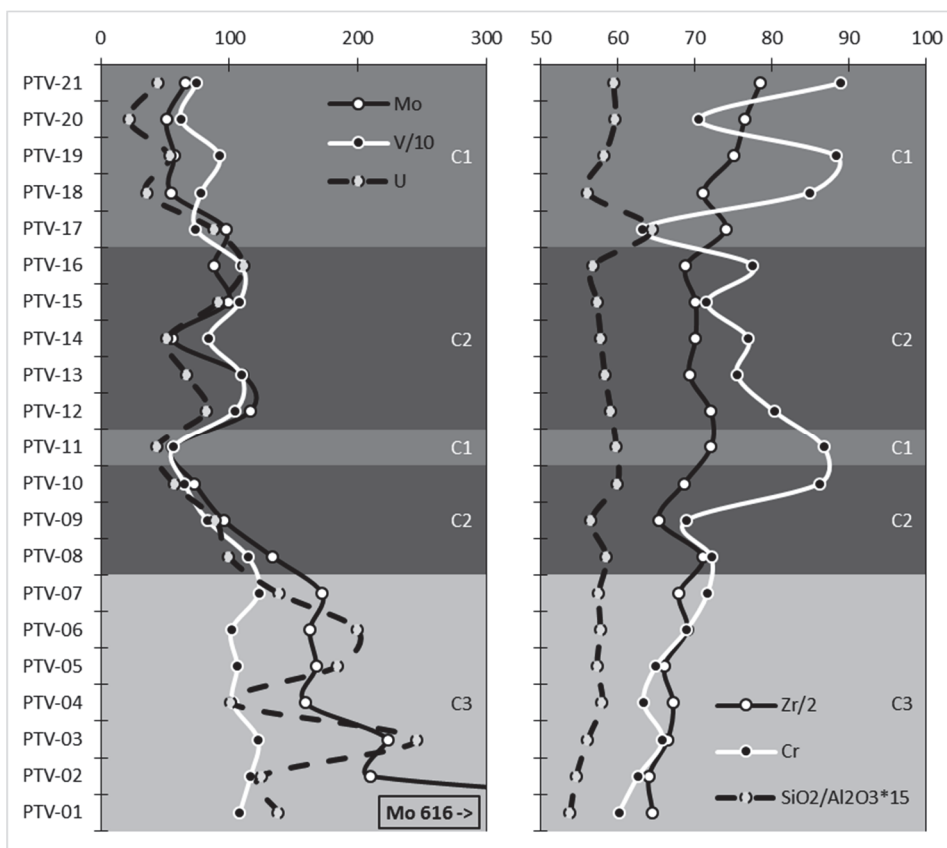


Fig. 14. Distribution of redox-sensitive elements Mo, V, and U in black shale sequence, the covariation pattern changes at C3-C2 border. Zr, Cr, $\text{SiO}_2/\text{Al}_2\text{O}_3$ display rather homogeneous pattern, however slightly increasing towards the upper part. At the base of C2 Cr deviates, showing higher content relative to Zr and $\text{SiO}_2/\text{Al}_2\text{O}_3$ and opposite trend in PTV-17. Note that for some elements the content is divided or multiplied with different coefficient for better visualization.

Nutrient-type trace metals Cu, Ni and Zn (Fig. 15) present rather different patterns. Zn, otherwise monotonously low, shows the highest concentrations together with Ni in organic-rich C3 samples. Zn and Ni peaks in the middle of C3 could indicate higher primary productivity that led to Zn depletion in surface waters, which in turn suggests semi-restricted rather shallow marine conditions preventing renewal of Zn reservoir. However, diagenetic enrichment cannot be excluded either as elevated concentration is limited with very narrow interval. Cu

content is rather monotonous, around 100 ppm, through the cross-section, being however slightly higher in C2 samples. Relative to Cu, Ni is following more closely the distribution of S and Fe.

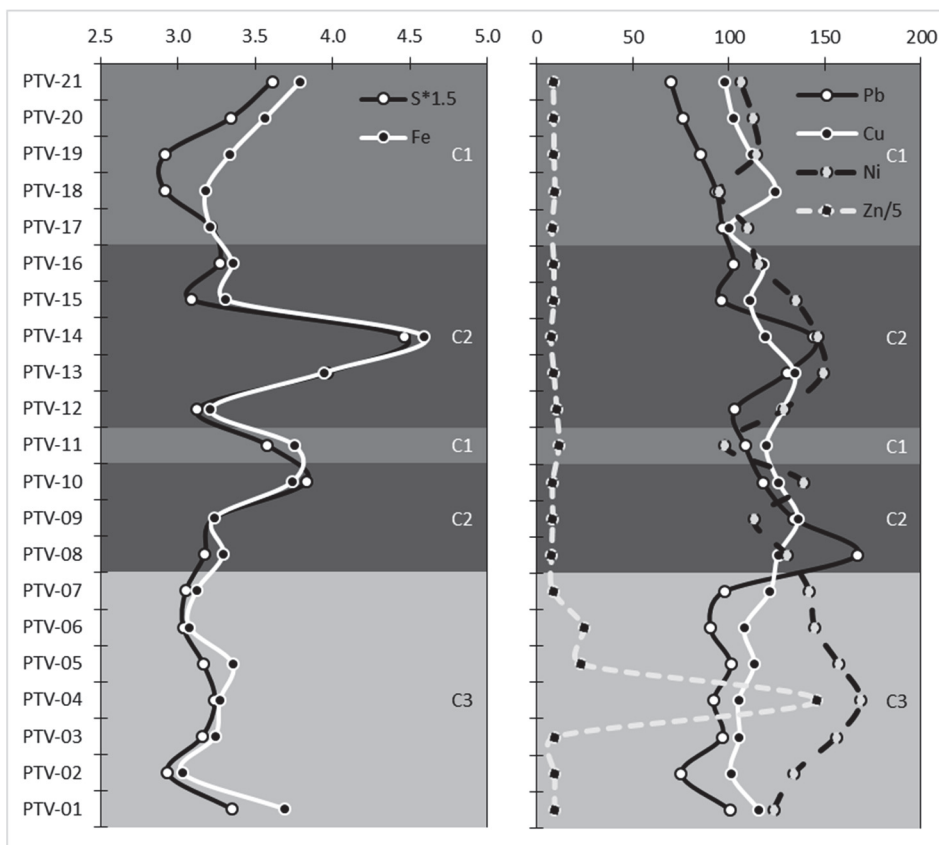


Fig. 15. Sulfide-forming and/or nutrient-type trace elements S, Fe, Pb, Cu, Ni, Zn distribution in black shale sequence. S and Fe display good covariation suggesting most of Fe residing in pyrite. In upper part of sequence (C2-C1 border) Fe deviates showing excess content relative to S. High Pb content marks the C3-C2 border; note also the Ni covariation with Fe and S in cluster C2. Zn enrichment is limited with narrow interval in the middle of the organic-rich cluster C3. (S, Fe in wt%; Pb, Cu, Ni, Zn in ppm).

The general positive covariance of U, V and Mo with OM in the studied samples from the Pakri outcrop confirms that the sequestration process of metals from seawater was in general controlled by metal reduction triggered by oxygen depleted seawater or anoxia below the sediment water interface and closely coupled with OM degradation, whereas organic-metal complexation could have acted as a major pathway for metal enrichment. Highest content of OM and nutrient-type trace metals Ni, especially Zn suggest higher productivity at the beginning of organic-rich mud accumulation. Intense decomposition of OM may have caused sulfidic bottom water conditions marked by C3-C2 border and

characterized by (i) changed behavior of redox-sensitive elements U, V, Mo and also currently not fully understandable Cr deviation relative to Zr; (ii) intense sulfide formation marked by Pb peak (galena), Ni covariation with Fe and S (pyrite); (iii) and also decreasing OM content; The top unit of the formation is characterized by decreasing OM content and increasing terrigenous input marked by Zr, SiO₂ peak at C2-C1 border (sample PTV17) as well as Fe deviation from S, suggesting increase of Fe content residing in siliciclastic minerals compared to otherwise dominantly pyritic Fe in the rest of deposit.

CONCLUSIONS

The major element composition of BS is rather monotonous, siliceous, high-K, Mn-poor and with variable Fe and S contents, while in OS sequence six different types can be distinguished, mostly defined by one dominating mineral or mixture of minerals (dolomite, calcite, apatite, quartz and tridymite-cristobalite, clay minerals) abundance. However, statistical analysis results on the OS dataset showed that OM carrying trace-metals is independent of major element composition, e.g. intervals of calcareous or siliceous as well as mixture of these OS intervals had similar amount of OM and trace-metals. Mineral matter only affected (diluted) the amount of OM present and had no effect on the assemblage of trace-metals or any trace-metal individually.

Several trace elements considered comparatively in this study are present in high concentrations, of which Zn and Cr display higher average values in OS, while Cu and V are more concentrated in BS. The average content of Ni and Mo is rather similar. BS is considerably enriched in U compared to OS, the content of U being <10 ppm in several intervals of the OS sequence. The biggest difference occurs in Pb content, that is absent in OS, but substantial in BS; the opposite behavior applies for Cd and Se.

Comparing the geochemical data of high resolution sample sets from ca 70-m thick OS (sampling interval 0.5-2.0 m) and 4.5-m thick BS (sampling interval 2 cm) deposits shows that:

1. Major element chemical composition shows strong terrigenous input for BS compared to OS dominantly biogenic mineral matter.
2. The enriched trace metal assemblage of OS may be explained by single hydrogenous source — redox-sensitive elements and micronutrients; in BS a mixed source for the elements considered is proposed. For Cr detrital provenance is suggested, while Pb and Zn may be influenced by additional hydrothermal source.
3. The dominance of common marine redox-sensitive elements (Mo, V, Cr) and micronutrients (Zn, Cu, Ni, Cd) among enriched metals in OS as well as their strong covariance with OM content favors syngenetic enrichment

and trapping mainly via OM tied species as the major process of trace metal sequestration;

Statistical analysis of BS samples from the Pakri outcrop highlighted two major changes in the deposit controlled by two main factors:

1. Organic matter and mineral matter inverse correlation, towards the upper part mineral matter content gradually increasing over organic matter.
2. Changes in bottom water redox conditions from anoxic to more reducing, possibly euxinic, during the deposition of the middle part of the deposit.

ACKNOWLEDGEMENTS

I thank my supervisor Prof. Alvar Soesoo for support and advice. I am grateful to Saima Peetermann for correcting the English. The study was financially supported by the Estonian Ministry of Education and Research with target research project no. SF0140016s09 (to A. Soesoo) and supported by grant no. 8963 (to A. Soesoo) from the Estonian Science Foundation. I thank companies Eesti Energia AS and JOSE for providing the geological material and permission to use the geochemical data in this work.

REFERENCES

- Abed, A. M., & Amireh, B. S. (1983). Petrography and geochemistry of some Jordanian oil shales from North Jordan. *Petroleum Geology*, 5(3), 261-274.
- Abed, A. M., Arouri, K., Amireh, B. S., & Al-Hawari, Z. (2009). Characterization and genesis of some Jordanian oil shales. *Dirasat: Pure Sciences*, 36, 7-17.
- Abed, M. A. (2013). The eastern Mediterranean phosphorite giants: An interplay between tectonics and upwelling. *GeoArabia*, 18(2), 67-94.
- Al-Harabsheh, A., Al-Otoom, A. Y., & Shawabkeh, R. A. (2005). Sulfur distribution in the oil fractions obtained by thermal cracking of Jordanian El-Lajjun oil Shale. *Energy*, 30, 2784-2795.
- Alali, J. (2006). Jordan Oil Shale, Availability, Distribution, and Investment Opportunity. *International Conference on Oil Shale: Recent Trends In Oil Shale*. Amman.
- Algeo, T. J., & Lyons, T. W. (2006). Mo-total organic carbon covariation in modern anoxic marine environments: implications for analysis of paleoredox and paleohydrographic conditions. *Paleoceanography*, 21, PA1016.
- Algeo, T. J., & Maynard, J. B. (2004). Trace element behavior and redox facies in core shales of Upper Pennsylvanian Kansas-type cyclothems. *Chemical Geology*, 206, 289-318.
- Algeo, T. J., & Tribovillard, N. (2009). Environmental analysis of paleoceanographic systems based on molybdenum - uranium covariation. *Chemical Geology*, 268, 211-225.
- Alnawafleh, H. M., & Fraige, F. Y. (2015). Analysis of Selected Oil Shale Samples from El-Lajjun, Central Jordan. *Geomaterials*, 5, 77-84.
- Alqudah, M., Ali Hussein, M., Van den Boorn, S., Giraldo, V., Kolonic, S., Podlaha, O. G., & Mutterlose, J. (2014b). Eocene oil shales from Jordan - paleoenvironmental implications from reworked microfossils. *Marine and Petroleum Geology*, 52, 93-106.
- Alqudah, M., Ali Hussein, M., Van den Boorn, S., Podlaha, O. G., & Mutterlose, J. (2014a). Calcareous nanofossils biostratigraphy of oil shales from Jordan. *GeoArabia*, 19(1), 117-140.
- Alqudah, M., Ali Hussein, M., Van den Boorn, S., Podlaha, O. G., & Mutterlose, J. (2015). Biostratigraphy and depositional setting of Maastrichtian - Eocene oil shales from Jordan. *Marine and Petroleum Geology*, 60, 87-104.
- Andersson, A., Dahlman, B., Gee, D. G., & Snäll, S. (1985). The Scandinavian Alum Shales. *Sveriges Geologiska Undersökning*, 56, 1-50.
- Amer, M. W., Marshall, M., Fei, Y., Jacson, R. W., Gorbaty, M. L., Cassidy, P. J., & Chaffee, A. L. (2013). Comparison of the yields and structure of

- fuels derived from freshwater algae (torbanite) and marine algae (El-Lajjun oil shale). *Fuel*, *105*, 83-89.
- Bai, Y., Liu, Z., Sun, P., Liu, R., Hu, X., Zhao, H., & Xu, Y. (2015). Rare earth and major element geochemistry of Eocene fine-grained sediments in oil shale- and coal-bearing layers of the Meihe Basin, Northeast China. *Journal of Asian Earth Sciences*, *97*, 89-101.
- Berry, W. N., Wilde, P., Quinby-Hunt, M. S., & Orth, C. J. (1986). Trace element signatures in Dictyonema shales and their geochemical and stratigraphic significance. *Norsk Geol. Tidsskr.*, *66*, 45-51.
- Boyle, E. A. (1983). Chemical accumulation variations under the Peru Current during the past 130,000 years. *Journal of Geophysical Research*, *88*, 7667-7680.
- Bruland, K. W., & Lohan, M. C. (2003). Controls of Trace Metals in Seawater. In H. Elderfield, H. D. Holland, & K. K. Turekian (Eds.), *Treatise on Geochemistry*, (Vol. 6, pp. 23-47). Elsevier.
- Brumsack, H. J. (2006). The trace metal content of recent organic carbon-rich sediments: implications for Cretaceous black shale formation. *Palaeogeogr. Palaeocl.*, *232*(2-4), 344-361.
- Buchardt, B., Nielsen, A. T., & Schovsbo, N. H. (1997). Alun skiferen i Skandinavien. *Geologisk Tidsskrift*, *3*, 1-30.
- Calvert, S. E., & Pedersen, T. F. (1993). Geochemistry of recent oxic and anoxic marine sediments - implications for the geological record. *Marine Geology*, *113*, 67-88.
- Chester, R. (2000). *Marine Geochemistry*. London: Blackwell.
- Cooper, R. A., & Sadler, P. M. (2012). The Ordovician Period. In F. M. Gradstein, J. G. Ogg, M. D. Schmitz, & G. M. Ogg (Eds.), *The Geological Time Scale* (pp. 489-523). Amsterdam: Elsevier.
- Coveney, R. M., & Glascock, M. D. (1989). A review of the origins of metal-rich Pennsylvanian black shales, central U.S.A., with an inferred role for basinal brines. *Appl. Geochem.*, *4*(4), 347-367.
- Coveney, R. M., Leventhal, J. S., Glascock, M. D., & Hatch, J. R. (1987). Origins of metals and organic matter in the Mecca Quarry Shale Member and stratigraphically equivalent beds across the Midwest. *Economic Geology*, *82*, 915-933.
- DeWolfe, J. C., Horne, E. J., & Morgan, C. A. (2010). Geology and Geochemistry of the Al Lajjun Oil Shale Deposit, Central Jordan. *AAPG Conference and Exhibition*. Calgary, Alberta, Canada, September 12–15.
- Dill, H. G., Bechtel, A., Berner, Z., Botz, R., Kus, J., Heunish, C., & Abu Hamad, A. M. (2012). The evaporite–coal transition: Chemical, mineralogical and organic composition of the Late Triassic Abu Ruweis Formation, NW Jordan—Reference type of the “Arabian Keuper”. *Chemical Geology*, *298-299*, 20-40.
- Dyni, J. R. (2006). Geology and Resources of Some World Oil-Shale Deposits. *U.S. Geological Survey Scientific Investigations Report 2005–5294*, 42.

- Dyni, J. R. (2003). Geology and resources of some world oil-shale deposits. *Oil Shale*, 20(3), 193-252
- Fu, X., Wang, J., Zeng, Y., Tan, F., Wenbing, C., & Feng, X. (2015a). The geochemistry of platinum group elements in marine oil shale — A case study from the Bilong Co oil shale, northern Tibet, China. *Chemie der Erde*, 75, 55-63.
- Fu, X., Jian, W., Feng, X., Chen, W., Wang, D., Song, C., & Zeng, S. (2015b). Mineralogy and geochemical anomalies of Lower Cretaceous marine oil shale from Changshe Mountain West, northern Tibet, China. *Journal of Geochemical Exploration*, 155, 62-75.
- Fu, X., Wang, J., Tan, F., Feng, X., Wang, D., & Song, C. (2012). Geochemistry of terrestrial oil shale from the Lunpola area, northern Tibet, China. *International Journal of Coal Geology*, 102, 1-11.
- Goren, O. (2015). Distribution and mineralogical residence of trace elements in the Israeli carbonate oil shales. *Fuel*, 143, 118-130.
- Grimmer, J. C., & Greiling, R. O. (2012). Serpentinites and low-K island arc metavolcanic rocks in the Lower Kõli Nappe of the central Scandinavian Caledonides: Late Cambrian – early Ordovician serpentinite mud volcanoes in a forearc basin? *Tectonophysics*, 541-543, 19-30.
- Hade, S., & Soesoo, A. (2014). Estonian graptolite argillites revisited: a future resource? *Oil Shale* 31(1), 4-18.
- Hakimi, M. H., Abdullah, W. H., Alqudah, M., Makeen, Y. M., & Mustapha, K. A. (2016). Organic geochemical and petrographic characteristics of the oil shales in the Lajjun area, Central Jordan: Origin of organic matter input and preservation conditions. *Fuel*, 181, 34-45.
- Hamareh, Y., Alali, J., & Sawaged, S. (2006). *Oil Shale Resources Development in Jordan*. Amman: Natural Resources Authority of Jordan (updated report), pp 98.
- Hatch, J. R., & Leventhal, J. S. (1992). Relationship between inferred redox potential of the depositional environment and geochemistry of the Upper Pennsylvanian (Missourian) Stark Shale Member of the Dennis Limestone, Wabaunsee County, Kansas, U.S.A. *Chemical Geology*, 99(1-3), 65-82.
- Heinsalu, H., & Bednarczyk, W. (1997). Tremadoc of the East European Platform: lithofacies and palaeogeography. *Proceedings of the Academy of Sciences of the Estonian SSR. Geology.*, 46, 59-74.
- Heinsalu, H., & Viira, V. (1997). Pakerort Stage. In: *Geology and Mineral Resources of Estonia*. (Raukas, A., & Teedumäe, A., Eds.) Tallinn: Estonian Academy Publishers. 52-58
- Heinsalu, H., Kaljo, D., Kurvits, T., & Viira, V. (2003). The stratotype of the Orasoja Member (Tremadocian, Northeast Estonia): lithology, mineralogy, and biostratigraphy. *Proceedings of the Estonian Academy of Sciences. Geology*, 52(3), 135-154.

- Hints, R., Hade, S., Soesoo, A., & Voolma, M. (2014). Depositional framework of the East Baltic Tremadocian marginal black shale revisited. *GFF*, 136(3), 464-482.
- Hints, R., Soesoo, A., Voolma, M., Tarros, S., Kallaste, T., & Hade, S. (2014). Centimetre-scale variability of redox-sensitive elements in Tremadocian black shales from the eastern Baltic Palaeobasin. *Estonian Journal of Earth Sciences*, 63(4), 233-239.
- Holland, H. D. (1979). Metals in black shales - A reassessment. *Economic geology*, 74, 1676-1680.
- Hufnagel, H. (1984). *Oil Shale in Jordan*. Geologische Jahrbuch 75.
- Husson, F., Josse, J. & Pages, J. (2010). Principal Component Methods–Hierarchical Clustering–Partitional Clustering: Why Would We Need to Choose for Visualizing Data? *Technical Report–Agrocampus Ouest, Applied Mathematics Department*, 17 pp.
- Husson, F., Le, S. & Pages, J. (2011). Exploratory Multivariate Analysis by Example Using R. 1st ed. Chapman & Hall/CRC, London, 228 pp.
- Hutton, A. C. (1987). Petrographic classification of oil shales. *International Journal of Coal Geology*, 8, 203-231.
- Jiang, S. Y., Yang, J. H., & Ling, H. F. (2007). Extreme enrichment of polymetallic Ni-Mo-PGE-Au in lower Cambrian black shales of south China: an Os isotope and PGE geochemical investigation. *Palaeogeography. Palaeoclimatology. Palaeoecology.*, 254, 217-228.
- Kaljo, D., Borovko, N., Heinsalu, H., Khazanovich, K., Mens, K., Popov, L., Sergejeva, S. & Sobolevskaja, R. (1986). The Cambrian-Ordovician boundary in the Baltic-Ladoga clint area (North Estonia and Leningrad Region, USSR). *Proceedings of the Academy of Sciences of the Estonian SSR. Geology.*, 35(3), 97-108.
- Kallaste, T., & Pukkonen, E. (1992). Pyrite varieties in Estonian Tremadocian argillite (Dictyonema shale). *Proc. Est. Acad. Sci. Geol.*, 2(1), 11-22.
- Kiipli, E. (1997). Geochemistry of Llandovery black shales in the Aizpute-41 core, West Latvia. *Proceedings of the Estonian Academy of Sciences Geology*, 46(3), 127-145.
- Kiipli, T., Batchelor, R. A., Bernal, J. P., Cowing, Ch., Hagel-Brunnström, M., Ingham, M. N., Johnson, D., Kivisilla, J., Knaack, Ch., Kump, P., Lozano, R., Michiels, D., Orlova, K., Pirrus, E., Rousseau, R. M., Ruzicka, J., Sandström, H. & Willis, J. P. (2000). Seven sedimentary rock reference samples from Estonia. *Oil Shale*, 17(3), 215-223.
- Kleesment, A., & Kurvits, T. (1987). Mineralogy of Tremadoc graptolitic argillites of North Estonia. *Oil Shale*, 4(2), 130-138.
- Le, S., Josse, J. & Husson, F. (2008). FactoMineR: An R Package for Multivariate Analysis. *Journal of Statistical Software*, 25(1), 1–18.
- Leventhal, J. S. (1990). Comparative geochemistry of metals and rare earth elements from the Cambrian alum shale and kolm of Sweden. *Sp. Publ. Int.*, 11, 203-215.

- Leventhal, J. S. (1991). Comparison of organic geochemistry and metal enrichment in two black shales: Cambrian Alum Shale of Sweden and Devonian Chattanooga Shale of United States. *Mineral Deposita*, 26, 104-112.
- Leventhal, J. S., & Hosterman, J. W. (1982). Chemical and mineralogical analysis of Devonian black-shale samples from Martin County, Kentucky; Carroll and Washington counties, Ohio; Wise County, Virginia; and Overton County, Tennessee, U.S.A. *Chem. Geol.*, 37(3-4), 239-264.
- Lewis, S. E., Henderson, R. A., Dickens, G. R., Shields, G. A., & Coxhell, S. (2010). The geochemistry of primary and weathered oil shale and coquina across the Julia Creek vanadium deposit (Queensland, Australia). *Mineralium Deposita*, 45(6), 599-620.
- Lippmaa, E., Maremäe, E., & Pihlak, A. T. (2011). Resources, production and processing of Baltoscandian multimetal black shales. *Oil Shale*, 28(1), 68-77.
- Lippmaa, E., Maremäe, E., Pihlak, A. T., & Agurauja, R. (2009). Estonian Graptolitic Argillites - Ancient Ores or Future Fuels? *Oil Shale*, 26(4), 530-539.
- Liu, R., Liu, Z., Sun, P., Xu, Y., Liu, D., Yang, X., & Zhang, C. (2015). Geochemistry of the Eocene Jijuntun Formation oil shale in the Fushun Basin, northeast China: Implications for source-area weathering, provenance and tectonic setting. *Chemie der Erde*, 75, 105-116.
- Loog, A. (1982). On the geochemistry of postsedimentary mineral formation in the Tremadoc graptolitic argillites of North Estonia. *Acta et Commentationes Universitatis Tartuensis*, 527, 44-49.
- Loog, A., & Petersell, V. (1994). The distribution of microelements in Tremadoc Graptolitic Argillite of Estonia. *Acta et Commentationes Universitatis Tartuensis*, 972, 57-75.
- Loog, A., & Petersell, V. (1995). Authigenic siliceous minerals in the Tremadoc graptolitic argillite of Estonia. *Proceedings of the Estonian Academy of Sciences*, 44(1), 26-32.
- Loog, A., Kurvits, T., Aruväli, J., & Petersell, V. (2001). Grain size analysis and mineralogy of the Tremadocian Dictyonema shale in Estonia. *Oil Shale*, 18(4), 281-297.
- Magharbeh, M., Fayyad, M., & Batarseh, M. (2012). Preparation of Natural Standard Reference Material (SRM) for El-lajjun Oil Shale/Jordan. *Jordan Journal of Earth and Environmental Sciences*, 4(2), 15-22.
- Morford, J., & Emerson, S. (1999). The geochemistry of redox sensitive trace metals in sediments. *Geochimica et Cosmochimica Acta*, 63, 1735-1750.
- Nijenhuis, I. A., Bosch, H. J., Sinninghe Damste, J. S., Brumsack, H. J., & De Lange, G. J. (1999). Organic matter and trace element rich sapropels and black shales: a geochemical comparison. *Earth Planet. Sc. Lett.*, 169(3-4), 277-290.

- Peacor, D. R., Coveney, R. M., & Zhao, G. (2000). Authigenic illite and organic matter: the principal hosts of vanadium in the Mecca Quarry shale at Velpen, Indiana. *Clay Miner.*, 48(3), 311-316.
- Petersell, V. (1997). Dictyonema argillite. In A. Raukas, & A. Teedumäe (Eds.), *Geology and Mineral Resources of Estonia* (pp. 327-331). Tallinn, Estonia: Estonian Academy Publishers.
- Petersell, V., Mineyev, D., & Loog, A. (1981). Mineralogy and geochemistry of obolus sandstones and dictyonema shale of North Estonia. *Acta et Commentationes Universitatis Tartuensis*, 561, 30-49.
- Petersell, V., Zhukov, F., Loog, A., & Fomin, Y. (1987). Origin of Tremadoc kerogeneous aleurolites and argillites of North Estonia. *Oil Shale*, 4(1), 8-13.
- Piper, D. Z., & Isaacs, C. M. (1995). Geochemistry of Minor Elements in the Monterey Formation, California: Seawater Chemistry of Deposition. *U. S. Geological Survey Professional Paper*, 1566, 1-44.
- Powell, H. J., & Moh'd, K. B. (2011). Evolution of Cretaceous to Eocene alluvial and carbonate platform sequences in central and south Jordan. *GeoArabia*, 16(4), 29-82.
- Pukkonen, E. (1989). Major and minor elements in Estonian Graptolite Argillite. *Oil Shale*, 6(1), 11-18.
- Pukkonen, E., & Rammo, M. (1992). Distribution of Molybdenum and Uranium in the Tremadoc Graptolite Argillite (Dictyonema Shale) of North-Western Estonia. *Bulletin of the Geological Survey of Estonia*, 2(1), 3-15.
- Puura, V., Soesoo, A., Hade, S., Voolma, M., & Aosaar, H. (2016). Chemical composition of the mineral matter of the Attarat Um Ghudran oil shale, Central Jordan. *Oil Shale*, 33(1), 18-30.
- Quinby-Hunt, M. S., Wilde, P., Orth, C. J., & Berry, W. B. (1989). Elemental geochemistry of black shales - statistical comparison of low-calcic shales with other shales. In R. I. Grauch, & J. S. Leventhal (Eds.), *Metalliferous Black Shales and Related Ore Deposits* (pp. 8-15). US Geological Survey Circular.
- Rudnick, R. L., & Gao, S. (2010). Composition of continental crust. In H. D. Holland, & K. K. Turekian (Eds.), *Readings from the Treatise of Geochemistry* (pp. 131-198). Amsterdam: Elsevier.
- Schovsbo, N. H. (2002). Uranium enrichment shorewards in black shales: A case study from Scandinavian Alum Shale. *GFF*, 124(2), 107-115.
- Sharland, R. P., Archer, R., Casey, M. D., Davies, B. R., Hall, H. S., Heward, P. A., Horbury, D. A., & Simmons, D. M. (2001). Arabian Plate Sequence Stratigraphy. *GeoArabia Special Publication 2*, Gulf PetroLink, Bahrain, 371.
- Snäll, S. (1988). Mineralogy and maturity of the alum shales of south-central Jämtland, Sweden. *Sveriges Geologiska Undersökning (SGU)*, 818(Serie C), 1-46.

- Soesoo, A., & Hade, S. (2012). Metalliferous organic-rich shales of Baltoscandia – a future resource or environmental/ecological problem? *Archiv Euro Eco*, 2(1), 11-14
- Soesoo, A., & Hade, S. (2014). Black shale of Estonia: moving towards a Fennoscandian - Baltoscandian database. *Transactions of Karelian Research Centre, Russian Academy of Science*, 1, 103-114
- Steiner, M., Wallis, E., Erdtmann, B. D., Zhao, Y. L., & Yang, R. D. (2001). Submarine hydrothermal exhalative ore layers in black shales from South China and associated fossils – insights into a Lower Cambrian facies and bio-evolution. *Palaeogeogr. Palaeocl.*, 169(3-4), 165-191.
- Sundblad, K., & Gee, D. G. (1984). Occurrence of a uraniferous-vanadiniferous graphitic phyllite in the Kõli Nappes of the Stekenjokk area, central Swedish Caledonides. *Geol. Foren. Stock. For.*, 106(3), 269-274.
- Zeng, S., Wang, J., Fu, X., Chen, W., Feng, X., Wang, D., Song, C. & Wang, Z. (2015). Geochemical characteristics, redox conditions, and organic matter accumulation of marine oil shale from the Changliang Mountain area, northern Tibet, China. *Marine and Petroleum Geology*, 64, 203-221.
- Taylor, S. R., & McLennan, S. M. (1985). The Continental Crust: Its Composition and Evolution. *Oxford: Blackwell Scientific Publications*.
- Tribovillard, N., Algeo, T. J., Lyons, T. W., & Riboulleau, A. (2006). Application of trace metals as paleoredox and paleoproductivity proxies. *Chemical Geology*, 232, 12-32.
- Utsal, K., Kivimägi, E., & Utsal, V. (1982). About method of investigating Estonian graptolithic argillite and its mineralogy. *Acta et Commentationes Universitatis Tartuensis*, 527, 116-136.
- Vaughan, D. J., Sweeney, M., Diedel, G. R., & Haranczyk, C. (1989). The Kupferschiefer: An overview with an appraisal of the different types of mineralization. *Economic Geology*, 84, 1003-1027.
- Wedepohl, K. H. (1971). Environmental influences on the chemical composition of shales and clays. in *Physics and Chemistry of the Earth*, 8, edited by L. H. Ahrens et al., pp. 305–333, Elsevier, New York.
- Wedepohl, K. H. (1991). The composition of the upper Earth's crust and the natural cycles of selected metals: Metals in natural raw materials: Natural resources, in *Metals and Their Compounds in the Environment*, edited by E. Merian, pp. 3–17, John Wiley, Hoboken, N. J.
- Wilde, P., Quinby-Hunt, M. S., Berry, W. N., & Orth, C. J. (1989). Palaeo-oceanography and biogeography in the Tremadoc (Ordovician) Iapetus Ocean and the origin of the chemostratigraphy of Dictyonema flabelliforme black shales. *Geological Magazine*, 126, 19-27.
- Vine, J. D., & Tourtelot, E. B. (1970). Geochemistry of Black Shale Deposits - A Summary Report. *Economic Geology*, 65, 253-272.
- Voolma, M., Soesoo, A., Hade, S., Hints, R., & Kallaste, T. (2013). Geochemical heterogeneity of the Estonian graptolite argillite. *Oil Shale*, 30(3), 377-401.

- Voolma, M., Soesoo, A., Puura, V., Hade, S. & Aosaar, H. (2016). Assessing geochemical variability of oil shale in the Attarat Um Ghudran deposit, Jordan. *Estonian Journal of Earth Sciences*, 65(2), 61-74.
- Xu, L., Lehmann, B., & Mao, J. (2013). Seawater contribution to polymetallic Ni–Mo–PGE–Au mineralization in Early Cambrian black shales of South China: Evidence from Mo isotope, PGE, trace element, and REE geochemistry. *Ore Geology Reviews*, 52, 66-84.
- Yu, B., Dong, H., Widom, E., Chen, J., & Lin, C. (2009). Geochemistry of basal Cambrian black shales and cherts from the Northern Tarim Basin, Northwest China: Implications for depositional setting and tectonic history. *J. Asian Earth Sci.*, 34(3), 418-436.

ABSTRACT

Geochemistry of organic-rich metalliferous oil shale/black shale of Jordan and Estonia

The organic-rich metalliferous fine-grained oil shale and black shale deposits with highly variable thickness as well as lateral extent, are found all over the world. These formations are commonly enriched with a number of heavy metals, commonly associated with the abundance of sulfide minerals and organic matter. In this study, the chemical composition of 410 oil shale samples of Jordan and 373 black shale samples of Estonia, is analyzed comparatively to determine similarities as well as main differences in elements concentrations and trace-metal assemblages allowing to interpret possible source and genesis of these formations. Mineralogical composition of the OS sequence (average thickness of 70 m) is highly variable: the content of calcite varies from 8 to 88%, quartz up to 51% (cristobalite+tridymite up to 47%), and dolomite from below the detection limit (approximately <2%) up to 80%, apatite up to 40% and clay minerals up to 31%, opposed to the 4.5 m thick BS cross-sections, siliceous and rather homogeneous mineral assemblage, dominated by quartz, K-feldspars, clay minerals and with abundant pyrite. The statistical analysis results on oil shale dataset show that organic matter carrying trace metals is independent of major element composition, e.g. intervals of dominantly calcareous or siliceous oil shales, as well as mixture of these oil shale intervals had similar/proportional amount of organic matter and trace metals. Mineral matter only affected (diluted) the amount of organic matter present and had no effect on the assemblage of trace metals or any trace metal individually. Both rock formations contain organic matter and are enriched with several trace metals. The enriched metals assemblage is partly overlapping (e.g. Mo, V, Ni, Cu), as well as contrasting, e.g. high Pb in black shale or Cd in oil shale. The comparative study of oil shale and black shale major elements content suggest strong terrigenous input for black shale compared to oil shales dominantly biogenic mineral matter. The dominance of common marine redox-sensitive elements (Mo, V, \pm U) and abundant pyrite incorporating/hosting also chalcophile elements Cu, Ni suggest formation under low oxygen (anoxic/euxinic) environment. However, U uneven distribution, absence (<10ppm) in some OS intervals and low concentration relative to other trace metals suggest that small quantities of dissolved oxygen may have caused the solubilization and loss of U. While in oil shale the correlation trends of organic matter with enriched element assemblage Zn, Cd, Ni, Cu, Mo, V, and Cr indicate single hydrogenous source, for black shale incoherent distribution of Zn (and Pb) may indicate influence of hydrothermal source. Additionally, chromium content near the average shale concentration and different trends highlight the detrital fraction influence in black shales. The dominance of common marine redox-sensitive elements (Mo, V, Cr) and micronutrients, (Zn, Cu, Ni, Cd) among the enriched metals in oil shale favours syngenetic enrichment as the major process of trace metal sequestration,

while observed complex distribution of trace elements in black shale was likely controlled by the interplay of different primary metal supply-sequestration factors/processes, such as synsedimentary redox-driven sequestration of redox-sensitive elements, the clastic and possible hydrothermal input. Statistical analysis of geochemical data of the 4.2-m thick BS formation enabled distinguishing three groups of samples. The results and distribution of samples in the black shale sequence suggest at least two major changes in accumulation conditions: (i) at approximately 1.4 m from the base redox-sensitive elements (U, V, Mo) and sulfide-forming elements (Pb, Ni, Cu) altered covariance patterns suggest increased reducing conditions, possibly from anoxic to euxinic, and (ii) although organic- and mineral matter inverse correlation is evident through the entire formation, at 3.2 m towards the upper part mineral matter content more sharply increases over organic matter. Slight change in mineral matter composition is indicated by different covariance patterns of Zr, Cr, Al/Ti, Si/Al, Fe₂O₃ and S.

KOKKUVÕTE

Orgaanika- ja metalliderikaste põlevkivide/mustade kiltade geokeemiast Jordaania ja Eestis

Orgaanika- ja metalliderikkaid põlevkivi- ning musta kilda lasundeid, mis varieeruvad oma mõõtmetelt nii paksuses kui ka pindalaliselt suurtes piirides, leidub kogu maailmas. Sellistele lasunditele on tihtipeale iseloomulik kõrge raskmetallide sisaldus, mida valdavalt seostatakse sulfiidsete mineraalide ja orgaanika (kõrge) sisaldusega. Doktoritöös on analüüsitud võrdlevalt 410 Jordaania põlevkivi ja 373 Eesti musta kilda (graptoliitargilliit) proovi keemilist koostist, et tuvastada geokeemilisi sarnasusi, aga ka kontrastseid erinevusi peamiselt raskmetallide kontsentratsioonide ja koosluste varieeruvuses eesmärgiga interpreteerida nende võimalikku päritolu ja geneesi.

Võrdluses kasutatud Jordaania keskmiselt 70 m paksust põlevkivilasundit iseloomustab väga muutlik mineraloogiline koostis: kaltsiidi sisaldus varieerub 8% ja 88% vahel, kvartsi on kuni 51% (ja SiO₂ erimit kristoballiit-tridüümi kuni 47%), dolomiiti 80%, apatiiti 40% ja savimineraale kuni 31%. Seevastu 4,5 m paksune musta kilda kiht on homogeensem ja valdavalt silikaatne, peamisteks mineraalideks on kvarts, K-päevakivi ja savimineraalid, lisaks esineb palju püriiti. Jordaania põlevkivi keemilise koostise andmestiku statistilise analüüsi tulemused näitasid, et mineraalosa koostise suurest varieeruvusest ei sõltunud orgaanikaga seostatud raskmetallide kooslus, küll aga mõjutas selle osakaal metallide üldist sisaldust erineva mineraalse koostisega intervallides. Seega, kahe lasundi põhielementide suur erinevus ei sega antud töö fookuses olevate jälgelementide koosluse ja esinemise seaduspärasuste võrdlust.

Põhielementide (Ca, Si, Al, Ti, Mg, Fe, S) sisalduse ja trendide võrdlus näitab, et põlevkivi mineraalosa on valdavalt biogeenset päritolu, samas kui musta kilda põhielementide kooslus viitab terrigeensele päritolule. Põlevkivi ja musta kilda raskmetallide kooslus on osaliselt kattuv, näiteks Mo, V, Ni, Cu osas. Seevastu Pb, mis on rikastunud mustas kildas, puudub põlevkivis, samas kui vastupidine trend iseloomustab Cd ja Se. Rikastunud metallide hulgas on valdavad muutuva oksüdatsiooniastmega elemendid (*redox sensitive elements*) (Mo, V, ±U), samuti sulfiididega seotud kalkofiilsed elemendid (Zn, Cd, Cu, Ni). Loetletud elementide ja orgaanilise aine suur sisaldus viitavad settimisele hapnikuvaeses redutseerivas (*anoxic*) keskkonnas. Uraani ebaühtlane jaotus põlevkivi läbilõikes ja madal kontsentratsioon (<10 ppm) võrreldes teiste raskmetallidega mõnedes intervallides võib viidata perioodilisele hapniku juurdepääsule põlevkivi settimiskeskkonda ja U mobiliseerimisele.

Kui põlevkivis rikastunud raskmetallide (Zn, Cd, Ni, Cu, Mo, V, Cr) tugev korrelatsioon omavahel ja ka orgaanilise ainega viitab pärinemisele ühest allikast, milleks on merevesi, siis mustas kildas võib Zn (ja Pb) seostamatu jaotus olla tingitud hüdrotermaalsetest mõjutustest. Samuti Cr madalam ja keskmisele

savikilda koostisele vastav sisaldus ning põlevkivist erinev jaotustrend viitab veel kord terrigeense fraktsiooni allikale mustas kildas.

Redokstundlike elementide (Mo, V, Cr) ja mikrotoitainete (Zn, Cu, Ni, Cd) domineerimine põlevkivi rikastunud metallide koosluses toetab süngeneetilist metallide fikseerimist settesse. Seevastu komplekssemad/mitmekülgsemad metallide jaotustrendid mustas kildas viitavad mitme erineva allika ja settesse fikseerimise protsessi koosmõjule nagu näiteks süngeneetiline redutseerivast keskkonnast tingitud muutuva oksüdatsiooniastmega elementide väljasettimine, terrigeense materjali sissekanne ja võimalik hüdrotermaalne allikas. Settekeskkonna muutustele ja mitme erineva protsessi koosmõjule viitab ka musta kilda 4,2 m paksuse lasundi keemilise andmestiku statistiline analüüs, mille tulemusel eristus kolm gruppi proove. Erinevatesse gruppidesse kuuluvate proovide jaotus läbilõikes viitab vähemalt kahele suuremale muutusele settekeskkonnas: (i) lasundi alumisest otsast umbes 1,4 m kõrgusel redokstundlike elementide (U, V, Mo) kovariatsiooni muutus ja kalkofiilsete elementide (Pb, Cu, Ni) suurenenud sisaldus viitab vaba vesiniksulfiidi (H_2S^-) tekkimisele settekeskkonnas; (ii) umbes 3,2 m kõrgusel mineraalosa osakaal suureneb järsumalt, seejuures Zr, Cr, Al/Ti, Si/Al, Fe_2O_3 ja S jaotuse muutused viitavad ka mineraalosa koostise muutusele.

ELULOOKIRJELDUS

Isikuandmed

Ees- ja perekonnanimi: Margus Voolma

Sünniaeg ja -koht: 13.03.1981 Eestis

Kodakondsus: Eesti

E-posti aadress: margus.voolma@ttu.ee

Hariduskäik

Tartu Ülikool, Geoloogia Instituut, 2000-2007, Geoloogia eriala, MSc

Keelteoskus

Inglise keel kesktase

Teenistuskäik

Alates 2007 Tallinna Tehnikaülikool, TTÜ Geoloogia Instituut; insener

Teadustegevus ja juhendatud lõputööd

Teadustegevuse valdkonnaks on geoloogilised ja geokeemilised uuringud. Graptoliitargilliit, põlevkivi, magnetiitkvartsiid.

2007-2010 osalemine Jordaania Attarati maardla põlevkivi geoloogilise uuringu projektis

2015-2017 osalemine projektis Eesti graptoliitargilliidis leiduvate raskmetallide ja teiste elementide keskkonnamõju mudel ning leostumise dünaamika

CURRICULUM VITAE

Personal data

Name: Margus Voolma
Date and place of birth: 13.03.1981 Estonia
Nationality: Estonian
E-posti address: margus.voolma@ttu.ee

Education

University of Tartu, Institute of Geology, 2000-2007, Geology, MSc

Language competence

English average

Professional employment

Since 2007 Tallinn University of Technology, Institute of Geology at
TUT; engineer

Research activity and thesis supervised

Main scientific interest: geology and geochemistry of graptolite argillite,
oil shale, magnetite quartzites

2007-2010 Participation in geological and geochemical study of the oil
shale of the Attarat Umm Ghudran deposit; Jordan

2015-2017 Participation in project: The environmental model of heavy
metals and other elements containing in Estonian graptolite argillite and
leaching dynamics

PUBLICATIONS

1. Voolma, Margus; Soesoo, Alvar; Hade, Sigrid; Hints, Rutt; Kallaste, Toivo (2013). Geochemical heterogeneity of the Estonian graptolite argillite. *Oil Shale*, 30(3), 377 - 401.

GEOCHEMICAL HETEROGENEITY OF ESTONIAN GRAPTOLITE ARGILLITE

MARGUS VOOLMA*, ALVAR SOESOO, SIGRID HADE,
RUTT HINTS, TOIVO KALLASTE

Institute of Geology, Tallinn University of Technology, Ehitajate tee 5, 19086
Tallinn, Estonia

Abstract. *This paper describes vertical fine-scale geochemical heterogeneity of Estonian graptolite argillite (GA). GA samples from Pakri and Saka outcrop sections were collected at 20 cm intervals for chemical analysis of major and trace elements, including rare earth elements. The study indicates GA enrichment in U, V, Mo and Pb with respect to the average black shales and thus confirms the formerly reported data on GA geochemistry in general. However, the content of enriched elements and other trace metals was recorded to vary greatly across the sequences suggesting that trace metal distribution in GA is notably more heterogeneous than previously assumed. The origin of the observed complex distribution of trace elements was likely controlled by the interplay of different primary metal supply-sequestration factors/processes, such as synsedimentary redox-driven sequestration of redox sensitive elements, the provenance of clastic input, the post-sedimentary redistribution, etc.*

Keywords: *graptolite argillite, black shale, geochemistry, trace metals, REE, Estonia.*

1. Introduction

The Estonian graptolite argillite (GA), Tremadoc in age, is distributed in northern Estonia and on Vormsi and Hiiumaa islands. It belongs to the Türi-salu Formation and is overlain by glauconitic sandstones and clays of the Varangu Stage and underlain by the phosphatic quartzose sandstone of the Kallavere Formation [1]. The GA is an argillaceous rock enriched with organic matter [2] and is characterized by high concentrations of a number of trace elements, including U, V and Mo. The thickness of GA reaches 7.4 m in NW Estonia and decreases towards the east and south. On a regional scale, GA belongs to the wide but patchy belt of Middle Cambrian

* Corresponding author: e-mail voolma@gi.ee

to Lower Ordovician black shales extending from Lake Onega district in the east to the Caledonian front, Oslo region and Jutland Peninsula in the west [3–6].

There are numerous studies conducted on various metalliferous black shale/oil shale deposits worldwide – black shale deposits in North America [7–12], China [13, 14], central Europe [15], and alum shale in Scandinavia [3, 16–20] – focusing on the general characteristics and different aspects of metallogenesis in those assemblages. Also, a series of investigations have been targeted on the general geochemistry and trace element distribution of Estonian GA [21–30].

The metalliferous nature of GA was well known already in the first half of the last century. A more systematic picture of GA outside its outcrop area near the Baltic Klint, however, was gathered thanks to the extensive geological mapping of basement, drilling and geochemical investigations, which started in the 1950s and were conducted by the Geological Survey of Estonia. The vast amount of detailed information on the GA lithology and geochemistry was collected during the prospecting of Estonian phosphorite resources, e.g. [23, 31, 32]. The previous investigations have allowed depicting general trends of trace element enrichment and lateral distributions within GA, demonstrating at the same time high trace metal heterogeneity of those deposits [26, 28, 29]. Still, relatively little is known about the source of metals and the mechanism that caused metal enrichment in many black shale deposits worldwide, including GA. Although several investigations have been conducted during the past decades [25–30], the origin of metals is still unclear, as why their content is so heterogeneous laterally and also vertically through the GA complex.

Based on previous geochemical investigations [26] three geochemical zones have been distinguished in Estonian GA: Western, Central and Eastern zones (Fig. 1). The zones differ mainly in concentration of metals which are characteristic of GA – Mo, V, U. However, based on the present study it will be shown that the distribution of metals in GA has a more complex pattern. This paper describes the vertical bed-to-bed variation of metals, with emphasis on two vertical cross-sections, and discusses some possible critical factors that may stand behind the trace metal enrichment and heterogeneity in those complexes. Samples for the study were collected from Pakerort cliff on Pakri Peninsula, NW Estonia and Saka cliff, NE Estonia (Fig. 1), selected to represent GA complex in different geochemical zones. According to biostratigraphic studies GA in those localities does not represent strictly coeval sedimentation: GA from Western Estonia is assigned to the Pakerort Stage, whereas GA within the Eastern Zone belongs to the younger Varangu Stage [33, 34].

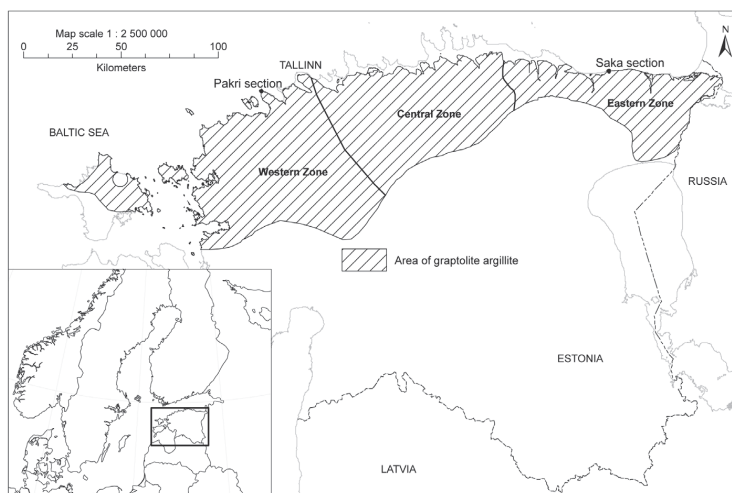


Fig. 1. Map of the location of GA and sampled outcrop sections.

2. Material and methods

Two outcrops, Pakri and Saka, were sampled at 20 cm intervals for geochemical analysis. Twenty-one fresh GA samples from Pakri and nine samples from Saka were collected from the outcrop sections of 4.2 m and 1.8 m, respectively. The weight of samples was approximately 2 kg. The samples were cleaned, dried, crushed and homogenized for chemical analysis. The sample powders were analyzed for major and trace element composition, including rare earth elements, in order to determine the geochemical changes across the section and general rock composition. Geochemical analysis was performed using X-ray fluorescence (XRF) and ICP-MS analysis.

XRF analysis was conducted at the Institute of Geology, Tallinn University of Technology (TUT), with an S4 Pioneer Spectrometer (Bruker AXS GmbH, Germany), using an X-ray tube with a rhodium anode, which operated with a power of 3 kW. The samples were measured with a manufacturer's standard as MultiRes modification (pre-calibrated standardless method). The in-house standard ES-2 ("Dictyonema Shale") was used as reference material [34]. Loss on ignition (LOI) was determined from 1 g of sample material at 500 °C and 920 °C. ICP-MS analysis was conducted at the Institute of Geology, TUT. Rare earth elements of Pakri samples were determined from solutions which were prepared following the nitric, hydrofluoric, hydrochloric and boric acids digestion of a 0.250 g pulverized sample in an Anton Paar MW3000 microwave oven. A set of samples from

Pakri and Saka were additionally re-analyzed for trace elements, including rare earths, at ACMELABS in Canada.

Mineralogical analysis of selected whole rock powdered samples was conducted using an X-ray diffractometry apparatus (HZG4 diffractometer) at the Institute of Geology, TUT. XRD analysis was performed using a Fe-filtered Co radiation (35 kV and 25 mA) and scintillation detector. The range from $5\text{--}45^\circ 2\theta$ was scanned with a step of $0.04^\circ 2\theta$. For selected samples complementary scanning electron microscope (SEM) analysis was used. SEM examination of uncoated rough and flat unpolished GA samples was carried out at the Institute of Geology, TUT, with a Zeiss EVO MA15 scanning electron microscope.

3. Mineralogy of graptolite argillite

GA is a fine-grained kerogen-rich siliceous deposit characterized by high content of organic matter (15–20%) and pyrite (2.4–6.0%) [2], and very low thermal maturity. The mineral assemblage of GA is according to previous studies dominated by K-feldspars, quartz and clay minerals [35, 36]. In the lateral as well as vertical dimension the contents of major rock-forming minerals show slight but pronounced variation patterns [35, 37, 36]. The average content of quartz in GA gradually rises eastward with the corresponding clay mineral decrease. In NE Estonia, the argillite complex is intercalated with numerous quartzose silt beds [30]. From authigenic sulfides, the occurrence of pyrite, marcasite, sphalerite and galena has been documented. In outcrops and drill cores secondary gypsum and jarosite commonly appear. In general, a higher degree of sulfide mineralization within GA is associated with the occurrence of silt interbeds. Those interbeds might also host a higher amount of other minor authigenic compounds typical for GA – phosphates (mainly apatite as biogenic detritus and nodules), carbonates (calcite and dolomite as cement and concretions), barite and glauconite. Besides the highly resistant terrigenous accessory phases, considerable abundance of micas in GA beds has been documented [35, 37].

Detailed mineralogical study is beyond the scope of the present paper. However, in order to record general mineralogical outline, XRD analysis of selected GA samples from the Pakri outcrop was performed. The study confirmed the presence of K-feldspar (sanidine), illite (illite-smectite, micas), quartz, pyrite, marcasite, apatite, calcite, dolomite, galena and chlorite. The analysis with SEM revealed high micrometer-scale morphological heterogeneity in the examined samples. The dominance of finely disseminated microcrystalline euhedral K-feldspar and quartz in argillite suggests that these minerals in GA are commonly authigenic in origin. The multistage development of syngenetic-diagenetic mineral assemblages and importance of redistribution processes in GA are suggested by the

occurrence of a high variety of pyrite crystal forms within the argillite matrix as well as in sulfide enriched interbeds.

4. Results and discussion on the geochemistry of the Estonian graptolite argillite

Detailed vertical geochemical heterogeneity in the GA has not been studied previously. There is little understanding of the scale of heterogeneity and distribution pattern of elements. Moreover, detailed lateral geochemical changes across the GA unit are unknown. As an example of elemental distribution, V, Mo and Pb within the Estonian GA unit are displayed in Figure 2. The initial data were selected from the database of the Geological

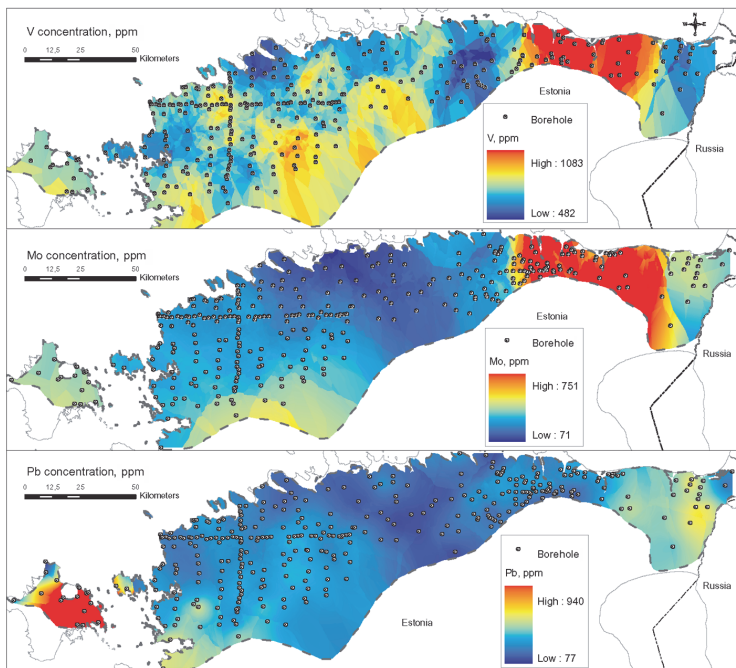


Fig. 2. V, Mo and Pb concentrations in Estonian GA as modeled using calculated average drill core analyses (data: Geological Survey of Estonia, 2008). Element concentration surfaces were modeled by the kriging method using spherical distances (ESRI ArcGIS). For distribution model of V data from 297 drill cores were selected, for Mo 325 and for Pb 345 drill cores were used.

Survey of Estonia. These elemental concentration data represent the calculated average concentration in the GA in the drill core. The central and western parts of the Eastern Zone show the highest concentrations for V and Mo (Figs. 2, 1). Generally, it can be concluded that the concentration of most of the metals is relatively low in the Central Zone (Figs. 2, 1). Pb shows the highest concentrations on Hiiumaa Island. It must be emphasized that the available data is relatively unevenly distributed, especially the southern margin of the GA bed. Therefore, geochemical generalizations of this kind are informative but must be taken with precaution. More drilling material and studies of the vertical geochemical change of elements in GA are needed to define spatial geochemical patterns.

4.1. Major elements

The bed-to-bed study performed on geochemical variation from Saka and Pakri sections show that major elements vary relatively little across the examined GA sequences (Table 1). Analyses indicate that the GA assemblage is siliceous, high-K, Mn-poor and with variable Fe and S contents.

The SiO₂ abundance in examined GA sections varies from 45.74 to 55.11 wt% and shows a general increase towards the upper part of the GA complex. The observed distribution pattern agrees with previously described lithological changes – general increase of the silt/clay ratio from bottom to top of the beds in Estonian GA sequences [37, 36]. Besides, there is an inverse correlation between LOI 500 °C (reflecting organic matter content in GA) and SiO₂. The Al₂O₃ content varies between 10.9 and 14.49 wt% and its average concentration is somewhat higher in GA from the Pakri locality. Titanium behavior shows a strong correlation with aluminum suggesting a possible detrital origin. The distinct feature of the Estonian GA is its elevated potassium content, in Pakri and Saka GA sequences K₂O ranges from 6.59 to 8.44 wt%. The high potassium content is likely connected with the abundance of authigenic K-feldspar in those beds, thus differentiating Estonian GAs from the Scandinavian alum shale, where clay minerals occur as the dominant K-rich phases [38]. Pronounced potassium enrichment is also evident when the detected chemical composition of GA is compared with the compositions of widely used standard shale compilations such as PAAS (Post Archaean Australian Shale) [39], and NASC (North American Shale Composite) [40] (Fig. 3). On the other hand, a number of major element compounds, such as MnO, Na₂O, CaO, MgO, appear to be considerably depleted with respect to the “standard shale” composition. The content of all those elements in the studied GA sequences is consistently well below 1.5 wt%.

The invariably low manganese content of Cambrian-Tremadoc black shales of the Baltoscandian region was interpreted by Wilde et al. [10] as an indicator of persistently euxinic environment during accumulation of the

Table 1. Major elements in Ga samples from Pakri and Saka sections

Interval, cm		GI XRF %													%		GI %	
From	To	Sample	SiO ₂	TiO ₂	Al ₂ O ₃	Fe ₂ O ₃	MnO	MgO	CaO	Na ₂ O	K ₂ O	P ₂ O ₅	Cl	S	SUM	LOI500°C	LOI920°C	
0	20	Pakri1	46.10	0.72	13.91	4.89	0.020	1.31	0.25	0.07	8.00	0.15	0.019	2.23	99.48	22.10	24.05	
20	40	Pakri2	45.74	0.71	13.60	4.01	0.020	1.33	0.22	0.07	7.77	0.11	0.020	1.96	99.69	24.46	26.09	
40	60	Pakri3	46.83	0.70	13.55	4.29	0.019	1.30	0.20	0.07	7.73	0.12	0.026	2.11	99.69	23.27	24.86	
60	80	Pakri4	48.77	0.72	13.66	4.33	0.020	1.27	0.23	0.06	7.95	0.14	0.022	2.16	99.16	20.46	21.99	
80	100	Pakri5	48.01	0.72	13.60	4.44	0.020	1.26	0.13	0.06	7.82	0.12	0.025	2.11	99.54	21.77	23.33	
100	120	Pakri6	47.57	0.72	13.38	4.07	0.019	1.22	0.12	0.06	7.85	0.10	0.023	2.02	98.87	22.21	23.73	
120	140	Pakri7	48.37	0.73	13.65	4.13	0.018	1.22	0.11	0.07	7.92	0.12	0.029	2.03	99.59	21.69	23.22	
140	160	Pakri8	49.91	0.75	13.85	4.36	0.019	1.23	0.10	0.07	8.02	0.12	0.023	2.12	99.87	19.79	21.42	
160	180	Pakri9	48.25	0.73	13.85	4.28	0.018	1.23	0.12	0.06	8.12	0.09	0.024	2.16	99.99	21.59	23.22	
180	200	Pakri10	49.63	0.70	13.45	4.95	0.017	1.17	0.16	0.06	7.88	0.14	0.018	2.56	99.54	19.73	21.36	
200	220	Pakri11	51.35	0.75	13.94	4.97	0.017	1.18	0.15	0.07	8.25	0.18	0.020	2.39	99.70	16.96	18.83	
220	240	Pakri12	49.71	0.75	13.65	4.25	0.018	1.19	0.13	0.07	8.12	0.14	0.023	2.08	99.03	19.30	20.99	
240	260	Pakri13	49.09	0.74	13.67	5.22	0.019	1.25	0.14	0.07	7.77	0.13	0.017	2.64	100.03	19.95	21.92	
260	280	Pakri14	49.41	0.74	13.88	6.08	0.018	1.25	0.21	0.07	7.72	0.19	0.017	2.98	99.98	18.45	20.40	
280	300	Pakri15	49.61	0.76	14.06	4.38	0.019	1.30	0.18	0.07	8.20	0.13	0.018	2.06	99.02	18.60	20.29	
300	320	Pakri16	48.97	0.75	14.00	4.44	0.018	1.24	0.10	0.07	8.15	0.13	0.019	2.18	99.15	19.50	21.27	
320	340	Pakri17	52.43	0.68	13.21	4.25	0.019	1.16	0.60	0.07	7.91	0.48	0.015	2.14	98.18	15.40	17.35	
340	360	Pakri18	50.03	0.79	14.49	4.21	0.021	1.33	0.18	0.07	8.44	0.14	0.017	1.95	100.12	18.58	20.40	
360	380	Pakri19	51.69	0.80	14.41	4.42	0.021	1.33	0.23	0.07	8.42	0.17	0.013	1.95	99.20	15.83	17.62	
380	400	Pakri20	51.87	0.78	14.12	4.72	0.020	1.23	0.18	0.07	8.32	0.11	0.014	2.23	99.33	16.10	17.89	
400	420	Pakri21	51.59	0.79	14.09	5.02	0.022	1.27	0.43	0.08	8.16	0.27	0.015	2.41	99.49	15.30	17.76	
0	20	Saka1	49.73	0.73	11.94	4.21	0.009	0.72	0.25	0.06	7.23	0.37	0.020	2.68	99.99	21.28	24.73	
20	40	Saka2	51.75	0.64	11.00	6.00	0.008	0.64	1.08	0.06	6.59	1.08	0.019	4.00	99.29	16.03	20.43	
40	60	Saka3	48.28	0.64	11.27	4.20	0.009	0.67	0.18	0.05	6.90	0.54	0.028	2.57	99.05	23.70	26.29	

Table 1 (continuation)

Interval, cm		GI, XRF %											%		GI %		
From	To	Sample	SiO ₂	TiO ₂	Al ₂ O ₃	Fe ₂ O ₃	MnO	MgO	CaO	Na ₂ O	K ₂ O	P ₂ O ₅	Cl	S	SUM	LOI500°C	LOI920°C
60	80	Saka4	46.54	0.68	11.84	3.93	0.012	0.87	0.11	0.06	7.17	0.25	0.021	2.05	99.91	26.19	28.43
80	100	Saka5	49.95	0.70	11.55	3.78	0.012	0.87	0.13	0.05	7.29	0.29	0.030	2.03	99.84	22.83	25.19
100	120	Saka6	52.02	0.67	10.90	3.81	0.011	0.78	0.13	0.05	6.90	0.24	0.020	1.95	99.77	22.61	24.25
120	140	Saka7	48.01	0.65	11.01	4.97	0.012	0.82	0.19	0.05	6.85	0.20	0.022	2.48	99.80	24.96	27.02
140	160	Saka8	55.11	0.75	12.38	4.82	0.018	0.98	0.25	0.06	7.51	0.23	0.019	1.34	99.38	14.63	17.24
160	180	Saka9	48.86	0.64	10.91	4.95	0.033	0.82	1.24	0.06	6.79	1.33	0.020	1.57	99.29	19.71	23.63

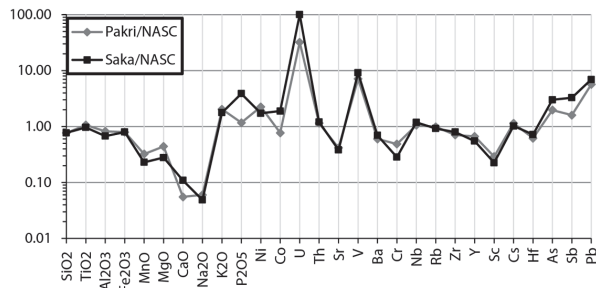


Fig. 3. Major and trace elements of GA samples normalized to NASC (North American Shale Composite) after [40].

black shale complexes. Typically for the organic-rich deposits formed under oxygen deficient environment, the Estonian GA suggests efficient sequestration of sulfur and iron. The content of these elements is, however, highly variable in different samples investigated. The content of Fe_2O_3 in the examined samples varied between 3.79 and 6.08 wt%. The sulfur concentration changed from 1.34 to 4 wt%. The strong correlation between the abundances of sulfur and iron in the Pakri GA sequence indicates that most of the sulfur is incorporated into iron sulfides rather than into organic matter. In the Saka section the correlation between the behaviors of sulfur and iron is less apparent, partly probably due to formation of secondary sulfates and phosphates. P_2O_5 and CaO, whose abundance in GA is generally low, are mainly included in apatite, as suggested by the covariance of those elements in the GA samples. Nevertheless, the detailed variance patterns of phosphorus in Saka and Pakri sequences reveal that on the background of generally monotonous phosphorus content some GA intervals (e.g. Saka2, Saka9, Pakri17) present anomalously high concentrations of P_2O_5 . Elevated phosphorus values might be due to the higher level of mixing with phosphatic detritus, suggested by the considerable abundance of phosphatic bioclastic fragments in these GA levels or due to the formation of diagenetic apatite.

If the two GA sequences under study are compared on the basis of major element composition, differences appear to be moderate – the Pakri samples have a slightly higher content of K_2O , Al_2O_3 , TiO_2 and MgO and a lower content of CaO and P_2O_5 . In general, the relatively homogeneous major element distribution gives limited clues for predicting the highly inhomogeneous trace element enrichment patterns and for unraveling the processes behind enrichment.

4.2. Trace elements

Trace metal enrichment in black shales is mostly explained by two alternative theories: 1) syngenetic sequestration of metals under oxygen-deficient conditions from marine water, e.g. [41, 12, 20], or 2) flushing of the sediments by metal-enriched syngenetic brines or contemporaneous exhalation of such brines into marine basin, e.g. [42, 14, 43, 25, 30]. However, these theories are challenged by works that underline the influence of source rocks and particulate precursor material on the final character of metal enrichment in black shales, e.g. [44], or the crucial role of diagenetic redistribution processes induced by late diagenetic brines, e.g. [8, 45].

In general, U-Mo-V-Pb enriched trace metal association with sporadically elevated concentrations of some other trace elements was detected in GA from Saka and Pakri sections (Table 2). For assessing the degree of enrichment of particular trace metals in GA, the detected average trace element abundances were compared with average shale and black shale standard compilations. With respect to PAAS and NASC values the GA appears to be extremely enriched in U and V (Fig. 3). For example, the average U concentration in the Saka section (267 ppm) is a hundred times higher than the corresponding values for NASC. There is a nine-fold difference in V concentration between NASC and Saka GA section (average 1190 ppm). If compared with the minimum enrichment values (m.e.v.) for metalliferous black shales (suggested by Vine and Tourtelot [7] on the basis of generalized data of numerous North-American black shales), the studied samples and the Estonian GA in general could be considered enriched with U (m.e.v. 30 ppm), Mo (m.e.v. 200 ppm), V (m.e.v. 1000 ppm), Pb (m.e.v. 100 ppm) and Co (m.e.v. 30 ppm; only in Saka samples) [28].

All previously listed enriched trace metals of GA as well as other abundant trace elements, like As, Sb, Ni, Cu, Re, belong to the group of redox sensitive and/or stable sulfide-forming metals and might undergo considerable partitioning in marine geochemical and biochemical cycles. As indicated by the studies of trace elements in modern marine environments, e.g. [46–48], the redox sensitive elements mostly occur as soluble species under oxidizing conditions. Under the oxygen-depleted conditions, however, the redox sensitive elements are typically present as insoluble species (metal-organic complexes, sulfides, metal oxyhydrates) and thus tend to sequester into sediments. The whole metal trapping process is strongly linked with organic matter breakdown and sulfate reduction processes, which inhibit the crystallization of sulfides. In addition to the redox sensitive trace elements, other elements like Fe and Mn found commonly enriched in black shales, are essential recyclers in redox partitioning in marine systems [49]. Consequently, based on numerous comparative studies of trace element accumulation in modern and ancient organic rich sediments, e.g. [50, 51], it has been suggested that oxygen availability in sedimentary environment could have had sole control over development of enriched trace metal associations in different black shales, e.g. [12].

Table 2. Trace elements in GA samples from Pakri and Saka sections

Interval, cm	Lab	Acme														PPM													
		Acme							GI XRF							Acme							GI XRF						
From	To	Sample	Mo	Cu	Pb	Zn	Ni	Co	As	U	Th	Sr	Sb	V	Ba	Cr	Se	Ga	Nb	Rb	Zr	Y	Sc	Be	Li				
0	20	Pakri1	639	146	105	45	130	18	55	126	13	62	5.4	1081	398	45	3.7	17.8	13.6	128	129	23	3.3	1.8	17.3				
20	40	Pakri2	181	115	75	40	124	16	39	108	12	65	4.3	1166	395	48	3.1	15.6	13.5	127	128	19	3.5	1.6	18.0				
40	60	Pakri3	203	134	101	49	166	33	56	206	13	65	5.0	1223	381	51	3.5	15.7	13.0	127	133	19	4.5	2.3	18.8				
60	80	Pakri4	148	133	98	845	178	27	51	82	13	63	3.9	1025	384	48	3.3	14.2	12.5	121	134	27	4.5	2.1	16.4				
80	100	Pakri5	155	143	116	138	170	24	56	164	14	62	4.2	1061	369	50	3.7	15.0	17.2	125	132	18	5.0	2.3	18.7				
100	120	Pakri6	151	133	98	134	144	15	52	172	13	64	4.4	1015	399	54	3.3	15.2	19.5	124	138	17	3.8	2.0	15.3				
120	140	Pakri7	157	148	105	42	147	22	55	117	15	63	4.0	1229	347	57	4.1	14.9	15.2	125	136	20	4.8	2.0	17.1				
140	160	Pakri8	126	151	193	39	141	21	52	93	15	64	3.3	1144	381	57	4.5	14.0	14.0	126	142	18	4.6	1.3	16.3				
160	180	Pakri9	88	162	143	39	115	18	47	78	14	61	2.6	827	374	54	3.1	15.6	14.3	124	131	13	4.4	1.4	15.3				
180	200	Pakri10	74	152	135	38	160	22	59	52	14	56	2.5	652	388	71	4.1	14.6	11.9	113	137	24	4.2	1.6	14.5				
200	220	Pakri11	61	151	135	60	107	15	72	41	16	57	2.4	563	376	72	3.8	14.5	12.8	117	144	17	4.2	1.3	14.6				
220	240	Pakri12	102	129	132	50	115	16	54	91	14	57	3.0	1040	387	65	4.7	12.9	12.6	125	144	21	n.a.	n.a.	n.a.				
240	260	Pakri13	110	161	152	40	172	19	68	65	15	55	4.4	1096	318	60	7.7	16.8	13.9	115	139	21	4.7	1.7	15.6				
260	280	Pakri14	60	162	174	37	185	21	118	52	14	54	5.2	839	344	62	5.8	12.5	10.7	105	140	31	4.2	2.0	14.6				
280	300	Pakri15	92	131	103	40	133	21	52	76	14	59	3.1	1081	408	57	4.3	15.0	14.0	128	140	21	4.5	1.2	16.1				
300	320	Pakri16	85	144	117	42	120	17	54	102	15	56	3.5	1096	358	63	4.0	16.2	15.9	128	138	13	4.6	1.0	15.4				
320	340	Pakri17	96	120	105	38	113	35	63	82	16	67	3.3	739	377	48	3.7	13.9	10.6	118	148	73	5.0	1.3	14.9				
340	360	Pakri18	53	141	103	41	96	17	45	35	14	54	2.2	781	377	70	2.9	16.7	13.2	131	142	21	4.9	1.2	16.7				
360	380	Pakri19	57	129	100	42	104	15	53	49	16	54	2.7	925	429	73	4.8	16.5	12.7	128	150	23	4.7	1.0	16.4				
380	400	Pakri20	52	125	94	40	116	17	55	19	14	48	2.0	622	393	56	2.6	15.9	12.3	121	153	21	4.1	1.0	14.6				
400	420	Pakri21	65	101	88	36	99	17	65	57	14	55	2.1	745	369	74	3.6	13.7	13.4	119	157	40	n.a.	n.a.	n.a.				
0	20	Saka1	1143	76	193	14	182	44	64	137	13	62	9.1	1266	390	36	5.3	15.0	16.0	120	168	9	2.8	0.5	3.9				
20	40	Saka2	85	85	187	10	103	102	76	182	16	56	5.3	946	409	36	5.7	12.0	10.0	92	171	31	3.6	0.6	3.1				

Table 2 (continuation)

Interval, cm		Acme														GI XRF										Acme			GI XRF			Acme		
From	To	Mo	Cu	Pb	Zn	Ni	Co	As	U	Th	Sr	Sb	V	Ba	Cr	Se	Ga	Nb	Rb	Zr	Y	Sc	Be	Li										
40	60	97	134	152	14	82	62	86	169	15	52	4.5	1093	406	32	5.3	16.0	17.0	108	155	12	3.2	0.8	4.1										
60	80	1844	176	101	25	89	31	72	805	16	51	9.9	1497	438	41	5.5	16.0	19.0	141	165	6	4.8	1.2	9.1										
80	100	202	122	135	22	89	43	54	111	16	49	5.5	1453	435	38	5.1	15.0	14.0	116	163	11	3.1	0.7	7.1										
100	120	408	106	124	21	88	25	57	433	14	47	5.7	1288	441	30	4.3	13.0	16.0	122	160	9	3.0	0.7	6.9										
120	140	413	108	137	36	127	28	50	239	14	50	7.2	1165	390	31	4.1	13.0	21.0	114	135	16	2.7	0.5	8.1										
140	160	279	116	125	116	118	51	75	145	16	56	6.5	1096	421	38	5.6	11.0	16.0	121	173	23	3.8	0.9	9.8										
160	180	299	148	95	23	125	53	236	184	15	66	8.0	908	650	38	7.1	10.0	10.0	102	149	57	3.2	0.8	7.8										

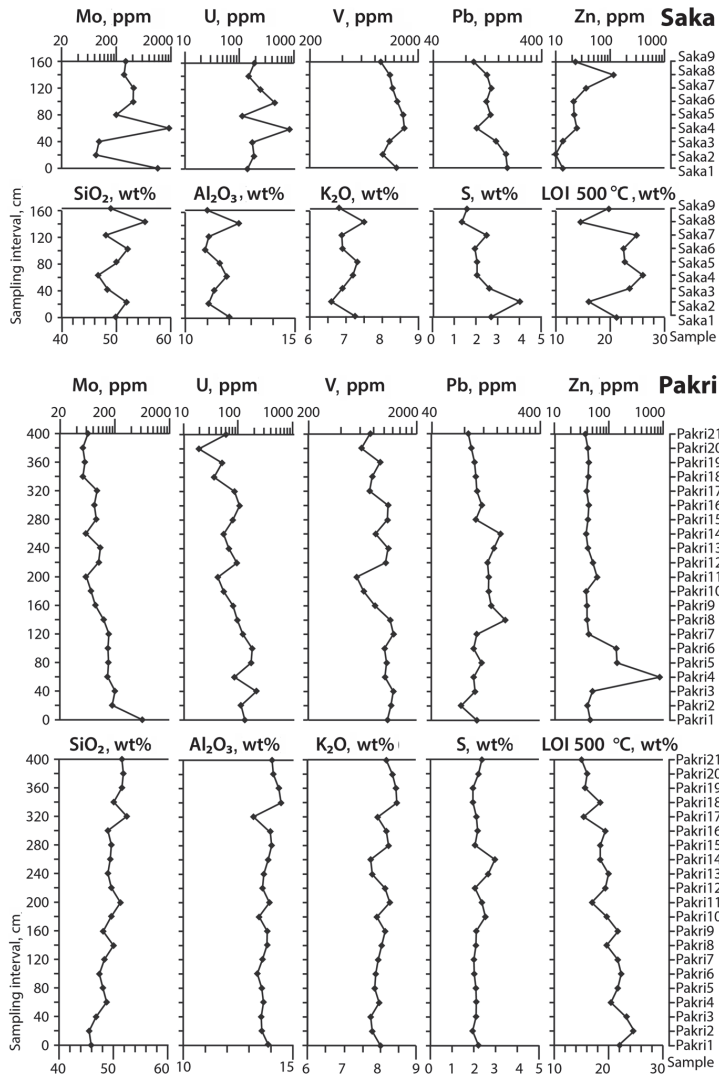


Fig. 4. Vertical distribution profiles of major compounds SiO₂, Al₂O₃, K₂O, S, and LOI 500 °C and enriched trace metals from Saka and Pakri GA sections.

The performed geochemical investigations revealed that the studied sequences present pronounced vertical variations in U, V, Mo and Zn con-

centrations (Fig. 4). The listed trace elements do not show completely matching variance patterns and the maximum (and minimum) enrichment intervals of different components mostly do not overlap. In case of the Pakri GA sequence one can separate about 1.3 m thick lower part, which is enriched with some trace metals like Mo, U and Sb, and also contains more organic matter as indicated by higher LOI 500 °C values. While Mo is gradually decreasing towards the upper part of the Pakri sequence, U and V contents are somewhat more erratic. The thinner GA complex from Saka, which on average contains more Mo, U and V than the Pakri GA, is also characterized by the larger variance of those elements. In Saka samples, no clear vertical distribution trends of Mo and U can be followed, the concentrations fluctuate on a large scale and very high values alternate with low ones. For example, in samples Saka1 and Saka4 the Mo content is 1143 and 1843 ppm, respectively, while between these samples it only varies between 85 and 97 ppm. In general, Mo and U contents in the Saka section show quite a strong positive covariance with organic matter content (LOI 500 °C). The sample Saka4, which presents anomalously high values of these elements, also yielded the highest LOI 500 °C value. These results agree with the observation that the contents of V, U and Mo in black shales typically correlate with the abundance of organic matter [7], likely indicating early fixation via metal-organic complexes. However, in case of V, which shows considerably high values throughout both studied GA sequences, the correlation with organic matter is less expressed.

The average content of Pb is similar in both investigated sections and its vertical distribution is rather homogeneous. Lead shows a positive covariance with elements presumably related with sulfides – Fe₂O₃, S, Cu, Se, Ag, Hg in Pakri samples, while in Saka there is a positive correlation with S and Ta, and a negative one with Cu, Li, Re, Sn. Zn generally demonstrates an opposite trend to internally enriched elements such as U, V, Mo. Its abundance is two times higher in Pakri samples compared to Saka ones. However, the elevated concentrations of Zn in the Pakri section (up to 761 ppm in Pakri4) are limited to the well-defined interval 60–120 cm from the bottom, whereas the rest of the sequence is characterized by a monotonous Zn concentration near 40–60 ppm. In the Saka section the content of Zn is very low in the lower part of the section, but shows a general increase toward the upper part of the complex. The pronounced positive covariance of Cd with Zn in the studied sequences likely indicates a coeval trapping of those phases during sphalerite formation.

U positive covariance with P₂O₅ was not detected in the samples under study. Trace metal partitioning into phosphates has been suggested by some studies [52] as a process responsible for the higher general concentration of U in the GA of NE Estonia.

In general, the dominance of common marine redox sensitive elements among enriched metals in GA favors syngenetic enrichment as the major process of trace metal sequestration. On the other hand, the remarkably high

concentration of enriched elements in GA and the variable covariance patterns imply that element sequestration solely from seawater due to Eh gradients is likely an insufficient model for explaining the observed large-scale trace metal heterogeneity in GA. Furthermore, the current data (Tables 2, 3) as well as previous studies [2] indicate that besides the elements, for which partitioning in marine systems is well known, GA sporadically presents elevated levels of some minor elements, e.g. PGE and W, characterized by generally very low abundance in average crust and modern marine sediments. The accumulation of such minor compounds in GA underlines the role of internal input of metals into the sedimentary or diagenetic environment.

The closeness of probable denudation areas (the peneplain of Proterozoic crystalline rocks in Southern Finland) to the sedimentary setting where GA accumulated hints that the trace elemental composition of sea water in these areas likely bore a distinct terrestrial signature, similarly to recent coastal marine environments [49]. Moreover, recent studies in Caledonian Nappe complexes, e.g. [53], suggest the existence of subduction zone related volcanic arc complexes within the Iapetus Ocean near the western border of the Baltica paleocontinent in the Late Cambrian and Tremadoc. The associated volcanic activity in these areas could supply overlying waters with extra trace metal budgets and modify regional marine trace metal signals enhancing, for example, Zn and V content of marine water. Then again, the likely introduction of the particulate volcanic matter to the sedimentary basin during the times of GA formation is suggested by clay mineral studies. According to Utsal et al. [35] the widespread occurrence of authigenic illite-smectite in GA indicates that at least 10% of its primary sedimentary matter was made up of volcanic ash.

The differences in trace element composition of GA might thus in some instances reflect variations in source material fluxes. First of all this relates to non-reactive elements with negligible solubility in surface environments transported to the sedimentary basin mainly in the composition of terrigenous (volcanic) matter such as residual heavy minerals, secondary weathering products or volcanic ash. According to Vine and Tourtelot [7], the detrital fraction of most black shales is characterized by the elements Al, Ti, Zr, Ga, Sc, and may also commonly include Be, B, Ba, Na, K, Mg, and Fe. Additional elements generally considered insensitive to secondary processes include Nb, Y, Th, Ta, Hf, and the REEs [39].

On the La-Al and La-Ti diagrams (Figs. 5A, 5B) the distribution of Al and Ti shows a similar pattern with respect to the lanthanum behavior. The Pakri samples with higher alumina and silica values and somewhat higher Ti content have enhanced La values as compared to Saka samples. The covariance of La with typical detrital compounds suggests that La may be dominantly bounded by detrital phases. However, the abnormally high La content detected in three phosphorus-rich samples may suggest a possible syngenetic incorporation into the biogenic detritus or diagenetic

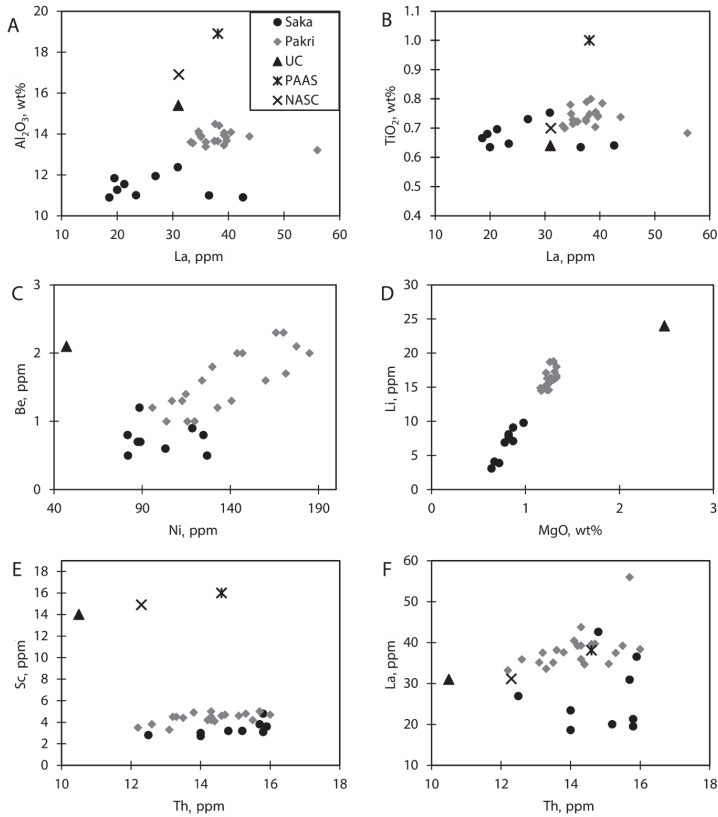


Fig. 5. Relationships between trace elements in graptolite argillite. UC = Upper Continental Crust [55]; PAAS = Post Archaean Australian Shale [39]; NASC = North American Shale Composite [40].

mobility of La. Be and Ni abundances in the Pakri section demonstrate a two-line positive covariance trend (Fig. 5C). Such a distribution pattern of two elements with generally different geochemical behavior in surface systems might reflect the terrigenous (volcanogenic) flux into the sedimentary environment from a distinct source during the initial period of accumulation of the GA or specific sedimentary conditions supporting Ni enrichment. The terrigenous flux controlled abundance is suggested also for Li and Mg (Fig. 5D). Both elements show a very well defined positive correlation, suggesting that Li and Mg are likely bonded into the crystal structure of micas and/or clay minerals. Figures 5E and 5F present the relations of Sc, Th,

and La, widely exploited for discriminating different magmatic rock types and settings. Numbers of studies have employed these variations to track possible precursor rocks of ancient shale and black shale complexes [39, 54]. On the Th-Sc graph the Pakri and Saka samples present anomalously low Sc and high Th/Sc content (Fig. 5E), thus suggesting a generally felsic upper crustal precursor for GA. The La/Th ratios of the analyzed GA samples demonstrate considerably higher scattering. As mentioned above, however, the enhanced La values in phosphorus-rich samples suggest that precursor rock signal had been in some cases evidently obscured by the synsedimentary incorporation or posterior redistribution of La.

In general, the clustering of non-reactive trace element data into the two fields may suggest that two different dominant source areas were involved in the supply of detrital material to the localities where organic-rich muds once accumulated.

4.3. Rare earth element variations

The REE patterns recorded for post-Archaean shales (PAAS) show striking similarity worldwide: they are light REE enriched, with a negative Eu anomaly and relatively flat heavy REEs [55, 39]. Samples from Pakri show chondrite-normalized (CN) REE patterns (Fig. 6C) generally similar to those recorded for PAAS, being considerably enriched in light rare earth elements (LREEs) with respect to heavy rare earth elements (HREEs). The main difference from the average shale compilations appears in content of MREEs (Fig. 6B). Like PAAS, all the studied samples exhibit negative Eu anomaly. The $\text{La}_{\text{CN}}/\text{Yb}_{\text{CN}}$ ratio ranges from 6.65 to 10.26, staying thus well below the upper crust's $\text{La}_{\text{CN}}/\text{Yb}_{\text{CN}}$ ratio. The $\text{Gd}_{\text{CN}}/\text{Yb}_{\text{CN}}$ ratio varies from 1.09 to 2.22 with an average of 1.44 which is close to the PAAS value. The PAAS-normalized REE patterns of the examined GA samples show generally flat shape (Figs. 6A, 6B). In respect of the considerably monotonous REE variations, three samples from the Pakri locality exhibit distinct behavior. Pakri21 and Pakri14 have similar REE fractionation patterns with a somewhat elevated content of MREEs compared to PAAS. A unique hat-shape REE shale-normalized pattern was recorded for Pakri17 sample, which also presents a clearly elevated absolute REE concentration and strong MREEs enrichment. Compared to the Pakri sequence the REE patterns for Saka samples show higher fractionation and variation in the content of REEs (Figs. 6A, 6C). The $\text{La}_{\text{CN}}/\text{Yb}_{\text{CN}}$ ratio is similar to that in Pakri samples, except in Saka1 and Saka4 where it reaches 15.56 and 14.27, respectively. The $\text{Gd}_{\text{CN}}/\text{Yb}_{\text{CN}}$ ratios show high variation from 0.66 to 2.76, being the highest in samples Saka2 and Saka3. The MREE pattern shows higher variation than in Pakri samples. The PAAS-normalized REE patterns of Saka1, Saka4, Saka5, and Saka6 show low REE absolute abundances, but are characterized by distinctive concave shape patterns with considerably enriched HREEs (Tm-Yb) with respect to depleted MREEs (Ce-Er). Remarkably, these samples have the lowest content of Fe_2O_3 and the highest

contents of Mo, U and V (though high contents of these trace elements also occur in other samples). The hat-shaped (similar to that of Pakri17), MREE enriched patterns characterize Saka2 and Saka3 samples. The REE patterns of samples Saka7, Saka8, and Saka9 are more flat-shaped, similar to a typical Pakri pattern.

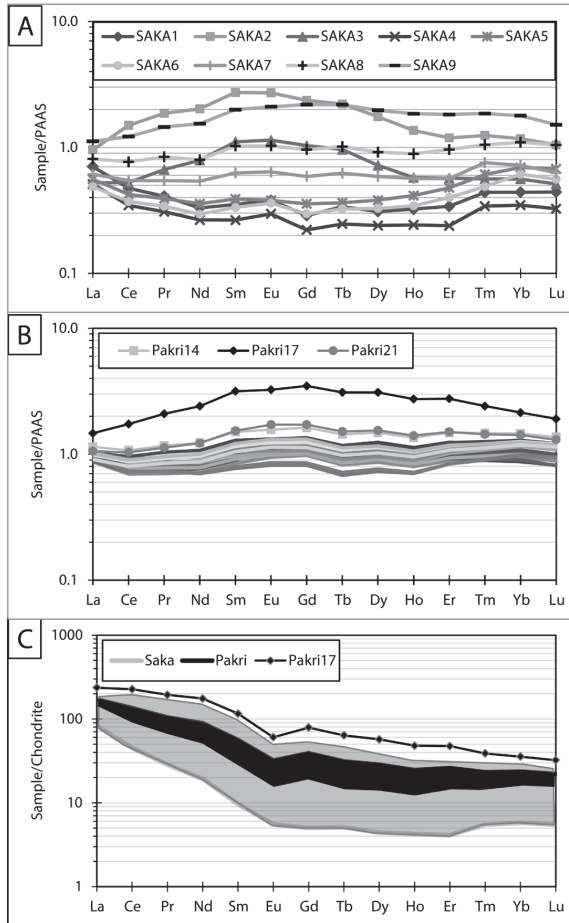


Fig. 6. Rare earth element patterns of GA samples normalized to PAAS (A; B) [39] and chondrite (C).

Table 3. Rare earth elements in GA samples from Pakri and Saka sections, ppm

Lab	Sample	La	Ce	Pr	Nd	Sm	Eu	Gd	Tb	Dy	Ho	Er	Tm	Yb	Lu
GI;	Pakri1	35.1	58.5	6.5	26.0	5.0	1.14	5.07	0.70	4.22	0.83	2.51	0.37	2.46	0.35
Acme															
GI;	Pakri2	33.2	55.4	6.2	24.2	4.7	1.02	4.56	0.63	4.03	0.79	2.53	0.37	2.67	0.38
Acme															
GI	Pakri3	33.6	57.7	6.6	26.1	5.3	1.12	4.92	0.70	4.43	0.85	2.63	0.37	2.56	0.35
GI	Pakri4	37.5	68.6	8.1	32.5	6.6	1.38	6.28	0.90	5.81	1.12	3.54	0.50	3.48	0.49
GI	Pakri5	35.9	62.4	7.2	28.1	5.6	1.16	5.11	0.72	4.62	0.89	2.85	0.42	2.90	0.41
GI;	Pakri6	35.9	61.0	6.9	26.5	5.1	1.07	4.70	0.66	4.25	0.82	2.66	0.40	2.81	0.40
Acme															
GI	Pakri7	37.5	65.8	7.6	29.6	5.8	1.17	5.09	0.72	4.54	0.88	2.83	0.42	3.05	0.43
GI	Pakri8	39.6	68.1	7.6	29.2	5.5	1.09	4.80	0.67	4.36	0.87	2.90	0.44	3.24	0.46
GI	Pakri9	35.1	58.5	6.4	23.8	4.3	0.88	3.81	0.52	3.42	0.70	2.38	0.37	2.79	0.41
GI	Pakri10	39.2	76.0	9.1	36.4	7.2	1.43	6.30	0.90	5.67	1.10	3.51	0.52	3.63	0.52
GI	Pakri11	39.2	72.4	8.3	31.5	5.9	1.14	4.98	0.70	4.49	0.89	2.99	0.46	3.40	0.50
GI;	Pakri12	38.1	70.0	8.2	31.9	6.2	1.23	5.41	0.77	4.93	0.96	3.15	0.47	3.37	0.49
Acme															
GI	Pakri13	39.7	71.8	8.3	32.3	6.2	1.25	5.45	0.78	5.00	0.98	3.21	0.49	3.48	0.50
GI	Pakri14	43.8	85.4	10.3	41.7	8.4	1.69	7.57	1.11	6.93	1.34	4.22	0.60	4.12	0.59
GI	Pakri15	39.2	72.0	8.4	33.2	6.6	1.36	5.91	0.84	5.28	1.01	3.23	0.48	3.40	0.48
GI	Pakri16	34.8	58.0	6.4	24.1	4.5	0.93	3.99	0.55	3.57	0.71	2.39	0.37	2.76	0.40
GI	Pakri17	56.0	138.2	18.4	81.6	17.7	3.51	16.23	2.38	14.48	2.71	7.86	0.99	6.04	0.82
GI	Pakri18	37.6	69.3	8.1	32.6	6.5	1.35	5.83	0.83	5.26	1.03	3.33	0.50	3.55	0.52
GI	Pakri19	38.4	71.6	8.4	33.9	6.8	1.42	6.13	0.87	5.44	1.05	3.36	0.49	3.51	0.51
GI	Pakri20	34.6	63.9	7.4	29.5	5.9	1.23	5.25	0.75	4.78	0.94	3.07	0.46	3.34	0.49
GI;	Pakri21	40.4	82.3	9.9	41.5	8.6	1.86	8.01	1.17	7.23	1.39	4.29	0.59	4.01	0.56
Acme															
Acme	Saka1	26.9	37.7	3.6	11.2	2.0	0.41	1.34	0.26	1.45	0.32	0.97	0.18	1.24	0.19
Acme	Saka2	36.5	119.0	16.4	68.6	15.3	2.93	11.00	1.70	8.19	1.35	3.39	0.51	3.30	0.45
Acme	Saka3	20.0	41.7	5.9	26.8	6.2	1.23	4.81	0.74	3.37	0.57	1.62	0.23	1.58	0.22
Acme	Saka4	19.5	27.6	2.7	9.0	1.5	0.32	1.03	0.19	1.12	0.24	0.68	0.14	0.98	0.14
Acme	Saka5	21.3	33.7	3.5	12.1	2.2	0.41	1.66	0.28	1.78	0.41	1.36	0.25	1.95	0.29
Acme	Saka6	18.6	29.6	3.0	10.0	1.9	0.39	1.38	0.25	1.53	0.34	1.14	0.20	1.73	0.24
Acme	Saka7	23.4	43.4	4.8	18.3	3.5	0.69	2.74	0.48	2.75	0.56	1.61	0.31	2.03	0.27
Acme	Saka8	30.9	61.1	7.4	27.0	5.7	1.11	4.47	0.78	4.29	0.88	2.74	0.43	3.09	0.45
Acme	Saka9	42.6	97.0	12.8	52.2	11.2	2.27	10.17	1.68	9.21	1.83	5.20	0.76	5.03	0.65

The observed large-scale variations in REE patterns – the encounter of normal flat shape as well as hat and concave like patterns – could be explained by variations in detrital input, e.g. variations in accessory mineral associations. However, alternatively it might point to the possibility that in most samples of the Saka sequence and in some intervals of Pakri the source rock inherited REE signals have been masked or obscured by the synsedimentary, diagenetic, hydrothermal or weathering induced redistribution-enrichment of REEs. The recent studies of black shales have indicated that authigenic phases such as sulfides, phosphates and carbonates as well as organic matter may host elevated REEs and their presence might influence

the absolute abundances of REEs as well as the fractionation patterns, e.g. [56]. Cruse et al. [57] interpreted the intermittent occurrence of hat and concave shape shale-normalized REE patterns in authigenic phosphate-rich and low-phosphate black shales as the evidence of an early diagenetic redistribution of REEs formed as the result of a preferential uptake of MREE in apatite and simultaneous depletion of phosphate-poor host shale beds. A similar enrichment process could be hypothesized for the MREE enriched samples of Saka and Pakri GA, all characterized by elevated phosphorus content compared to the rest of the samples under study. This agrees with high REE values detected by SEM analysis of authigenic as well as bioclastic phosphates in the studied sequences. Lev et al. [58] demonstrated the importance of post-/syn-depositional mineralizing fluid induced disturbance in REE-systems together with redistribution of U in black shales. Consequently, the encountered REE fractionation patterns could theoretically indicate also the influence of short-term low temperature brines. In case of GA the possible influence of deep source brines on the formation of its mineral assemblage has been suggested previously by sulfur isotope studies of pyrite [25]. However, the influence of deep brines on the Estonian Lower Paleozoic sedimentary assemblage is problematic as the whole complex is thermally almost unaltered. On the other hand, Somelar et al. (2010) [59] suggested intrusion of low temperature K-rich brines as the mechanism behind the illitization of Estonian Ordovician K-bentonites, pointing to the possible wide-scale influence of alkaline brines on the region in the Late Silurian.

Nevertheless, despite the lack of knowledge of the precise formation mechanism of the observed variability of REEs, it might suggest REE mobility in sedimentary or diagenetic environments. One could also speculate that the co-appearance of MREE depleted patterns and enhanced U, V and Mo abundances in GA from the Saka outcrop might indicate that those enriched elements were affected by the same redistribution processes which resulted in the formation of MREE depleted patterns.

5. Conclusions

The studies of two vertical sequences of graptolite argillite (GA) show the existence of pronounced fine-scale trace metal variability in GA. The examined samples were detected to be enriched in U, V, Mo and Pb with respect to average black shales, the obtained results thus agreeing with previously published data on the geochemistry of GA. The content of enriched elements was, however, recorded to change greatly over the examined sequences, suggesting a notably more complex nature of trace metal distribution in GA than previously assumed. Redox sensitive metals U and Mo, and also V to a lesser extent, showed loose covariance with organic matter content (LOI 500 °C), apparently indicating their trapping mainly via

organic matter tied species, and the enrichment primary linked to organic matter sequestration. The elevated abundance of a number of other trace metals, e.g. Pb, Zn, Cd, Cu, As and La, was detected in samples with an enhanced content of sulfur or phosphorus. The remarkably different behavior of the listed elements in two examined GA sequences could suggest that somewhat different sets of metal sequestration driving processes were responsible for the development of trace elemental assemblages in E and NW Estonian settings. As the trace element composition of GA is dominated by common marine redox sensitive and/or stable sulfide forming metals, the syngenetic trapping of metals from sea and interstitial water in redox boundary zones probably had first rate control over the development of trace element enrichment patterns. However, the observed high variability in the trace metal composition of GA, including heterogeneous REE patterns, points to the polygenetic nature of metal assemblages, apparently formed as the cumulative product of multistage evolution. On the whole, the study demonstrates that the knowledge base about metal distribution in GA is still rather fragmentary and that detailed geochemical, as well as multi-disciplinary investigations are essential for adequately predicting potential metal resources of GA in the future.

Acknowledgements

The authors are thankful to the reviewers for their constructive criticism and for helping to improve the manuscript. This study was funded by the Estonian Science Foundation Grant No. 8963 and the Estonian Ministry of Education and Research target research project No. SF0140016s09.

REFERENCES

1. Heinsalu, H., Viira, V. Pakerort Stage. In: *Geology and Mineral Resources of Estonia* (Raukas, A., Teedumäe, A., eds.). Estonian Academy Publishers, Tallinn, 1997, 52–58.
2. Petersell, V. Dictyonema argillite. In: *Geology and Mineral Resources of Estonia* (Raukas, A., Teedumäe, A., eds.). Estonian Academy Publishers, Tallinn, 1997, 313–326.
3. Andersson, A., Dahlman, B., Gee, D. G., Snäll, S. The Scandinavian Alum Shales. *Sveriges Geologiska Undersökning (SGU)*, 1985, **56**, 1–50.
4. Kaljo, D., Borovko, N., Heinsalu, H., Khazanovich, K., Mens, K., Popov, L., Sergeeva, S., Sobolevskaya, R., Viira, V. The Cambrian-Ordovician boundary in the Baltic-Ladoga clint area (North Estonia and Leningrad Region, USSR). *Proc. Acad. Sci. Estonian SSR, Geology*, 1986, **35**(3), 97–108.
5. Heinsalu, H., Bednarczyk, W. Tremadoc of the East European Platform: Lithofacies and palaeogeography. *Proc. Est. Acad. Sci. Geol.*, 1997, **46**(2), 59–74.

6. Buchardt, B., Nielsen, A. T., Schovsbo, N. H. Alum shale in Scandinavia (Alum skiferen i Skandinavien). *Geologisk Tidsskrift*, 1997, 3, 1–30 (in Danish).
7. Vine, J. D., Tourtelot, E. B. Geochemistry of black shale deposits – a summary report. *Econ. Geol.*, 1970, **65**, 253–272.
8. Coveney, R. M. Jr., Leventhal, J. S., Glascock, M. D., Hatch, J. R. Origins of metals and organic matter in the Mecca Quarry Shale Member and stratigraphically equivalent beds across the Midwest. *Econ. Geol.*, 1987, **82**, 915–933.
9. Quinby-Hunt, M. S., Wilde, P., Orth, C. J., Berry, W. B. N. Elemental geochemistry of black shales – statistical comparison of low-calcic shales with other shales. In: *Metalliferous Black Shales and Related Ore Deposits* (Grauch, R. I., Leventhal, J. S., eds.), US Geological Survey Circular, 1989, No. **1037**, 8–15.
10. Wilde, P., Quinby-Hunt, M. S., Berry, W. B. N., Orth, C. J. Palaeo-oceanography and biogeography in the Tremadoc (Ordovician) Iapetus Ocean and the origin of the chemostratigraphy of *Dictyonema flabelliforme* black shales. *Geol. Mag.*, 1989, **126**(1), 19–27.
11. Hatch, J. R., Leventhal, J. S. Relationship between inferred redox potential of the depositional environment and geochemistry of the Upper Pennsylvanian (Missourian) Stark Shale Member of the Dennis Limestone, Wabaunsee County, Kansas, U.S.A. *Chem. Geol.*, 1992, **99**(1–3), 65–82.
12. Algeo, T. J., Maynard, J. B. Trace-element behavior and redox facies in core shales of Upper Pennsylvanian Kansas-type cyclothems. *Chem. Geol.*, 2004, **206**, 289–318.
13. Steiner, M., Wallis, E., Erdtmann, B.-D., Zhao, Y. L., Yang, R. D. Submarine-hydrothermal exhalative ore layers in black shales from South China and associated fossils – insights into a Lower Cambrian facies and bio-evolution. *Palaeogeogr. Palaeocl.*, 2001, **169**(3–4), 165–191.
14. Jiang, S. Y., Yang, J. H., Ling, H. F., Chen, Y. Q., Feng, H. Z., Zhao, K. D., Ni, P. Extreme enrichment of polymetallic Ni- Mo-PGE-Au in Lower Cambrian black shales of South China: an Os isotope and PGE geochemical investigation. *Palaeogeogr. Palaeocl.*, 2007, **254**(1–2), 217–228.
15. Vaughan, D. J., Sweeney, M., Diedel, G. F. R., Haranczyk, C. The Kupferschiefer: An overview with an appraisal of the different types of mineralization. *Econ. Geol.*, 1989, **84**, 1003–1027.
16. Sundblad, K., Gee, D. G. Occurrence of a uraniferous-vanadiferous graphitic phyllite in the Kõli Nappes of the Stekenjokk area, central Swedish Caledonides. *Geol. Foren. Stock. For.*, 1984, **106**(3), 269–274.
17. Berry, W. B. N., Wilde, P., Quinby-Hunt, M. S., Orth, C. J. Trace element signatures in *Dictyonema* shales and their geochemical and stratigraphic significance. *Norsk Geol. Tidsskr.*, 1986, **66**, 45–51.
18. Leventhal, J. S. Comparative geochemistry of metals and rare earth elements from the Cambrian alum shale and kolm of Sweden. *Sp. Publ. Int.*, 1990, **11**, 203–215.
19. Leventhal, J. S. Comparison of organic geochemistry and metal enrichment in two black shales: Cambrian Alum Shale of Sweden and Devonian Chattanooga Shale of United States. *Miner. Deposita*, 1991, **26**, 104–112.
20. Schovsbo, N. H. Uranium enrichment shorewards in black shales: A case study from the Scandinavian Alum Shale. *Geol. Foren. Stock. For.*, 2002, **124**(2), 107–115.

21. Loog, A. Geochemistry of Lower Ordovician of Estonia. In: *Studies of the Institute of Geology, ESSR Academy of Sciences*. Tallinn, 1962. No. 10, 273–291 (in Russian).
22. Baukov, S. S. General characteristics of dictyonema shale. In: *Geology of Coal and Oil Shale Deposits of the USSR*, **11**. Nedra, Moscow, 1968, 145–148 (in Russian).
23. Petersell, V., Mineyev, D., Loog, A. Mineralogy and geochemistry of obolus sandstones and dictyonema shale of North Estonia. *Acta et Commentationes Universitatis Tartuensis*, No. 561, Tartu, 1981, 30–49 (in Russian).
24. Loog, A. On the geochemistry of postsedimentary mineral formation in the Tremadoc graptolitic argillites of North Estonia. *Acta et Commentationes Universitatis Tartuensis*, No. 527, Tartu, 1982, 44–49 (in Russian).
25. Petersell, V. H., Zhukov, F. I., Loog, A. R., Fomin, Y. A. Origin of Tremadoc kerogenous-bearing siltstones and argillites of North Estonia. *Oil Shale*, 1987, **4**(1), 8–13 (in Russian).
26. Pukkonen, E. M. Major and minor elements in Estonian graptolite argillite. *Oil Shale*, 1989, **6**(1), 11–18 (in Russian).
27. Kallaste, T., Pukkonen, E. Pyrite varieties in Estonian Tremadocian argillite (Dictyonema shale). *Proc. Est. Acad. Sci. Geol.*, 1992, **41**(1), 11–22.
28. Pukkonen, E., Rammo, M. Distribution of molybdenum and uranium in the Tremadoc graptolitic argillite (Dictyonema shale) of North-Western Estonia. *Bulletin of the Geological Survey of Estonia*, 1992, **2**(1), 3–15.
29. Loog, A., Petersell, V. The distribution of microelements in Tremadoc graptolitic argillite of Estonia. *Acta et Commentationes Universitatis Tartuensis*, No. 972, Tartu, 1994, 57–75.
30. Loog, A., Petersell, V. Authigenic siliceous minerals in the Tremadoc graptolitic argillite of Estonia. *Proc. Est. Acad. Sci. Geol.*, 1995, **44**(1), 26–32.
31. Heinsalu, H. Lithostratigraphical subdivision of Tremadoc deposits of North Estonia. *Proc. Acad. Sci. Estonian SSR, Geology*, 1987, **36**(2), 66–78 (in Russian).
32. Raudsep, R. Ordovician. Pakerort Stage. Ceratopyge Stage. In: *Geology and mineral resources of the Rakvere phosphorite-bearing area* (Puura, V., ed.). Valgus, Tallinn, 1987, 29–39 (in Russian).
33. Kaljo, D., Kivimägi, E. On the distribution of graptolites in the Dictyonema shale of Estonia and the noncontemporaneity of its different facies. *Proc. Acad. Sci. Estonian SSR, Chem., Geol.*, 1970, **19**(4), 334–341 (in Russian).
34. Kiipli, T., Batchelor, R. A., Bernal, J. P., Cowing, C., Hagel-Brunnström, M., Ingham, M. N., Johnson, D., Kivisilla, J., Knaack, C., Kump, P., Lozano, R., Michiels, D., Orlova, K., Pirrus, E., Rousseau, R. M., Ruzicka, J., Sandström, H., Willis, J. P. Seven sedimentary rock reference samples from Estonia. *Oil Shale*, 2000, **17**(3), 215–223.
35. Utsal, K., Kivimägi, E., Utsal, V. About the method of investigating Estonian graptolitic argillite and its mineralogy. *Acta et Commentationes Universitatis Tartuensis*, No. 527, Tartu, 1982, 116–136 (in Russian).
36. Loog, A., Kurvits, T., Aruväli, J., Petersell, V. Grain size analysis and mineralogy of the Tremadocian Dictyonema shale in Estonia. *Oil Shale*, 2001, **18**(4), 281–297.
37. Kleesment, A.-L., Kurvits, T. U. Mineralogy of Tremadoc graptolitic argillites of North Estonia. *Oil Shale*, 1987, **4**(2), 130–138 (in Russian).

38. Snäll, S. Mineralogy and maturity of the alum shales of south-central Jämtland, Sweden. *Sveriges Geologiska Undersökning (SGU)*, 1988, Serie C, **818**, 1–46.
39. Taylor, S. R., McLennan, S. M. *The Continental Crust: its Composition and Evolution*. Blackwell Scientific Publication, Oxford, 1985.
40. Gromet, L. P., Dymek, R. F., Haskin, L. A., Korotev, R. L. The “North American shale composite”: its compilation, major and trace element characteristics. *Geochim. Cosmochim. Ac.*, 1984, **48**, 2469–2482.
41. Holland, H. D. Metals in black shales – A reassessment. *Econ. Geol.*, 1979, **74**, 1676–1680.
42. Coveney, R. M. Jr., Glascock, M. D. A review of the origins of metal-rich Pennsylvanian black shales, central U.S.A., with an inferred role for basinal brines. *Appl. Geochem.*, 1989, **4**(4), 347–367.
43. Yu, B., Dong, H., Widom, E., Chen, J., Lin, C. Geochemistry of basal Cambrian black shales and cherts from the Northern Tarim Basin, Northwest China: Implications for depositional setting and tectonic history. *J. Asian Earth Sci.*, 2009, **34**(3), 418–436.
44. Leventhal, J. S., Hosterman, J. W. Chemical and mineralogical analysis of Devonian black-shale samples from Martin County, Kentucky; Carroll and Washington counties, Ohio; Wise County, Virginia; and Overton County, Tennessee, U.S.A. *Chem. Geol.*, 1982, **37**(3–4), 239–264.
45. Peacor, D. R., Coveney, R. M. Jr., Zhao, G. Authigenic illite and organic matter: the principal hosts of vanadium in the Mecca Quarry shale at Velpen, Indiana. *Clay. Clay Miner.*, 2000, **48**(3), 311–316.
46. Calvert, S. E., Pedersen, T. F. Geochemistry of recent oxic and anoxic marine sediments: Implications for the geological record. *Mar. Geol.*, 1993, **113**(1–2), 67–88.
47. Nameroff, T. J., Balistrieri, L. S., Murray, J. W. Suboxic trace metal geochemistry in the Eastern Tropical North Pacific. *Geochim. Cosmochim. Ac.*, 2002, **66**(7), 1139–1158.
48. Morford, J. L., Emerson, S. The geochemistry of redox sensitive trace metals in sediments. *Geochim. Cosmochim. Ac.*, 1999, **63**(11–12), 1735–1750.
49. Chester, R. *Marine Geochemistry*. Blackwell, London, 2000.
50. Nijenhuis, I. A., Bosch, H.-J., Sinnighe Damsté, J. S., Brumsack, H.-J., De Lange, G. J. Organic matter and trace element rich sapropels and black shales: a geochemical comparison. *Earth Planet. Sc. Lett.*, 1999, **169**(3–4), 277–290.
51. Brumsack, H.-J. The trace metal content of recent organic carbon-rich sediments: implications for Cretaceous black shale formation. *Palaeogeogr. Palaeoclimatol.*, 2006, **232**(2–4), 344–361.
52. Kochenov, A. V., Baturin, G. N. The paragenesis of organic matter, phosphorus and uranium in marine sediments. *Lithology and Mineral Resources*, 2002, **37**(2), 107–120.
53. Grimmer, J. C., Greiling, R. O. Serpentinites and low-K island arc meta-volcanic rocks in the Lower Köli Nappe of the central Scandinavian Caledonides: Late Cambrian – early Ordovician serpentinite mud volcanoes in a forearc basin? *Tectonophysics*, 2012, **541–543**, 19–30.
54. Quinby-Hunt, M. S., Wilde, P., Orth, C. J., Berry, W. B. N. The provenance of low-calcic black shales. *Miner. Deposita*, 1991, **26**(2), 113–121.

55. Rudnick R. L., Gao, S. Composition of the continental crust. In: *Readings from the Treatise on Geochemistry* (Holland, H. D., Turekian, K. K., eds.). Elsevier, Amsterdam, 2010, 131–198.
56. Lev, S. M., McLennan, S. M., Hanson, G. N. Mineralogic controls on REE mobility during black-shale diagenesis. *J. Sediment. Res.*, 1999. Vol. 69. P. 1071–1082.
57. Cruse, A. M., Lyons, T. W., Kidder, D. L. Rare-earth element behavior in phosphates and organic-rich host shales: An example from the Upper Carboniferous of Midcontinent North America. In: *Marine Authigenesis: From Global to Microbial* (Glenn, C. R., Prévôt-Lucas, L., Lucas, J., eds.), SEPM Special Publication, 2000, **66**, 445–453.
58. Lev, S. M., Filer, J. K., Tomascak, P. Orogenesis vs. Diagenesis: Can we use organic-rich shales to interpret the tectonic evolution of a depositional basin? *Earth Sci. Rev.*, 2008, **86**(1–4), 1–14.
59. Somelar, P., Kirsimäe, K., Hints, R., Kirs, J. Illitization of Early Paleozoic K-Bentonites in the Baltic Basin: decoupling of burial- and fluid-driven processes. *Clay. Clay Miner.*, 2010, **58**(3), 388–398.

Presented by J. Boak

Received October 30, 2012

2. Hints, Rutt; Hade, Sigrid; Soesoo, Alvar; Voolma, Margus (2014). Depositional framework of the East Baltic Tremadocian black shale revisited. *GFF*, 136, 464 - 482.

Depositional framework of the East Baltic Tremadocian black shale revisited

RUTT HINTS, SIGRID HADE, ALVAR SOESOO and MARGUS VOOLMA

Hints, R., Hade, S., Soesoo, A. & Voolma, M., 2014: Depositional framework of the East Baltic Tremadocian black shale revisited. *GFF*, Vol. 00 (Pt. 1,), pp. 1–19. © Geologiska Föreningen. doi: <http://dx.doi.org/10.1080/11035897.2013.866978>.

Abstract: This article presents a centimetre- to micrometre-scale study of sedimentary fabrics from Lower Ordovician metalliferous black shale from the Baltic palaeobasin. Two sections of the Türisalu Fm. NW and NE Estonia were analysed with light microscopy and scanning electron microscopy. This rock unit is characterised by mostly thin bedding (<10 mm), common occurrence of minor erosional features, and a large variety of sedimentary fabrics, including graded, cross-laminated and massive fabrics. Based on this, we suggest that dynamic sedimentation events, rather than commonly assumed slow net sedimentation, may be the dominant mechanism behind the accumulation of these beds. The storm-related near-bottom flows and the bed-load transport of mud particles were likely common distribution agents of organic-rich mud. The mud (re)distribution, mainly via near-bottom flows and controlled by flat seafloor topography and general clastic starvation, might explain the present lateral distribution and diachronous character of the Türisalu Fm. Documented traces of microbial mat growth and siliceous sponges in the NW Estonia indicate that in more sheltered settings, biogenic factors played a vital role in developing primary mud characteristics. The geochemical palaeoredox proxies, and high trace metal and organic matter content suggest that mud sedimentation could occur under anoxic conditions. The observed sedimentary fabrics and traces of bioturbation, however, favour prevailing oscillating redox conditions in the lower water column. The recorded heterogeneity of microfossils indicates that dynamic transport and intermittent deposition together with biogenic factors likely forced the development of an array of unique (bio)geochemical microenvironments for syngenetic trace element sequestration.

Keywords: black shale; sedimentary fabrics; Türisalu Fm.; event sedimentation; microbial mat; trace elements.

Institute of Geology at Tallinn University of Technology, Ehitajate tee 5, 19086 Tallinn, Estonia; Rutt.Hints@ttu.ee, sigrid.hade@gmail.com, Alvar.Soesoo@gi.ee, Margus.Voolma@gi.ee
Manuscript received 12 July 2013. Revised manuscript accepted 14 November 2013.

1. Introduction

Distal deep marine settings with stratified water columns were long considered a unique environment of black shale formation, and accumulation processes were envisioned as a slow, continuous net sedimentation of fine-grained organic and inorganic particles from a starved, persistently anoxic water column, which resulted in the formation of finely laminated mud intervals (Potter et al. 1980). Reports of shallow-water marginal black shales from many locations (e.g. Leckie et al. 1990; Schieber 1994; Wignall & Newton 2001), as well as the accumulation of a wealth of data in the modern marine research of organic-rich muds and their ancient analogues (e.g. Ganeshram et al. 1999; Lyons & Kashgarian 2005), in modern and ancient mud sedimentology and mudstone lithology (e.g. Traykovksi et al. 2000; Schieber et al. 2007; Macquaker et al. 2010a; Ghadeer & Macquaker 2011; Plint et al. 2012), advances in experimental mud research (e.g. Baas et al. 2011; Schieber 2011 and references there in) and in organic-rich mudstone geochemistry (e.g. Algeo & Maynard 2004), organic geochem-

istry (e.g. Blumenberg & Wiese 2012) and geobiology (e.g. Pacton et al. 2007) have revealed that many variable formation paths might have produced different black shales. Those discoveries indicate that organic-rich mud intervals might form under an agitated water column in shallow settings (e.g. Schieber 1994), and they in places contain event beds, erosion surfaces and other signs of a discontinuous sedimentary record (e.g. Schieber & Yawar 2009). Likewise, the occurrence of black shale does not necessarily reflect a permanently anoxic water column (e.g. Pedersen & Calvert 1990; Murphy et al. 2000; Schovsbo 2001; Egenhoff & Maletz 2012), and typical fossil black shales can contain various signs of benthic life (e.g. Kazmierczak et al. 2012).

The new discoveries allow us to revisit some of the controversial aspects of the sedimentary framework of the black shales that have long been known in Estonian Tremadocian succession. Those organic-rich and metalliferous black shales, formed in proximal settings of the vast

epicontinental sea of the Baltica palaeocontinent during an overall eustatic sea-level rise (Dronov et al. 2011), have been mainly described as shallow-water deposits (e.g. Scupin 1922; Kivimägi & Loog 1972), which accumulated in water depth near storm wave base (e.g. Heinsalu 1990; Artyushkov et al. 2000). In basin scale, Schovsbo (2002) places Estonia within the inner-shelf environment of the Cambrian–Tremadocian black shales, i.e. to innermost and shallowest area of black shale formation in the Baltic palaeobasin. However, a considerably deeper water origin of more than 130 m has been suggested by some researchers for considered black shales (e.g. Pukkonen & Rammo 1992). The previous studies have indicated spatial regional-scale lithological heterogeneity and facies differences of the Türisalu Fm. between western and north-eastern Estonian settings, as well as the existence of small-scale lithological features, such as the random occurrence of cross-lamination, small ripple marks, irregular silt intercalations, traces of bioturbation and benthic sessile communities (Müürisepp 1964; Kaljo & Kivimägi 1970; Kivimägi & Teedumäe 1971; Kivimägi & Loog 1972; Heinsalu 1990; Pukkonen & Rammo 1992; Loog & Petersell 1995). However, the sedimentary framework behind those lithological features remains poorly understood. Recently, submillimetre- to millimetre-scale vertical lithological heterogeneity has been recognised as a common feature in a wide variety of mudstones, including organic-rich mudstones (Aplin & Macquaker 2011 and references there in). In the case of the Türisalu Fm., the existence of pronounced spatial and subtle decimetre-scale vertical trace metal variability has been documented (Pukkonen & Rammo 1992; Soesoo & Hade 2012; Voolma et al. 2013). Whereas the syngenetic enrichment of redox-sensitive trace metals is a widely accepted pathway for metal sequestration in typical black shales (e.g. Algeo & Maynard 2004), the enrichment models are commonly based on the generalisation that sedimentation rates of primary mud remained constant over long periods, thus suspension–re-deposition of sediments and bioturbation are negligible according to their accumulation, and the physicochemical character of primary mud was not notably variable. Such simplifications, however, might not be appropriate for interpreting enrichment processes in shallow-water marginal black shales.

This article is based on the analysis of micrometre- to centimetre-scale fabrics of two sections from the Baltic Klint area, both representing the proximal settings of the Türisalu Fm. on Estonian territory. The aims of the study were to (1) document the vertical variability of small-scale sedimentary fabrics in the Türisalu Fm., (2) discuss a possible accumulation dynamics (physical factors) and the biogenic factors forming the observed fabrics, (3) outline the main features of sedimentary environment of ancient mud successions based on combined lithological and geochemical palaeoredox signals and (4) examine the possible influence of sedimentary dynamics and syndimentary biogenic processes on organic matter (OM) and trace metal sequestration processes.

2. Geological background

The black shale of the Türisalu Fm. (historically known as *Dictyonema* shale or *Dictyonema* argillite, also the term “graptolite argillite” is widely used in recent local literature) is an organic-rich black shale that formed in the proximal settings of the Baltic palaeobasin in the Early Ordovician (Männil 1966) when Baltica was at approximately 40–50° southern latitudes

(Fig. 1A and B) (Cocks & Torsvik 2005). Between Mid-Cambrian and Early Ordovician, the Baltica made through anti-clockwise rotation. At the beginning of Tremadocian, Baltic palaeobasin was situated at western margins of the continent, facing the Iapetus Ocean in the west and the Tornquist Sea in the south and south-west (Cocks & Torsvik 2005). On a regional scale, the Türisalu Fm. is part of a patchy (modern distribution) but vast Mid-Cambrian–Lower Ordovician black shale belt in the Baltoscandian region, extending in the east–west dimension from Lake Onega to Jutland (Andersson et al. 1985; Kaljo et al. 1986). It was accumulated in a large, exceptionally flat-floored epicontinental sea (Nielsen & Schovsbo 2011). Nielsen & Schovsbo (2006) considered the Estonian and Russian Tremadocian black shale to be a shallow-water tongue of the Alum Shale Fm. In Estonia, the almost flat-lying Türisalu Fm. occurs within the tectonically undisturbed lower Palaeozoic sedimentary succession, and the entire Palaeozoic sedimentary complex is generally characterised by very low thermal maturity (Kirsimäe et al. 1999). Its distribution in Estonia and Russia has been considered one of the best examples of very shallow-marine near-shore Cambrian and Early Ordovician deposits with siliciclastic sedimentation (Kaljo et al. 1986; Mens & Pirrus 1997; Artyushkov et al. 2000).

Dark-brown black shale of the Türisalu Fm., which contains fossilised fragments of early planktonic graptolites, is characterised by high OM content ranging from 10% to 20%, fine silt fraction dominating the composition and variable pyrite abundance (Kaljo & Kivimägi 1970; Loog et al. 2001). Another characteristic feature of the black shale is its high but spatially variable content of redox-sensitive trace elements, such as V, U and Mo, showing general positive covariance with OM abundance (Pukkonen & Rammo 1992). In Estonia, the thickness of the formation remains between 1 and 8 m, generally decreasing eastward and southward from the area of maximum thickness in north-western Estonia. The Türisalu Fm. occurs on top of a complex of commonly cross-bedded siltstone and sandstone (Kallavere Fm.) containing debris or rich coquinas of phosphatic brachiopods denoting a large-scale skeletal phosphorite accumulation episode during the Cambrian–Ordovician transition (Ilyin & Heinsalu 1990; Hiller 1993). These siliciclastic deposits also contain interbeds and lenses of black shales. In NW Estonia, a thick organic-rich mudstone bed caps a subaerial regional unconformity at the base of the transgressive Kallavere Fm. (Nemliher & Puura 1996). In NE Estonia, the black shale overlies the siliciclastic beds of the Kallavere Fm., presenting dense interfingerings of siltstone with phosphatic detritus and organic-rich mudstone beds (Heinsalu et al. 2003). The onset of accumulation of primary organic-rich muds of the Türisalu Fm. across Estonia was not concurrent (Kaljo & Kivimägi 1970) (Fig. 1C). The older black shales in western Estonia belong to the *Cordylodus lindstromi/angulatus* conodont biozones (Pakerort Regional Stage). Eastwards the black shales become gradually younger, and in NE Estonia, the succession is assigned to the *Paltodus deltifer pristinus* conodont zone (Varangu Regional Stage; Kaljo et al. 1986; Heinsalu et al. 2003). The Varangu age generally denotes a major regressive episode in the region (e.g. Dronov et al. 2011). The upper boundary of the Türisalu Fm. comprises a regional unconformity that is capped by organic-poor grey shales or glauconitic sandstones (Heinsalu 1980) and marks a sea-level drop that terminated organic-rich mud accumulation in the proximal settings of the Baltic palaeobasin.

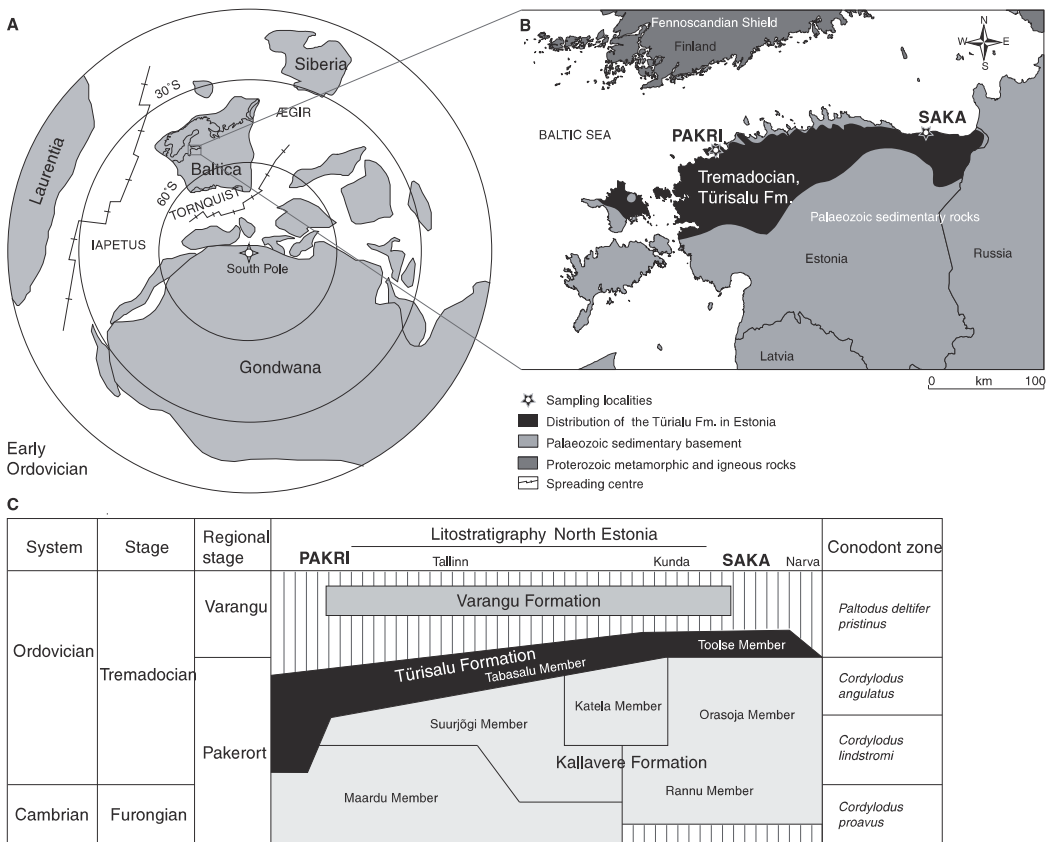


Fig. 1. A. Palaeogeography of Baltica in the Early Ordovician (after Cocks & Torsvik 2005). B. Modern distribution of the Türişalu Fm. and sampling localities on Baltic Klint. C. Lithostratigraphy of the Tremadocian deposits of Estonia (after Heinsalu et al. 2003).

Lithology and facies of the Türişalu Fm. have been targeted by several studies, including Mürişsepp (1960), Kaljo & Kivimägi (1970), Kivimägi & Teedumäe (1971), Heinsalu (1980) and Heinsalu (1990). In western and north-central Estonia, the Türişalu Fm. has been described as a considerably homogeneous black shale comprising laminated or massive lithologies (Tabasalu Member). The massive black shale varieties that are dominant in somewhat younger north-central Estonian settings have supposedly accumulated under more active hydrodynamic regime than the beds in the western settings (Pukkonen & Rammo 1992). However, Heinsalu (1990) reported irregular encounters of cross- and wavy-lamination, trace fossils and minor ripple marks in older western Estonian black shales. In NE Estonia, the Türişalu Fm. becomes thinner and more variable (Toolse Member). It embodies numerous silt intercalations that are regularly associated with authigenic carbonate or sulphide mineralisation, and the entire Türişalu Fm. has been suggested to represent a shallower-water setting and a more variegated sedimentation environment than represented by the Tabasalu Mb. (Kaljo & Kivimägi 1970; Kivimägi & Loog 1972; Loog et al. 2001). For example, in the Toolse area, the Türişalu Fm. was divided into four distinct intervals with different textural

and structural characteristics and trace metal content (Kivimägi & Teedumäe 1971). Furthermore, Heinsalu et al. (1994) suggested that the areas around Toolse and Rakvere (Rakvere Phosphorite Area) acted as a border zone between subenvironments with different hydrodynamic regimes in this proximal part of the palaeobasin during the Early Tremadocian and that subaerial highs likely existed in this shallow-water area before a main organic-rich mud accumulation episode.

In the rather homogenous mineral assemblages of the Türişalu Fm., K-feldspar has been found to be dominant over quartz, illite–smectite and illite (Utsal et al. 1982; Kleesment & Kurvits 1987; Loog & Petersell 1995; Loog et al. 2001). High K-feldspar content is the characteristic feature of the Türişalu Fm., distinguishing the complex from the typical Alum Shale Fm. in which K-rich clay minerals (illite and illite–smectite) tend to dominate in mineral assemblages, and which have been reported to present generally lower K_2O/Al_2O_3 molar ratio than Tremadocian black shales from Estonia (Snäll 1988; Lindgreen et al. 2000; Schovsbo 2003). It is remarkable that substantial amounts of K-feldspar in the Türişalu Fm. is likely authigenic in origin (Utsal et al. 1982; Loog et al. 2001; unpublished data). For quartz, a genetic link with primary biogenic silica has been

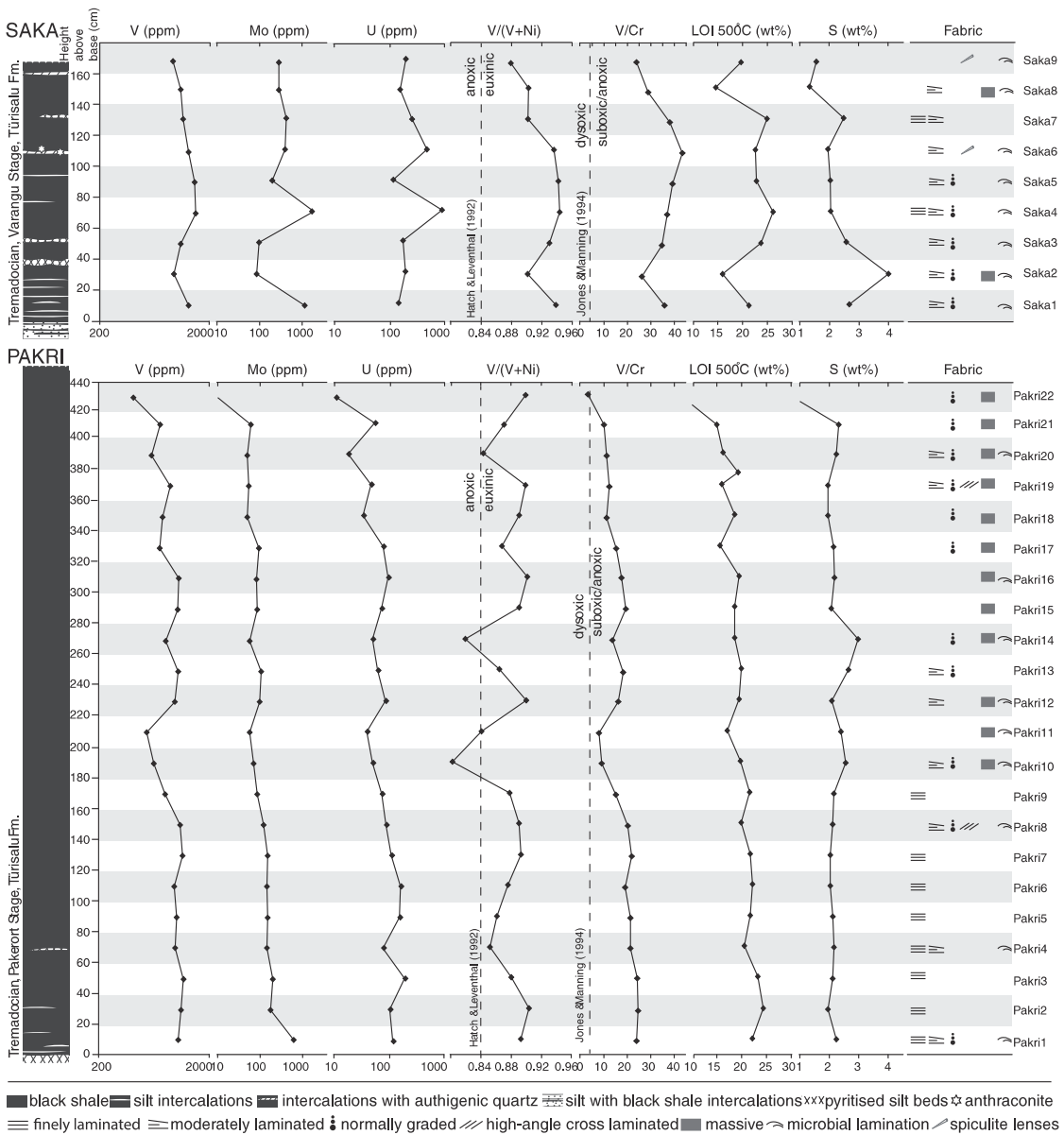


Fig. 2. The cross-section of the Saka and Pakri sections, with sampling intervals, vertical profiles of redox-sensitive trace elements, palaeoredox proxies (after Hatch & Leventhal 1992; Jones & Manning 1994), environmental indices based on data by Voolma et al. (2013) and observed sedimentary fabrics.

suggested in NE Estonia, where lenticular intercalations of siliceous sponges are common (Müürisepp 1964; Loog & Petersell 1995). The OM of the Türisalu Fm. is N-rich, highly aromatic and, according to previous studies, composed dominantly of transformation–condensation products of marine microbial matter (Klesment & Urov 1980; Sumberg et al. 1990;

Lille 2003). From other biogenic components, early planktonic graptolites, fragments of phosphatic lingulid brachiopods, conodonts, acritarchs and polychaete jaws have been reported (e.g. Kaljo & Kivimägi 1970; Kaljo et al. 1986; Paalits 1995; Hints & Nölvak 2006). A characteristic of the Türisalu Fm. is the absence of calcareous fossils.

3. Materials and methods

This study is based on two sections of the Türisalu Fm. from the Saka Cliff (59.4419°N, 27.2150°E) and the Pakri Peninsula Uuga Cliff (59.3766°N, 24.0364°E). Thick and rather homogeneous Pakri section (Pakerort Stage, Türisalu Fm. and Tabasalu Member (after Mens et al. 1996)) represents transitional black shale setting between western Estonian considerably organic- and metal-rich and the more massive and trace metal poor northern central Estonian settings (cf. Heinsalu 1990; Pukkonen & Rammo 1992). The lithologically more variable Saka section is part of the heterogeneous NE Estonian Toole Member (Varangu Stage, Türisalu Fm. and Toole Member (after Heinsalu et al. 2003)) and is known to contain abundant lenses of siliceous spicules and small anthraconites (Müürisepp 1964).

For this study, the Pakri and Saka sections were sampled at 20-cm intervals. From each collected field sample, approximately half was crushed and homogenised for major and trace element analyses (Voolma et al. 2013). The rest was used for lithological study. For fabric analysis presented in this article, five to seven subsamples from every field sample were selected randomly, cut perpendicular to bedding and roughly polished. The polished surfaces of the subsamples were scanned with a high-resolution flatbed scanner and studied with a light microscopy (Leica M205 A) to establish small-scale fabrics and stacking successions. In selected subsamples, the morphology of bedding planes was also studied on surfaces that were fractured parallel to bedding. Microfabric study and microanalyses of selected samples from both sections were carried out with a scanning electron microscopy (SEM) (Zeiss EVO MA15) equipped with EDS (Oxford INCA) at the Institute of Geology at Tallinn University of Technology. Fig. 2 presents schematic sections of both study locations, sampling intervals together with enriched trace metal profiles, and some commonly used geochemical palaeoredox and environmental indices based on data of Voolma et al. (2013). Note that the geochemical data are results of analyses of homogenised whole-rock samples, each representing average chemical composition of 20 cm long interval of studied sections. The presented loss on ignition (LOI, at 500°C) values can be used as rough estimates of the OM content. Fig. 2 also summarises the main fabric types recorded in both sections. The studied samples and data are deposited at the Institute of Geology at Tallinn University of Technology.

4. Observations

4.1 Small sedimentary fabrics

The examination of samples from the Pakri and Saka sections demonstrated the existence of submillimetre-to-centimetre range vertical in homogeneity of the black shale. Based on variations in bed thickness and continuity, lamination and bedding boundary characteristics, and the existence of grading and biogenic features, a number of distinct black shale varieties with dominant sedimentary-fabric types were distinguished. However, the listed varieties do not cover the complete array of encountered fabrics, as in several cases beds with mixed characteristic features, or the later overprinting (e.g. diagenetic growth of carbonate concretions and secondary gypsum) of primary fabrics was observed. The samples from both sections were mostly organised into rather thin beds with a common thickness of less than 10 mm. The bed boundaries were traceable by thin silt intercalations or by colour, fabric or macrocomponent contrast between the beds. The thicker

average bed sizes of up to 5 cm (and rarely more) were encountered in the upper portion of the Pakri section, in the part dominated by massive varieties.

4.2 Beds with laminated fabrics

Fig. 3A demonstrates black shale samples with millimetre-scale laminated planar fabric, a characteristic of the lowest organic-rich part of the Pakri section, but encountered also at some levels of the Saka section. Those beds were fine grained and well sorted. The lamination appeared as an alteration of darker, more organic-rich, and lighter, less organic containing thin continuous laminae. However, many finely laminated beds from the studied sections appear to present subtle discontinuous lamination with minor asymmetric mud lenses and uneven bedding surfaces (Fig. 3B). Furthermore, in the case of somewhat less sorted samples, low-angle cross-lamination was observed, showing curved down-dipping laminae or inclined non-parallel bedding surfaces (Fig. 3B–D). Few bedding planes of finely laminated beds from the lower part of the Pakri section revealed poorly preserved remains of *Rhabdinopora* sp. (Pakri 2 and 4).

4.3 Graded beds

In addition to laminated fabrics, graded black shale varieties were regularly encountered in the studied sections. The upward-fining beds recorded in the Türisalu Fm. had typical average thicknesses between 0.5 and 5 mm and were invariably sharp-based with flat or rough basal surfaces, the latter presenting common scour-like structures. The normal graded fabrics were widespread in the Saka section and in the upper part of the Pakri section. The beds with well-pronounced normal grading (Fig. 4A–D) comprised either couplets of silt- and organic-rich lamina sets or, in some cases, exhibited a triplet motive similar to that described by Macquaker et al. (2010a). In some intervals, the lower lamina sets of such graded beds presented distinct curved ripple-laminated fabrics. The proportion of graded beds from the upper part of the Pakri section and a few subsamples from the middle and upper part of the Saka section showed more gradational changes. In those cases, the grading appeared as a decrease in grain size or in the marine detritus content and as a colour shift from light brown to darker brown, indicating an increase in organic fraction in upper part of beds (Fig. 4E). Sharp and flat lower contacts were the characteristics for such beds.

4.4 Cross-laminated beds with soft sediment deformation structures

High-angle cross-laminated black shales with ripple sets were encountered in distinct intervals of the Pakri section (Pakri 8 and 19; Fig. 5A and B). The curved bedding surfaces, as well as abundant soft sediment deformation features, such as load structures, were typical for such beds, indicating sediment loading on uncompacted and water-enriched mud.

4.5 Beds with massive fabrics

The examination of the upper portion of the Pakri section revealed several intervals dominated by massive and thick beds compared with the rest of the section. The observed lithologies varied from isotropic massive fabric to poorly sorted irregular varieties (Fig. 5C and D), the latter containing detritus of phosphatic brachiopods. The other typical features were the absence of erosional features at the bed base, sharp bedding

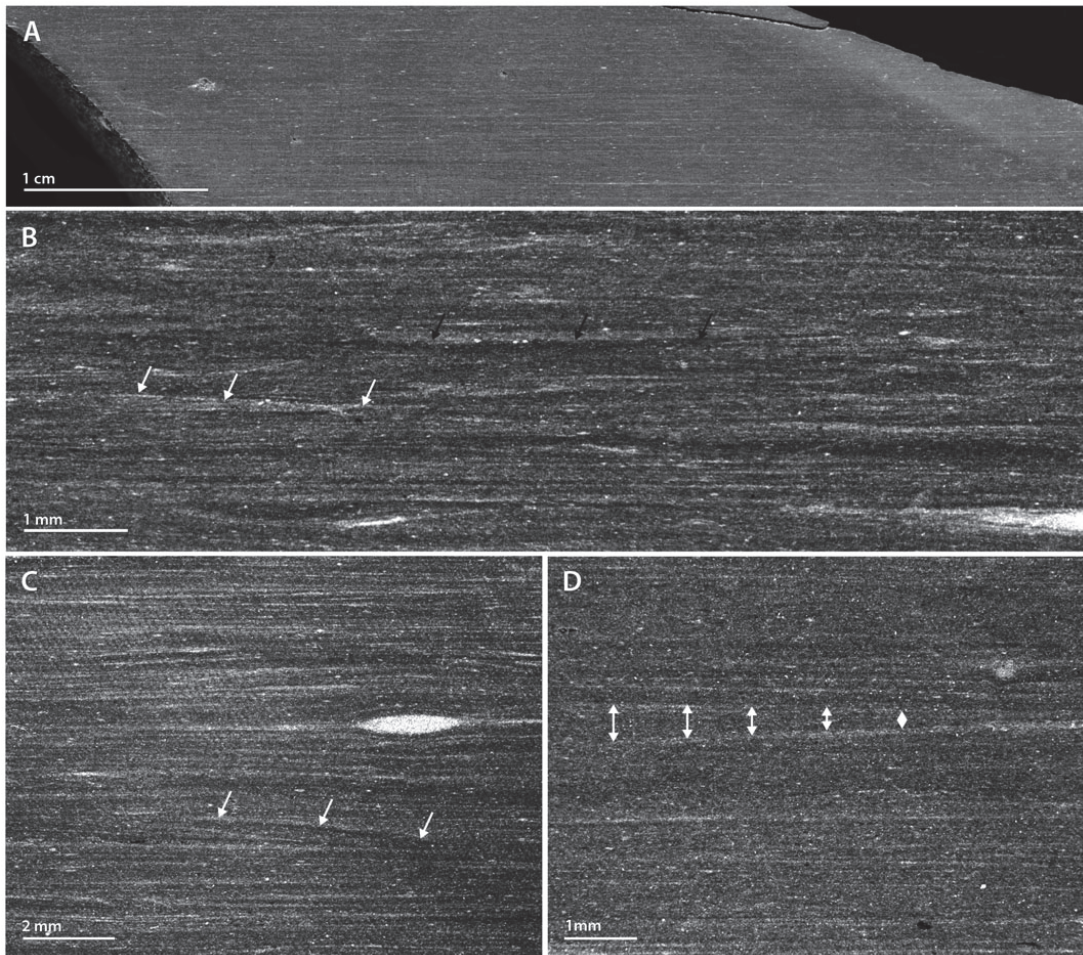


Fig. 3. Scanned image (A) and micrographs (B–D) of small-scale laminated fabrics. **A.** Subsample Pakri 4-1 with finely laminated planar fabric. **B.** Laminated fabric (Pakri 2-1) with subtle non-parallel lamina geometry showing thin, discontinuous black shale laminae (white arrows) and eroded uneven bedding surfaces (black arrows). **C.** Pakri 4-2 exhibits discontinuous fine lenticular lamination; arrows mark down-dipping surface of the possible ripple lamina. **D.** Pakri 9-1 with inclined non-parallel planar bedding boundaries.

boundaries and the irregular thickness distribution of intimately stacked beds. Some massive beds from the middle part of the Pakri section presented different characters with indistinct bedding boundaries and halo zones (see also section on biogenic fabrics).

4.6 Siliciclastic intercalations

The siliciclastic intercalations and lenses with thickness of a few grains to several centimetres were recorded throughout both sections, whereas their frequency was higher in the Saka section. In both sections, the thickest intercalations were confined to the lowermost ~60 cm of the Türisalu Fm. Siliciclastic intercalations were sharp-based and regularly with scoured lower contacts. In addition to angular to subrounded quartz, the thicker studied

intercalation contained variegated sulphide paragenesis, rare glauconitic grains and marine detritus including phosphatic brachiopods and conodonts. Rather typical for the siliciclastic beds of the lower part of the Saka section was the occurrence of well-preserved, coarse euhedral muscovite. In the lower part of the same section, thin silty laminae were occasionally observed on the top of gradational upper contact of black shales beds, whereas grain sizes of silt particles matched with those from the underlying strata.

4.7 Beds with biogenic fabrics (biolamination, spiculite lenses and bioturbation)

The studied sections revealed a number of fabrics, which were likely formed by biogenic factors. Throughout the Saka section

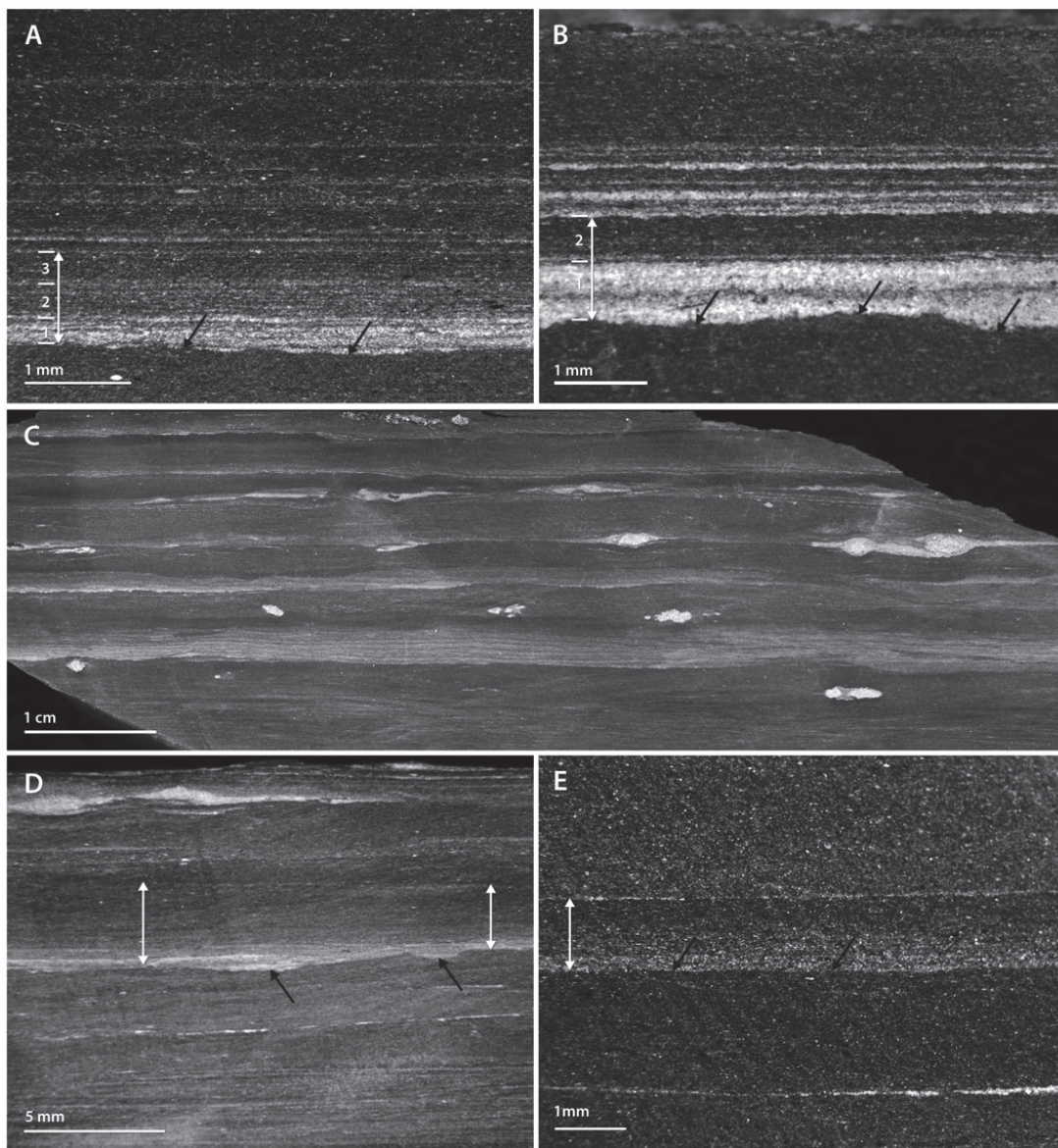


Fig. 4. Micrographs (A, B, D and E) and scanned image (C) of the studied black shales with normal graded fabrics. **A.** Pakri 10-1 presents sharp grading with triple fabric (individual lamina sets of single bed marked by numbers) comprising a lower silt-rich, an intercalated silt-rich and an organic/clay-rich lamina set and upper organic/clay-rich lamina set. Note the irregular surface below the bed (black arrows). **B.** Saka 1-1 presents fabric with a graded appearance, with silt-rich lower and dark organic-rich upper lamina sets (individual lamina sets marked by numbers). Black arrows mark the irregular bedding boundary. **C.** Succession of graded beds of sample OM8-105 from the uppermost half metre of the Pakri section; the lower silt-rich lamina set shows small-scale hummocky cross-lamination. **D.** Pakri 13-1 with graded fabric and scour structures (black arrows) at bedding surface; note the irregular thickness of the graded bed. **E.** Gradually graded bed of Saka 4-1 with smooth lower contact.

and in some intervals of the Pakri section, beds with wavy-crinkly lamination were observed (Fig. 6C–E). They appeared as very dark brown to black, dense, subparallel curved laminae,

best visible at the top lamina set of beds, or as wavy crinkly intercalations in silt interlayers. A different type of supposed biolamination was encountered in some intervals of the Pakri

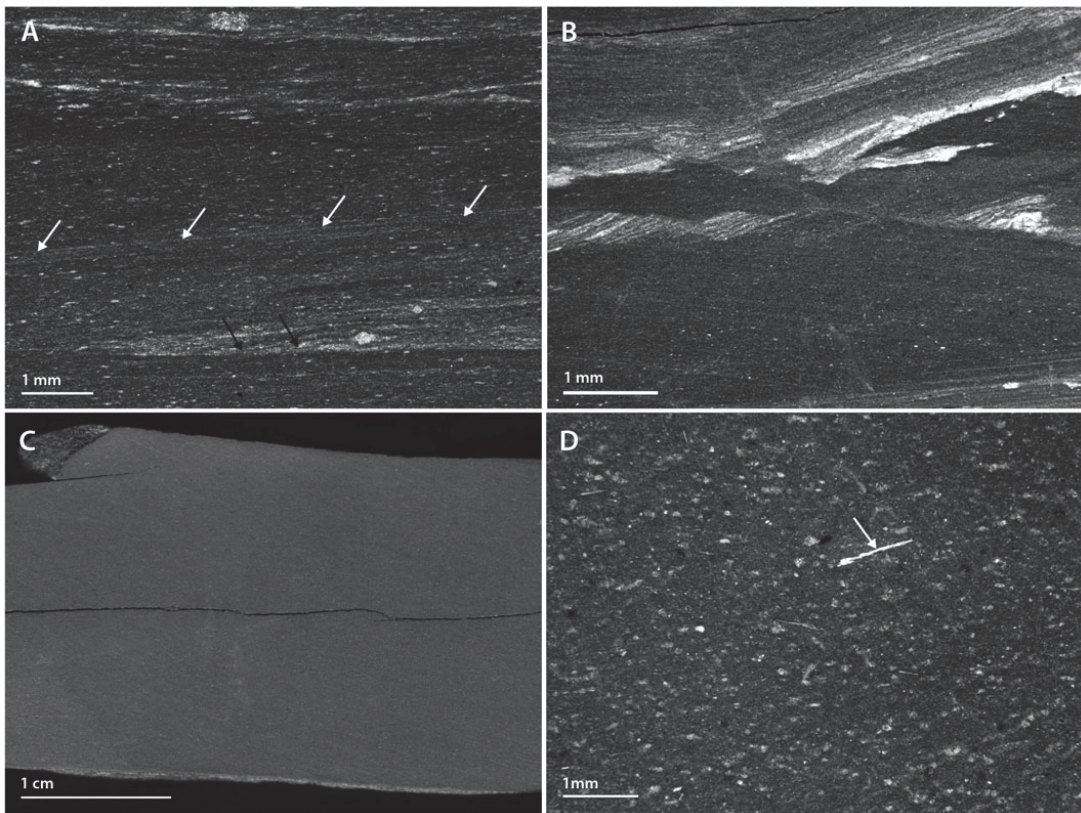


Fig. 5. Micrographs (A, B and D) and scanned image (C) of the black shales with high-angle cross-laminated and massive fabrics. **A.** Subsample Pakri 8-1 exhibits cross-lamination, grading and curved bedding boundaries. Note inclined laminae (white arrows) and down dipping of laminae to the basal surface (black arrow). **B.** Black shale (Pakri 19-1) with ripple sets, grading, curved bedding boundaries and flame structures. **C.** Well-sorted black shale (Pakri 19-2) with featureless massive fabric. **D.** Black shale with massive fabric from Pakri 17-1, white arrow marks the randomly oriented platy fragments in the poorly sorted bed.

section, where firm organic-rich filaments comprised an irregular web in black shale and presented features such as coated mineral grains and vertically oriented filaments (Fig. 6A and B). The additional features of probable biolaminated beds were mica flakes at wavy bed surfaces and the layer-specific distribution of pyrite. In the Saka section, distinctive cross-laminated fabrics were encountered in two intervals in which the thoroughly cross-laminated nature of the beds was traceable thanks to inclined lenses of spicules and quartz (Fig. 7A and B). It is noteworthy that such cross-laminated spicule-rich fabrics occur in an organic-rich and rather metalliferous part of the section (Fig. 2). In the upper part of the Saka section (starting from sample Saka 4), the intercalations commonly comprised rather poor microcrystalline quartz, which is probably a recrystallisation product of biogenic silica (cf. Loog & Petersell 1995). Furthermore, various traces of horizontal bioturbation throughout the studied black shale sections were observed (Fig. 7C–F). At bedding boundaries of finely laminated organic-rich beds of the Pakri section, the pyritised horizontal flattened tubular traces up to a few millimetres thick were occasionally

recorded. The features of the traces resemble those of ichnofossil *Planolites* (e.g. Egenhoff & Fishman 2013). More silty laminated beds and some massive beds in the Pakri section showed discontinuous indistinct lamination, halo zones, partly destroyed probable biolamination, diffused surface boundaries and, less commonly, mottled appearances (see also the massive fabric section). Those fabric elements were likely a product of homogenisation by bioturbation (Fig. 7C and D). In discrete intervals, the Saka section (Saka 6 and 9) yielded rare vertical traces with height of up to a few centimetres, and mottled fabrics, in both cases visible due to the mixing of organic-rich mud, spicules and quartz (Fig. 7E). The observed vertical traces may represent “escape traces” of zoobenthos.

4.8 Microfabrics by SEM

SEM observations were conducted to study how the above-described centimetre- to millimetre-scale features are connected to the micrometre-scale morphology of the deposit. It appears that finely laminated samples (Fig. 8A) are characterised

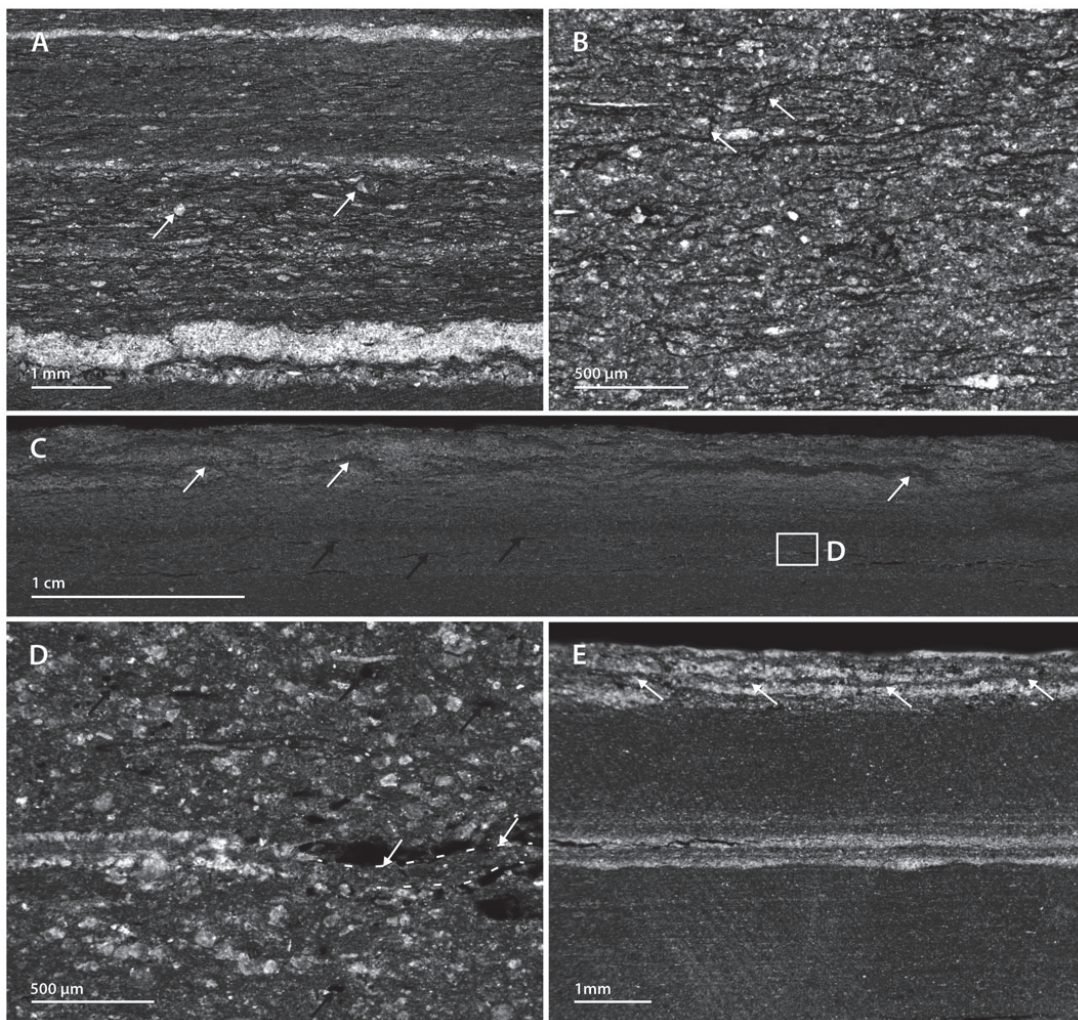
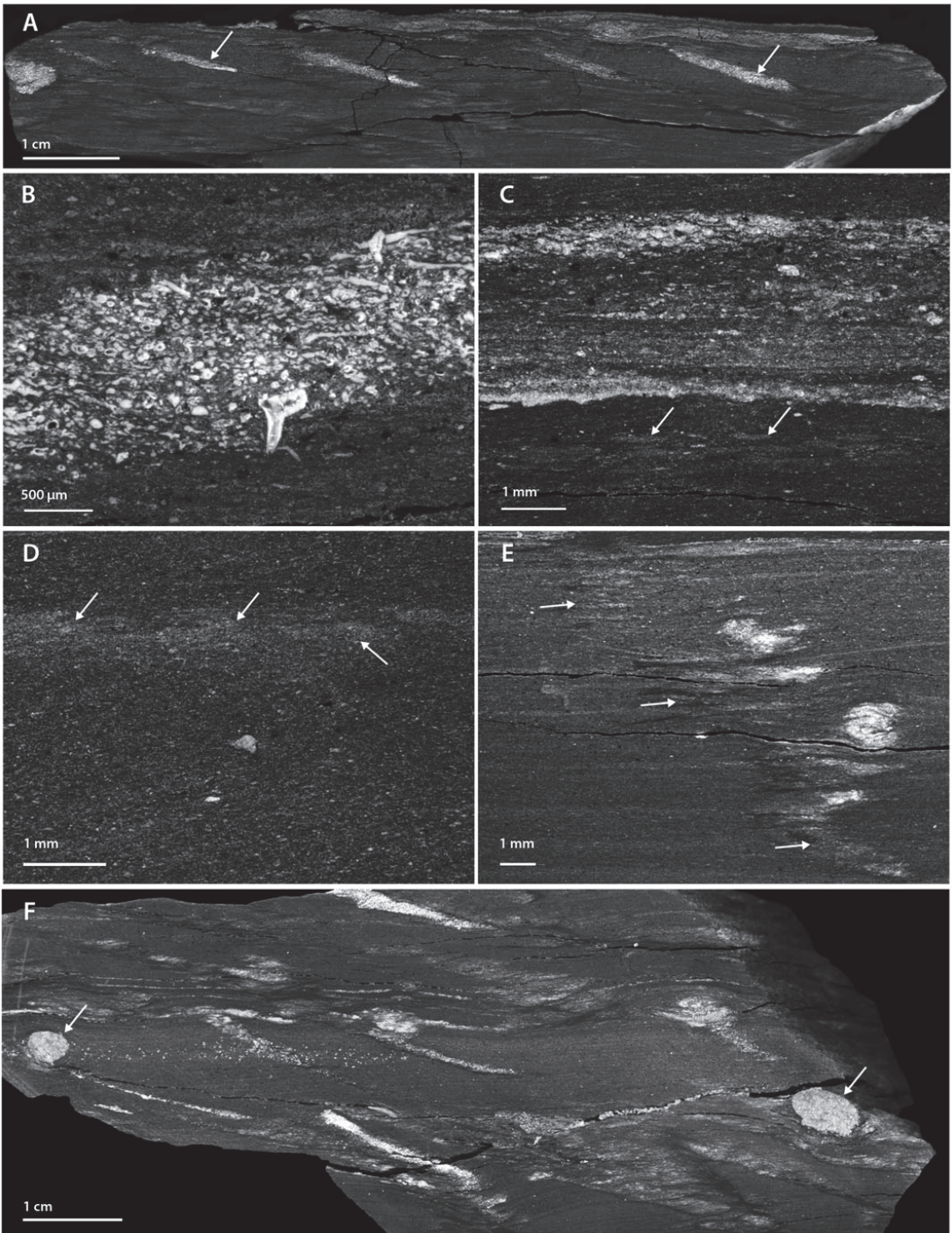


Fig. 6. Micrographs (A, B, D and E) and scanned images (C) of samples with probable biolaminated microfabrics. **A.** Fabric with a dense network of organic-rich laminae in black shale (Pakri 14-1). Arrows mark the grains coated by organic-rich filaments. **B.** Higher magnification micrograph of fabric of Pakri 14-1. Note the widespread occurrence of vertically oriented organic-rich filaments (arrows). **C.** Scanned slab of probable biolaminated fabric of Saka 3-1, with thick wavy slightly upward convex dark organic-rich bands (white arrows) within a lighter matrix. The black arrows mark the elongated pores in less contrast parts of subsample. **D.** Higher magnification micrograph of Saka 3-1. Wavy-crinkly organic-rich lamina (white arrows, dotted lines) in black shale. Note the rather granular character of fabric and large open pores (black arrows). **E.** Series of wavy organic-rich laminae on the top of black shale bed, Saka 4-2.

by anisotropic microfabric with a preferred orientation of platy minerals and bioclastic compounds and evenly distributed regular-size elongated small interparticle micropores (micropores >0.75 μm; pore size classification after Loucks et al. 2009). By contrast, in samples with massive morphology (Fig. 8B), the observed isotropic microfabrics presented a random orientation of mineral platelets and detritus in the matrix and randomly distributed closed interparticle micropores. The probable biolaminated fabrics from the Saka section revealed

heterogeneous and highly porous microfabrics (Fig. 8C) with loosely packed and randomly oriented grains and a connected network of large irregularly shaped micropores. SEM studies of supposed biolaminated samples also indicated the presence of abundant curved, convoluted, folded organic-rich filaments, with thicknesses from less than 1 to several tens of microns (Fig. 8D–F). Some samples revealed convoluted homogenous laminae, or few micrometre-thick layers with laminar structures that most likely are remnants of palynomorphs. The presence of



thicker heterogeneous laminae with bumpy surfaces and uneven thickness distribution was also rather a characteristic for biolaminated samples. The conducted SEM–EDS analysis of such filaments suggested a high carbon content and the presence of Si, Fe, S and Al. Similar organic-rich sheaths, commonly partly mineralised by silica or Fe–Al silicates, have been recognised from different siliciclastic rocks, including black shales, and interpreted as fossilised remnants of microbial mats (e.g. Noffke et al. 2001; Gorin et al. 2009; Kazmierczak et al. 2012).

5. Interpretation of sedimentary fabrics

The finely laminated fabrics in mudstones are traditionally interpreted as products of slow deposition of fine, loose particles or organomineralic aggregates from a generally stagnant water column (Potter et al. 1980) and widely recognised as a characteristic of black shales. Occurrence of finely laminated beds with discontinuous inclined laminae in the Türisalu Fm., however, suggests that such beds were not formed simply by gravitational settling. Similar low-angle cross-laminated fabrics have been recently recognised in several black shales and interpreted as a product of lateral mud accumulation by near-seabed flows (Schieber et al. 2007; Macquaker et al. 2010a; Ghadeer & Macquaker 2011). The flume experiments by Schieber (2011) demonstrated that flocculated clay–silt particles could sustain integrity under high flow speeds and that such flocs could actually move by bed-load transport. Compaction of water-enriched mud ripples has been shown to result in the formation of microlaminated beds, very similar to those found in black shales (Schieber & Yawar 2009). Moreover, research of modern mud dynamics has revealed many quick dispersal mechanisms, some of which could form widespread “event mud blankets”, even in the case of low topographic gradient (e.g. Traykovski et al. 2000). Such mechanisms may involve the formation of sediment-laden unidirectional near-bed flows – eroding, dispersing and depositing the sediments during one and the same flow event (e.g. Macquaker et al. 2010a). Wider acknowledgement that dynamically deposited muds could have been voluminously important in the geologic history of shallow seas has been achieved because of several recent studies of ancient low-gradient mud dominated settings. These investigations indicate that the cross-shelf drift of fine cohesive particles in various settings could have been partly or dominantly driven by short-lived sediment-laden currents (Macquaker et al. 2010a; Plint et al. 2012). The encounter of stacked successions of finely parallel and subtle lenticular laminated fabric in the lower part of the Pakri section indicates that the intermittent advective transport-controlled deposition of mud was likely one of the major mechanisms behind laminated mud accumulation. However, the same interval is also characterised by the high content of OM (LOI 500°C) and V, Mo and U (Voolma et al. 2013; Fig. 2), which designate that the sedimentary environment

should have been favourable for accumulating and preserving biogenic matter and redox-sensitive trace metal enrichment. Based on the recorded fabric characteristics, it is difficult to adequately differentiate the role of suggested dynamic sedimentation and that of slow background suspension settling in the formation of finely laminated muds. Overall, however, the finely laminated beds likely represent a subenvironment with the lowest hydrodynamic energy among the observed black shale varieties of the Türisalu Fm.

Also, other fabrics observed in the Türisalu Fm., such as normally graded and high angle cross-laminated beds, support organic-rich mud formation by sediment-laden flows. Appearance of grading in marine sedimentary record is typically interpreted as deposition in environment where the speed of sediment-loaded current changes over time (e.g. the formation of tempestites). The occurrence of normal grading with distinct lamina sets in studied section of the Türisalu Fm., together with erosional features on the lower bedding surfaces, suggests that those elements are likely products of the same turbulent near-bed flow event (e.g. Macquaker et al. 2010a). Furthermore, the occurrence of ripple-laminated lamina sets in the lower silt-rich lighter part of graded beds clearly points to the bed-load transport of mud particles. Macquaker et al. (2010a) interpreted normally graded beds composed of three distinct lamina sets as products of wave-enhanced sediment gravity flows. Importantly, such combined flows do not require steep slopes like typical turbidites, but can progress in low-gradient shallow settings thanks to energy derived from orbital motion of surface waves, which help to maintain sediment in suspension (Traykovski et al. 2000; Macquaker et al. 2010a). Dynamically deposited mudbeds with thicknesses comparable to those observed in the Türisalu Fm. have been attributed to low-density diluted flows with sediment loads of 1–10 g/l (Mackay & Dalrymple 2011). On the other hand, the absence of erosional features below beds with more gradational grading also observed in the Türisalu Fm., coupled with mostly rather silty composition of such beds, could indicate that the primary mud settled from a suspended sediment (storm) cloud during considerably short time intervals. The observed high-angle cross-laminated fabrics in the Türisalu Fm. unequivocally point to high-energy sedimentation event most likely controlled by surface storm waves. The accompanying soft sediment deformation features in such beds suggest rapid sediment loading on seabed, whereas resistance of those fabrics to later compaction indicates the general grain supported nature of the primary sediments.

Deciphering of formation of observed massive fabrics is more problematic as different pathways and sedimentary settings can lead to formation of massive fabrics in mudstones. Massive varieties could appear as products of the simple gravitational settling of fluidised mud, deposition from fluid mud flows, products of settling from a suspended sediment cloud in slack shallow-water settings (e.g. Traykovski et al. 2000; Baas & Best 2002; Ichnas & Dalrymple 2009; Mackay & Dalrymple 2011) or as products of post-sedimentary homogenisation by bioturbation.

Fig. 7. Micrographs (B, C, D and E) and scanned image (A and F) of beds with lenses of spiculite and traces of bioturbation. **A.** Thorough cross-lamination of the black shale (Saka 6-1) is traceable thanks to inclined lenses of spicules of siliceous sponges (white arrow). **B.** Close-up of Saka 6-1 presenting the detail of spicule-rich lens. **C.** Black shale (Pakri 16-1) shows low-contrast burrow mottled fabric in its lower part (arrows). **D.** Massive bed of Pakri 12-1 with a lighter halo zone (arrows). **E.** Vertical trace (arrows) in subsample Saka 6-2. **F.** Black shale (Saka 9-2) with composite spicules cross-laminated and partly biturbated fabric with pyritised traces (arrows).

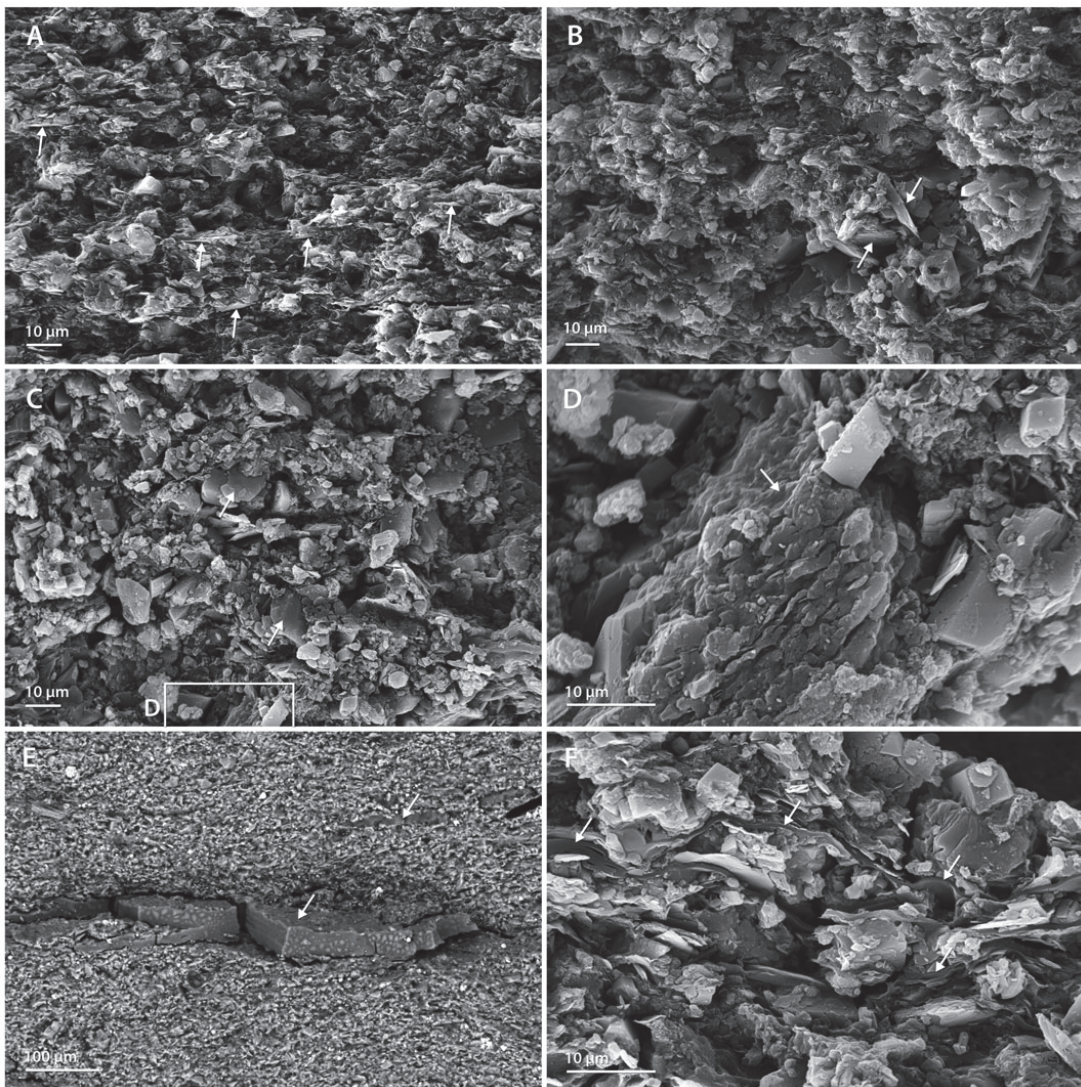


Fig. 8. Representative secondary (A–D and F) and backscattered electron (E) images of microfabrics. **A.** Microfabric of finely laminated bed (Pakri 4). Note the preferred planar parallel orientation of platy particles (arrows). **B.** Microfabric of massive black shale (Pakri 20) presents irregular orientation of large platy mineral particles (arrows). **C.** Biolaminated microfabric (Saka 3) with random orientation of mineral grains (white arrows) and OM laminae. **D.** Detail from image C with thick partly mineralised organic-rich lamina in the centre (white arrow). **E.** Microfabric of black shale (Saka 2) presenting thick partly mineralised organic-rich laminae (arrows) interpreted as remnants of microbial mat. **F.** Thin organic-rich convoluted laminae (arrows) of problematic biogenic origin (Saka 3).

tion. The preservation of sharp bedding surfaces in studied black shale samples suggests that the major part of observed massive fabrics in the Türisalu Fm. are likely primary sedimentary features and might thus reflect an accumulation of mud in an environment that was shallow enough to support surficial mud fluidisation by storm waves. However, as shown by studies of modern muddy shallow-marine areas like the Eel river shelf

(Traykovski et al. 2000; Macquaker et al. 2010a), the massive fabrics in mud might be as well produced by deposition from dense fluid mud flows, which on the Eel river shelf act as the major agents of offshore transport of cohesive flood sediments. In the case of the Türisalu Fm., considerably immature siliciclastic fresh input into palaeobasin and proximity of terrestrial feeding systems of sediment supply could be argued

based on the heterolithic character of Lower Tremadocian successions and by the abundance of both mica flakes and subangular quartz in siliciclastic intercalations in the studied black shale sections. Those intercalations are traditionally considered to be products of distal storm flows, which very infrequently disturbed the otherwise tranquil environment of black shale accumulation (e.g. Heinsalu 1990). However, as suggested by our study, both siliciclastic intercalations and shale beds likely originated from sediment-laden wave-aided flows, which plausibly controlled cohesive sediment dispersal in the inner-shelf settings of the Tremadocian epicontinental palaeobasin. Gradational silty upper contact of black shale beds observed in the Saka section suggests that additionally to deposition by the storm flows, the winnowing of surface mud by bottom currents could also cause the formation of the observed silty laminae.

Besides physical factors which controlled the accumulation of black shales of the Türisalu Fm., biogenic processes had considerable role on the final character of those beds. Carbon-rich wrinkled structures, similar to those observed in the Saka section have been documented in different siliciclastic rocks including mudstones (e.g. Schieber 1999) starting from Archean (e.g. Noffke 2009). These features have been interpreted as recalcitrant remnants of benthic microbial mats, supposedly produced by phototrophic bacteria, encapsulated into thick films of extracellular polymeric substances (EPSs) or by more complex multitrophic microbial consortia (e.g. Gorin et al. 2009). EPS is a general term for sticky substances composed dominantly of polysaccharides and secreted by different types of microorganisms (e.g. Decho 1990). The EPS-rich microbial mats are found to be typical for high-energy well-lit shallow-water environments, whereas EPS has a considerable role in biostabilisation of mat-covered seabed (e.g. Noffke 2009). The somewhat different types of supposed biolamination recorded in the Pakri section with vertical organic-rich filaments were probably formed as the result of an upward migration of the microbial mat during its life cycle (Noffke et al. 2001). Synsedimentary detrital grain trapping by sticky mat surfaces and the benthic community-controlled subsurface sulphate reduction could be suggested based on common encounters of abundant mica flakes at wavy mat surfaces and the observed layer-specific distribution of pyrite in biolaminated samples (e.g. Schieber 1999).

The influence of zoobenthos is conventionally considered to be negligible in the case of typical laminated black shales (Wignall 1994); however, our research as well as previous studies (Heinsalu 1990) report traces of bioturbation throughout the Türisalu Fm. Furthermore, recent investigations of Lower Ordovician black shales in Scandinavia have suggested that black shales might actually present abundant traces of bioturbation even in levels rich in graptolite fossils. This is in contrast to commonly upheld notion that such beds should have accumulated in anoxic environment (Egenhoff & Maletz 2012). Although a detailed study of benthic communities in the Türisalu Fm. is beyond the scope of this article, the observed traces of bottom colonisation (bioturbation and sponge spicules) suggest the availability of free oxygen at the sediment–water interface regularly, or at least episodically, throughout the accumulation history of the Türisalu Fm. However, the heterogeneity of the observed biogenic fabrics denotes that the conditions for benthic life varied through time.

The comparison of microfabrics of black shales showed that notable difference exists between samples with distinct small-

scale sedimentary features. General feature of all studied black shale varieties was the large volume of micropores and a low level of compaction, which is consistent with low diagenetic maturity and silt-fraction dominated size fractions of the deposit. SEM observations also confirmed profound effect of biogenic processes, such as *in situ* formation of microbial mats, on the development of microfabrics of black shales by supporting the formation of highly heterogeneous, porous and relatively fragile varieties. The storm ripped up cohesive fragments of such microbial mats (e.g. Schieber 1999) could have been the source of the convoluted organic-rich fragments that were commonly observed in the matrix of the Saka and the Pakri samples.

The results of this research demonstrate that vertical sections of the Türisalu Fm. are lithologically heterogeneous, even in intervals dominated by well-laminated beds. We suggest that the observed fabric variability with elements such as ripple and high-angle cross-lamination, grading, common microbial lamination, lenticular intercalations of siliceous sponges, submarine erosional surfaces, silty massive fabrics with marine detritus and traces of bioturbation indicate a shallow-water surface-wave-controlled sedimentary environment of primary mud accumulation. The interpretation of a shallow-water origin is consistent with the conclusion that was previously made by numerous studies (e.g. Scupin 1922; Heinsalu 1990). However, accumulation pathways of primary mud in those settings were obviously much more variable than the commonly assumed “slow suspension settling in stagnant water column inferred by rather infrequent storm events” (e.g. Heinsalu 1990). In their landmark paper, Rine & Ginsburg (1985) demonstrated, based on studies of modern equatorial Atlantic mud shore faces, that siliciclastic mud deposits can form in high-energy dynamic shallow-water environment. Furthermore, their study hinted that actual mud- or sand-dominated facies distribution in shallow-water settings can be rather different from traditional sandy near-shore–muddy offshore facies zonation.

The well-documented occurrence of typical marine fauna in the Türisalu Fm. such as early planktic graptolites *Rhabdinopora* sp. (Kaljo et al. 1986) designates that inner-shelf organic-rich muds deposited under normal marine conditions with non-restricted surface circulation. The documented fabric successions of the Pakri black shale shows general change from the laminated fabrics-dominated lower part to massive varieties-dominated upper part. This could possibly reflect a major shift in the character of sediment-laden flows during the accumulation of studied black shale section, from diluted turbulent flows to more dense fluid mud flows. According to Baltoscandian sea-level reconstruction of Nielsen (2004), the initial Early Ordovician transgression, which reached to its maximum in *Rhabdinopora* spp. *interval* (lower part of the Pakerort Stage), was followed by shallowing at the base of the *Adelographus hunnebergensis* graptolite zone and then by more moderate sea-level rise, which culminated during the *Kiaerograptus* Drowning Event (lower part of the Varangu Stage). Thus, the shift from more laminated to massive fabrics observed in the Pakri section could be related to eustatic sea-level fall. A limited occurrence of massive fabrics and widespread biogenic fabrics in the stratigraphically younger Saka section suggests that, besides water depth control, different sediment accumulation patterns and related hydrodynamic and sediment supply regimes were dominant in the two studied localities. The Saka section most likely represented a more sheltered shallow-marine setting, protected from storm waves by submerged sand bars or ridges between the Vihula and Toolse

areas as proposed by Heinsalu et al. (1994). Such sheltered, but not stagnant environments favoured an increase in benthic biogenic factors, including the development of benthic microbial mats and abundant shallow-water sponges.

6. Discussion

6.1 Sedimentary framework of organic-rich mud accumulation

In the early Palaeozoic, the considered marginal area of the Baltic palaeobasin was situated in the interior of the palaeocontinent, hundreds of kilometres away from deep water settings, facing the Iapetus Ocean and the Tornquist Sea, and hosting the Alum Shale Fm. For Alum Shale, which was deposited from the Mid-Cambrian to the early Tremadocian, the average net accumulation rate of 1–10 mm/1000 years has been suggested (Thickpenney 1987; Schovsbo 2001). Based on the available biostratigraphic framework and the latest time-scale calibration, black shales of the Türisalu Fm. deposited within a maximum time frame of ~5 My (Cooper & Sadler 2012). Thus, the average net accumulation rates stayed very low both in the deeper basin and in the marginal settings. The very low level of terrestrial input into the primary sedimentary environment was controlled by the peneplained nature of the main input area – low-altitude Proterozoic hard rock terrain of the Fennoscandian Shield in the present day north and northeast (Utsal et al. 1982; Artyushkov et al. 2000). Furthermore, a drop in fluvial particulate input into more distal settings at the start of the organic-rich mud accumulation was apparently supported by the sea-level rise and trapping riverine fluxes in back-stepping estuarine-coastal systems (e.g. Wignall 1991; Nielsen & Schovsbo 2011). At the time of high sea level (Nielsen 2004; Dronov et al. 2011) in early Tremadocian, the Finland–Russian part of the Fennoscandian Shield (adjacent to the accumulation area of the Türisalu Fm.) likely remained the main terrestrial source area of siliciclastic input for this part of the palaeobasin, as indicated by the occurrence of relatively immature siliciclastic deposits in Estonian settings (e.g. Heinsalu et al. 2003). The encounter of regular small-scale erosional features and the bedded character of the studied black shale successions indicate that the Türisalu Fm. is not a condensed deposit *sensu stricto* but presents evidence of intermittent dynamic sedimentation and reworking.

Formation of cohesive sediment-laden flows (as well as sediment storm clouds) in the accumulation environment of the Türisalu Fm. could have either been connected with the reactivation of muds that were trapped in coastal/estuarine settings, with the resuspension of seabed muds or alternatively with “fresh” fine sediment load into the basin from extensive flooding events (e.g. Arthur & Sageman 2005). The rivers of the pre-vegetational era were likely far more prone to the generation of sediment surges during flooding events compared with modern rivers (Davies & Gibling 2010). On other hand, the storm wave activity at dynamic estuaries (supposedly rather typical for pre-Devonian rivers according to Davies & Gibling (2010)) or in related coastal systems most likely had a higher potential for triggering the formation of long-travelling sediment-laden flows and for causing the dispersal of fine sediments.

In the early Palaeozoic, the study area was characterised by high tectonic and sedimentary facies zone stability (Männil 1966; Jaanusson 1976). In settings with very flat seabed, additional wave energy was needed to allow the progression of

sediment-laden flows over long distances (e.g. Plint et al. 2012). Such seabed topography was not probably favourable for the formation and progression of sediment-laden density currents in water depth below storm wave base. Furthermore, the innermost shelf position also meant that the Estonian area was situated far from strong currents and upwelling systems at the continental margins, which thus had likely minor influence on sediment dispersal. The flow deposition features observed in the Türisalu Fm. together with palaeogeographic position therefore favour shallow-water storm-wave-controlled deposition rather than a deeper water origin of primary muds. Several general features in the architecture of the Türisalu Fm. indicate a tight supply–transport–accommodation space-controlled nature of the black shale distribution: (1) the belt of the Estonian–Russian Tremadocian black shales (e.g. Heinsalu 1986) along the supposed terrestrial areas, (2) diachronous accumulation in different localities, (3) the gradual thinning towards the most distal (southern) part with respect to supposed terrestrial sources and (4) the gradual thinning and decrease in age towards more shallow-water settings in the NW Estonia (Fig. 9). The intimate association of black shales with the peritidal shell phosphorite-containing Kallavere Fm. has been commonly considered as a strong evidence for a shallow-water origin of the Türisalu Fm. (e.g. Scupin 1922; Heinsalu 1990). Furthermore, the Türisalu Fm. is set within the limits of shallow-water North Estonian facies belt in terms of post-Tremadocian Ordovician carbonate sedimentary basin being absent in the deeper water settings of the Livonian Tongue facies belt (Jaanusson 1976). Thus, based on the thickness distribution of the Kallavere and Türisalu formations (and the absence of evidence on major tectonic movements in the considered setting in the Tremadocian), the migration of the sedimentation locus towards near-shore settings during sea-level rise and diminished clastic input is suggested. Alternatively, however, the absence of organic-rich Tremadocian sediments in presumably deeper water settings in southern Estonia could be related to post-Tremadocian erosion of mudbeds (Mens & Pirrus 1997). Nevertheless, the rather irregular thickness of the Kallavere Fm., juxtaposed with the established litho- and bio-stratigraphy of the Türisalu Fm., suggest that the sedimentary architecture of the primary organic-rich mud was strongly influenced by inherited seafloor topography, i.e. drowning of complex sets of sand–silt bed forms formed during the previous stages of transgression (cf. Heinsalu et al. 1994).

Previous studies by Heinsalu (1990) and Artyushkov et al. (2000) have suggested that the black shales of the Türisalu Fm. should have been deposited at a depth near storm-wave base (40–60 m). The results of this research, however, indicate that the accumulation of primary mud could also probably occur in shallower depths depending on the local physiography, material supply and patterns of wind-forced storm waves. Thus, spatial and stratigraphic changes in the lithology within the Türisalu Fm. cannot be directly interpreted in terms of water depth, but reflect an interlinked effect of proximity to hinterlands, the volume and type of distributed sediment, seafloor gradients, seafloor morphology and variegated hydrodynamic energy patterns (e.g. Macquaker et al. 2010a). We suggest that storm-induced sediment dispersal and sedimentation characteristic of the later Early Ordovician sedimentary record in the north Estonian shelf (Dronov et al. 2002), dominated also in the Tremadocian and storm-wave-

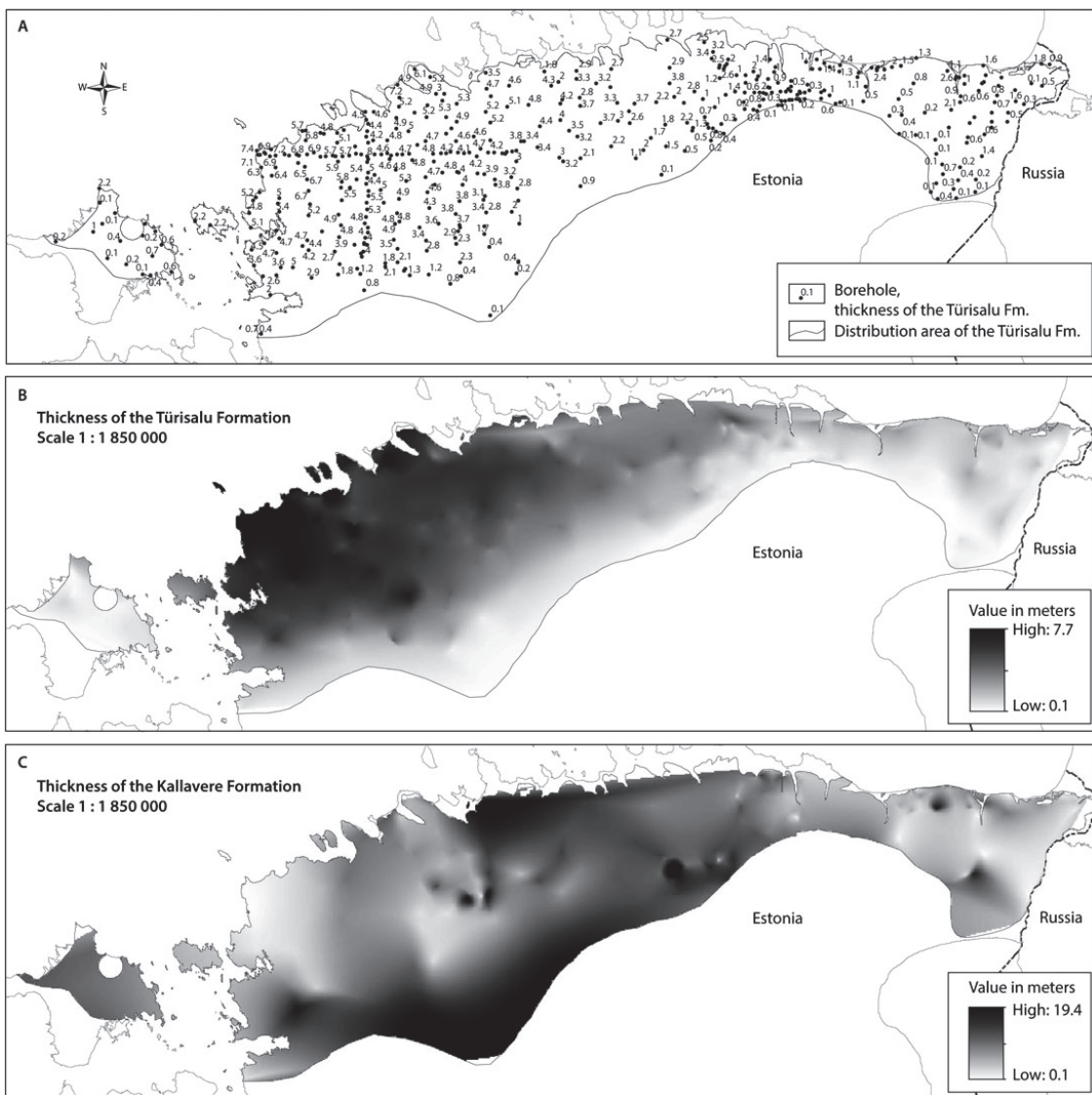


Fig. 9. Thickness of the Türisalu and Kallavere Fm. A. Location of drill cores used for thickness calculations and representative thicknesses of the Türisalu Fm. Data of Geological Survey of Estonia (Niin et al. 2008). B. Scheme of interpolated thicknesses of Türisalu Fm. C. Scheme of interpolated thicknesses of the Kallavere Fm. Note that only thicknesses within the distribution area of the Türisalu Fm. are provided on the scheme.

aided near-bed flows, acted as major agents of mud reworking, dispersal and accumulation in the studied black shale localities.

6.2 Sequestration of OM and trace metals in the context of dynamic deposition

Evidence of physical and biogenic mixing of precursor muds of the Türisalu Fm. suggests a shallow-water hydrodynamically

variegated marine environments and makes permanent anoxia (euxinia) in the lower water column questionable. However, an O₂ deficit has been shown to be a critical factor for the preservation of labile marine OM and trace metal enrichment in black shales (e.g. Algeo & Maynard 2004). Both studied sections presented a high content of redox-sensitive elements such as V, Mo and U (recorded maximum content: V = 1500 ppm, Mo = 1800 ppm, U = 800 ppm; Voolma et al.

2013). The average concentration of those metals was detected to be considerably higher in the Saka section (enrichment factor $V = 1.2$, $U = 2.95$, $Mo = 3.9$ respective to the average content in the Pakri section; Voolma et al. 2013). Widely used geochemical palaeoredox proxies, such as $V/(V + Ni)$ and V/Cr (Fig. 2; Hatch & Leventhal 1992; Jones & Manning 1994), suggest that the studied organic-rich mud deposit is formed under anoxic (euxinic) conditions. Thus, lithologically more heterogeneous and an average more metalliferous, the Saka section yielded results varying from anoxic to euxinic conditions. Somewhat less anoxic conditions were deduced for the Pakri section. The few element-based indices might have, however, limited value for interpreting the palaeoredox situation without a detailed knowledge of the local geological situation (e.g. Tribovillard et al. 2006). Schovsbo (2001) calibrated the combined $V/(V + Ni)$ and sulphur values in the Alum Shale Fm. against trilobite and brachiopod occurrence data. According to this classification, most of the Türisalu Fm. belong to an upper dysoxic zone, where V enrichment was favoured by advective transport of the trace elements (Schovsbo 2001). The latter author also suggested crucial role of advective transport by U enrichment of the near-shore Cambrian Alum Shale Fm. and Tremadocian black shales.

Global-scale processes, such as the development of a strongly stratified ocean with anoxic deep waters, are commonly seen as the triggers of widespread contemporary black shale development (Schlanger & Jenkyns 1976). The Upper Cambrian part of the metalliferous Alum Shale Fm. in deeper basinal settings of the Baltic palaeobasin could have been linked to one such ocean anoxic event in the Late Cambrian (Gill et al. 2011). Wilde et al. (1989) suggested a build-up of strong upwelling at the western margin of Baltica in the Tremadocian and a transgression of deep anoxic nutrient-rich ocean waters to the shelf. However, Schovsbo (2001) argued that at the beginning of the Ordovician, less oxygen-depleted conditions and better circulation had been restored in the Baltic palaeobasin compared with the Upper Cambrian marine environments. Despite the uncertainty about deep water redox conditions, it is evident that the primary muds of the Türisalu Fm. accumulated well within the photic zone (e.g. Chester 2003). In present-day seas, photic zone anoxia can be found under specific conditions that are related to strongly stratified water column limiting the O_2 supply and/or high bioproduction–decomposition rates and is confined to closed or barred marine to brackish water bodies (e.g. Yao & Millero 1995) and/or to environments with high anthropogenic nutrient input fuelling eutrophication (e.g. Rabalais et al. 2002). In mid-latitude epicontinental shallow seas, such as the Baltic palaeobasin in the Tremadocian, strong thermohaline stratification could possibly develop because of a combined effect of high freshwater fluxes and seasonal temperature variations. However, modern and ancient analogues suggest that such stratification most likely had temporal character because large seasonal climate variation at mid-latitudes also supports perturbation and regular mixing of the water column, thus favouring oscillatory redox conditions (cf. Murphy et al. 2000). Another critical factor of black shale development is bioproduction. The formation of rich skeletal phosphorite complexes during the initial stage of the Late Cambrian–early Tremadocian transgression suggests enhanced bioproduction in considered marginal settings of the Baltic palaeobasin (Ilyin & Heinsalu 1990). The primary OM of the Türisalu Fm. was likely produced by cyanobacteria and possibly by green sulphur bacteria (Klesment & Urov 1980;

Lille 2003). Both those groups contain species capable of fixing N_2 . The dominance of nitrogen-fixing primary production pathways during the accumulation of Tremadocian black shales in Estonia has been lately proposed by Kiipli & Kiipli (2013) based on low $\delta^{15}N$ values. Blumenberg & Wiese (2012) suggested that high bioavailable P loading versus bioavailable N could have been the main trigger of black shale formation in shallow seas during late phases of Cenomanian/Turonian ocean anoxic event. The rather low P content (average P_2O_5 concentration of the studied section remains less than 0.5 wt%) in the studied black shale sections versus the high OM content (Voolma et al. 2013) could indicate the effective recycling of this element in a primary marine environment. This process was likely supported by the anoxic conditions in the sediment column, seasonal mixing of water masses, but possibly also by constant reworking and lateral transport of sediments (e.g. Emeis et al. 2000). Consequently, the deposition of primary organic-rich muds of the Türisalu Fm. might have been controlled by a feedback loop to the supply of biolimiting elements (most importantly bioavailable P) to the marginal photic settings, enhanced bioproductivity and build-up of strong P bioproduction–regeneration cycling (e.g. Tribovillard et al. 2006; Blumenberg & Wiese 2012).

The role of bioproduction and the OM incorporation into primary mudbeds of the Türisalu Fm. are nevertheless rather poorly understood. The herein documented occurrence of microbial mats is the first direct evidence of the existence of microbial consortia at the sediment–water interface of primary organic-rich muds and suggests that microbial mats could have been major primary producers of OM of the Türisalu Fm. (cf. Gorin et al. 2009). Buchardt et al. (1997) proposed that widespread thick algal mats could have been the source of OM in the Alum Shale Fm. The oxygen production by benthic photosynthesising microbes in the photic zone and the degradation of the OM below mat surface could support the formation of steep redox gradients at sediment–water interface (e.g. Kazmierczak et al. 2012). On the other hand, several recent studies have implied a crucial role of the formation of organomineral aggregates in the water column (e.g. during phytoplankton blooms) and the related quick sequestration of OM into sediments (Macquaker et al. 2010b). Inside such aggregates, and also in benthic microbial mats, the OM could be protected by EPS (Pacton et al. 2007) or by physicochemical interactions with mineral particles (Salmon et al. 2000), thus supporting selective OM preservation in generally oxygenated environments. Consequently, the aggregation of organic and mineral matter might explain the preservation of the organic fraction in dynamic sedimentary processes in shallow-water oxic settings. Event deposition could also promote the preservation of OM by increasing episodic burial rates and limiting the residence time of OM at sediment–water interface (Macquaker et al. 2010b; Ghadeer & Macquaker 2012). Studies of microfibrils in the Saka section hinted that rather different physicochemical (biological) conditions of primary mud layers (including permeability, diffusion and microbially mediated processes) possibly developed in those settings compared with the Pakri section. Higher porosity and simultaneous supposedly steep redox gradients at the sediment–water interface braced fluxes of redox-sensitive elements between mudbeds and marine water (cf. Schovsbo 2001). The development of high trace metal heterogeneity in the Türisalu Fm. (Voolma et al. 2013) has thus been partly forced by variegated fabric characteristics of the

primary mud. We suggest that during the accumulation of primary mud of the Türisalu Fm., the lower water column was characterised by oscillating redox systems with H₂S-rich conditions mostly confined below the sediment–water interface. The OM supply, intermittent deposition, contact time of mud with seawater and heterogeneity of mud fabrics and porosity likely had a profound influence on trace metal enrichment processes in the examined settings. Not less importantly, advective transport and redeposition of particulate and colloidal matter most likely acted as major controllers of element cycling, including P recycling and trace element supply.

7. Conclusions

The results of this research are consistent with previous studies on the shallow-water origin of the Türisalu Fm., further suggesting that the water depth remained above the storm wave base within the photic zone throughout the deposition of the studied proximal complexes. The observed lithological characteristics provide evidence that the sedimentary dynamics of the Türisalu Fm. varied spatially and temporally, whereas intermittent accumulation with rapid short-term sedimentary fluxes prevailed. The cohesive sediment dispersal and deposition were mainly controlled by the near-bed storm-induced flows, which, besides causing the dynamic deposition of mud, also acted as eroding and reworking agents on muddy seafloor.

The rather shallow-water organic-rich mud settings in NE Estonia were protected from storm wave action by a complex set of drowned transgressive sand bodies that favoured the formation and preservation of more mosaic fabric patterns in primary mud successions, including common biogenic fabrics. This study is the first to report the occurrence of fossilised microbial mats in these settings of the Türisalu Fm.

Some geochemical indices, enrichment of redox-sensitive elements and high OM content seems to favour the idea that the primary mud formed in anoxic environment. In contrast, the observed traces of bioturbation and dynamic sedimentation features suggest oscillating redox conditions in the lower water column during primary mud accumulation. Metal sequestration in such environments could have been favoured by steep redox gradients at sediment–water interfaces covered by microbial mats.

This work suggests that a thorough understanding of syngenetic metal sequestration pathways in the Türisalu Fm. requires further studies on sedimentary environments. In particular, we need to learn more about (1) variability of accumulation rates, (2) proximity to fluvial sources, (3) sediment transport routes within the basin, (4) element cycling because of redeposition, (5) OM production and preservation, (6) supply of dissolved and colloidal species to sediment–water interface, (7) chemocline character, (8) the physicochemical character of primary mudbeds, (9) benthic microbial consortiums and (10) the role of diagenetic overprinting.

Acknowledgements. — We greatly appreciate constructive criticism and numerous helpful comments of the reviewers Niels Schovsbo and Sven Egenhoff. This study was supported by the Estonian Research Council (projects ETF8963 and SF014001609).

References

Algeo, T.J. & Maynard, J.B., 2004: Trace element behavior and redox facies in core shales of Upper Pennsylvanian Kansas-type cyclothems. *Chemical Geology* 206, 289–318.

Andersson, A., Dahlman, B., Gee, D.G. & Snäll, S., 1985: The Scandinavian Alum Shales. *Sveriges Geologiska Undersökning Serie Ca 56*, 1–50.

Apin, A.C. & Macquaker, J.H.S., 2011: Mudstone diversity: origin and implications for source, seal and reservoir properties in petroleum systems. *AAPG Bulletin* 95 (12), 2031–2059.

Arthur, M.A. & Sageman, B.B., 2005: Sea level control on source rock development: perspectives from the Holocene Black Sea, the mid-Cretaceous Western Interior Basin of North America, and the Late Devonian Appalachian Basin. In N.B. Harris & B. Pradier (eds.): *The Deposition of Organic Carbon-rich Sediments: Models, Mechanisms and Consequences*. *SEPM Special Publication* 82, 35–59.

Artyushkov, E.V., Lindstrom, M. & Popov, L.E., 2000: Relative sea-level changes in Baltoscandia in the Cambrian and early Ordovician: the predominance of tectonic factors and the absence of large scale eustatic fluctuations. *Tectonophysics* 320, 375–407.

Baas, J.H. & Best, J.L., 2002: Turbulence modulation in clay-rich sediment-laden flows and some implications for sediment deposition. *Journal of Sedimentary Research* 72, 336–340.

Baas, J.H., Best, J.L. & Peakall, J., 2011: Depositional processes, bedform development and hybrid bed formation in rapidly decelerated cohesive (mud-sand) sediment flows. *Sedimentology* 58, 1953–1987.

Blumenberg, M. & Wiese, F., 2012: Imbalanced nutrients as triggers for black shale formation in a shallow shelf setting during the OAE 2 (Wunstorf, Germany). *Biogeosciences* 9 (10), 4139–4153.

Buchardt, B., Nielsen, A.T. & Schovsbo, N.H., 1997: Alun skiferen i Skandinavien. *Geologisk Tidsskrift* 3, 1–30.

Chester, R., 2003: *Marine Geochemistry*. Blackwell Publishing, London. 506 pp.

Cocks, L.R.M. & Torsvik, T.H., 2005: Baltica from the late Precambrian to mid-Palaeozoic times: the gain and loss of a terrane's identity. *Earth-Science Reviews* 72, 39–66.

Cooper, R.A. & Sadler, P.M., 2012: Chapter 20. The Ordovician Period. In F.M. Gradstein, J.G. Ogg, M.D. Schmitz & G.M. Ogg (eds.): *The Geological Time Scale 2012*, 489–523. Elsevier, Amsterdam.

Davies, N.S. & Gibling, M.R., 2010: Cambrian to Devonian evolution of alluvial systems: the sedimentological impact of the earliest land plants. *Earth-Science Reviews* 98, 171–200.

Decho, A.W., 1990: Microbial exopolymer secretions in ocean environments: their role(s) in food webs and marine processes. *Oceanography & Marine Biology. Annual Review* 28, 73–154.

Dronov, A.V., Ainsaar, L., Kaljo, D., Meidla, T., Saadre, T. & Einasto, R., 2011: Ordovician of Baltoscandia: facies, sequences and sea-level changes. In J.C. Gutierrez-Marco, I. Rabano & D. Garcia-Bellido (eds.): *Ordovician of the World*, 143–150. Instituto Geológico y Minero de España, Madrid.

Dronov, A.V., Mikuláš, R. & Loginova, M., 2002: Trace fossils and ichnofabrics across the Volkhov depositional sequence (Ordovician, Arenigian of St. Petersburg Region, Russia). *Journal of the Czech Geological Society* 47 (3–4), 133–146.

Egenhoff, S.O. & Fishman, N.S., 2013: Traces in the dark-sedimentary processes and facies gradients in the upper shale member of the Upper Devonian–Lower Mississippian Bakken Formation, Williston Basin, North Dakota, USA. *Journal of Sedimentary Research* 83, 803–824.

Egenhoff, S.O. & Maletz, J., 2012: The sediments of the Flojan GSSP: depositional history of the Ordovician succession at Mount Hunneberg, Västergötland, Sweden. *GFF* 134 (4), 237–249.

Emeis, K.C., Struck, U., Leipe, T., Pollehn, F., Kunzendorf, H. & Christiansen, C., 2000: Changes in the C, N, P burial rates in some Baltic Sea sediments over the last 150 years – relevance to P regeneration rates and the phosphorus cycle. *Marine Geology* 167, 43–59.

Ganeshram, R.S., Calvert, S.E., Pedersen, T.F. & Cowie, G.A., 1999: Factors controlling the burial of organic carbon in laminated and bioturbated sediments off NW Mexico: implications for hydrocarbon preservation. *Geochimica et Cosmochimica Acta* 63, 1723–1734.

Ghadeer, S.G. & Macquaker, J.H.S., 2011: Sediment transport processes in an ancient mud-dominated succession: a comparison of processes operating in marine offshore settings and anoxic basinal environments. *Journal of the Geological Society* 168, 1121–1132.

Ghadeer, S.G. & Macquaker, J.H.S., 2012: The role of event beds in the preservation of organic carbon in fine-grained sediments: analyses of the sedimentological processes operating during deposition of the Whitby Mudstone Formation (Toarcian, Lower Jurassic) preserved in northeast England. *Marine and Petroleum Geology* 35 (1), 309–320.

Gill, B.C., Lyons, T.W., Young, S.A., Kump, L.R., Knoll, A.H. & Saltzman, M. R., 2011: Geochemical evidence for widespread euxinia in the Later Cambrian ocean. *Nature* 469, 80–83.

Gorin, G., Fiet, N. & Pacton, M., 2009: Benthic microbial mats: a possible major component of organic matter accumulation in the Lower Aptian oceanic anoxic event. *Terra Nova* 21, 21–27.

Hatch, J.R. & Leventhal, J.S., 1992: Relationship between inferred redox potential of the depositional environment and geochemistry of the Upper Pennsylvanian (Missourian) Stark Shale Member of the Dennis Limestone, Wabaunsee County, Kansas, U.S.A. *Chemical Geology* 99, 65–82.

Heinsalu, H., 1980: On the facial relations of upper Tremadocian deposits in North Estonia. *Proceedings of the Academy of Sciences of the Estonian SSR, Geology* 29 (1), 1–7 (in Russian).

Heinsalu, H., 1986: The lithofacial zonality of Early Tremadoc deposits in the East-European Platform. *Proceedings of the Academy of Sciences of the Estonian SSR, Geology* 35 (3), 115–121 (in Russian with English summary).

- Heinsalu, H., 1990: On the lithology and stratigraphy of the late Tremadoc graptolitic argillites of North-West Estonia. *Proceedings of the Estonian Academy of Sciences, Geology* 39 (4), 142–151 (in Russian with English summary).
- Heinsalu, H., Kaljo, D., Kurvits, T. & Viira, V., 2003: The stratotype of the Orasoja Member (Tremadocian, Northeast Estonia): lithology, mineralogy, and biostratigraphy. *Proceedings of the Estonian Academy of Sciences, Geology* 52 (3), 135–154.
- Heinsalu, H., Viira, V. & Raudsep, R., 1994: Environmental conditions of shelly phosphorite accumulation in the Rakvere phosphorite region, northern Estonia. *Proceedings of the Estonian Academy of Sciences, Geology* 43 (3), 109–121.
- Hiller, N., 1993: A modern analogue for the Lower Ordovician Obolus conglomerate of Estonia. *Geological Magazine* 130, 265–267.
- Hints, O. & Nõlvak, J., 2006: Early Ordovician scolecodonts and chitinozoans from Tallinn, North Estonia. *Review of Palaeobotany and Palynology* 139, 189–209.
- Ichaso, A.A. & Dalrymple, R.W., 2009: Tide- and wave generated fluid mud deposits in the Tilje Formation (Jurassic), offshore Norway. *Geology* 37, 539–542.
- Ilyin, A.V. & Heinsalu, H.N., 1990: Early Ordovician shelly phosphorites of the Baltic Phosphate Basin. In A.J.G. Notholt & I. Jarvis (eds.): *Phosphorite research and development. Geological Society of London Special Publication* 52, 253–259.
- Jaanusson, V., 1976: Faunal dynamics in the Middle Ordovician (Viruan) of Balto-Scandia. In M.G. Bassett (ed.): *The Ordovician system. Proceedings of the Palaeontological Association*, 301–326. University of Wales Press, Cardiff.
- Jones, B. & Manning, D.A.C., 1994: Comparison of geochemical indices used for the interpretation of paleoredox conditions in ancient mudstones. *Chemical Geology* 111, 111–129.
- Kaljo, D., Borovko, N., Heinsalu, H., Khazanovich, K., Mens, K., Popov, L., Sergejeva, S., Sobolevskaia, R. & Viira, V., 1986: The Cambrian–Ordovician boundary in the Baltic-Ladoga Clint area (North Estonia and Leningrad Region, USSR). *Proceedings of the Academy of Sciences of the Estonian SSR, Geology* 35 (3), 97–108.
- Kaljo, D. & Kivimägi, E., 1970: On the distribution of graptolites in the Dictyonema shale of Estonia and the untemporaneity of its different facies. *Proceedings of the Academy of Sciences of the Estonian SSR, Chemistry and Geology* 19 (4), 334–341 (in Russian with English summary).
- Kazmierczak, J., Kremer, B. & Racki, G., 2012: Late Devonian marine anoxia challenged by benthic cyanobacterial mats. *Geobiology* 10, 371–383.
- Kiipli, E. & Kiipli, T., 2013: Nitrogen isotopes in kukersite and black shale, implying Ordovician–Silurian seawater redox conditions. *Oil Shale* 30 (1), 60–75.
- Kirsimäe, K., Jørgensen, P. & Kalm, V., 1999: Low-temperature diagenetic illite-smectite in Lower Cambrian clays in North Estonia. *Clay Minerals* 34 (1), 151–163.
- Kivimägi, E. & Loog, A., 1972: The main structural types of graptolitic argillites of the Toolese deposit. *Proceedings of the Academy of Sciences of the Estonian SSR, Chemistry and Geology* 21 (2), 143–147 (in Russian with English summary).
- Kivimägi, E. & Teedumäe, A., 1971: Results of a complex estimation of the rocks in the phosphorite deposit of Toolese. *Proceedings of the Academy of Sciences of the Estonian SSR, Chemistry and Geology* 20 (3), 243–250 (in Russian with English summary).
- Kleesment, A. & Kurvits, T., 1987: Mineralogy of Tremadoc graptolitic argillites of North Estonia. *Oil Shale* 4 (2), 130–138 (in Russian with English summary).
- Klesment, I. & Urov, K., 1980: Role of bacterial lipids in the formation of geolipids and kerogens. *Proceedings of the Academy of Sciences of the Estonian SSR, Chemistry* 29 (4), 241–245.
- Leckie, D.A., Singh, C., Goodarzi, F. & Wall, J.H., 1990: Organic-rich, radioactive marine shale: a case study of a shallow-water condensed section, Cretaceous Shaftesbury Formation, Alberta, Canada. *Journal of Sedimentary Petrology* 60, 101–117.
- Lille, U., 2003: Current knowledge on the origin and structure of Estonian kukersite kerogen. *Oil Shale* 20 (3), 253–263.
- Lindgreen, H., Drits, V.A., Sakharov, B.A., Salyu, A.L. & Dainyak, L.G., 2000: Illite-smectite structural changes during metamorphism in black Cambrian Alum Shales from the Baltic area. *American Mineralogist* 85, 1223–1238.
- Loog, A., Kurvits, T., Aruväli, J. & Petersell, V., 2001: Grain size analysis and mineralogy of the Tremadocian Dictyonema shale in Estonia. *Oil Shale* 18 (4), 281–297.
- Loog, A. & Petersell, V., 1995: Authigenic siliceous minerals in the Tremadoc graptolitic argillite of Estonia. *Proceedings of the Estonian Academy of Sciences, Geology* 44 (1), 26–32.
- Loucks, R.G., Reed, R.M., Ruppel, S.C. & Jarvie, D.M., 2009: Morphology, Genesis, and Distribution of Nanometer-Scale Pores in Siliceous Mudstones of the Mississippian Barnett Shale. *Journal of Sedimentary Research* 79, 848–861.
- Lyons, T.W. & Kashgarian, M., 2005: Paradigm lost, paradigm found. The Black Sea-black shale connection as viewed from the Anoxic Basin Margin. *Oceanography* 18, 86–99.
- Mackay, D.A. & Dalrymple, R.W., 2011: Dynamic mud deposition in a tidal environment: the record of fluid-mud deposition in the Cretaceous Bluesky Formation, Alberta, Canada. *Journal of Sedimentary Research* 81, 901–920.
- Macquaker, J.H.S., Bentley, S.J. & Bohacs, K.M., 2010a: Wave enhanced sediment-gravity flows and mud dispersal across continental shelves: reappraising sediment transport processes operating in ancient mudstone successions. *Geology* 38, 947–950.
- Macquaker, J.H.S., Keller, M.A. & Davies, S.J., 2010b: Algal blooms and “Marine snow”: mechanisms that enhance preservation of organic carbon in ancient fine-grained sediments. *Journal of Sedimentary Research* 80, 934–942.
- Männil, R., 1966: *Evolution of the Baltic basin during the Ordovician*. Valgus, Tallinn. 201 pp (in Russian).
- Mens, K., Heinsalu, H., Jegonjan, K., Kurvits, T., Puura, I. & Viira, V., 1996: Cambrian–Ordovician boundary beds in the Pakri Cape section, NW Estonia. *Proceedings of the Estonian Academy of Sciences, Geology* 45, 9–21.
- Mens, K. & Pirrus, E., 1997: Vendian - Tremadocian clastogenic sedimentation basins. In A. Raukas & A. Teedumäe (eds.): *Geology and Mineral Resources of Estonia*, 184–191.
- Murphy, A.E., Sageman, B.B., Hollander, D.J., Lyons, T.W. & Brett, C.E., 2000: Black shale deposition and faunal overturn in the Devonian Appalachian basin: clastic starvation, seasonal water-column mixing and efficient biolimiting nutrient recycling. *Paleoceanography* 15, 280–291.
- Müürisepp, K., 1960: Die Lithostratigraphie der Packerort-Stufe nach den Angaben der Aufschlüsse in der Estnischen SSR. In *ENSV Teaduste Akadeemia, Tallinn*. (in Russian with German summary).
- Müürisepp, K., 1964: Käsnlaätestest Pakerordi lademes. In *ENSV Teaduste Akadeemia Looduseuurijate Selti aastaraamat* 56, 17–24. Valgus, Tallinn.
- Nemliher, J. & Puura, I., 1996: Upper Cambrian basal conglomerate of the Kallavere Formation on the Pakri peninsula, NW Estonia. *Proceedings of the Estonian Academy of Sciences, Geology* 45, 1–8.
- Nielsen, A.T., 2004: Sea-level changes – a Baltoscandian perspective. In B.D. Webby, F. Paris, M.L. Droser & I.G. Percival (eds.): *The Great Ordovician Biodiversification Event*, 84–93. Columbia University Press, New York.
- Nielsen, A.T. & Schovsbo, N.H., 2006: Cambrian to basal Ordovician lithostratigraphy in southern Scandinavia. *Bulletin of the Geological Society of Denmark* 53, 47–92.
- Nielsen, A.T. & Schovsbo, N.H., 2011: The Lower Cambrian of Scandinavia: depositional environment, sequence stratigraphy and paleogeography. *Earth-Science Reviews* 107, 207–310.
- Niin, M., Rammo, M. & Saadre, R., 2008: Eesti Maavarade kaart. V etapp. 1:400 000 (1:200 000). Diktiooneemakilt (graptolitaargilliid). Seletuskiri. Eesti Geoloogiakeskus, Tallinn.
- Nofke, N., 2009: The criteria for the biogenicity of microbially induced sedimentary structures (MISS) in Archean and younger, sandy deposits. *Earth-Science Reviews* 96 (3), 173–180.
- Nofke, N., Gerdes, G., Klenke, T. & Krumbein, W.E., 2001: Microbially induced sedimentary structures: a new category within the classification of primary sedimentary structures. *Journal of Sedimentary Research* 71 (5), 649.
- Paalits, I., 1995: Acritarchs from the Cambrian–Ordovician boundary beds at Tõnismägi, Tallinn, North Estonia. *Proceedings of the Estonian Academy of Sciences, Geology* 44 (2), 87–96.
- Pacton, M., Fiet, N. & Gorin, G., 2007: Bacterial activity and preservation of sedimentary organic matter: the role of copolymeric substances. *Geomicrobiology Journal* 24, 571–581.
- Pedersen, T.F. & Calvert, S.E., 1990: Anoxia vs. productivity: what controls the formation of organic-carbon-rich sediments and sedimentary rocks? *AAPG Bulletin* 74 (4), 454–466.
- Plint, A.G., Macquaker, J.H.S. & Varban, B.L., 2012: Bedload transport of mud across a wide, storm-influenced ramp: Cenomanian–Turonian Kaskapau Formation, Western Canada Foreland Basin. *Journal of Sedimentary Research* 82 (11), 801–822.
- Potter, P.E., Maynard, J.B. & Pryor, W.A., 1980: *Sedimentology of Shale. Study Guide and Reference Source*. Springer-Verlag, New York. 303 pp.
- Pukkonen, E. & Rammo, M., 1992: Distribution of molybdenum and uranium in the Tremadoc Graptolite Argillite (Dictyonema Shale) of North-Western Estonia. *Bulletin of the Geological Survey of Estonia* 2 (1), 3–15.
- Rabalais, N.N., Turner, R.E. & Scavia, D., 2002: Beyond science into policy: Gulf of Mexico hypoxia and the Mississippi River. *Bioscience* 52, 129–142.
- Rine, J.M. & Ginsburg, R.N., 1985: Depositional facies of a mud shoreface in Suriname, South America: a mud analogue to sandy, shallow-marine deposits. *Journal of Sedimentary Research* 55, 633–652.
- Salmon, V., Drenne, S., Lallier-Vergès, E., Largeau, C. & Beaudoin, B., 2000: Protection of organic matter by mineral matrix in a Cenomanian black shale. *Organic Geochemistry* 31, 463–474.
- Schieber, J., 1994: Evidence for high-energy events and shallow water deposition in the Chattanooga Shale, Devonian, central Tennessee, USA. *Sedimentary Geology* 93, 193–208.
- Schieber, J., 1999: Microbial mats in terrigenous clastics: the challenges of identification in the rock record. *Palaiois* 14, 3–12.
- Schieber, J., 2011: Reverse engineering Mother Nature – shale sedimentology from an experimental perspective. *Sedimentary Geology* 238, 1–22.
- Schieber, J., Southard, J.B. & Thaisen, K., 2007: Accretion of mudstone beds from migrating floccule ripples. *Science* 318, 1760–1763.

- Schieber, J. & Yawar, Z., 2009: A new twist on mud deposition—mud ripples in experiment and rock record. *The Sedimentary Record* 7 (2), 4–8.
- Schlanger, S.O. & Jenkyns, H.C., 1976: Cretaceous oceanic anoxic events: causes and consequences. *Geologie en Mijnbouw* 55, 179–184.
- Schovsbo, N.H., 2001: Why barren intervals? A taphonomic case study of the Scandinavian Alum Shale and its faunas. *Lethaia* 34, 271–285.
- Schovsbo, N.H., 2002: Uranium enrichment shorewards in black shales: a case study from the Scandinavian Alum Shale. *GFF* 124, 107–115.
- Schovsbo, N.H., 2003: The geochemistry of Lower Paleozoic sediments deposited on the margins of Baltica. *Bulletin of the Geological Society of Denmark* 50 (1), 11–27.
- Scupin, H., 1922: Ist der Dictyonemaschiefer eine Tiefseeablagerung? *Zeitschrift Deutschen Geologischen Gesellschaft* 73 (6/7), 153–155.
- Snäll, S., 1988: Mineralogy and maturity of the alum shales of south-central Jämtland, Sweden. *Sveriges Geologiska Undersökning Serie C 818*, 1–46.
- Soesoo, A. & Hade, S., 2012: Metalliferous organic-rich shales of Baltoscandia - a future resource or environmental/ecological problem. *Archiv Euro Eco* 2, 11–14.
- Sumberg, A.I., Urov, K.E. & Aasmäe, E.E., 1990: Characteristic of the Estonian Lower Ordovician fossil organic matter (Maardu member of the Pakerort horizon). *Oil Shale* 7 (3–4), 238–244 (in Russian with English summary).
- Thickpenny, A., 1987: Palaeoceanography and depositional environment of the Scandinavian Alum shales: sedimentological and geochemical evidence. In J. K. Leggett & G.G. Zuffa (eds.): *Marine Clastic Sedimentology—Concepts and Case Studies*, 156–171. Graham & Trotman, London.
- Traykovski, P., Geyer, W.R., Irish, J.D. & Lynch, J.F., 2000: The role of wave-induced density-driven fluid mud flows for cross-shelf transport on the Eel River continental shelf. *Continental Shelf Research* 20, 2113–2140.
- Tribouillard, N., Algeo, T.J., Lyons, T.W. & Riboulleau, A., 2006: Application of trace metals as paleoredox and paleoproductivity proxies. *Chemical Geology* 232, 12–32.
- Utsal, K., Kivimägi, E. & Utsal, V., 1982: About method of investigating Estonian graptolitic argillite and its mineralogy. *Acta et Commentationes Universitatis Tartuensis* 527, 116–136. Tartu Riiklik Ülikool, Tartu (in Russian with English summary).
- Voolma, M., Soesoo, A., Hade, S., Hints, R. & Kallaste, T., 2013: Geochemical heterogeneity of the Estonian graptolite argillite. *Oil Shale* 30 (3), 377–401.
- Wignall, P.B., 1991: Model for transgressive black shales? *Geology* 19, 167–170.
- Wignall, P.B., 1994: *Black Shales. Geology and Geophysics Monographs* 30. Oxford University Press, Oxford. 130 pp.
- Wignall, P.B. & Newton, R., 2001: Black shales on the basin margin: a model based on examples from the Upper Jurassic of the Boulonnais, northern France. *Sedimentary Geology* 144, 335–356.
- Wilde, P., Quinby-Hunt, M.S., Berry, W.B.N. & Orth, C.J., 1989: Palaeoceanography and biogeography in the Tremadoc (Ordovician) Iapetus Ocean and the origin of the chemostratigraphy of *Dictyonema flabelliforme* black shales. *Geological Magazine* 126, 19–27.
- Yao, W. & Millero, F.J., 1995: The chemistry of anoxic waters in the Framvaren Fjord, Norway. *Aquatic Geochemistry* 1 (1), 53–88.

3. Hints, Rutt; Soesoo, Alvar; Voolma, Margus; Tarros, Siim; Kallaste, Toivo; Hade, Sigrid (2014). Centimetre-scale variability of redox-sensitive elements in Tremadocian black shales from the eastern Baltic Palaeobasin. *Estonian Journal of Earth Sciences*, 63(4), 233 - 239.

Centimetre-scale variability of redox-sensitive elements in Tremadocian black shales from the eastern Baltic Palaeobasin

Rutt Hints, Alvar Soesoo, Margus Voolma, Siim Tarros, Toivo Kallaste and Sigrid Hade

Institute of Geology at Tallinn University of Technology, Ehitajate tee 5, 19086 Tallinn, Estonia; Rutt.Hints@ttu.ee, Alvar.Soesoo@gi.ee, Margus.Voolma@gi.ee, siimtarros@gmail.com, Toivo.Kallaste@ttu.ee, Sigrid.Hade@ttu.ee

Received 16 July 2014, accepted 30 September 2014

Abstract. The high-resolution study of vertical geochemical variability of shallow-water Tremadocian black shales of the Türisalu Formation targeted two drill core sections from Suur-Pakri Island, NW Estonia. Altogether 374 samples from 4.6 m thick shale were analysed by XRF. The metalliferous and organic-rich black shales revealed significant centimetre-scale variation in the concentration of redox-sensitive trace metals – U, Mo and V. The V profiles show cyclic variations in half a metre- to metre-scale and the strongest correlation with loss on ignition (LOI) 500 °C (interpreted to reflect organic matter abundance). The abundance of Mo presents high values near the lower and upper contacts of black shale and otherwise moderate covariance with LOI. The distribution of U is not coupled with LOI, being characterized by irregular local enrichment anomalies in the profiles of both sections. This suggests that sequestration of U may have been time-dependent and possibly favoured by dissimilatory U-reduction at the sediment–water interface under iron-reducing conditions. Significant depositional variability of the studied organic-rich muds apparently supported dynamic physicochemical and biological microenvironments at the sediment–water interface and thus temporally and spatially diversified the paths and efficiency of syndimentary redox-sensitive trace element enrichment.

Key words: black shale, geochemistry, redox-sensitive elements, Tremadocian, Baltica.

INTRODUCTION

Organic-rich deposits ranging from shallow estuarine to ocean floor varieties act as a significant sink for a number of redox-sensitive elements (e.g. Calvert & Pedersen 1993; Morford & Emerson 1999). The distribution of redox-sensitive elements in ancient organic-rich deposits have shown to be useful proxies for interpreting the redox-structure of palaeoseawater, primary productivity and palaeohydrography (e.g. Algeo & Maynard 2004; Algeo & Lyons 2006; Brumsack 2006; März et al. 2008; Algeo & Tribovillard 2009). The interpretations rely on enrichment models compiled mostly on the basis of data from anoxic deposits from relatively deep-water settings. Nevertheless, black shales can also be found in shallow-water proximal sedimentary environments (Schieber 1994; Hints et al. 2014). The high-resolution case studies of such assemblages help to test the usefulness of trace-metal proxies for palaeoenvironments that are likely prone to a much higher influence of short-term (including annual oscillations) environmental changes compared to deep-water settings. Furthermore, such investigations are essential for providing new insights into the set of palaeoenvironment conditions, which could support the development of proximal black shales, including some rather metalliferous varieties (e.g. Coveney et al. 1991).

The Tremadocian black shales of the Türisalu Formation (Fm.) make up a laterally extensive organic-rich siliceous mudstone bed in northern Estonia, eastern part of the Baltic Palaeobasin. Characterized by a high content of U, Mo, V and some chalcophile elements, the complex is a potential resource of a variety of metals (Hade & Soesoo 2014). Recent findings suggest that the Türisalu Fm. exemplifies transgressive, but rather shallow-water reducing marine muds with spatially heterogeneous properties (Voolma et al. 2013; Hints et al. 2014). According to biostratigraphic data, the unit is diachronous and varies in thickness from less than half a metre in northeast Estonia to more than 6 m in northwest Estonia (Heinsalu et al. 2003) (Fig. 1). The average distribution of enriched redox-sensitive elements shows significant lateral variations in the Türisalu Fm. (Pukkonen & Rammo 1992). However, the genetic factors behind the documented spatial and temporal trace metal heterogeneity are not well understood. Based on the biostratigraphic framework and a recent time scale calibration (Cooper & Sadler 2012), one could argue that the primary muds of the Türisalu Fm. should have been deposited within a maximum time frame of ~5 My (Hints et al. 2014). Whereas the long-term accumulation rates apparently stayed very low during sedimentation of the primary organic-rich muds of the Türisalu Fm., the sedimentary fabrics in the black shales suggest dynamic deposition,

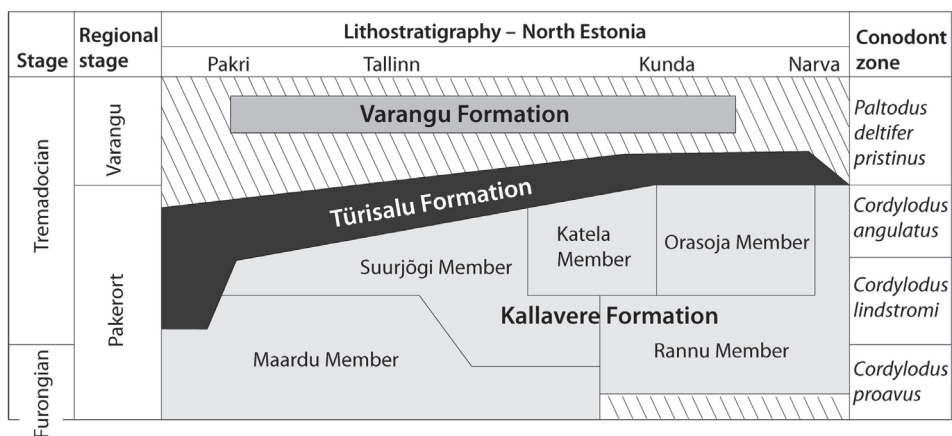


Fig. 1. Stratigraphic position of the Türisalu Fm. (modified after Heinsalu et al. 2003).

frequent reworking of sea bottom and changes in deposition rates (Hints et al. 2014). The studies of modern organic-rich muds have revealed usefulness of high-resolution sampling within a limited geographic range (e.g. Algeo & Lyons 2006), allowing more reliable distinction between possible driving factors behind the syndimentary trace metal sequestration and more consistent environmental interpretations.

In this paper we report the first results of a centimetre-scale study of redox-sensitive trace metal distribution in the Tremadocian black shales in two closely spaced drill core sections from NW Estonia, Baltica. The study was carried out in order to record and interpret detailed enrichment patterns of redox-sensitive elements in the Türisalu Fm.

MATERIAL AND METHODS

The study material comes from two drill cores from Suur-Pakri Island, NW Estonia, located less than a kilometre apart: SP2 (59°20'13.07"N, 23°53'54.74"E, WGS84) and SP3 (59°20'15.33"N, 23°54'33.8"E, WGS84). The ca 4.6 m thick black shale successions show high lithological variability, including the presence of finely laminated, ripple laminated, graded, massive, biolaminated, bioturbated fabrics and small-scale syndimentary faulting. The dominant fabric types and thickness of individual beds vary as well.

A quarter of the black shale in both drill cores was sampled and analysed by 2-cm intervals. Siliciclastic beds belonging to the Kallavere Fm. and the Varangu Fm. near the lower and upper contacts of the Türisalu Fm.

were also sampled. Altogether 374 homogenized samples were analysed for major and trace element composition with Bruker S4 PIONEER XRF spectrometer (X-ray tube with a rhodium anode, operated at 3 kW) at the Institute of Geology at Tallinn University of Technology. The samples were measured with a manufacturer's standard as MultiRes modification. In-house standard ES-2 ('Dictyonema Shale') was used as a reference sample (Kiipli et al. 2000).

In the current overview we focus on the results of vertical variability of enriched redox-sensitive elements in the studied sections. Other trace element data will be published elsewhere. From all samples loss of ignition at 500°C (LOI 500°C) was determined from 1 g of sample material and used as an indicator of organic matter abundance (except in case of sulphide-rich samples).

RESULTS

The studied black shales of the Türisalu Fm. revealed a remarkably homogeneous major element composition of mineral matter. The average values of major elements and redox-sensitive trace elements are summarized in Table 1. The recorded high content of Si and K are typical features of the black shales of the Türisalu Fm., where silt-size particles dominate over clay fraction and which contains abundant authigenic K-feldspar (Loog et al. 2001). Aluminium content shows low variability, being on average smallest in the middle part of the sections. Furthermore, Ti/Al ratios, commonly interpreted to reflect changes in terrigenous input and provenance

Table 1. Summarized results of XRF analyses of major elements (wt%) and redox-sensitive elements (ppm), recorded loss on ignition values (wt%) and calculated Ti/Al molar ratios of the black shales of the Türisalu Fm. from SP2 and SP3 drill cores

Component	SP2 <i>n</i> = 183				SP3 <i>n</i> = 168			
	Mean	SD	Max	Min	Mean	SD	Max	Min
SiO ₂	49.82	1.48	54.47	46.35	50.36	1.49	54.29	47.08
TiO ₂	0.75	0.03	0.86	0.67	0.74	0.03	0.81	0.63
Al ₂ O ₃	12.90	0.32	14.06	11.93	13.21	0.35	13.90	11.84
Fe ₂ O ₃	5.27	0.77	9.22	4.54	5.05	0.77	10.93	4.29
MnO	0.020	0.001	0.022	0.016	0.020	0.004	0.066	0.014
MgO	1.20	0.05	1.34	1.03	1.25	0.11	2.20	1.05
CaO	0.24	0.09	1.05	0.16	0.30	0.42	4.45	0.16
Na ₂ O	0.07	0.01	0.09	0.02	0.07	0.01	0.11	0.01
K ₂ O	7.75	0.20	8.56	7.11	7.70	0.23	8.31	6.86
P ₂ O ₅	0.14	0.07	0.72	0.07	0.16	0.12	1.00	0.09
S	2.76	0.45	4.76	2.05	2.51	0.42	5.63	1.94
LOI 500 °C	20.628	1.887	24.9	15.05	21.183	2.48	25.874	12.67
100Al/Ti	3.74	0.11	4.166	3.478	3.58	0.09	3.78	3.302
Mo	151	51	323	55	156	58	589	62
U	114	40	257	33	118	36	229	40
V	1101	172	1520	752	1097	175	1474	508

areas (e.g. Boyle 1983), showed invariable patterns in both of the studied cores. The average recorded LOI 500 °C value in the shale samples is ca 21 wt%, decreasing slightly in the upper parts of both sections (Table 1, Fig. 2). The LOI 500 °C variations, which could in most part be interpreted in terms of organic matter abundance in organic-rich deposits, are, however, dependent on other additional processes such as decomposition of sulphides and carbonates and dehydration of clays. The gathered compositional data agree with the rather low carbonate content and uniform clay mineral abundance in the studied profiles. Therefore, those components have apparently a minor role in the observed mass loss. On the other hand, the analyses indicate the occurrence of a few highly sulphidic samples (S > 5 wt%), mostly close to the upper and lower contacts of the formation. Such samples were excluded from the dataset used to calculate descriptive statistics for the black shale geochemistry. The calculated determination coefficient for S and LOI ($r^2 = 0.05$, $n = 351$) for samples with S < 5 wt% does not indicate covariance between those variables, thus likely no general strong linear relationship exists between LOI and sulphide content in the black shale samples. The recorded distribution trends of Fe in the studied black shales largely mimic that of S, suggesting that the higher abundance of the metal could largely be attributed to the elevated content of pyrite.

In contrast to the major components, the studied enriched redox-sensitive trace elements show rather

heterogeneous centimetre-scale vertical distribution patterns (Fig. 2). The average estimated content of V is 1100 ppm, Mo 150 ppm and U 115 ppm. According to these values, the studied sections represent the less-enriched area of the Türisalu Fm. (cf. Pukkonen & Rammo 1992). However, the concentration of the considered redox-sensitive elements is markedly elevated in the samples from the Türisalu Fm. compared to the underlying and overlying siltstones. To minimize the effect of terrigenous dilution, the trace element contents of marine deposits are commonly presented as ratios of the trace element to Al. However, normalization was not used in this study due to rather low variability of Al content and to avoid possible appearance of spurious correlations between variables (Van der Weijden 2002). Whereas in general the recorded V and Mo show positive covariance with LOI 500 °C (and supposedly organic matter content), the behaviour of each redox-sensitive trace element is rather distinct in detail. Vanadium shows moderate positive covariance with LOI 500 °C ($r^2 = 0.42$, $n = 351$) and cyclic variations in half a metre- to metre-scale in both of the studied cores. Considerably similar V distribution patterns in the middle part of the two sections may serve as a basis for chemostratigraphic correlation. Distribution profiles of Mo exhibit weak covariance with LOI 500 °C ($r^2 = 0.28$, $n = 351$) and are characterized by enrichment peaks near the upper and lower contacts of the black shale in close vicinity of sulphide-rich beds. The average Mo content shows slight

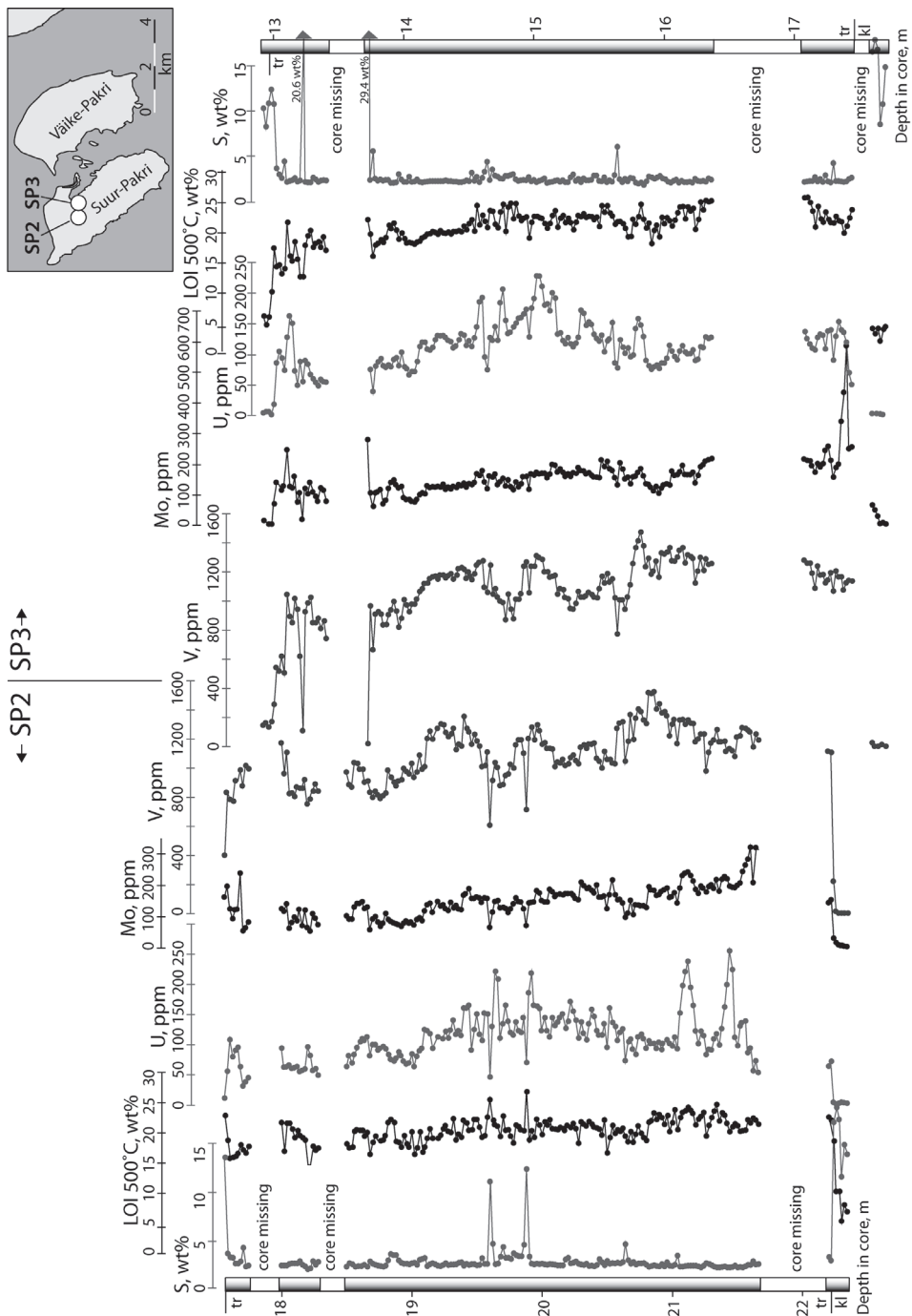


Fig. 2. Vertical distribution profiles of U, V, Mo, LOI 500°C and S in the black shales of the Türisalu Fm. and underlying siliciclastic complexes from drill cores SP2 and SP3, Suur-Pakri Island, NW Estonia. tr – Türisalu Fm.; kl – Kallaveri Fm.

decrease towards the upper part in both of the studied profiles. Uranium displays no obvious covariance with LOI 500°C ($r^2 = 0.19$, $n = 351$). Its average content tends to be the highest in the middle part of the successions. However, U distribution is characterized by irregular enrichment peaks, which mostly do not coincide with peak V and Mo values, nor does U show clear covariance with the distribution of S. Furthermore, the enrichment peaks of U, which show sharp centimetre-scale deviations from general distribution trends of the element, appear to be local in character, as there is no good match between such U peaks in the two studied localities. This suggests that some local factor(s) affected the speciation and enrichment process of uranium, in addition to the changing redox state of seawater or organic matter input.

DISCUSSION AND CONCLUSIONS

Redox-sensitive metals tend to form mobile species under oxic conditions and immobile species in reducing environments, therefore typically accumulating in sediments near redox boundaries. However, several recent investigations suggest that the reduction and sequestration of U, Mo and V occurs via various speciation pathways and thus parallel assessment of the behaviour of different redox-sensitive elements might potentially give a much more detailed picture of primary environments than single-element-based approaches (e.g. Algeo & Maynard 2004; Tribouillard et al. 2006). According to Gill et al. (2011), widespread euxinia characterized the Late Cambrian oceans. The ocean redox structure at the beginning of the Tremadocian is nevertheless poorly known, as is the redox structure in the shallow-water proximal part of the vast epicontinental Baltic Palaeobasin, where primary organic-rich muds of the Türisalu Fm. deposited. Based on the high content of redox-sensitive metals and organic matter in the Türisalu Fm., Pukkonen & Rammo (1992) suggested that kerogenous muds in northwestern Estonia were once deposited under a stagnant, stratified and permanently euxinic water column. However, bioturbation, which could be fairly intensive in some intervals of the studied sections (e.g. SP2 between 14.1 and 14.5 m, note rather homogeneous abundance of redox-sensitive elements there), favours a more complex syndimentary environment with free oxygen present at the sediment–water interface (SWI) more or less regularly. The general positive covariance of V and Mo with that of organic matter in the studied drill cores from Suur-Pakri Island confirms that the sequestration process of metals from seawater was in general controlled by metal reduction triggered by oxygen depleted seawater or anoxia below the SWI

and closely coupled with organic matter degradation, whereas organic–metal complexation could have acted as a major pathway for metal enrichment (cf. Algeo & Maynard 2004). The herein documented complex distribution patterns of elements imply that other factors besides redox should be considered as potential sources of variance, including the influence of the presence of free HS^- , possible role of particulate shuttles, position and stability of the chemocline in the enrichment environment, influence of microbial mediation, bioturbation and redeposition. For example, Mo enrichment near the formation boundaries, which is not coupled with enhanced U and V abundances, may indicate that euxinic conditions favourable for activation of thiomolybdate switch (Helz et al. 1996) quickly turned prevailing in the lower water column during the start of organic-rich mud accumulation, facilitating sequestration of Mo via sulphide formation. The recorded Mo-enrichment may as well reflect an episode of more efficient scavenging of the metal by Mn–Fe-oxyhydroxide under intermittent redox conditions and fluctuating chemocline (Algeo & Tribouillard 2009) during the initial phases of transgression. Early diagenetic enrichment of Mo cannot be excluded either, as elevated abundances of the element appear near black shale contacts with more permeability siltstones. The Mo/U ratio for the studied profiles, whose variations could potentially indicate restriction of palaeoseawater masses (Algeo & Tribouillard 2009), does not suggest draw-down of aqueous concentration of Mo during organic-rich mud deposition. Slight decrease in the average Mo/U ratio in the upper part of the sections is interpreted to reflect somewhat less reducing conditions at the SWI rather than depletion of an aqueous Mo reservoir. Accordingly, open to semi-restricted marine conditions likely prevailed during most of the organic-rich mud accumulation period.

The forcing mechanisms behind the observed cyclic distribution patterns of V, whose reduction could start under slightly less reducing conditions than that of U and Mo (Algeo & Maynard 2004), are far from clear. The data presented here indicate low variability in terrigenous influx and thus lack of major terrigenous control (e.g. due to climatic or eustatic changes) over V sequestration. The cyclicity of V abundance might be linked to factors such as alteration of thermohaline circulation or water depth fluctuations and related cyclic changes in dissolved oxygen availability near the sea bottom. On the other hand, Hints et al. (2014) suggested that high primary productivity rates driven by phosphate loading and effective recycling in the shallow water column (sea bottom within the photic zone) characterized the accumulation of the muds of the Türisalu Fm. The recorded V pattern might thus be connected to cyclic changes in nutrient loading and palaeoproductivity.

Nevertheless, a more consistent interpretation of the triggering forces behind V behaviour requires considering additional datasets.

Unlike that of Mo and V, which could be reduced both within the marine water column and in sediments, U reduction is known to occur only within sediments (e.g. Algeo & Maynard 2004). Based on shoreward increase in U in the Cambrian Alum Shales in Scandinavia, Schovsbo (2002) suggested that synsedimentary U enrichment had been controlled by a more efficient advective transport of U in those settings. Both sections of the Türisalu Fm. studied herein show sedimentary features indicative of deposition under a hydrodynamically active water column, and thus the dominance of advective rather than diffusive transport of elements to the SWI is likely. Furthermore, the average thickness of shale beds and Al content drops in the middle part of the studied black shale sections, while the abundance of bioclastic fragments increases, generally coinciding with a high U content. Those changes could have favoured more efficient element exchange over the SWI and the longevity of the SWI. We hypothesize that under such conditions the U enrichment anomalies could record enhanced efficiency of local U reduction at the SWI, possibly favoured by the dominance of an iron-reducing rather than H₂S-enriched environment and microbially controlled processes within pore waters of the upper sediment layer. Numerous recent studies of the modern aquatic system and experimental works (e.g. Komlos et al. 2008) have indicated that efficient U-trapping through microbially mediated dissimilatory metal reduction could occur simultaneously with Fe(III)–Fe(II) transition under iron-reducing conditions. It is noteworthy that the middle parts of the studied black shale successions, which show the highest U abundances, also contain common remains of probable microbial mats.

In summary, the two sections of the Türisalu Fm. studied are characterized by high centimetre-scale vertical variability of V, Mo and U. Significant depositional heterogeneity of shallow-water kerogenous muds likely favoured dynamic physicochemical and biological micro-environments at the SWI and thus spatially and temporally diversified pathways and efficiency of synsedimentary enrichment of Mo and especially U, even in rather closely set localities. Due to considerable influence of local enrichment factors, the application of redox-sensitive elements as indicators of palaeoredox conditions of seawater is limited in the Türisalu Fm.

Acknowledgements. We are grateful to N. H. Schovsbo and C. März, whose critical comments helped to improve the manuscript. We thank Eesti Energia AS for providing the drill cores used for the study. The study was supported by the Estonian Research Council projects ETF8963 and SF0140016s09 and is a contribution to IGCP Project 591.

REFERENCES

- Algeo, T. J. & Lyons, T. W. 2006. Mo-total organic carbon covariation in modern anoxic marine environments: implications for analysis of paleoredox and paleohydrographic conditions. *Paleoceanography*, **21**, PA1016.
- Algeo, T. J. & Maynard, J. B. 2004. Trace element behavior and redox facies in core shales of Upper Pennsylvanian Kansas-type cyclothems. *Chemical Geology*, **206**, 289–318.
- Algeo, T. J. & Tribouillard, N. 2009. Environmental analysis of paleoceanographic systems based on molybdenum–uranium covariation. *Chemical Geology*, **268**, 211–225.
- Boyle, E. A. 1983. Chemical accumulation variations under the Peru Current during the past 130,000 years. *Journal of Geophysical Research*, **88**, 7667–7680.
- Brumsack, H. J. 2006. The trace metal content of recent organic carbon-rich sediments: implications for Cretaceous black shale formation. *Palaeogeography, Palaeoclimatology, Palaeoecology*, **232**, 344–361.
- Calvert, S. E. & Pedersen, T. F. 1993. Geochemistry of recent oxic and anoxic marine sediments – implications for the geological record. *Marine Geology*, **113**, 67–88.
- Cooper, R. A. & Sadler, P. M. 2012. Chapter 20. The Ordovician Period. In *The Geological Time Scale 2012* (Gradstein, F. M., Ogg, J. G., Schmitz, M. D. & Ogg, G. M., eds), pp. 489–523. Elsevier, Amsterdam.
- Coveney Jr., R. M., Watney, W. L. & Maples, C. G. 1991. Contrasting depositional models for Pennsylvanian black shale discerned from molybdenum abundances. *Geology*, **19**, 147–150.
- Gill, B. C., Lyons, T. W., Young, S. A., Kump, L. R., Knoll, A. H. & Saltzman, M. R. 2011. Geochemical evidence for widespread euxinia in the Later Cambrian ocean. *Nature*, **469**, 80–83.
- Hade, S. & Soesoo, A. 2014. Estonian graptolite argillites revisited: a future resource. *Oil Shale*, **13**, 4–18.
- Heinsalu, H., Kaljo, D., Kurvits, T. & Viira, V. 2003. The stratotype of the Orasoja Member (Tremadocian, Northeast Estonia): lithology, mineralogy, and biostratigraphy. *Proceedings of the Estonian Academy of Sciences, Geology*, **52**, 135–154.
- Helz, G. R., Miller, C. V., Charnock, J. M., Mosselmans, J. F. W., Patrick, R. A. D., Garner, C. D. & Vaughan, D. J. 1996. Mechanism of molybdenum removal from the sea and its concentration in black shales: EXAFS evidence. *Geochimica et Cosmochimica Acta*, **60**, 3631–3642.
- Hints, R., Hade, S., Soesoo, A. & Voolma, M. 2014. Depositional framework of the East Baltic Tremadocian marginal black shale revisited. *GFF*, doi: 10.1080/11035897.2013.866978.
- Kiipli, T., Batchelor, R. A., Bernal, J. P., Cowing, C., Hagel-Brunstrom, M., Ingham, M. N., Johnson, D., Kivisilla, J., Knaack, C., Kump, P., Lozano, R., Michiels, D., Orlova, K., Pirrus, E., Rousseau, R. M., Ruzicka, J., Sandstrom, H. & Willis, J. P. 2000. Seven sedimentary rock reference samples from Estonia. *Oil Shale*, **17**, 215–223.
- Komlos, J., Peacock, A., Kukkadapu, R. K. & Jaffé, P. R. 2008. Long-term dynamics of uranium reduction/reoxidation

- under low sulfate conditions. *Geochimica et Cosmochimica Acta*, **72**, 3603–3615.
- Loog, A., Kurvits, T., Aruväli, J. & Petersell, V. 2001. Grain size analysis and mineralogy of the Tremadocian Dictyonema shale in Estonia. *Oil Shale*, **18**, 281–297.
- März, C., Poulton, S. W., Beckmann, B., Küster, K., Wagner, T. & Kasten, S. 2008. Redox sensitivity of P cycling during marine black shale formation: dynamics of sulfidic and anoxic, non-sulfidic bottom waters. *Geochimica et Cosmochimica Acta*, **72**, 3703–3717.
- Morford, J. & Emerson, S. 1999. The geochemistry of redox sensitive trace metals in sediments. *Geochimica et Cosmochimica Acta*, **63**, 1735–1750.
- Pukkonen, E. & Rammo, M., 1992. Distribution of molybdenum and uranium in the Tremadoc Graptolite Argillite (Dictyonema Shale) of north-western Estonia. *Bulletin of the Geological Survey of Estonia*, **2**(1), 3–15.
- Schieber, J. 1994. Evidence for high-energy events and shallow-water deposition in the Chattanooga Shale, Devonian, central Tennessee, USA. *Sedimentary Geology*, **93**, 193–208.
- Schovsbo, N. H. 2002. Uranium enrichment shorewards in black shales: a case study from the Scandinavian Alum Shale. *GFF*, **124**, 107–115.
- Tribouvillard, N., Algeo, T. J., Lyons, T. W. & Riboulleau, A. 2006. Application of trace metals as paleoredox and paleoproductivity proxies. *Chemical Geology*, **232**, 12–32.
- Van der Weijden, C. H. 2002. Pitfalls of normalization of marine geochemical data using a common divisor. *Marine Geology*, **184**, 167–187.
- Voolma, M., Soesoo, A., Hade, S., Hints, R. & Kallaste, T. 2013. Geochemical heterogeneity of Estonian graptolite argillite. *Oil Shale*, **30**, 377–401.

4. Puura, Väino; Soesoo, Alvar; Voolma, Margus; Hade, Sigrid; Aosaar, Hardi (2016). Chemical composition of the mineral matter of the Attarat Um Ghudran oil shale, Central Jordan. *Oil Shale*, 33(1), 18-30

CHEMICAL COMPOSITION OF THE MINERAL MATTER OF THE ATTARAT UM GHUDRAN OIL SHALE, CENTRAL JORDAN

VÄINO PUURA^{(a)*}, ALVAR SOESOO^(b),
MARGUS VOOLMA^(b), SIGRID HADE^(b), HARDI AOSAAR^(c)

^(a) Department of Geology, Institute of Ecology and Earth Sciences, University of Tartu, Ravila 14A, 50411 Tartu, Estonia

^(b) Institute of Geology, Tallinn University of Technology, Ehitajate tee 5, 19086 Tallinn, Estonia

^(c) Eesti Energia AS, Lelle 22, 11318 Tallinn, Estonia

Abstract. *The concession area of the Jordan Oil Shale Energy Co (JOSE) is located in the southern border zone of the Attarat Um Ghudran deposit, next to the Wadi Maghara deposit, both consisting of marinite type oil shale (OS). These deposits of the Late Cretaceous to Early Paleogene Muwaqqar Chalk-Marl Formation form a huge north-southward elongated oil shale basin in Central Jordan, with resources over 55 billion tons. JOSE has drilled a regular grid of boreholes with a full coring of the up to 90 m thick OS seam and its lower and upper contact layers. Visually, the OS unit is a rather homogenous dark-colored (grey, black, brownish grey) succession of finely bedded (laminated) kerogen-bearing carbonate rocks that has been in earlier papers described as a uniform lithological unit. The aim of the geological and lithological studies of the JOSE exploration area was (i) to investigate the vertical variation of OS composition and, if present, to define layers within the OS unit, and (ii) to identify lithological varieties and chemical composition of OS present in different layers.*

On the basis of field evidence, downhole gamma-logging, chemical analyses and other criteria, an original detailed scheme of the layered structure of oil shale and barren rocks was introduced. A total of eight OS layers (indexed as A, B1, B2, C, D, E1, E2, E3) and at least four barren dolomitic limestone interlayers were distinguished. The present publication is dedicated to the chemical study of the layers and the total OS seam. A representative gapless collection of 632 conventional core samples from 12 cores serves as the base for the comparative study of the layers. Two main (SiO₂, CaO) and two subordinate chemical (Al₂O₃ and P₂O₅) components of the mineral matter (MM), and loss on ignition (LOI @500 °C) approximately reflecting the content of organic matter (OM), are the basic variables discussed. Contents of SiO₂ and CaO always show negative correlation,

* Corresponding author: e-mail vaino.puura@ut.ee

whereas local enrichment with Al_2O_3 and P_2O_5 occurs in certain interbeds. OM content in samples has no strong correlation with mineral matter abundances. The eight distinguished OS layers comprise both those strongly enriched in CaO, or oppositely in SiO_2 . The layers differ in rate of internal heterogeneity reflected in variation of standard deviation values. With rare exceptions, the barren limestone interlayers are dolomitized, strongly enriched with MgO and depleted of CaO. The database on the distribution of mineral compounds and trace elements serves for the 3-D block modelling of the deposit composition. However, further data analysis is required for the understanding of lateral changes of the layers' mineral composition, and geological and geochemical structure.

Keywords: oil shale, mineral matter, chemical composition, Maastrichtian, Attarat Um Ghudran deposit, Central Jordan.

1. Introduction

Cretaceous to Paleogene sedimentary sequences of the Afro-Arabian shelf sea contain vast volumes of organic matter [1, 2]. Abed and Amireh [3] have summarized the early (1959–1980) publications on the occurrence of oil shale (OS) in Jordan. The authors admitted that at this time oil shale was considered as a major future energy resource in Jordan devoid of oil. During the following more than 30 years a number of geological explorations resulted in the discovery of many new deposits (Fig. 1), and development of oil shale utilization technologies has continued since then [4–6]. A significant recent practical achievement is that after the geological survey, mining studies and engineering design efforts by the Jordanian Oil Shale Energy Co (JOSE), construction of an electric power plant is presently in an active preparation stage. It will be fueled with oil shale from the Attarat Um Ghudran deposit. The geological survey materials on the chemical composition of oil shale layers of the area have been used for the present publication.

Jordan has huge resources of oil shale [5–7], especially if calculated per unit of territory. When compared to many other thick oil shale suites [7], it is impressive that the whole thickness of the main OS unit, belonging to the Muwaqqar Chalk-Marl Formation (MCM), is often of considerably high organic matter (OM) content. In Central Jordan, OS lies near the surface with a thin overburden and shows a higher percentage of OM compared to other localities [8]. The richest oil shale-grade deposits are of the Late Cretaceous Maastrichtian age, in which OM is present as kerogen [3]. It originates from fossilized phytoplankton and zooplankton that flourished and deposited on the southern continental shelf of the Tethys Ocean [8]. Kerogen is the minor component in OS (from 0 to 36 wt%). According to the classification by Hutton [10], the largest Jordanian oil shale deposits belong to the family of marinite oil shales [5, 11]. The dominant minerals of

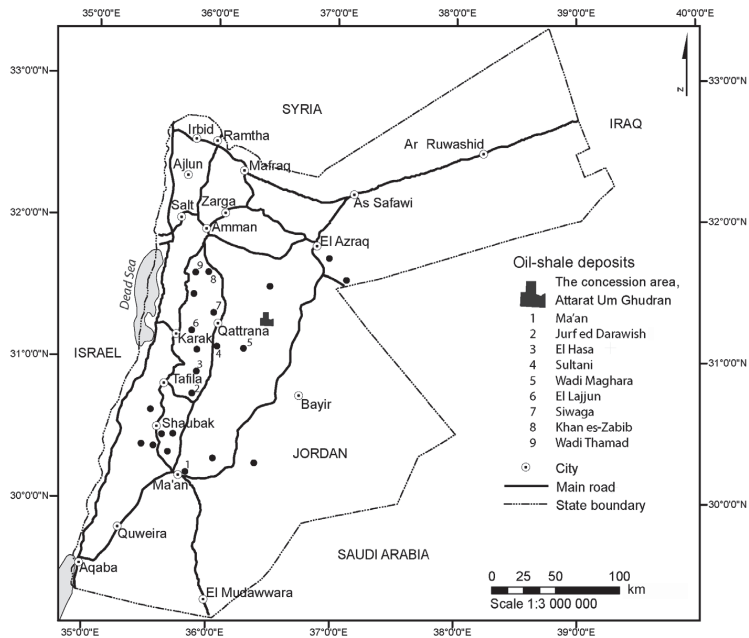


Fig. 1. Location of the Attarat Um Ghudran deposit comprising the concession area and other deposits in Jordan. Modified after [7].

Jordanian OS are calcite (calcium carbonate, from 31% to a maximum of 90%) and quartz (free silica, 0–37%), and occasionally minor mineral components, such as clay minerals, apatite (carbonate-flour apatite ($\text{Ca}_3(\text{PO}_4)_2 \text{Ca}_2\text{PO}_4(\text{CO}_3, \text{F})$) and pyrite (FeS_2) [8, 9].

The Attarat Um Ghudran (AUG) and Wadi Maghara (WM) oil shale deposits (Fig. 1) form a uniform, north-south striking elongated Attarat Um Ghudran-Wadi Maghara basin that covers an area over 1000 km² in Central Jordan with total geological resources over 55 billion tons of OS [5, 6].

Previous studies [3–6, 8, 11, 13] have shown certain differences in the average composition of mineral matter within and between different deposits of Jordan. Also the Maastrichtian OS of Southern Syria is of similar variable composition [12]. In more detail, variation in average mineral contents between different core intervals with different oil contents in the El Lajjun deposit have been demonstrated [13, 5, 6]. Compared with compositions of many other oil shales of the world [7], including the Estonian Paleozoic kukersite [14], and graptolite argillite [15–18], the Near East oil shales have specifically high contents of carbonate (calcite), silica (quartz, in places with

admixture of tridymite and cristobalite – unpublished data by the authors) and sulfur [8]. During 2007–2013, JOSE explored a concession area of about 73 km² situated in the southern border zone of AUG, next to WM. It is located about 40 km east of the town of Qattrana.

When starting the exploration, analysis of the historical research and exploration data demonstrated that, first, the Maastrichtian oil shale of Jordan and of its surroundings belongs to a principally uniform highly carbonaceous type of marinite, and second, a certain variability of its mineral composition occurs. However, the internal changeable mineralogical and chemical composition of the OS suite in Jordan including the exploration area has remained poorly understood as yet.

JOSE started geological exploration in Central Jordan in 2006. Through the previous geological exploration, the organic-rich rocks of the OS seam were usually described just as bituminous (or kerogen-bearing or OM-bearing) chalky marls or marls with limestone interlayers. In practice, it overshadowed the variability of OS mineral and chemical composition. Herein the study is focused on mineral components while the content of organic matter is determined using LOI (500 °C) data only. Planning technologies for OS use requires a more precise definition and classification of raw material composition, structure and texture. Oil shales with different mineralogical/chemical composition exhibit different properties in the thermal processing. This is especially revealed when the ENEFIT technologies that are focused on the ample use of OM potential in OS are applied [19]. Herein, in particular XRD and XRF data on concentrations of mineral components are used. Evidence on the OM content is restricted to LOI (loss on ignition @500 °C) data.

The aim of the geological and lithological studies carried out in the JOSE exploration area was (i) to investigate the vertical variation of OS composition and, if present, to define layers within the OS unit, and (ii) to identify lithological varieties and chemical composition of OS present in different layers. Layered structure is characteristic of many oil shale deposits and basins. As an example, the layering-focused model of the Baltic Kukersite basin well serves for the demonstration of the spread of the oil shale lateral distribution and variation of quantitative and qualitative parameters [20, 21].

During the field campaign in 2008–2013, JOSE drilled a regular grid of boreholes with a full coring of the up to 90 m thick OS seam and of its lower and upper contact layers that were neither targeted nor reached in previous studies. From the beginning of exploration, a practical task was to create an easily applicable stratification scheme of the OS suite that would serve for the process of borehole logging and sampling. Using a variety of field and laboratory techniques, in the total succession of the oil shale unit eight OS layers (indexed as A, B1, B2, C, D, E1, E2, E3) with four dolomitic limestone interlayers were distinguished. Step by step, the validity of it within the entire exploration area was verified.

In order to understand the nature of both vertical and lateral compositional changes of individual layers as well as of natural typical and specific varieties of oil shale for their classification, further integrated petrographic, mineralogical and geochemical (including trace elements) studies are underway. The dataset obtained on the downhole gamma-logging, as well as micropaleontological and other studies enable further confirmation of the credibility of the detailed stratification scheme of the Attarat Um Ghudran deposit. The introductory interpretation of the large massif of analytical data in order to outline geochemical patterns of the OS seam and its individual layers in the JOSE concession area is the subject of the present writing.

2. Materials and methods

The paper presents results of the study of original drill core material carried out in the JOSE concession area. Drill cores obtained from owners of the previous oil shale projects conducted in the concession area were also examined and analyzed. JOSE is the owner of drill cores and detailed field and laboratory study data. A core-drilling grid of over 150 boreholes was created. In order to establish and study the chemical layered structure of the OS seam and certain lithologies, chemical analyses of 1284 gapless core samples from 39 boreholes were completed. A most representative collection of 632 conventional core samples from 12 gapless sampled cores (with usual full core recovery) was chosen for the following comparative chemical study of separate layers. In the process of sampling and sample preparation, half of the bisected core material was subjected to coarse crushing into a fraction below 2 mm, and then split by separating a 1 kg homogenized portion to be forwarded to laboratories. Part of this 1 kg homogenized sample was fine-crushed and pulverized for the laboratory study of MM using mineralogical and geochemical analyses. Throughout the study, exploration quality control procedures were followed.

A database for the systematic studies of vertical and lateral variations of the composition of separate OS layers and the entire OS seam was created. It equally characterizes every defined OS layer of the OS seam from bottom to top and takes into account the internal variability of subunits thicker than 0.5 m within each layer. Barren interlayers have been omitted here. For the study of petrographic and chemical differences between the layers and spatial chemical variability within layers lithology-dependent sampling techniques were adopted. Visually, the OS unit of the Muwaqqar Chalk-Marl Formation is dominantly a rather unvaried dark-colored (dark grey to brownish grey) succession of finely bedded (laminated) very finely grained kerogen-bearing, highly carbonate rocks. Detailed visual observations as well as XRD and SEM-EDS studies revealed that the richest OS is actually composed of the dominating groundmass of about $< 5 \mu\text{m}$ carbonate and siliceous mud particles mixed with the unstructured OM – kerogen, and a

small amount of usually < 0.1 mm grains of carbonate and rare phosphate skeletal debris and random microfossils. Depending on the share and distribution of groundmass and grains, two main types of OS structure and texture dominate: (i) the most common thinly bedded (laminated) to almost massive mudstone composed of variably calcareous to siliceous share and kerogen+/-clay minerals, with small or no admixture of grain-rich films (Fig. 2a), (ii) occasionally at certain levels, a dense alternation of thin beds of the above mudstone and < 2 mm thick microbeds, lenses or laminae of dominantly carbonate grain-bearing wackestone or packstone (visual volume share $> 10\%$ (rarely up to 50–70%)) appear (Fig. 2b). Intervals of mudstone and packstone+mudstone rich OS, each > 0.5 m thick, have been sampled separately, enabling us to follow the reflection of the main lithological changes in chemical composition and quality parameters in OS successions. In the succession of thinly bedded OS layers, more often in the lower part of the OS seam, rarely from mm- to many cm-size allochems (diagenetic concretions and/or lenses) occur. They are composed of either carbonate (calcite and/or dolomite sparite concretions; Fig. 2c) or silicified or phosphatized lenses or interbeds of barren rock varieties. However, they are of limited volume and therefore sampled together with the surrounding OS. Their texture and composition are studied using SEM-EDS techniques. X-ray Fluorescence (XRF) analysis was conducted at the Institute of Geology, Tallinn University of Technology (TUT), with an S4 Pioneer Spectrometer (Bruker AXS GmbH, Germany), using an X-ray tube with a rhodium anode, which operated with the power of 3 kW. The samples were measured with a manufacturer's standard as MultiRes modification (pre-

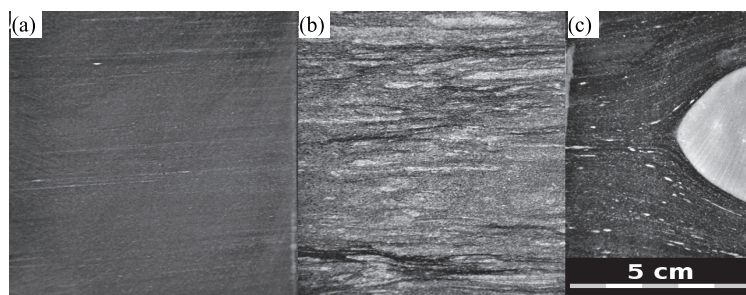


Fig. 2. Sedimentary (depositional and diagenetic) structures and textures of the Attarat oil shale, (a) and (b) representing the two main varieties of OS in the JOSE concession area of the Attarat Um Ghudran deposit: (a) – finely bedded mudstone with very thin parallel films of packstone and wackestone, both mostly composed of grains (carbonate shell debris) cemented with mudstone; (b) up to 2–3 mm thick packstone and wackestone laminae and lenses (carbonate shell debris dominating) intercalated with mudstone; (c) a rounded diagenetic concretion of silicified limestone deforming the laminated mudstone OS with few grain-bearing lenses (the lower-middle part of the OS seam). The scale is the same for all the photos.

calibrated standardless method). The in-house standard ES-2 (“Dictyonema Shale”) was used as reference material [22]. Loss on ignition was determined from 1 g of sample material at 500 °C and 920 °C. As background information for the present paper, also the data of ICP-MS analysis of OS, mineralogical studies by X-ray diffraction and SEM-EDS methods of a selection of OS and its insoluble residue samples (completed at the Institute of Geology) were taken into consideration. These data, however, need additional publication. For understanding the distribution of components in the OS layers, descriptive statistical analysis was performed. Inter-relationship between concentrations of major and trace elements and contents of mineral carriers was studied using correlation analysis.

3. Chemical composition of oil shale layers

According to the existing exploration data, the OM in the sequence of the Attarat OS unit is represented by kerogen, usually forming 5 to 30 wt% of the total OS. Volumetrically, it corresponds to approximately 12 to 53 volume% of OM (with the density of around 1 g/cm³) among the, accordingly, 88 to 47 volume% of MM (with an average density of about 2.6 g/cm³). In the most common OS, with 16 mass% of OM, its calculated volumetric content is about 33%. Consequently, the visual share of OM in oil shale is much higher than expressed in its wt% values. It is significant to consider when integrating visual and analytical weighted data.

Table 1 summarizes the average contents of macrocompounds and trace elements detected in the representative collection of conventional core samples. Table 2 characterizes variations of two main (SiO₂, CaO), and two subordinate (Al₂O₃, P₂O₅) chemical components of the mineral matter in the Attarat OS layered sequence, and of LOI (500 °C), in most cases approximately reflecting the content of OM. However, in intervals with higher contents of clay minerals (especially in layer D – see Al₂O₃ in Table 2) the LOI 500 °C value may tend to slightly overestimate the OM content. Systematized analytical data only on the productive OS layers and the total of OS layers are used here, whereas the considerably thick (> 0.5 m) barren dolomite and limestone interlayers also present within the OS seam have been omitted.

Comparing the average compositions of separate layers (Table 2) and the total average composition of the sum of all samples (Table 1), a certain specialization of layers concerning the contents of the three main components CaO, SiO₂ and LOI 500 °C is obvious (Table 3).

In the frames of minimal to maximal average concentrations of the compounds, three of them show extraordinarily high values in certain but different layers: compositions of layers E1 and E3 are strongly dominated by CaO; layer D is extraordinarily rich in SiO₂ but remarkably poor in CaO; and in samples from layer E2 the LOI 500 °C value is extraordinarily high,

Table 1. Average chemical composition and standard deviations of OS layers A to E3 (see also Fig. 3) in the JOSE concession area, AUG deposit, based on the results of XRF and LOI analyses of dominantly gapless sampling of the shale seam from 39 drill cores

Mass%	Content	SD	ppm	Content	SD
SiO ₂	20.63	11.65	Sr	657	116
TiO ₂	0.08	0.04	V	430	267
Al ₂ O ₃	2.06	1.05	Zr	38	11
Fe ₂ O ₃	0.65	0.23	Y	16	6
MnO	0.002	0.00	Mo	167	100
MgO	0.71	0.20	Cu	60	18
CaO	33.57	7.84	Zn	891	378
Na ₂ O	0.19	0.05	Ni	180	66
K ₂ O	0.26	0.09	Cr	289	81
P ₂ O ₅	2.99	1.36	As	18	10
Cl	0.07	0.01	Cd	95	48
S	2.70	0.72	F	2633	1482
LOI 500 °C	15.93	4.48	Se	36	45
LOI 920 °C	35.65	6.41			

SD = standard deviation.

Table 2. Variation of the oil shale composition by layers. Average contents and standard deviations of the five main macrocomponents in 8 OS layers and average of the total collection (the representative collection of 395 samples with a total length of 672.1 m from selected 12 representative drill cores)

Layer	E3	E2	E1	D	C	B2	B1	A	Total OS of layers E–A
Boreholes No	5	6	6	12	12	12	12	12	12
Samples No	30	14	25	33	57	109	49	78	395
Analyzed total thickness, m	48.40	22.30	42.30	54.40	99.10	193.40	84.90	127.30	672.10
SiO ₂ , wt%	7.21	8.12	8.02	43.33	24.20	21.85	21.56	27.91	20.63
SD	0.65	1.21	0.60	4.67	2.22	1.36	1.50	3.30	11.65
Al ₂ O ₃ , wt%	1.78	1.53	1.95	4.89	2.57	2.35	1.15	1.40	2.06
SD	0.49	0.12	0.12	0.46	0.20	0.12	0.08	1.40	2.06
CaO, wt%	43.58	34.96	42.48	17.12	29.71	31.67	35.15	31.18	33.57
SD	1.69	1.81	0.90	3.68	1.86	1.00	1.02	2.00	7.84
P ₂ O ₅ , wt%	1.25	0.95	1.89	1.91	3.06	2.94	3.91	5.30	2.99
SD	0.16	0.12	0.16	0.18	0.41	0.14	0.24	0.81	1.36
LOI 500 °C, wt%	13.18	28.26	13.87	15.70	18.56	17.36	14.53	13.18	15.93
SD	2.20	2.10	0.75	4.90	2.44	0.62	1.18	1.18	4.48

SD = standard deviation.

Table 3. Average ranking of chemical components in OS layers (data from Table 2)

	CaO, wt%	SiO ₂ , wt%	LOI 500 °C, wt%	Al ₂ O ₃ , wt%	P ₂ O ₅ , wt%
E3	40–45	7–9	13–15	1–2	0.9–2
E2	29–36	7–9	26–30	1–2	0.9–2
E1	40–45	7–9	13–15	1–2	0.9–2
D	15–20	40–45	15–19	4.5–5	0.9–2
C	29–36	20–28	15–19	2–2.6	2.5–5
B2	29–36	20–28	15–19	2–2.6	2.5–5
B1	29–36	20–28	13–15	1–2	2.5–5
A	29–36	20–28	13–15	1–2	5–5.5
A–E3	29–36	20–28	15–19	2–2.6	2.5–5
Legend: Notional concentration ranks	Very high	Considerably high	Ordinary	Low	

suggesting its high energetic potential. In the distribution of the three compounds certain specific patterns are observed. The contents of CaO are considerably high in the lower layers (A–C) and very high in the dominant part of layer E, with the extremely low content in layer D. Contrarily, in the lower layers A–C the SiO₂ contents are ordinary, in the upper layers E1–E3 very low and in layer D extremely high. The LOI 500 °C values reflecting the OM content are not dependent on the CaO versus SiO₂ ratio in the sequence. OM-lean samples with low LOI (< 13%) have been occasionally found within the layers. Average Al₂O₃ contents are considerably high in the SiO₂-rich layer D but low or ordinary in the other layers. In fact, usually only certain thin sublayers are enriched with Al₂O₃ (Fig. 3). Concentrations of P₂O₅ decrease from the bottom of the OS seam upwards, being considerably high in layer A (overlying the phosphate-bearing Al-Hisa Formation e.g. [2]), ordinary in layers B1–C, and low in D–E3. The most homogeneous mudstone intervals may show maximal LOI 500 °C values, whereas the grain-rich intervals tend to show lower OM content.

Regularities found in the distribution of key components are manifested in all analyzed cores. Similarly, regularities in the spread of almost all the remaining macrocomponents and also of all trace elements in the OS sequence are quasi stable across the entire JOSE study area. Individual OS layers substantially differ in concentrations of all analyzed components. The produced dataset on the average concentrations by layers is reliable. However, it has to be noted that the nature of Na₂O and Cl concentrations differs from that of all other compounds. Namely, in many localities it is affected by infiltration of NaCl from surface continental waterbodies during recent continental epochs. It requires explanation in a special paper. Detailed visual, microscopic and SEM observations of thin beds, lenses and laminae show that on the detailed scale (mm-s and cm-s) the concentrations of all

compounds are even more variable, and the concentration maxima and minima of thin interlayers may significantly differ from the averages of OS layers.

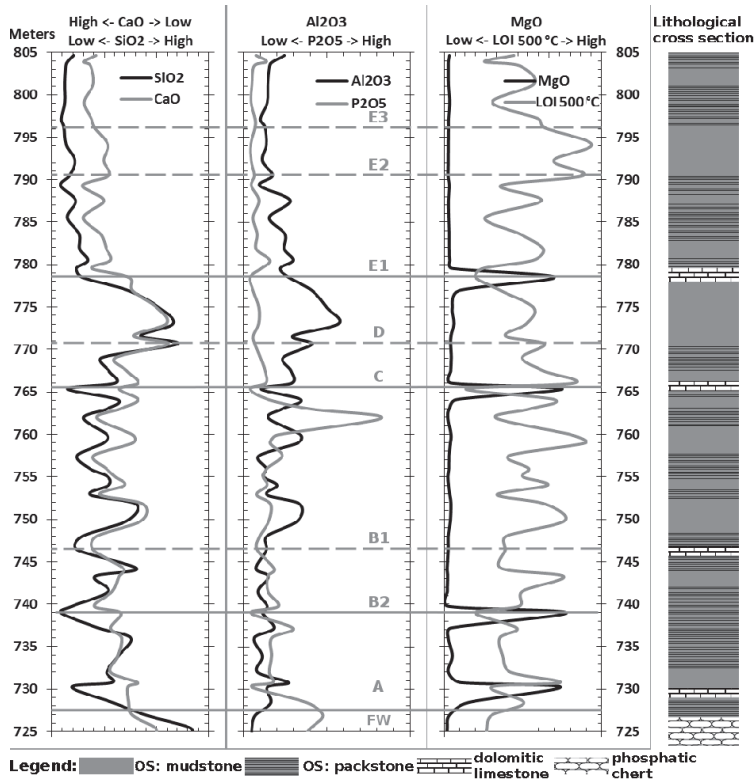


Fig. 3. Selected major element composition of MM and LOI @500 °C (reflecting the OM content) variation in a core section from the JOSE concession area. Average content values of individual 0.5–2 m long sample intervals are visualized. Note that the scales of CaO and SiO₂ contents are reverse. The OS layers are defined using complex data of visual lithological description, downhole natural gamma-logging and chemical data on the distribution of macrocompounds and trace elements.

On a 0.5–2 meter long sample scale, the internal compositional variance of each OS layer is reflected in the variation of standard deviation values (Tables 1 and 2). Comparing different components of the total sample collection from layers A–E3, the concentrations of CaO and LOI 500 °C

show considerably low variation, whereas concentrations of SiO_2 , Al_2O_3 and P_2O_5 are highly variable (Table 1). Comparing standard deviations of components' concentrations for separate layers from A to E3, the differences in the variability of components within a layer become evident (Table 2). The relatively low variability of SiO_2 as well as the lowest variability of CaO concentrations for layers B1, B2, E1 and E3 suggests a more homogeneous composition. The considerably high standard deviation values of SiO_2 and CaO for layers A, D and E2 are indicative of a more heterogeneous composition. A short analysis demonstrates that the changes of mineral composition most influence the chemical heterogeneity. Increase of the standard deviation of the five main chemical components depends on compositional changes: calcite versus silica in mudstone, a variable share of mudstone versus wackestone+packstone, and content variations of apatite, clay minerals and OM. As an example, the relative homogeneity of some layers and heterogeneity of others is visualized in Figure 3. The vertical distribution of compounds concentrations in layers from A to E3 in all 12 studied core sections is principally similar, suggesting a considerable lateral stability of the defined layers compositions.

In the succession of layers A–E3 (Fig. 3) the peaks of the MgO curve mark well the interlayers of barren dolomitic limestones. In some sequences, few minor barren limestone interbeds occur that are not separately depicted in Figure 3. In OS layers, the contents of CaO and SiO_2 usually show up negative correlation, the most remarkable are the SiO_2 peak and CaO low corresponding to layer D. The Al_2O_3 curve is well congruent to the SiO_2 curve, with a significant peak corresponding to layer D (Fig. 3). The LOI 500 °C curve is occasionally congruent to SiO_2 - Al_2O_3 peaks, but is usually poorly connected to mineral components.

Table 1 also presents the average contents and standard deviations of additional 10 major and 13 trace elements of the studied samples. The contents of usual major elements in a sedimentary rock (Fe_2O_3 , MgO, Na_2O , K_2O) remain below 1 wt%, whereas TiO_2 , MnO, and Cl are below 0.1 wt%. The average contents of P_2O_5 (2.99 wt%) and S (2.7 wt%) are considerably high. Standard deviation values of the average concentrations of certain major and trace elements are variable, mostly depending on the content variance of carrier minerals such as calcite, silica, phosphate, clay minerals and OM. Many trace elements are present in concentrations higher than normal for carbonate rocks. Carrier minerals and macro- and trace-element content details are worthy of a separate approach to statistical methods.

4. Conclusions

The new analytical data on the representative sample collection of the entire OS sequence in the JOSE concession area enabled the authors to describe the stable layered internal chemical structure of the whole OS seam and to

discover its spatial variation of composition and energetic potential in a 73 km² portion of the Attarat Um Ghudran-Wadi Maghara oil shale basin. The data principally confirmed the concentration ranges of components reported by Abed and Amireh [3], Hufnagel [13], Hamarneh et al. [4, 5], Abed and Arouri [8] and Alali [6]. However, the regularities in the vertical distribution of chemical components and their variation patterns are new original information. The vertical distribution of the studied chemical element concentrations in all studied core successions, i.e. the layered structure, is principally similar but still remarkably changeable in details over the whole study area. It is revealed from the analytical dataset on the 37 core sections and additional data of visual and photo documentation and gamma-logging of over 150 core and percussion boreholes. The structure and composition of the OS seam suggest that its primary depositional nature has principally survived. In places, the identified layers show minor local tendencies of synsedimentary thickening or thinning. The OS layers have only locally slightly changed in the diagenetic processes, whereas the barren limestone interlayers are strongly enriched with MgO and depleted of CaO that is caused by diagenetic dolomitization.

The data obtained on the variation of the average chemical composition are probably applicable for the comparison of OS layers' compositions across the large Attarat Um Ghudran-Wadi Maghara OS basin of Central Jordan and possibly with the other OS basins and deposits in Jordan and farther. The chemical patterns firmly support the introduced original detailed stratification scheme of the studied oil shale unit that is deduced from the complex database. However, comprehensive comparative analysis of the chemical composition might be more fertile with the results of mineralogical studies, which is, however, the next separate research task.

The data on the layered chemical structure serve as geological and chemical base information for the OS quality and compositional modelling of the deposit, and for the design of mining and OS processing technologies.

REFERENCES

1. Sharland, P. R., Archer, R., Casey, D. M., Davies, R. B., Hall, S. H., Heward, A. P., Horbury, A. D., Simmons, M. D. *Arabian Plate Sequence Stratigraphy*. GeoArabia Special Publication 2. Gulf PetroLink, Manama, Bahrain, 2001, p. 372.
2. Powell, H. J., Moh'd, K. B. Evolution of Cretaceous to Eocene alluvial and carbonate platform sequences in central and south Jordan, *GeoArabia – Middle East Petroleum Geosciences*, 2011, **16**(4), 29–82.
3. Abed, A. M., Amireh, B. S. Petrography and geochemistry of some Jordanian oil shales from North Jordan. *J. Petrol. Geol.*, 1983, **5**(3), 261–274.
4. Hamarneh, Y. *Oil Shale Resources Development in Jordan*. Natural Resources Authority, Hasemite Kingdom of Jordan, Amman, 1998.
5. Hamarneh, Y., Alali, J., Sawaged, S. *Oil Shale Resources Development in Jordan*. Natural Resources Authority of Jordan (updated report), Amman, 2006.

6. Alali, J. Jordan oil shale, availability, distribution, and investment opportunity. *Int. Conf. on Oil Shale: "Recent Trends in Oil Shale"*, Amman, Jordan 7–9 November 2006, Paper no. rtos-A 117.
7. Dyni, J. R. *Geology and Resources of Some World Oil-Shale Deposits*. Scientific Investigations Report 2005-5294. U.S. Geological Survey, Reston, Virginia, 2006.
8. Abed, A. M., Arouri, K. Characterization and genesis of oil shales from Jordan. *Int. Conf. on Oil Shale: "Recent Trends in Oil Shale"*, Amman, Jordan 7–9 November 2006, Paper no. rtos-A121.
9. Abed, A. M., Fakhouri, K. On the chemical variability of phosphatic particles from Jordanian phosphorite deposits. *Chem. Geol.*, 1996, **131**(1–4), 1–13.
10. Hutton, A. C. Petrographic classification of oil shales. *Int. J. Coal Geol.*, 1987, **8**(3), 203–231.
11. DeWolfe, C., Horne, E. J., Morgan, C. A. *Geology and Geochemistry of the Al Lajjun Oil Shale Deposit, Central Jordan*, AAPG Conference and Exhibition, Calgary, Alberta, Canada, September 12–15, 2010.
12. Puura, V., Martins, A., Baalbaki, M. Kh., Al-Khatib, K. Occurrence of oil shales in the south of Syrian Arab Republic. *Oil Shale*, 1984, **1**(4), 333–340.
13. Hufnagel, H. Die Ölschiefer Jordaniens. In: *Geologisches Jahrbuch*, Reihe A, Heft 75, Hannover, 1984, 295–312 (in German).
14. Bauert, H., Kattai, V. Kukersite oil shale. In: *Geology and Mineral Resources of Estonia* (Raukas, A., Teedumäe, A., eds.). Estonian Academy Publishers, Tallinn, 1997, 313–327.
15. Petersell, V. Dictyonema argillite. In: *Geology and Mineral Resources of Estonia* (Raukas, A., Teedumäe, A., eds.). Estonian Academy Publishers, Tallinn, 1997, 327–331.
16. Voolma, M., Soesoo, A., Hade, S., Hints, R., Kallaste, T. Geochemical heterogeneity of Estonian graptolite argillite. *Oil Shale*, 2013, **30**(3), 377–401.
17. Hade, S., Soesoo, A. Estonian graptolite argillites revisited: a future resource? *Oil Shale*, 2014, **31**(1), 4–18.
18. Soesoo, A., Hade, S. Black shales of Estonia: moving towards a Fenno-scandian-Baltoscandian database. *Transactions of Karelian Research Centre of Russian Academy of Sciences: Precambrian Geology*, 2014, **1**, 103–114.
19. Enefit Outotec Technology. 2015. www.enefit.com/en/eot (accessed 15 November 2015).
20. Puura, V., Bauert, H., Männil, R. The Conditions of Kukersite Deposition. In: *Proc. Int. Conf. Oil Shale and Shale Oil*, Beijing, China, May 16–19, 1988. Chemical Industry Press, Beijing, 1988, 42–51.
21. Kattai, V., Puura, V. Commercial Zonation of the Estonian Oil Shale Deposit. In: *Proc. Int. Conf. Oil Shale and Shale Oil*, Beijing, China, May 16–19, 1988. Chemical Industry Press, Beijing, 1988, 51–60.
22. Kiipli, T., Batchelor, R. A., Bernal, J. P., Cowing, Ch., Hagel-Brunnström, M., Ingham, M. N., Johnson, D., Kivisilla, J., Knaack, Ch., Kump, P., Lozano, R., Michiels, D., Orlova, K., Pirrus, E., Rousseau, R. M., Ruzicka, J., Sandström, H., Willis, J. P. Seven sedimentary rock reference samples from Estonia. *Oil Shale*, 2000, **17**(3), 215–223.

Presented by

Received

5. Voolma, Margus; Soesoo, Alvar; Puura, Väino; Hade, Sigrid; Aosaar, Hardi (2016). Assessing geochemical variability of oil shale in the Attarat Um Ghudran deposit, Jordan. *Estonian Journal of Earth Sciences*, 65(2), 61-74.

Assessing the geochemical variability of oil shale in the Attarat Um Ghudran deposit, Jordan

Margus Voolma^a, Alvar Soesoo^a, Väino Puura^b, Sigrid Hade^a and Hardi Aosaar^c

^a Institute of Geology at Tallinn University of Technology, Ehitajate tee 5, 19086 Tallinn, Estonia; margus.voolma@ttu.ee

^b Department of Geology, Institute of Ecology and Earth Sciences, University of Tartu, Ravila 14A, 50411 Tartu, Estonia

^c Eesti Energia AS, Lelle 22, 11318 Tallinn, Estonia

Received 4 January 2016, accepted 16 March 2016

Abstract. The Cretaceous to Palaeogene oil shale (OS) of Jordan is predominantly calcareous mudstone with intervals of mostly siliceous minerals, quartz and cristobalite–tridymite. Oil shale is rich in organic sulphur and trace elements. According to preliminary micropalaeontological data, the OS succession of the studied area, the south-central part of the Attarat Um Ghudran (AUG) deposit in central Jordan, is of Maastrichtian age. A representative collection of 392 samples from 9 drill cores reliably characterizes the sequence of the OS seam, on average 70 m thick. The composition of AUG OS varies significantly. The major compounds CaO and SiO₂ range within 3–70 wt% and 10–50 wt%, respectively, and also the contents of organic matter, MgO, P₂O₅, Al₂O₃ and S change. The concentrations of metals (especially Zn, V, Cr, Ni and Mo) change many dozens of times in the cross section. The aim of our statistical analysis was to determine the most significant OS types and their positions in the OS sequence. Two multivariate statistical analysis methods, principal components analysis (PCA) and hierarchical clustering of PCA groups, gave an interpretable result. Four principal components account for 88.6% of data variability. Variation in six main chemical components or groups of components is reflected in parameters of the four principal components. The component PC1 accounts for 47% of the data variance, expressing the highest correlation with organic matter, S, Cr, Cu, Ni, Zn, Mo, and PC2 accounts for 22.82% of the data variability, being strongly correlated with TiO₂, Al₂O₃, Fe₂O₃, SiO₂ and K₂O and negatively correlated with CaO. The next two significant component groups express covariance with CaO and MgO. The applied statistical analysis proves to be a powerful tool for the interpretation of the chemically variable structure of the OS unit when using a representative enough sample collection. In the complex study of the OS unit, variation in the chemical composition is of interest, especially in the context of genetic and mining aspects.

Key words: oil shale, Maastrichtian, mineral matter, geochemical variability, Attarat Um Ghudran deposit, central Jordan.

INTRODUCTION

Jordan is extraordinarily rich in oil shale (OS) resources. Abed & Amireh (1983) have summarized the early (1959–1980) publications on the occurrences of OS in Jordan. At that time, OS was considered as a major future energy resource in Jordan devoid of oil. Subsequent prospecting and exploration campaigns organized by the Government (Hamarnah et al. 2006) cleared the way for developers interested in acquiring concessions in order to initiate the resource exploration and feasibility studies by interested companies. The Estonian–Jordanian company Jordan Oil Shale Energy (JOSE) applied for the concession in the southern part of the Attarat Um Ghudran (AUG) deposit (Fig. 1).

Nevertheless, systematic study of OS chemical composition and its variation in connection with the internal

structure of the OS unit was never performed, within the AUG deposit or elsewhere in Jordan. However, recent facies (Powell & Moh'd 2011) and micro-biostratigraphic (Alqudah et al. 2014a, 2014b, 2015) studies enable us to converge to the interpretation of the observed variable geochemical nature of OS accumulation. During 2008–2013, JOSE committed a detailed exploration campaign on its concession area. Analyses of the chemical composition were included in these studies.

Chemical investigation was designed to identify the compositions of and variations in the OS layers and resulted with the definition of subunits – OS layers and barren interlayers (Puura et al. 2016). Certain regularities of average composition and contrast anomalies of macro-component and trace element distribution in the total OS unit and its separate layers were defined. Linking the data on palaeogeography and facies with

exposed in wadi valleys and lower slopes of hills. A hiatus between the MCM and the overlying Umm Riham Chert Limestone Formation corresponds to the Paleocene. The Eocene Riham Chert Limestone Formation, up to 50 m thick, is represented by non-OS chert and marl beds composing tops of jabels (watersheds between the wadi valleys).

The AUG deposit, together with the Wadi Maghara deposit, form a uniform north–southerly elongated OS deposit on a territory of over 1000 km² with total resources over 55 billion tons (Hamarnah et al. 2006). The basin and the exploration area have an east-central position among a large number of OS deposits known in Central Jordan (Fig. 1). Detailed lithological and chemical studies conducted in the JOSE concession area suggest that the OS unit consists of lithologically differing OS layers and dolomitic limestone interlayers (Puura et al. 2016). Data on average concentrations of macro- and trace element contents demonstrate significant differences between the layers and variations within the layers. Consequently, the conditions of OS accumulation in the basin have repeatedly changed, which has neither been described nor interpreted so far.

Geological setting of the Attarat Um Ghudran and Wadi Maghara deposits

Geologically, the territory of Jordan is located in the northwest part of the Arabian Plate. Starting in the Palaeozoic, a thick sedimentary cover evolved during several phases (Sharland et al. 2001; Powell & Moh'd 2011). Systematic lithofacies studies of the Cretaceous to Eocene succession in central and southern Jordan (Powell & Moh'd 2011) revealed that (i) the area is characterized by passive continental margin depositional sequences, which pass upwards from alluvial/paralic to carbonate shelf and pelagic ramp settings, and (ii) sedimentation during the Santonian to Maastrichtian was characterized by a hemipelagic chalk–chert–phosphorite lithofacies association, deposited in shallow to moderate water depths on a homoclinal ramp setting, although thicker coeval sequences were deposited in extensional rifts.

Throughout the Early Cretaceous to Eocene, the large temporarily submerged shallow marine clastic and carbonate platform surrounded the continental area of the Arabian Shield in the south and was surrounded by a deep marine clastic and carbonate platform of Neo-Tethys in the northwest (the Mediterranean Neo-Tethys Domain) and northeast (the Eastern Neo-Tethys Domain) (see fig. 1A in Alqudah et al. 2015). Due to upwelling systems, there, the shallow marine deposits contain rich OS and phosphate accumulations (Abed 2013).

A comprehensive and representative study of nannofossils from OS sequences of Jordan was committed and OS sequences of Maastrichtian, Paleocene, Early Eocene and Middle Eocene age were identified by Alqudah et al. (2014a, 2014b, 2015). The data revealed that the thickest OS sequences occur in deep sub-basins that developed due to synsedimentary subsidence of the seabed in active fault zones. The accumulation of the OS-bearing and other deposits in the rifting-induced sub-basins and on swells was strongly influenced by climate, tectonic processes and relief of the hinterland. All these factors are supposed to have controlled the influx of terrigenous material (Alqudah et al. 2015). Due to asynchronous subsidence histories of the basins, the location of Maastrichtian, Paleocene and Eocene OS suites in Jordan varies substantially.

Based on reconstructions by Alqudah et al. (2015), the uniform area of the AUG and Wadi Maghara oil shale deposits lies in the transition zone between the deepest zones of the El-Lajjun Sub-basin with Maastrichtian OS (in the west) and the Azraq-Hamza Sub-basin with Maastrichtian–Eocene and locally with over 500 m thick Eocene OS (in the east). The Jafr Sub-basin with Maastrichtian–Eocene OS (locally over 250 m thick) is situated some 100 km to the south. The maximum up to almost 100 m thickness of the Maastrichtian OS unit of the JOSE concession area is less than the deepest parts of the listed sub-basins, but still considerable.

Within the exploration area, the OS unit is of stable internal structure – eight OS layers and three dolomitic limestone interlayers have accumulated uniformly. However, its structure probably changes markedly away from the JOSE concession area. The relatively shallow JOSE sedimentation area is detached by deep basins and swells from both the Arabian-African continent far (over 200 km) in the south and from the Mediterranean Neo-Tethys Domain (palaeo-ocean) in the NE (150 km). Alqudah et al. (2014a, 2015) describe changes in sea-level and land-sea configurations and provide data on synchronous or asynchronous as well as compressional or tensile tectonic stresses causing uplift or subsidence in different fault belt-related deep sub-basins.

MATERIAL AND METHODS

An overview of the chemical composition of Jordan oil shales from different localities has been presented by Abed et al. (2009) and Dyni (2003). In historical studies, however, sampling was sparse and random, and the list of the components analysed was usually incomplete. Unlike previous studies, the present study is based on a representative, systematic sample collection. The samples

are owned by JOSE and only abstract contents of elements can be presented here. Using different analytical techniques (XRF and ICP-MS), the concentrations of more than 40 elements were determined in OS and the surrounding rocks. Geological field and laboratory studies confirmed that primarily the OS layers have accumulated as continuous layers across the whole exploration area. In places, the topmost layers have altered due to weathering, hence the varying thickness of the OS sequence in different drill cores; those samples have been omitted from the data handling and interpretations. For the present detailed geochemical study, 392 samples from nine representative drill cores out of 36, characterizing the full sequence of OS in the JOSE area, were selected. The average thickness of one sample is 1.58 m; the number of samples in a drill core varies from 37 to 55, representing on average 70.1 m of the OS sequence. For the variation and position of lithologically different OS types and thicknesses of individual OS layers along with the chemical composition variation of major elements in the cross section see figure 3 in Puura et al. (2016).

Bisected drill cores were logged and photographed in Jordan. Samples for quality assessment were taken from lithologically uniform intervals with a 0.5–2.0 m step, continuously without any gaps (breaks) between the intervals, coarse-crushed and sent for analyses. The sampling and sample preparation methodology used guarantees a high reliability of (weighted) average compositions of sample intervals, separate OS layers and barren interlayers and the total OS seam.

About 60 g of material was separated from a coarse-crushed sample (< 2 mm) for chemical and mineralogical analysis, using a Humboldt riffle-type sample splitter. The samples were dried in an oven over 24 h at 105°C. For XRF, XRD and ICP-MS analysis the samples were fine-crushed (pulverized) in a ring mill. Loss on ignition (LOI) was determined from 1 g of pulverized sample material at 500°C and 920°C. X-ray fluorescence analysis was conducted at the Institute of Geology at Tallinn University of Technology (IG TUT) with an S4 Pioneer Spectrometer (Bruker AXS GmbH), using an X-ray tube with a rhodium anode, which operated with the power of 3 kW. The samples were measured with a manufacturer's standard as MultiRes modification (pre-calibrated standardless method). The in-house standard ES-2 ('Dictyonema Shale') was used as reference material (Kiipli et al. 2000). The detection limits for trace elements analysed with XRF at the IG TUT are 10 ppm for Ni, Cu, Zn, Ga, Ge, As, Se, Br, Rb, Sr, Y, Zr, Nb, Mo, U, Th, 20 ppm for Sc, V, Cr, Co, Ag, Cd, Sn, Sb, Te, Pb, W, 50 ppm for I, Cs, Ba, La, Ce, Nd and 0.1% for F.

All lithological layers more than 0.5 m thick were sampled separately, however, thin (<50 cm) interbeds

seldom observed in the sequences are mixed with material of surrounding thick layers. Therefore certain anomalous varieties of OS or barren rock remain chemically unrecorded. The chemical composition of 1284 samples was analysed. All geochemical data used in this work were acquired during the exploratory programme according to the contract between Enefit/JOSE and the IG TUT. Variation in the chemical composition of 392 samples, forming a regular dataset, from nine representative drill cores (with complete OS sequences) is described by 18 elements whose concentrations constantly exceed the analytical detection limit. The elements and components used in this study are SiO₂, TiO₂, Al₂O₃, Fe₂O₃, MgO, CaO, K₂O, P₂O₅, S, LOI500°C reflecting organic matter (OM), Zn, Ni, Cr, Cu, Mo, V, Zr and Sr. The rest of the analytical dataset (over 600 more samples and over 20 more components in all samples appearing partially in concentrations below the detection level) is used in ongoing geochemical studies and serves as background information herein.

Linking geochemical patterns of a sediment succession with a number of known and unknown geological factors requires a complex multi-step multivariate analysis. As a first step, the statistical analysis is applied in order to define variations and highlight changes in major and trace element compositions that may be linked to certain fluctuations in the course of accumulation of the primary OS sediment and other contemporary and later processes. One of the well-known statistical tools is principal component analysis (PCA), which is the general name for a technique that uses sophisticated underlying mathematical principles to transform a number of possibly correlated variables into a smaller number of variables called principal components. In general terms, PCA uses a vector space transform to reduce the dimensionality of large datasets (like geochemical analyses). Using mathematical projection, the original dataset, which may have involved many variables, can often be interpreted in just a few variables (the principal components). The examination of the reduced dimension dataset will allow the user to spot trends, patterns and outliers in the data, far more easily than would have been possible without performing the PCA.

The dataset for present statistical analyses is composed of 392 data rows as chemical analyses and 18 columns as elements (9 drill cores by 18 elements). Two methods of multivariate analysis were used for data assessment: (i) PCA and (ii) hierarchical clustering of PCA groups. Both analyses were carried out by using software 'R' (package 'FactoMineR') and RExcel. A detailed description, the formulas used and the mechanism of the construction for these parameters are given by Le et al. (2008) and Husson et al. (2010, 2011).

General geochemical characteristics of oil shale in the Attarat Um Ghudran deposit

In addition to small-scale dolomitic limestone layers, two large types of OS can be distinguished in the cross section: (i) mudstone OS that is dark brown to black, almost massive or very finely laminated and (ii) wackestone OS that contains varying amounts of grains (fossil shells and shell debris) and concretions (Puura et al. 2016). According to SEM-EDS observations, grains and concretions in the OS are predominantly calcitic or, in places, carbonate fluorapatite in composition.

In general, according to XRD studies, the mineral composition of OS is limited to calcite, carbonate fluorapatite, quartz (with additional tridymite–cristobalite in certain intervals) and smectite with minor pyrite, sphalerite and barite identified so far (Puura et al. 2016). The variation through the cross section is significant. The content of calcite varies from 8% to 88%, quartz to 51% (cristobalite + tridymite to 47%), and dolomite from below the detection limits (approximately <2%) to 80%, apatite to 40% and clay minerals range to 31%. The corresponding chemical and mineralogical composition is similar to that of the Lajjun deposit, located westwards from the current study area as described by Hufnagel (1984) and Abed et al. (2009).

Despite the dominating carbonate composition of the OS suite, the mineral and chemical composition of the AUG OS seam still varies significantly in cross section (Table 1). Major element composition studies indicate that SiO₂ and CaO range within 3–70 wt% and 10–50 wt%, respectively, and show strong inverse correlation (Fig. 2). The usually low MgO and P₂O₅ content rises randomly up to 16 wt%. The Al₂O₃ and S concentrations are locally up to 7 wt% and 6 wt%, respectively. The OM content in the deposit varies from 4 wt% to 38 wt%. A significant variation occurs also in trace metal contents, for Zn and V ranging within 100–2784 ppm and 78–2040 ppm. Ni, Cr and Mo show concentrations from a few tens of ppm to 488, 626 and 614 ppm, respectively.

Geochemical variation in major and trace elements significantly depends on the layered structure of the OS unit (Table 1). Apart from lithological OS types, there are geochemical distinctions separating different OS layers, indexed A to E3. Unlike the rest of the layers, certain OS layers show distinct enrichment in some elements, for example, kerogen- and trace metal-rich layer E2 (Fig. 2, Zn vs Ni plot), SiO₂-rich layer D, CaO-rich and SiO₂-poor layers E3 and E1 (Fig. 2, SiO₂ vs CaO plot) and P₂O₅-rich layer A (Fig. 2, P₂O₅ vs CaO plot). The dolomitic limestone

Table 1. Mean, minimum and maximum concentrations of chemical elements in 392 samples and average thickness of 398 samples from nine drill cores; and average thickness and concentrations by different oil shale and barren rock layers (A–E3) distinguished in the concession area, Attarat Um Ghudran deposit, Jordan. Organic matter (OM) reflected by LOI500°C. Major elements in wt%, trace elements in ppm. (The chemical composition of dolomitic limestone layers A/B, B/C and D/E was not analysed in two drill cores)

	Total data			Average by distinguished layers										
	Mean	Min	Max	A	A/B	B1	B2	B/C	C	D	D/E	E1	E2	E3
Number of samples	392 (398)			66	7 (9)	38	84	7 (9)	44	28	7 (9)	45	22	44
Thickness (m)	1.59	0.50	2.00	1.51	0.78	1.70	1.73	0.55	1.68	1.54	1.15	1.63	1.57	1.69
SiO ₂	18.90	2.59	71.70	29.23	5.97	19.75	19.88	8.79	22.21	40.13	9.21	8.84	7.59	5.13
TiO ₂	0.08	0.02	0.29	0.05	0.04	0.05	0.09	0.05	0.10	0.20	0.07	0.08	0.06	0.05
Al ₂ O ₃	2.02	0.38	6.97	1.28	1.15	1.18	2.29	1.67	2.56	4.84	1.99	2.20	1.64	1.20
Fe ₂ O ₃	0.63	0.21	1.77	0.49	0.37	0.46	0.65	0.43	0.76	1.27	0.49	0.65	0.66	0.44
MgO	1.37	0.22	15.50	1.13	11.99	0.46	0.84	9.88	0.77	1.28	12.29	0.63	0.54	0.59
CaO	33.91	10.79	49.26	30.34	34.73	36.20	32.98	33.13	30.82	18.87	31.97	41.48	34.75	43.84
K ₂ O	0.25	0.06	0.62	0.22	0.11	0.18	0.34	0.21	0.35	0.41	0.13	0.22	0.19	0.12
P ₂ O ₅	2.82	0.47	16.58	5.03	1.38	3.85	3.01	1.63	3.20	1.80	0.72	1.91	0.97	1.12
S	2.68	0.54	6.22	2.65	0.80	2.66	2.82	1.18	2.98	2.81	0.72	2.24	4.73	2.37
OM	16.02	4.13	38.28	13.17	6.13	14.85	17.30	8.03	18.65	16.37	5.77	14.53	29.13	15.43
Zn	862	100	2784	876	176	764	769	288	946	856	149	657	2035	954
Ni	173	28	488	148	43	158	167	66	193	163	35	151	378	203
Cr	292	83	626	230	108	241	312	152	331	328	105	284	488	320
Cu	60	<10	131	61	16	62	61	25	65	53	12	53	106	60
Mo	143	12	614	136	17	96	133	36	170	180	19	103	348	157
V	436	78	2040	508	113	341	292	114	388	427	98	347	1395	508
Zr	38	<10	85	28	16	33	43	21	43	48	29	39	44	36
Sr	680	229	1855	585	375	729	697	432	710	568	565	759	769	770

interlayers show compositionally extreme values for certain elements, especially MgO (layers A/B, B/C, D/E) (Fig. 2, MgO vs CaO plot). The OS layers (A–E3) and barren interlayers can be followed at least across the JOSE study area. A selection of X–Y correlation graphs (Fig. 2) illustrates cases of strong positive, negative and less significant correlation relationships of main and trace elements, varying also by the layers. However, the internal chemical structure and the compositional changeability within the layers are difficult to assess visually or by using simple correlation methods. This is the reason why statistical multivariate methods have been applied to transform a number of possibly correlated variables (chemical elements) into a smaller number of variables, which can be later interpreted through geological processes and elemental composition.

DISCUSSION

Traditionally, the oil shales of the Muwaqqar Chalk-Marl Formation of Jordan are described as predominantly uniform kerogen-bearing calcareous rocks, most frequently named just as chalk and marl (Abed 2013; Alqudah et al. 2014a, 2015). Systematic and regular sampling and analyses of the full OS succession in Central Jordan have changed the image. The JOSE exploration process revealed the stable internal layered structure of the OS unit caused by compositional variations (Puura et al. 2016). Together with general lithological data, mineral composition and gamma-log survey, the specific chemical compositions and geochemical contrasts of layers served for the complex definition of OS layers and barren interlayers in the OS unit of the JOSE exploration area. The dominating thick OS suite is separated into subunits by thin but continuous barren interlayers of dolomitized limestones, and other marker surfaces. Besides the principal layered structure of the OS unit, regular differences between mineral and average chemical compositions of layers were established, as presented in Table 1.

As the first step in assessing the geochemical variability, statistical analysis is applied in order to define major and trace element variations and contrast main changes in the sedimentary sequence of OS and barren rock. The definition of distinct geochemical patterns among and also inside the distinguished layers is an additional result of the study. Further on, the integration of statistical and geological results will help to study trends and changes in the accumulation of original sediments – OS layers, barren rock interlayers, and their internal variability.

Principal component analysis for distinguishing the geochemical characteristics and clustering of samples

Nine drill cores across the AUG OS deposit, each represented by approximately 45 samples described by 18 variables (chemical elements), were chosen for PCA. The aim of the statistical analysis is to determine significant types of different OS and barren rock and their position in the overall sequence of the OS unit in combination with geochemical patterns.

Principal component analysis and the hierarchical clustering of PCA groups are used for geochemical data assessment. Eigenvalue, derived from PCA, is a measure of quality of data representation and shows the relative importance of the components. In the present dataset, four principal components are significant, as each of those accounts for over 10% of variability. The first principal component (PC) accounts for 47.11% of data variability, the second component for 22.82%, while four components together account for nearly 90% of data variability (70% by the first two components; Fig. 3). In order to visualize interrelationships between PC and chemical elements (Table 2), the planes constructed by pairs of principal components PC1 to PC4 (Fig. 4) are presented. Plots of single samples (grouped into clusters) on the planes PC1–PC2 and PC1–PC3 demonstrate association between clusters and principal components (Fig. 5). When interpreting the geochemical data and elemental variation parameters, it is important to consider the main carriers of major and trace elements: calcite as the carrier of CaO; dolomite as the carrier of CaO and MgO; quartz (and modifications) – SiO₂; clay minerals – Al₂O₃, SiO₂, K₂O, TiO₂; carbonate-fluorapatite – P₂O₅, CaO; organic matter – expressed as LOI500°C (includes part of sulphur and carries Zn and many other trace metals).

Relying upon the described methodology, the interpretation of significant principal components is given below.

PC1 – The first PC describes 47% of the data variance. It is strongly correlated with many variables (Table 2), with the highest correlation with S and OM (LOI500°C), and also Cr, Cu, Ni, Zn and Mo. Very strong correlation between OM, S, and trace metals suggests that these elements vary together. This component can be interpreted as a measure of sulphur- and trace-element-carrying OM versus carbonate-silicate mineral matter (calcite, dolomite, silica) content.

PC2 – The second PC accounts for 22.82% of the data variability. It is strongly correlated with TiO₂, Al₂O₃, Fe₂O₃, SiO₂ and K₂O. Strong negative correlation occurs with CaO (Table 2). The component can be

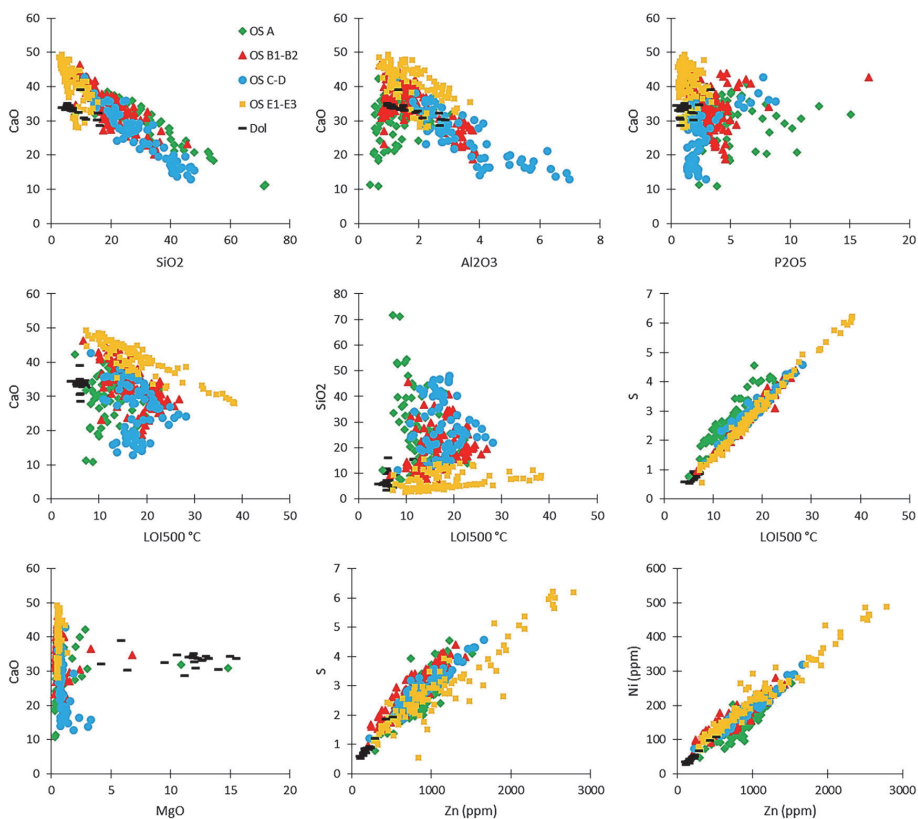


Fig. 2. A selection of X–Y plots between 9 elements, selected out of the studied 18 using analytical data on single samples. The plots demonstrate the best examples of variable nature of correlations between certain different components of the oil shale (OS) unit in total: (i) strong negative (CaO vs SiO_2) or moderate negative (CaO vs Al_2O_3) or scattered (CaO vs P_2O_5) correlation between the main mineral components of OS, (ii) scattered (diffuse) correlation between CaO and SiO_2 contents and LOI500°C, the latter reflecting the content of organic matter, (iii) strong positive correlation between LOI500°C and S, and further on between S and Zn, and Zn and Ni. The plots reflect also distinct geochemical differences between certain layers and the rest of samples, e.g. layers C and D on the CaO vs Al_2O_3 plot and layers E1–E3 on many plots. The MgO vs CaO plot expresses the presence of elevated MgO contents only in barren dolomitic limestone layers.

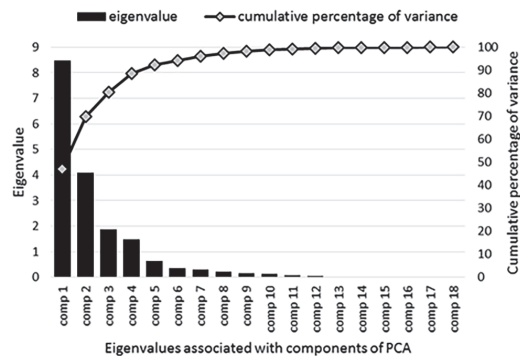


Fig. 3. Bar plot of the eigenvalues showing the number of components significant for interpretation. In the present dataset, the first four components account for 88.66% of variability.

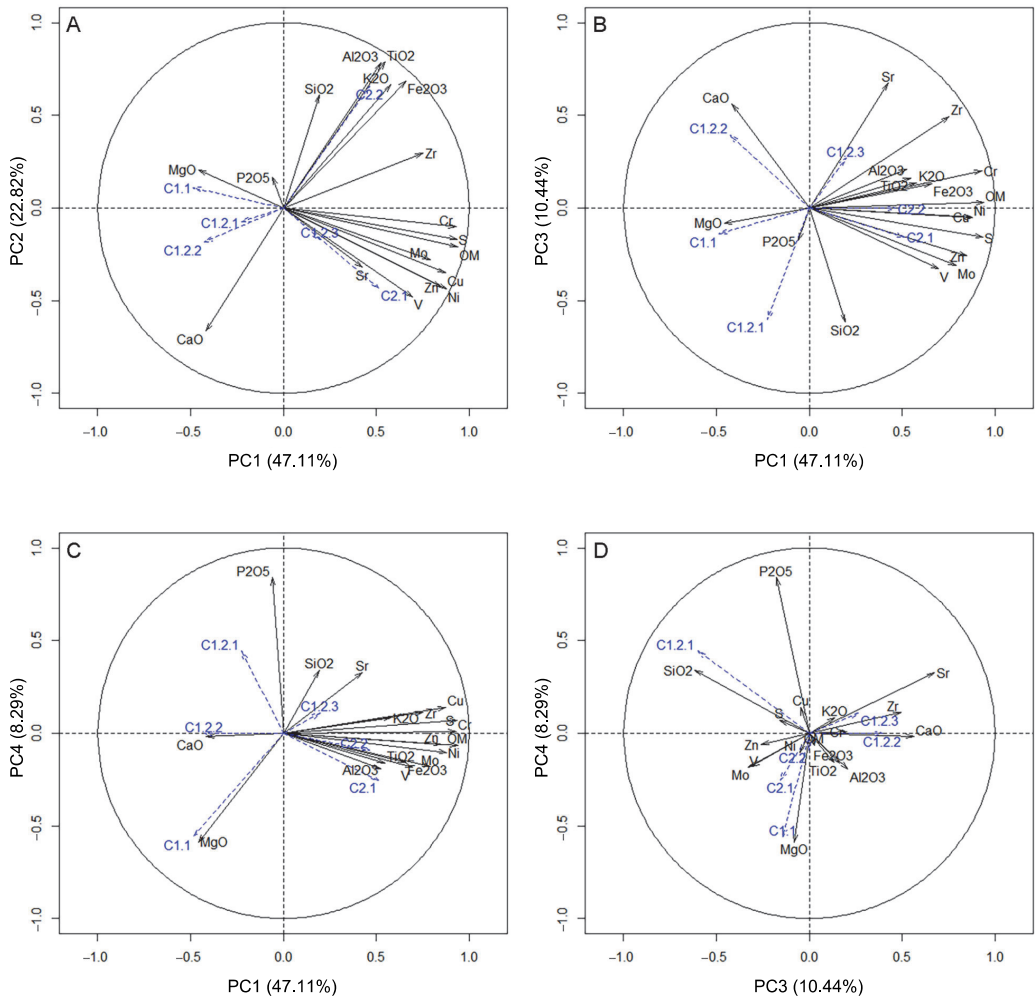


Fig. 4. Graphs of the analysed major and trace elements on the planes constructed by principal components. The distance between the chemical component projected onto a plane and the correlation circle with radius 1 demonstrates the correlation of the variable and principal components (Table 2). The distance from an axis shows the quality of how well the element is projected onto a corresponding plane. The proximity of variables on the plane means also strong association between individual elements (for example OM and S on planes A, B and C; see also Fig. 2 LOI500°C vs S plot). Clusters (C1.1 to C2.2) are presented to demonstrate the association between chemical components and principal components (see text for the explanations). On a main plane (explains 69% of variability) constructed by principal components PC1 and PC2, OM (LOI500°C), S, Cr, Mo, Cu, Zn and V are positively correlated to PC1, while MgO and CaO are negatively correlated to PC1. It means that samples with a high concentration of MgO have a low content of OM (LOI500°C), S, Cr, Mo, Cu, Zn and V, and vice versa. Strong positive correlation is between TiO₂, Al₂O₃, Fe₂O₃, SiO₂, K₂O and PC2, while CaO is negatively correlated to PC2. Thus the samples with a high CaO content have low TiO₂, Al₂O₃, Fe₂O₃, SiO₂ and K₂O contents, and vice versa.

interpreted as ‘silicates’ (clay, silica in mud ground mass and chert) versus ‘calcic’ components in the OS.

PC3 – Sr, SiO₂ and CaO contribute the most to the formation of the third component that describes 10.44% of the data variance. The third PC has a positive correlation with Sr and CaO, while the correlation with SiO₂ is also strong but negative (Table 2). This component can be interpreted as a measure of biogenic calcite (calcite mud, foraminifera shells, carbonate skeletal debris) versus silica amounts in OS.

PC4 – The fourth component accounts for 8.29% of data variability. Significant positive correlation with P₂O₅ contents, weaker negative correlation with MgO and lack or low correlations with all other elements suggest that PC4 describes processes of phosphorus enrichment, including apatite skeleton debris in OS.

Principal component analysis proves that considerable variation exists in chemical composition among the studied OS and barren rock samples. Based on Figs 4 and 5, it can be concluded that the OS sequence contains OS subtypes with very high OM and metal contents, and dolomite samples with a very low content of metals. There are samples with a high calcite content and a low quartz content and vice versa, and samples with a considerable amount of OM accompanied by a variable mixture of calcareous and siliceous mineral matrix. In addition, samples with a high apatite content are also found in the OS succession.

Table 2. Correlation between principal components and variables. The first two variables contributing the most to the construction of the corresponding component are in bold. Variables on the plane induced by different components are presented also in Fig. 4

	PC1	PC2	PC3	PC4
SiO ₂	0.19	0.61	-0.62	0.34
TiO ₂	0.55	0.79	0.16	-0.16
Al ₂ O ₃	0.52	0.78	0.21	-0.19
Fe ₂ O ₃	0.66	0.69	0.13	-0.16
MgO	-0.46	0.21	-0.08	-0.59
CaO	-0.42	-0.67	0.56	-0.02
K ₂ O	0.58	0.66	0.14	0.08
P ₂ O ₅	-0.06	0.17	-0.18	0.84
S	0.93	-0.17	-0.16	0.07
OM	0.94	-0.21	0.03	-0.06
Zn	0.85	-0.43	-0.26	-0.06
Ni	0.88	-0.44	-0.05	-0.10
Cr	0.93	-0.10	0.20	0.01
Cu	0.87	-0.35	-0.05	0.14
Mo	0.79	-0.28	-0.31	-0.18
V	0.70	-0.48	-0.33	-0.18
Zr	0.75	0.30	0.49	0.11
Sr	0.42	-0.32	0.67	0.33

The current dataset consists of samples from nine drill cores covering the lateral and vertical extent of the OS deposit. Approximately 45 samples from each core represent an on average 70 m thick vertical cross section of the 72 km² deposit area. As recorded from the chemical composition of the OS sequence, the deposition of 70 m of OS took place in a considerable time period (by indirect assessment, a few millions of years), during which stable and variable conditions of accumulation alternated. These variations become visible by the help of hierarchical clustering of samples using PCA.

The hierarchical classification of 392 samples is presented in Fig. 6. Two distinct groups are separated, C1 and C2, which are further subclustered into C1.1, C1.2, and C2.1, C2.2, respectively. Cluster C1.2 is additionally subdivided into three subclusters: C1.2.1, C1.2.2 and C1.2.3. The principal components describing different clusters are plotted in Fig. 5, and the relation of elements to clusters on planes constructed by components is visualized in Fig. 4.

The geochemical pattern is plotted using the average of the element in the cluster, normalized to the average of the element concentration in the whole dataset. It enables us to highlight the range of variation of different elements (including those non-significant for defining a certain cluster) in the limits of a geochemical group and between the groups (Fig. 7).

Positioning of clusters in oil shale sequences reflecting changes during oil shale accumulation

The properties of the studied OS subunits (Table 1) are shortly summarized as follows: **OS layer A** is described as phosphate-bearing OS; **OS layer B1** is terminated by OS layer B2 with the disappearance of phosphate concretions in OS; **OS layer B2** is currently separated as calcareous-siliceous OS; **OS layer C** is currently defined as calcareous-siliceous OS; **OS layer D** is described as SiO₂-rich; **OS layer E1** is calcareous; **OS layer E2** is OM-rich and has a high content of metals; **OS layer E3** is calcareous. Three dolomitic limestone interlayers (A/B, B/C, D/E – in the geochemical study altogether indexed as Dol) subdivide the OS seam into four parts: A, B1+B2, C+D and E1+E2+E3.

The positions of individual samples in OS cross sections are plotted in Fig. 8, using the cluster colour legend from Fig. 7 and others. The cluster analysis proves that samples are clustered along the lateral extent of OS layers referring (i) to the persistence of the composition of the layers in the horizontal direction over the exploration area and (ii) to the layering-related alternation of OS chemical types from the bottom to the

top of the unit. Consequently, the results suggest that distinct laterally uniform conditions of the accumulation of OS layers and barren rock interlayers principally (with minor local variations, however) governed the formation of each layer over the whole exploration field. In the vertical succession, uniform variations in the composition of layers and their subunits reflect respective alternation and also trends of sedimentation conditions. Visualizing the distribution of sample groups (corresponding to different clusters) using the colour-coded legend enables us to observe the structure of the OS unit in more different aspects: (i) variability of the unit in general, (ii) co-existence of certain sample groups, (iii) specific assemblages of chemical groups in different layers, (iv) specific composition of the barren interlayers, etc.

The distribution of cluster groups of samples (Fig. 8) expresses also the chemical variability of the OS unit and its separate layers in aspects of the appearance of certain specifically characteristic patterns. Specific characteristics of the sample groups (clusters), presented below, highlight the individual elements or group of elements with high or low levels.

C1.1 – Samples in this group are described by elements (MgO) having low values on a plane constructed by PC1 vs PC4 (Figs 4C, 5). The chemical pattern presented in Fig. 7 shows the MgO concentration several times higher in this group, while other elements are below average. The group is present in only barren dolomitic interbeds A/B, B/C and C/D.

C1.2.1 – The samples in this group are described by elements (P_2O_5 , SiO_2) having high values on axis PC4 and low values on axis PC3 on a plane constructed by principal components (Figs 4D, 5). This group is characterized by above-average P_2O_5 , together with SiO_2 content (Fig. 7) due to the high apatite (and quartz-chert) contents, while OM, trace metals and clay content are suppressed. The samples of C1.2.1 occur from the footwall and dominate in the OS layers A and B1 (Fig. 8). Minor alternation with other OS types decreases upwards.

C1.2.2 – This group is defined by high values of CaO on axis PC3 and low values on axis PC1 (Figs 4B, 5). The chemical pattern shows the slightly above-average contents of CaO and Sr and the below-average contents of all other elements. These samples are likely representing wackestone-type OS intervals. In the deposit this type of OS appears in 3–4 intervals alternating with other types of OS in layers B1 and B2, and becomes more dominating in the upper part of the OS sequence (Fig. 8).

C1.2.3 – The samples of this group are described by elements having high values on a plane constructed

by PC1 vs PC3 (Figs 4B, 5). With slight ‘negative SiO_2 anomaly’ the chemical pattern of these samples represents the average composition of other types of OS (Fig. 7). This type of OS is present in several OS layers, forming one interval in OS layer B2, major part of layer C, and several continuous intervals in E1 and E3 (Fig. 8).

C2.1 – The samples of this group are described by OM carrying S and trace metals having high values on axis PC1 and low values on axis PC2 (Figs 4A, 5). The differentiating feature of this cluster is OM nearly two times higher and a very high content of trace metals (Fig. 7). These samples form a distinct interval, layer E2, which separates otherwise similar OS layers E1 and E3 (Fig. 8).

C2.2 – The samples of this group are described by elements (TiO_2 , Al_2O_3 , K_2O , Fe_2O_3) having high values on the plane constructed by PC1 vs PC2 (Figs 4A, 5). The distinctive feature of these samples is the above-average content of Al_2O_3 , TiO_2 , Fe_2O_3 , K_2O and SiO_2 (Fig. 7). In the cross section these samples form a distinct interval in the middle part of the OS unit corresponding to OS layer D; however, three continuous minor intervals also occur at lower levels (Fig. 8).

CONCLUSION

A representative collection of gapless core samples reliably characterizes the chemical composition of the full OS sequence and, within it, of the eight separate OS layers and three dolomitic interlayers forming the OS unit in a limited area of the AUG deposit. The results of PCA and hierarchical clustering of the sample collection provide considerable information about the geochemical pattern – regularities in the distribution of sample clusters within and between the different OS layers. The variation in the chemical composition of the OS unit is basically expressed and visualized with six specific geochemical groups (clusters) of samples, whose spatial distribution allows summarizing the main changes in the composition and shapes of the general chemical patterns of the deposit. The study reveals that significant general trends and fluctuations in the entire OS unit as well as differences in the chemical composition of the individual OS layers occur namely in accordance with the layered structure and have most likely been established by considerable changes in sedimentation conditions. Minor variations as well as specific geochemical stability intervals occur in the internal structure of layers.

The inconstant composition of the OS unit has resulted from different intensity of the accumulation of chemical components that are almost independent

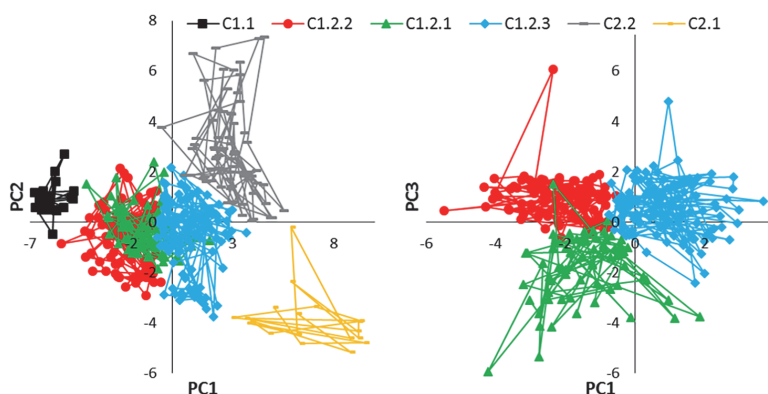


Fig. 5. On principal components planes constructed by PC1–PC2 and PC1–PC3 (and others not presented here), the cloud of the analysed samples grouped into clusters (C1.1, C1.2.1, etc.) demonstrates the correlation between samples and principal components. Note the different positioning of clusters on different planes, showing which component (and elements forming the corresponding component) best describe the samples in the cluster. On the plane PC1 (S, OM, trace metals) – PC2 (‘clay components’) clusters C1.2.1 (P_2O_5 with SiO_2 , typical for the layers A and B1), C1.2.2 (Sr with CaO) and C1.2.3 (nearly corresponding to average oil shale) partially overlap, whereas on the plane PC1–PC3 (Sr and CaO with SiO_2) these clusters are located separately.

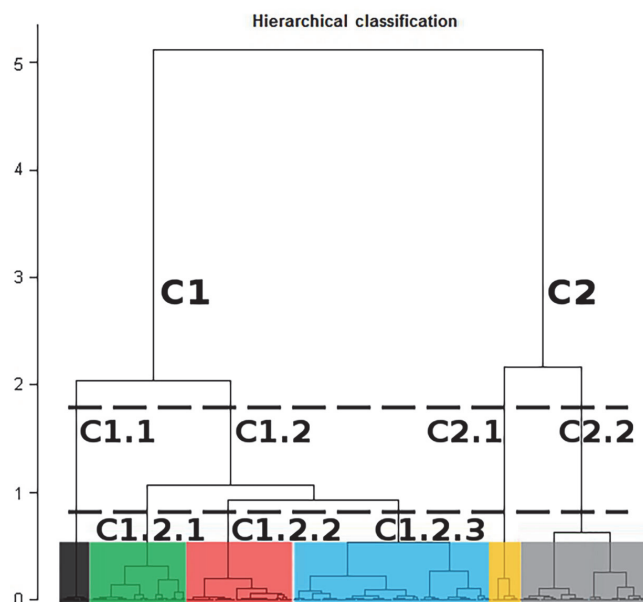


Fig. 6. Hierarchical classification dendrogram. The distance of linkage between samples/clusters is a measure of similarity of individual samples within the cluster or between clusters. The most distant linkage bonds two groups of samples that are further subdivided and samples can be described by a distinguishing component: C1.1 – dolomite (MgO); C1.2.1 – apatite (P_2O_5); C1.2.2 – calcite (CaO); C1.2.3 – ‘average oil shale’; C2.1 – organic matter (OM, S, trace metals); C2.2 – silicate (clay-related elements). For the full pattern of 18 elements see Fig. 7. Note that the diagram reflects the number of samples and also the number of varieties in the clusters that are described in the text.

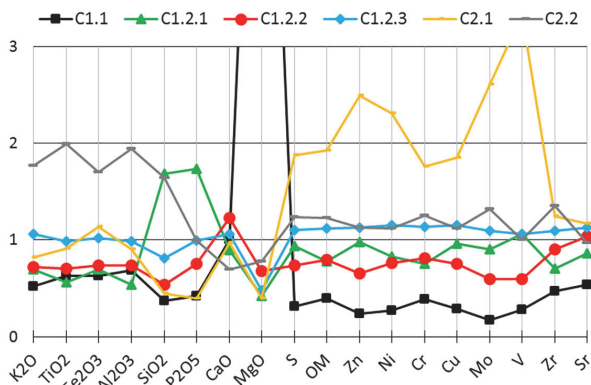


Fig. 7. Geochemical ‘patterns’ of different clusters showing specific elements that have elevated or low concentrations, thus defining the cluster’s geochemical properties: very high MgO defining C1.1 and representing dolomite samples; peak of P₂O₅ (SiO₂) distinguishing apatite-rich samples of the C1.2.1 group; peak of CaO (Sr) with a below the average and flat pattern of other elements representing wackestone oil shale samples of C1.2.2; C1.2.3 being characterized by a flat pattern and close to the average composition; samples of C2.1 distinguished by elevated OM carrying S and trace metals; C2.2 groups samples with above the average content of elements related to silicates.

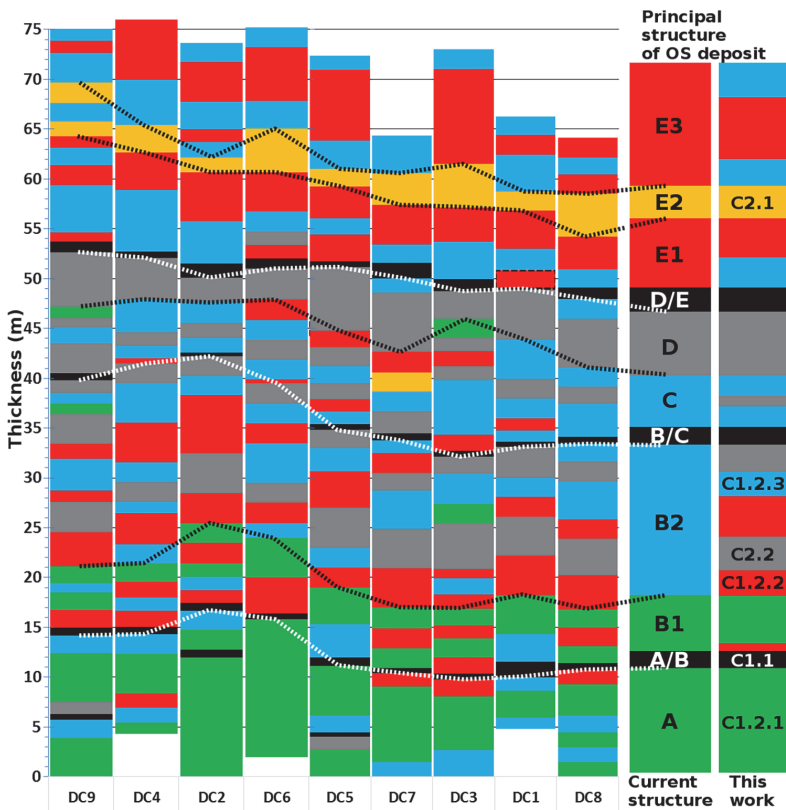


Fig. 8. The position of samples belonging to different clusters in nine oil shale sequences (wells DC1–DC9) revealing the complex structure of the deposit. For better reading three cross sections are uplifted and dashed lines are indicating the base of currently separated oil shale and barren dolomitic limestone layers. For comparison a simplified column of the current structure (NB! layer thicknesses are approximate) with corresponding chemical properties indicated by colours is plotted aside the summarized column of nine cross sections, illustrating the alternation of chemically different types of oil shale/dolomite samples in the sequence.

of each other: (i) CaO of calcite; (ii) SiO₂ of quartz (cristobalite–tridymite); (iii) Al₂O₃ and related elements of clay minerals; (iv) P₂O₅ of apatite and (v) OM carrying S and trace metals (Zn, Mo, Cr, etc.). Exceptional elevated concentrations of MgO in barren carbonate interlayers are likely due to diagenetic processes but derived from specific limestones deposited without load of clay components, apatite and OM carrying sulphur and trace metals.

Principal component analysis integrated with cluster analysis proved to be a powerful tool for the interpretation of the chemically variable structure of the OS unit when using a representative enough sample collection. The integration of chemical data and results of their statistical processing with lithological, mineralogical, palaeontological, petrophysical and other datasets potentially serves for the further interpretation of the origin of OS and barren interlayers. The data are useful also for the development of OS utilization technologies having in mind the variability of their composition.

Huge amounts of OS have accumulated in the Late Cretaceous epicontinental sea ‘carbonate shelf’ basins of Jordan and neighbouring territories. In these basins, oil shales and leaner kerogen-bearing rocks have similar OM of marinite type and similar predominantly calcareous mineral matter. Surprisingly, the presence of barren rock layers is strongly suppressed. Variations in compositions and respective changes in accumulation conditions expressed in OS profiles of different sub-basins and OS units of different age (from Early Maastrichtian to Early Eocene) are poorly studied so far. Sources of accumulated marine mineral matter in the epicontinental shallow marine maze of pools and swells also remain poorly known. The results of the geochemical studies of the JOSE exploration area within the Attarat Um Ghudran deposit show that integrated geochemical investigations together with nannofossil stratigraphic studies are probably the most promising tool for the comparative research into OS profiles of different sub-basins and of different age units in the region. The integration of mineralogical and more detailed geochemical studies (including the use of components not treated here) could contribute to resolving unanswered questions.

Acknowledgements. We thank companies Eesti Energia AS and JOSE for providing the geological material and permission to use the geochemical data in this work. We are grateful to J. Mutterlose and the anonymous referee whose remarks and comments helped to improve the manuscript.

REFERENCES

- Abed, A. M. 2013. The eastern Mediterranean phosphorite giants: an interplay between tectonics and upwelling. *GeoArabia*, **18**, 67–94.
- Abed, A. M. & Amireh, B. S. 1983. Petrography and geochemistry of some Jordanian oil shales from North Jordan. *Petroleum Geology*, **5**, 261–274.
- Abed, A. M., Aroui, K., Amireh, B. S. & Al-Hawari, Z. 2009. Characterization and genesis of some Jordanian oil shales. *Dirasat: Pure Sciences*, **36**, 7–17.
- Alqudah, M., Ali Hussein, M., Van den Boorn, S., Podlaha, O. G. & Mutterlose, J. 2014a. Calcareous nannofossils biostratigraphy of oil shales from Jordan. *GeoArabia*, **19**, 117–140.
- Alqudah, M., Ali Hussein, M., Van den Boorn, S., Giraldo, V. M., Kolonic, S., Podlaha, O. G. & Mutterlose, J. 2014b. Eocene oil shales from Jordan – paleoenvironmental implications from reworked microfossils. *Marine and Petroleum Geology*, **52**, 93–106.
- Alqudah, M., Ali Hussein, M., Van den Boorn, S., Podlaha, O. G. & Mutterlose, J. 2015. Biostratigraphy and depositional setting of Maastrichtian–Eocene oil shales from Jordan. *Marine and Petroleum Geology*, **60**, 87–104.
- Dyni, R. J. 2003. Geology and resources of some world oil-shale deposits. *Oil Shale*, **20**, 193–252.
- Hamarnah, Y., Alali, J. & Sawaged, S. 2006. *Oil Shale Resources Development in Jordan*. Natural Resources Authority of Jordan, Amman (updated report), 98 pp.
- Hufnagel, H. 1984. Die Ölschiefer Jordanien. *Geologisches Jahrbuch*, Reihe A, Heft 75, 295–312.
- Husson, F., Josse, J. & Pages, J. 2010. *Principal Component Methods–Hierarchical Clustering–Partitional Clustering: Why Would We Need to Choose for Visualizing Data?* Technical Report–Agrocampus Ovest, Applied Mathematics Department, 17 pp.
- Husson, F., Le, S. & Pages, J. 2011. *Exploratory Multivariate Analysis by Example Using R*. 1st ed. Chapman & Hall/CRC, London, 228 pp.
- Kiipli, T., Batchelor, R. A., Bernal, J. P., Cowing, Ch., Hagel-Brunnstrom, M., Ingham, M. N., Johnson, D., Kivisilla, J., Knaack, Ch., Kump, P., Lozano, R., Michiels, D., Orlova, K., Pirrus, E., Rousseau, R. M., Ruzicka, J., Sandstrom, H. & Willis, J. P. 2000. Seven sedimentary rock reference samples from Estonia. *Oil Shale*, **17**, 215–223.
- Le, S., Josse, J. & Husson, F. 2008. FactoMineR: An R Package for Multivariate Analysis. *Journal of Statistical Software*, **25**(1), 1–18.
- Powell, H. J. & Moh’d, K. B. 2011. Evolution of Cretaceous to Eocene alluvial and carbonate platform sequences in central and south Jordan. *GeoArabia*, **16**, 29–82.
- Puura, V., Soesoo, A., Voolma, M., Hade, S. & Aosaar, H. 2016. Chemical composition of the mineral matter of the Attarat Um Ghudran oil shale, Central Jordan. *Oil Shale*, **33**, 18–30.
- Sharland, R. P., Archer, R., Casey, M. D., Davies, B. R., Hall, H. S., Heward, P. A., Horbury, D. A. & Simmons, D. M. 2001. *Arabian Plate Sequence Stratigraphy*. *GeoArabia Special Publication 2: Gulf PetroLink, Bahrain*, 371 pp.

Jordaania Attarat Um Ghudrani maardla põlevkivikihtide geokeemilise muutlikkuse hinnang

Margus Voolma, Alvar Soesoo, Väino Puura, Sigrid Hade ja Hardi Aosaar

Jordaania Kriidi ja Paleogeeni vanusega põlevkivid on valdavalt lubjarikkad mudakivid, mõningate ränirikaste intervallidega, kus domineerivateks mineraalideks on kvarts ning kristobaliit-tridümiit. Esmaste mikropaleontoloogiliste andmete põhjal on käesolevas töös uuritud põlevkivid Maastrichti vanusega. Kesk-Jordaania paikneva Attarat Um Ghudrani maardla põlevkivilasundi keskmine paksus on 70 meetrit. Nimetatud kihtide keemilise koostise muutlikkuse uurimiseks kasutati 9 puursüdamikust võetud 392 proovi keemilise analüüsi andmeid. Proovid võeti intervalliga 0,5–2 meetrit. Põlevkivi põhielementide (MgO , P_2O_5 , Al_2O_3) sisaldused varieeruvad läbilõikes suurtes piirides, näiteks CaO sisaldus muutub 3 kuni 70 massiprotsenti ja SiO_2 sisaldus 10 kuni 50 massiprotsenti, ka orgaanikasisaldus on muutlik. Lisaks on põlevkivis palju orgaanilist väävlit ja jälgelemente. Mõnede metallide (Zn , V , Cr , Ni , Mo) sisaldused läbilõikes muutuvad mitmekordselt. Keemilise koostise (18 elementi) muutlikkuse hindamiseks kasutati statistilisi meetodeid: (i) põhikomponentide analüüs, (ii) hierarhiline klasteranalüüs. Põhikomponentide analüüs näitas, et esimene põhikomponent kirjeldas 47% muutlikkust, teine 22,82%. Esimest komponenti kirjeldab orgaanikaga seotud väävli ja metallide (Cr , Cu , Ni , Zn , Mo) sisaldus ning teist positiivne korrelatsioon TiO_2 , Al_2O_3 , Fe_2O_3 , SiO_2 ja K_2O ning negatiivne seos CaO -ga. Tulemused näitasid et, neli põhikomponenti kirjeldavad kokku ligi 89% geokeemilisest erinevusest ja nende abil on võimalik defineerida kuut erinevat põlevkiviläbilõike kivimtüüpi. Väljaeraldatud kivimtüüpide paigutus ja esinemisregulaarsus läbilõikes peegeldab lasundi sisestruktuuri. Eristunud kihid on seletatavad põhielementide/mineraalide kuhjumise intensiivsuse vaheldumisega, mis omakorda on põhjustatud märkimisväärtsetest settimiskeskonna muutustest. Põlevkivilasundi geokeemilise muutlikkuse mõistmine on oluline põlevkivi tekke-tingimuste selgitamise ja kaevandamise ning töötlemise seisukohalt.

**DISSERTATIONS DEFENDED AT
TALLINN UNIVERSITY OF TECHNOLOGY ON
NATURAL AND EXACT SCIENCES**

1. **Olav Kongas**. Nonlinear Dynamics in Modeling Cardiac Arrhythmias. 1998.
2. **Kalju Vanatalu**. Optimization of Processes of Microbial Biosynthesis of Isotopically Labeled Biomolecules and Their Complexes. 1999.
3. **Ahto Buldas**. An Algebraic Approach to the Structure of Graphs. 1999.
4. **Monika Drews**. A Metabolic Study of Insect Cells in Batch and Continuous Culture: Application of Chemostat and Turbidostat to the Production of Recombinant Proteins. 1999.
5. **Eola Valdre**. Endothelial-Specific Regulation of Vessel Formation: Role of Receptor Tyrosine Kinases. 2000.
6. **Kalju Lott**. Doping and Defect Thermodynamic Equilibrium in ZnS. 2000.
7. **Reet Koljak**. Novel Fatty Acid Dioxygenases from the Corals *Plexaura homomalla* and *Gersemia fruticosa*. 2001.
8. **Anne Paju**. Asymmetric oxidation of Prochiral and Racemic Ketones by Using Sharpless Catalyst. 2001.
9. **Marko Vendelin**. Cardiac Mechanoenergetics *in silico*. 2001.
10. **Pearu Peterson**. Multi-Soliton Interactions and the Inverse Problem of Wave Crest. 2001.
11. **Anne Menert**. Microcalorimetry of Anaerobic Digestion. 2001.
12. **Toomas Tiivel**. The Role of the Mitochondrial Outer Membrane in *in vivo* Regulation of Respiration in Normal Heart and Skeletal Muscle Cell. 2002.
13. **Olle Hints**. Ordovician Scolecodonts of Estonia and Neighbouring Areas: Taxonomy, Distribution, Palaeoecology, and Application. 2002.
14. **Jaak Nõlvak**. Chitinozoan Biostratigraphy in the Ordovician of Baltoscandia. 2002.
15. **Liivi Kluge**. On Algebraic Structure of Pre-Operad. 2002.
16. **Jaanus Lass**. Biosignal Interpretation: Study of Cardiac Arrhythmias and Electromagnetic Field Effects on Human Nervous System. 2002.
17. **Janek Peterson**. Synthesis, Structural Characterization and Modification of PAMAM Dendrimers. 2002.
18. **Merike Vaher**. Room Temperature Ionic Liquids as Background Electrolyte Additives in Capillary Electrophoresis. 2002.
19. **Valdek Mikli**. Electron Microscopy and Image Analysis Study of Powdered Hardmetal Materials and Optoelectronic Thin Films. 2003.
20. **Mart Viljus**. The Microstructure and Properties of Fine-Grained Cermets. 2003.
21. **Signe Kask**. Identification and Characterization of Dairy-Related *Lactobacillus*. 2003.
22. **Tiiu-Mai Laht**. Influence of Microstructure of the Curd on Enzymatic and Microbiological Processes in Swiss-Type Cheese. 2003.
23. **Anne Kuusksalu**. 2–5A Synthetase in the Marine Sponge *Geodia cydonium*. 2003.
24. **Sergei Bereznev**. Solar Cells Based on Polycrystalline Copper-Indium Chalcogenides and Conductive Polymers. 2003.

25. **Kadri Kriis.** Asymmetric Synthesis of C₂-Symmetric Bimorpholines and Their Application as Chiral Ligands in the Transfer Hydrogenation of Aromatic Ketones. 2004.
26. **Jekaterina Reut.** Polypyrrole Coatings on Conducting and Insulating Substrates. 2004.
27. **Sven Nõmm.** Realization and Identification of Discrete-Time Nonlinear Systems. 2004.
28. **Olga Kijatkina.** Deposition of Copper Indium Disulphide Films by Chemical Spray Pyrolysis. 2004.
29. **Gert Tamberg.** On Sampling Operators Defined by Rogosinski, Hann and Blackman Windows. 2004.
30. **Monika Übner.** Interaction of Humic Substances with Metal Cations. 2004.
31. **Kaarel Adamberg.** Growth Characteristics of Non-Starter Lactic Acid Bacteria from Cheese. 2004.
32. **Imre Vallikivi.** Lipase-Catalysed Reactions of Prostaglandins. 2004.
33. **Merike Peld.** Substituted Apatites as Sorbents for Heavy Metals. 2005.
34. **Vitali Syritski.** Study of Synthesis and Redox Switching of Polypyrrole and Poly(3,4-ethylenedioxythiophene) by Using *in-situ* Techniques. 2004.
35. **Lee Põllumaa.** Evaluation of Ecotoxicological Effects Related to Oil Shale Industry. 2004.
36. **Riina Aav.** Synthesis of 9,11-Secosterols Intermediates. 2005.
37. **Andres Braunbrück.** Wave Interaction in Weakly Inhomogeneous Materials. 2005.
38. **Robert Kitt.** Generalised Scale-Invariance in Financial Time Series. 2005.
39. **Juss Pavelson.** Mesoscale Physical Processes and the Related Impact on the Summer Nutrient Fields and Phytoplankton Blooms in the Western Gulf of Finland. 2005.
40. **Olari Ilison.** Solitons and Solitary Waves in Media with Higher Order Dispersive and Nonlinear Effects. 2005.
41. **Maksim Säkki.** Intermittency and Long-Range Structurization of Heart Rate. 2005.
42. **Enli Kiipli.** Modelling Seawater Chemistry of the East Baltic Basin in the Late Ordovician–Early Silurian. 2005.
43. **Igor Golovtsov.** Modification of Conductive Properties and Processability of Polyparaphenylene, Polypyrrole and polyaniline. 2005.
44. **Katrin Laos.** Interaction Between Furcellaran and the Globular Proteins (Bovine Serum Albumin β -Lactoglobulin). 2005.
45. **Arvo Mere.** Structural and Electrical Properties of Spray Deposited Copper Indium Disulphide Films for Solar Cells. 2006.
46. **Sille Ehala.** Development and Application of Various On- and Off-Line Analytical Methods for the Analysis of Bioactive Compounds. 2006.
47. **Maria Kulp.** Capillary Electrophoretic Monitoring of Biochemical Reaction Kinetics. 2006.
48. **Anu Aaspõllu.** Proteinases from *Vipera lebetina* Snake Venom Affecting Hemostasis. 2006.

49. **Lyudmila Chekulayeva.** Photosensitized Inactivation of Tumor Cells by Porphyrins and Chlorins. 2006.
50. **Merle Uudsemaa.** Quantum-Chemical Modeling of Solvated First Row Transition Metal Ions. 2006.
51. **Tagli Pitsi.** Nutrition Situation of Pre-School Children in Estonia from 1995 to 2004. 2006.
52. **Angela Ivask.** Luminescent Recombinant Sensor Bacteria for the Analysis of Bioavailable Heavy Metals. 2006.
53. **Tiina Lõugas.** Study on Physico-Chemical Properties and Some Bioactive Compounds of Sea Buckthorn (*Hippophae rhamnoides* L.). 2006.
54. **Kaja Kasemets.** Effect of Changing Environmental Conditions on the Fermentative Growth of *Saccharomyces cerevisiae* S288C: Auxo-accelerostat Study. 2006.
55. **Ildar Nisamedtinov.** Application of ^{13}C and Fluorescence Labeling in Metabolic Studies of *Saccharomyces* spp. 2006.
56. **Alar Leibak.** On Additive Generalisation of Voronoï's Theory of Perfect Forms over Algebraic Number Fields. 2006.
57. **Andri Jagomägi.** Photoluminescence of Chalcopyrite Tellurides. 2006.
58. **Tõnu Martma.** Application of Carbon Isotopes to the Study of the Ordovician and Silurian of the Baltic. 2006.
59. **Marit Kauk.** Chemical Composition of CuInSe_2 Monograin Powders for Solar Cell Application. 2006.
60. **Julia Kois.** Electrochemical Deposition of CuInSe_2 Thin Films for Photovoltaic Applications. 2006.
61. **Iiona Oja Açıık.** Sol-Gel Deposition of Titanium Dioxide Films. 2007.
62. **Tiia Anmann.** Integrated and Organized Cellular Bioenergetic Systems in Heart and Brain. 2007.
63. **Katrin Trummal.** Purification, Characterization and Specificity Studies of Metalloproteinases from *Vipera lebetina* Snake Venom. 2007.
64. **Gennadi Lessin.** Biochemical Definition of Coastal Zone Using Numerical Modeling and Measurement Data. 2007.
65. **Enno Pais.** Inverse problems to determine non-homogeneous degenerate memory kernels in heat flow. 2007.
66. **Maria Borissova.** Capillary Electrophoresis on Alkylimidazolium Salts. 2007.
67. **Karin Valmsen.** Prostaglandin Synthesis in the Coral *Plexaura homomalla*: Control of Prostaglandin Stereochemistry at Carbon 15 by Cyclooxygenases. 2007.
68. **Kristjan Piirimäe.** Long-Term Changes of Nutrient Fluxes in the Drainage Basin of the Gulf of Finland – Application of the PolFlow Model. 2007.
69. **Tatjana Dedova.** Chemical Spray Pyrolysis Deposition of Zinc Sulfide Thin Films and Zinc Oxide Nanostructured Layers. 2007.
70. **Katrin Tomson.** Production of Labelled Recombinant Proteins in Fed-Batch Systems in *Escherichia coli*. 2007.
71. **Cecilia Sarmiento.** Suppressors of RNA Silencing in Plants. 2008.
72. **Vilja Mardla.** Inhibition of Platelet Aggregation with Combination of Antiplatelet Agents. 2008.

73. **Maie Bachmann.** Effect of Modulated Microwave Radiation on Human Resting Electroencephalographic Signal. 2008.
74. **Dan Hvonen.** Terahertz Spectroscopy of Low-Dimensional Spin Systems. 2008.
75. **Ly Villo.** Stereoselective Chemoenzymatic Synthesis of Deoxy Sugar Esters Involving *Candida antarctica* Lipase B. 2008.
76. **Johan Anton.** Technology of Integrated Photoelasticity for Residual Stress Measurement in Glass Articles of Axisymmetric Shape. 2008.
77. **Olga Volobujeva.** SEM Study of Selenization of Different Thin Metallic Films. 2008.
78. **Artur Jgi.** Synthesis of 4'-Substituted 2,3'-dideoxynucleoside Analogues. 2008.
79. **Mario Kadastik.** Doubly Charged Higgs Boson Decays and Implications on Neutrino Physics. 2008.
80. **Fernando Prez-Caballero.** Carbon Aerogels from 5-Methylresorcinol-Formaldehyde Gels. 2008.
81. **Sirje Vaask.** The Comparability, Reproducibility and Validity of Estonian Food Consumption Surveys. 2008.
82. **Anna Menaker.** Electrosynthesized Conducting Polymers, Polypyrrole and Poly(3,4-ethylenedioxythiophene), for Molecular Imprinting. 2009.
83. **Lauri Ilison.** Solitons and Solitary Waves in Hierarchical Korteweg-de Vries Type Systems. 2009.
84. **Kaia Ernits.** Study of In₂S₃ and ZnS Thin Films Deposited by Ultrasonic Spray Pyrolysis and Chemical Deposition. 2009.
85. **Veljo Sinivee.** Portable Spectrometer for Ionizing Radiation "Gammamapper". 2009.
86. **Jri Virkepu.** On Lagrange Formalism for Lie Theory and Operadic Harmonic Oscillator in Low Dimensions. 2009.
87. **Marko Piirsoo.** Deciphering Molecular Basis of Schwann Cell Development. 2009.
88. **Kati Helmja.** Determination of Phenolic Compounds and Their Antioxidative Capability in Plant Extracts. 2010.
89. **Merike Smera.** Sobemoviruses: Genomic Organization, Potential for Recombination and Necessity of P1 in Systemic Infection. 2010.
90. **Kristjan Laes.** Preparation and Impedance Spectroscopy of Hybrid Structures Based on CuIn₃Se₅ Photoabsorber. 2010.
91. **Kristin Lippur.** Asymmetric Synthesis of 2,2'-Bimorpholine and its 5,5'-Substituted Derivatives. 2010.
92. **Merike Luman.** Dialysis Dose and Nutrition Assessment by an Optical Method. 2010.
93. **Mihhail Berezovski.** Numerical Simulation of Wave Propagation in Heterogeneous and Microstructured Materials. 2010.
94. **Tamara Aid-Pavlidis.** Structure and Regulation of BDNF Gene. 2010.
95. **Olga Bragina.** The Role of Sonic Hedgehog Pathway in Neuro- and Tumorigenesis. 2010.
96. **Merle Randrt.** Wave Propagation in Microstructured Solids: Solitary and Periodic Waves. 2010.

97. **Marju Laars.** Asymmetric Organocatalytic Michael and Aldol Reactions Mediated by Cyclic Amines. 2010.
98. **Maarja Grossberg.** Optical Properties of Multinary Semiconductor Compounds for Photovoltaic Applications. 2010.
99. **Alla Maloverjan.** Vertebrate Homologues of Drosophila Fused Kinase and Their Role in Sonic Hedgehog Signalling Pathway. 2010.
100. **Priit Pruunsild.** Neuronal Activity-Dependent Transcription Factors and Regulation of Human *BDNF* Gene. 2010.
101. **Tatjana Knjazeva.** New Approaches in Capillary Electrophoresis for Separation and Study of Proteins. 2011.
102. **Atanas Katerski.** Chemical Composition of Sprayed Copper Indium Disulfide Films for Nanostructured Solar Cells. 2011.
103. **Kristi Timmo.** Formation of Properties of CuInSe_2 and $\text{Cu}_2\text{ZnSn}(\text{S,Se})_4$ Monograin Powders Synthesized in Molten KI. 2011.
104. **Kert Tamm.** Wave Propagation and Interaction in Mindlin-Type Microstructured Solids: Numerical Simulation. 2011.
105. **Adrian Popp.** Ordovician Proetid Trilobites in Baltoscandia and Germany. 2011.
106. **Ove Pärn.** Sea Ice Deformation Events in the Gulf of Finland and This Impact on Shipping. 2011.
107. **Germo Väli.** Numerical Experiments on Matter Transport in the Baltic Sea. 2011.
108. **Andrus Seiman.** Point-of-Care Analyser Based on Capillary Electrophoresis. 2011.
109. **Olga Katargina.** Tick-Borne Pathogens Circulating in Estonia (Tick-Borne Encephalitis Virus, *Anaplasma phagocytophilum*, *Babesia* Species): Their Prevalence and Genetic Characterization. 2011.
110. **Ingrid Sumeri.** The Study of Probiotic Bacteria in Human Gastrointestinal Tract Simulator. 2011.
111. **Kairit Zovo.** Functional Characterization of Cellular Copper Proteome. 2011.
112. **Natalja Makarytsheva.** Analysis of Organic Species in Sediments and Soil by High Performance Separation Methods. 2011.
113. **Monika Mortimer.** Evaluation of the Biological Effects of Engineered Nanoparticles on Unicellular Pro- and Eukaryotic Organisms. 2011.
114. **Kersti Tepp.** Molecular System Bioenergetics of Cardiac Cells: Quantitative Analysis of Structure-Function Relationship. 2011.
115. **Anna-Liisa Peikolainen.** Organic Aerogels Based on 5-Methylresorcinol. 2011.
116. **Leeli Amon.** Palaeoecological Reconstruction of Late-Glacial Vegetation Dynamics in Eastern Baltic Area: A View Based on Plant Macrofossil Analysis. 2011.
117. **Tanel Peets.** Dispersion Analysis of Wave Motion in Microstructured Solids. 2011.
118. **Liina Kaupmees.** Selenization of Molybdenum as Contact Material in Solar Cells. 2011.
119. **Allan Olsper.** Properties of VPg and Coat Protein of Sobemoviruses. 2011.
120. **Kadri Koppel.** Food Category Appraisal Using Sensory Methods. 2011.

121. **Jelena Gorbatšova**. Development of Methods for CE Analysis of Plant Phenolics and Vitamins. 2011.
122. **Karin Viipsi**. Impact of EDTA and Humic Substances on the Removal of Cd and Zn from Aqueous Solutions by Apatite. 2012.
123. **David Schryer**. Metabolic Flux Analysis of Compartmentalized Systems Using Dynamic Isotopologue Modeling. 2012.
124. **Ardo Illaste**. Analysis of Molecular Movements in Cardiac Myocytes. 2012.
125. **Indrek Reile**. 3-Alkylcyclopentane-1,2-Diones in Asymmetric Oxidation and Alkylation Reactions. 2012.
126. **Tatjana Tamberg**. Some Classes of Finite 2-Groups and Their Endomorphism Semigroups. 2012.
127. **Taavi Liblik**. Variability of Thermohaline Structure in the Gulf of Finland in Summer. 2012.
128. **Priidik Lagemaa**. Operational Forecasting in Estonian Marine Waters. 2012.
129. **Andrei Errapart**. Photoelastic Tomography in Linear and Non-linear Approximation. 2012.
130. **Külliki Krabbi**. Biochemical Diagnosis of Classical Galactosemia and Mucopolysaccharidoses in Estonia. 2012.
131. **Kristel Kaseleht**. Identification of Aroma Compounds in Food using SPME-GC/MS and GC-Olfactometry. 2012.
132. **Kristel Kodar**. Immunoglobulin G Glycosylation Profiling in Patients with Gastric Cancer. 2012.
133. **Kai Rosin**. Solar Radiation and Wind as Agents of the Formation of the Radiation Regime in Water Bodies. 2012.
134. **Ann Tiiman**. Interactions of Alzheimer's Amyloid-Beta Peptides with Zn(II) and Cu(II) Ions. 2012.
135. **Olga Gavrilova**. Application and Elaboration of Accounting Approaches for Sustainable Development. 2012.
136. **Olesja Bondarenko**. Development of Bacterial Biosensors and Human Stem Cell-Based *In Vitro* Assays for the Toxicological Profiling of Synthetic Nanoparticles. 2012.
137. **Katri Muska**. Study of Composition and Thermal Treatments of Quaternary Compounds for Monograin Layer Solar Cells. 2012.
138. **Ranno Nahku**. Validation of Critical Factors for the Quantitative Characterization of Bacterial Physiology in Accelerostat Cultures. 2012.
139. **Petri-Jaan Lahtvee**. Quantitative Omics-level Analysis of Growth Rate Dependent Energy Metabolism in *Lactococcus lactis*. 2012.
140. **Kerti Orumets**. Molecular Mechanisms Controlling Intracellular Glutathione Levels in Baker's Yeast *Saccharomyces cerevisiae* and its Random Mutagenized Glutathione Over-Accumulating Isolate. 2012.
141. **Loreida Timberg**. Spice-Cured Sprats Ripening, Sensory Parameters Development, and Quality Indicators. 2012.
142. **Anna Mihhalevski**. Rye Sourdough Fermentation and Bread Stability. 2012.
143. **Liisa Arike**. Quantitative Proteomics of *Escherichia coli*: From Relative to Absolute Scale. 2012.
144. **Kairi Otto**. Deposition of In₂S₃ Thin Films by Chemical Spray Pyrolysis. 2012.

145. **Mari Sepp.** Functions of the Basic Helix-Loop-Helix Transcription Factor TCF4 in Health and Disease. 2012.
146. **Anna Suhhova.** Detection of the Effect of Weak Stressors on Human Resting Electroencephalographic Signal. 2012.
147. **Aram Kazarjan.** Development and Production of Extruded Food and Feed Products Containing Probiotic Microorganisms. 2012.
148. **Rivo Uiboupin.** Application of Remote Sensing Methods for the Investigation of Spatio-Temporal Variability of Sea Surface Temperature and Chlorophyll Fields in the Gulf of Finland. 2013.
149. **Tiina Kriščiunaite.** A Study of Milk Coagulability. 2013.
150. **Tuuli Levandi.** Comparative Study of Cereal Varieties by Analytical Separation Methods and Chemometrics. 2013.
151. **Natalja Kabanova.** Development of a Microcalorimetric Method for the Study of Fermentation Processes. 2013.
152. **Himani Khanduri.** Magnetic Properties of Functional Oxides. 2013.
153. **Julia Smirnova.** Investigation of Properties and Reaction Mechanisms of Redox-Active Proteins by ESI MS. 2013.
154. **Mervi Sepp.** Estimation of Diffusion Restrictions in Cardiomyocytes Using Kinetic Measurements. 2013.
155. **Kersti Jääger.** Differentiation and Heterogeneity of Mesenchymal Stem Cells. 2013.
156. **Victor Alari.** Multi-Scale Wind Wave Modeling in the Baltic Sea. 2013.
157. **Taavi Päll.** Studies of CD44 Hyaluronan Binding Domain as Novel Angiogenesis Inhibitor. 2013.
158. **Allan Niidu.** Synthesis of Cyclopentane and Tetrahydrofuran Derivatives. 2013.
159. **Julia Geller.** Detection and Genetic Characterization of *Borrelia* Species Circulating in Tick Population in Estonia. 2013.
160. **Irina Stulova.** The Effects of Milk Composition and Treatment on the Growth of Lactic Acid Bacteria. 2013.
161. **Jana Holmar.** Optical Method for Uric Acid Removal Assessment During Dialysis. 2013.
162. **Kerti Ausmees.** Synthesis of Heterobicyclo[3.2.0]heptane Derivatives *via* Multicomponent Cascade Reaction. 2013.
163. **Minna Varikmaa.** Structural and Functional Studies of Mitochondrial Respiration Regulation in Muscle Cells. 2013.
164. **Indrek Koppel.** Transcriptional Mechanisms of BDNF Gene Regulation. 2014.
165. **Kristjan Pilt.** Optical Pulse Wave Signal Analysis for Determination of Early Arterial Ageing in Diabetic Patients. 2014.
166. **Andres Anier.** Estimation of the Complexity of the Electroencephalogram for Brain Monitoring in Intensive Care. 2014.
167. **Toivo Kallaste.** Pyroclastic Sanidine in the Lower Palaeozoic Bentonites – A Tool for Regional Geological Correlations. 2014.
168. **Erki Kärber.** Properties of ZnO-nanorod/In₂S₃/CuInS₂ Solar Cell and the Constituent Layers Deposited by Chemical Spray Method. 2014.
169. **Julia Lehner.** Formation of Cu₂ZnSnS₄ and Cu₂ZnSnSe₄ by Chalcogenisation of Electrochemically Deposited Precursor Layers. 2014.

170. **Peep Pitk.** Protein- and Lipid-rich Solid Slaughterhouse Waste Anaerobic Co-digestion: Resource Analysis and Process Optimization. 2014.
171. **Kaspar Valgepea.** Absolute Quantitative Multi-omics Characterization of Specific Growth Rate-dependent Metabolism of *Escherichia coli*. 2014.
172. **Artur Noole.** Asymmetric Organocatalytic Synthesis of 3,3'-Disubstituted Oxindoles. 2014.
173. **Robert Tsanev.** Identification and Structure-Functional Characterisation of the Gene Transcriptional Repressor Domain of Human Gli Proteins. 2014.
174. **Dmitri Kartofelev.** Nonlinear Sound Generation Mechanisms in Musical Acoustic. 2014.
175. **Sigrid Hade.** GIS Applications in the Studies of the Palaeozoic Graptolite Argillite and Landscape Change. 2014.
176. **Agne Velthut-Meikas.** Ovarian Follicle as the Environment of Oocyte Maturation: The Role of Granulosa Cells and Follicular Fluid at Pre-Ovulatory Development. 2014.
177. **Kristel Hälvin.** Determination of B-group Vitamins in Food Using an LC-MS Stable Isotope Dilution Assay. 2014.
178. **Mailis Pääri.** Characterization of the Oligoadenylate Synthetase Subgroup from Phylum Porifera. 2014.
179. **Jekaterina Kazantseva.** Alternative Splicing of *TAF4*: A Dynamic Switch between Distinct Cell Functions. 2014.
180. **Jaanus Suurväli.** Regulator of G Protein Signalling 16 (RGS16): Functions in Immunity and Genomic Location in an Ancient MHC-Related Evolutionarily Conserved Synteny Group. 2014.
181. **Ene Viiard.** Diversity and Stability of Lactic Acid Bacteria During Rye Sourdough Propagation. 2014.
182. **Kristella Hansen.** Prostaglandin Synthesis in Marine Arthropods and Red Algae. 2014.
183. **Helike Lõhelaid.** Allene Oxide Synthase-lipoxygenase Pathway in Coral Stress Response. 2015.
184. **Normunds Stivrīnš.** Postglacial Environmental Conditions, Vegetation Succession and Human Impact in Latvia. 2015.
185. **Mary-Liis Kütt.** Identification and Characterization of Bioactive Peptides with Antimicrobial and Immunoregulating Properties Derived from Bovine Colostrum and Milk. 2015.
186. **Kazbulat Šogenov.** Petrophysical Models of the CO₂ Plume at Prospective Storage Sites in the Baltic Basin. 2015.
187. **Taavi Raadik.** Application of Modulation Spectroscopy Methods in Photovoltaic Materials Research. 2015.
188. **Reio Pöder.** Study of Oxygen Vacancy Dynamics in Sc-doped Ceria with NMR Techniques. 2015.
189. **Sven Siir.** Internal Geochemical Stratification of Bentonites (Altered Volcanic Ash Beds) and its Interpretation. 2015.
190. **Kaur Jaanson.** Novel Transgenic Models Based on Bacterial Artificial Chromosomes for Studying BDNF Gene Regulation. 2015.

191. **Niina Karro**. Analysis of ADP Compartmentation in Cardiomyocytes and Its Role in Protection Against Mitochondrial Permeability Transition Pore Opening. 2015.
192. **Piret Laht**. B-plexins Regulate the Maturation of Neurons Through Microtubule Dynamics. 2015.
193. **Sergei Žari**. Organocatalytic Asymmetric Addition to Unsaturated 1,4-Dicarbonyl Compounds. 2015.
194. **Natalja Buhhalko**. Processes Influencing the Spatio-temporal Dynamics of Nutrients and Phytoplankton in Summer in the Gulf of Finland, Baltic Sea. 2015.
195. **Natalia Maticiu**. Mechanism of Changes in the Properties of Chemically Deposited CdS Thin Films Induced by Thermal Annealing. 2015.
196. **Mario Öeren**. Computational Study of Cyclohexylhemicucurbiturils. 2015.
197. **Mari Kalda**. Mechanoenergetics of a Single Cardiomyocyte. 2015.
198. **Ieva Grudzinska**. Diatom Stratigraphy and Relative Sea Level Changes of the Eastern Baltic Sea over the Holocene. 2015.
199. **Anna Kazantseva**. Alternative Splicing in Health and Disease. 2015.
200. **Jana Kazarjan**. Investigation of Endogenous Antioxidants and Their Synthetic Analogues by Capillary Electrophoresis. 2016.
201. **Maria Safonova**. SnS Thin Films Deposition by Chemical Solution Method and Characterization. 2016.
202. **Jekaterina Mazina**. Detection of Psycho- and Bioactive Drugs in Different Sample Matrices by Fluorescence Spectroscopy and Capillary Electrophoresis. 2016.
203. **Karin Rosenstein**. Genes Regulated by Estrogen and Progesterone in Human Endometrium. 2016.
204. **Aleksei Tretjakov**. A Macromolecular Imprinting Approach to Design Synthetic Receptors for Label-Free Biosensing Applications. 2016.
205. **Mati Danilson**. Temperature Dependent Electrical Properties of Kesterite Monograin Layer Solar Cells. 2016.
206. **Kaspar Kevvai**. Applications of ¹⁵N-labeled Yeast Hydrolysates in Metabolic Studies of *Lactococcus lactis* and *Saccharomyces Cerevisiae*. 2016.
207. **Kadri Aller**. Development and Applications of Chemically Defined Media for Lactic Acid Bacteria. 2016.
208. **Gert Preegel**. Cyclopentane-1,2-dione and Cyclopent-2-en-1-one in Asymmetric Organocatalytic Reactions. 2016.
209. **Jekaterina Služenikina**. Applications of Marine Scatterometer Winds and Quality Aspects of their Assimilation into Numerical Weather Prediction Model HIRLAM. 2016.
210. **Erkki Kask**. Study of Kesterite Solar Cell Absorbers by Capacitance Spectroscopy Methods. 2016.
211. **Jürgen Arund**. Major Chromophores and Fluorophores in the Spent Dialysate as Cornerstones for Optical Monitoring of Kidney Replacement Therapy. 2016.
212. **Andrei Šamarin**. Hybrid PET/MR Imaging of Bone Metabolism and Morphology. 2016.
213. **Kairi Kasemets**. Inverse Problems for Parabolic Integro-Differential Equations with Instant and Integral Conditions. 2016.